The effect of locally secreted mediators on endothelial and mesothelial cell function during metastasis of epithelial ovarian cancer to the omentum

Submitted by Gillian Shih Yen Phua to the University of Exeter as a thesis for the degree of Doctor of Philosophy in Medical Studies, April 2022.

I certify that all material in this thesis which is not my own work has been identified and that any material that has previously been submitted and approved for the award of a degree by this or any other University has been acknowledged.

Gillian Phua

Acknowledgements

First and foremost, I am grateful to God for the good health and wellbeing which He has granted throughout this PhD journey.

From the bottom of my heart, my sincerest gratitude to Dr Jacqueline Whatmore for her guidance, and most especially her patience. Special thanks to Dr Nicholas Gutowski for his unwavering support and encouragement, and to Dr Katarina Kos. Our supervisory meetings kept me grounded and focussed throughout the project.

I would like to appreciate Mrs Susan Westoby and the NIHR Exeter Clinical Research Facility team for coordinating tissue sample collection. Thank you also to the patients who kindly donated.

Many thanks to members of the Endothelial Cell Biology Group and to lab members of the Institute of Biomedical and Clinical Science, who made learning and lab work fun. Shoutout to Joanna ‘jojofish’ and the HOMEC to my meso, Annelie ‘pompomfish.’

Thank you to the University of Exeter for the International Excellence Scholarship and also to FORCE Cancer Charity.

Most importantly, thank you to my parents and sisters. To Inosaurus and Tiagosaurus, this thesis is a testament to your love and encouragement.

Dedicated to the beautiful women of Ward 2B and the gynae-oncology team of Hospital Sultanah Bahiyah.

Abstract

Epithelial ovarian cancer (EOC) is the most lethal of all gynaecologic cancers, principally because the early stages are relatively asymptomatic, resulting in many patients having advanced, metastatic disease at diagnosis. A major site of metastasis is the omentum, a large abdominal adipose tissue bed mainly comprised of adipocytes encased in an outer mesothelial cell layer. For EOC cells metastasising to the omentum, via the transcoelomic route, the mesothelium is the first point of contact. After successful invasion through the mesothelium into the omental tissue, the EOC cells are able to activate angiogenesis i.e. new blood vessel formation, in the existing host microvasculature to supply the growing tumour with nutrients and oxygen. The initiation of angiogenesis requires activation of the endothelial cells (ECs) lining the omental microvasculature by pro-angiogenic factors, and it is possible that the production of these factors by both the metastasising tumour cells themselves and the resident cells within the omentum (e.g. adipocytes) jointly contribute to form a rich microenvironment for metastasis growth. However, the signalling interactions between the ovarian cancer cells and the cells of the omentum are poorly understood. Therefore, the aim of this thesis is to investigate the crosstalk between EOCs and omental adipocytes, mesothelial cells and microvascular ECs which may support the induction of metastasis and angiogenesis during secondary spread of EOC to the omentum.

Initially, improved and reliable methodologies for the isolation of primary human omental microvascular ECs (HOMECs) and omental mesothelial cells from donated human omentum were developed, thus providing disease relevant cell types for further study. The EOC cancer cell lines SKOV3 and A2780 were used as model cancer cells. HOMEC proliferation (to model EC activation during angiogenesis) was assessed by WST8 and BrdU assays. Commercially available antibody-based arrays and ELISA were used to investigate the secretome of omental adipose tissue and HOMEC signalling pathways.

Conditioned medium (CM) from omental adipose tissue significantly enhanced HOMEC proliferation via a signalling mechanism which involved STAT3 activation. Thus, secreted adipokines were screened to investigate the pro-proliferative factors responsible, highlighting adiponectin, cathepsin L, MIF, leptin and lipocalin-2. However, no increase in proliferation was observed when HOMECs were treated with any of these selected adipokines, either individually or in combination.

In contrast, treatment of HOMECs with CM collected from ovarian cancer cells which had been pre-incubated with the adipokines leptin or lipocalin-2 did significantly increase HOMEC proliferation compared with CM from untreated cancer cells. Activation of VEGFR2 by its ligand VEGF was implicated, as confirmed by ELISA and receptor inhibitor proliferation studies. Alongside VEGF/VEGFR2, the signalling mechanism may be potentiated by PDGFRβ activation leading to downstream activation of ERK1/2 and subsequent cell proliferation. Importantly, the ERK1/2 and STAT3 signalling pathways may be additive, suggesting that in the omentum, interaction between the adipocytes and the EOC cells can jointly drive angiogenic changes in the omental microvasculature during metastasis.

Cancer cell adhesion onto the mesothelial layer under experimental conditions mimicking peritoneal fluid shear stress was also examined. While CM from adipose tissue or EOCs had no effect, CM from mesothelial cells themselves decreased cancer cell adhesion (implying a protective effect) at a shorter timepoint.

The data presented suggest that while secreted omental adipokines do not impact the initial adhesion of metastasising EOC to the omentum, following invasion of the cancer cells into the omental tissue the microenvironment created is able to support angiogenesis and secondary tumor growth. Specifically, the adipocytes secrete (as yet unidentified) factors that can induce proliferation directly in HOMECs, in addition to secreting leptin and lipocalin-2 which act indirectly on the cancer cells to induce increased production of VEGF, which then also activates pro-angiogenic changes in the HOMECs. Thus, the omental microenvironment provides a rich metastatic niche for the growing secondary tumour, which may partly explain the high rates of omental metastasis in EOC patients.

In conclusion, tumour angiogenesis within the omentum is enhanced by interactions between adipokines secreted from resident adipocytes and metastatic cancer cells. A better understanding of the mechanisms involved may highlight reasons why current therapies are relatively ineffective and better direct the development of future therapies.

List of contents

List of figures

List of tables

List of abbreviations

ADP	adenosine diphosphate
ALK	anaplastic lymphoma kinase
AMPK	adenosine monophosphate-activated protein kinase
ATP	adenosine triphosphate
BCA	bicinchoninic acid
BMI	body mass index
BRCA1/2	breast cancer gene ½
BrdU	bromodeoxyuridine
BSA	bovine serum albumin
CCL	CC chemokine ligand
CCR	CC chemokine receptor
CFD	complement factor D
CM	conditioned medium
COX	cyclo-oxygenase
CRP	c-reactive protein
CXCL	C-X-C motif chemokine ligand
CXCR	CXC chemokine receptor
DAPI	4',6-diamidino-2-phenylindole
DLL4	delta-like ligand 4
DMEM	Dulbecco's Modified Eagle's Medium
DMEM/F12	DMEM/Nutrient Mixture F-12
DMSO	dimethyl sulfoxide
DNA	deoxyribonucleic acid
EC	endothelial cell
ECM	extracellular matrix
EDHF	endothelium-derived hyperpolarising factor
EDTA	ethylenediaminetetraacetic acid
EGF	epidermal growth factor
EGFR	epidermal growth factor receptor

EG-VEGF	endocrine-gland-derived VEGF
ELISA	enzyme-linked immunosorbent assay
EMT	epithelial-mesenchymal transition
EOC	epithelial ovarian cancer
ERK1/2	extracellular regulated kinase ½
ET-1	endothelin-1
FABP4	fatty acid-binding protein 4
FBS	foetal bovine serum
FGF	fibroblast growth factor
FGFR	fibroblast growth factor receptor
FIGO	The International Federation of Gynaecology and Obstetrics
G-CSF	granulocyte colony stimulating factor
GM-CSF	granulocyte macrophage colony-stimulating factor
HBSS	Hank's balanced salt solution
hCMEC	human cerebral microvascular endothelial cell
HEPES	4-(2-hydroxyethyl)-1-piperazineethanesulfonic acid
HGF	hepatocyte growth factor
HGSC	high grade serous carcinoma
HIF-1	hypoxia-inducible factor 1
HMEC	human microvascular endothelial cell
HOMEC	human omental microvascular endothelial cell
HPMEC	human placental microvascular endothelial cell
HRP	horseradish peroxidase
HSL	hormone-sensitive lipase
HSP	heat shock protein
HUVEC	human umbilical vein endothelial cell
ICAM-1	intercellular cell adhesion molecule
IGF	insulin-like growth factor
IGFBP	insulin-like growth factor binding protein
IL	interleukin

MCP-1	monocyte chemoattractant protein-1
MET	mesenchymal-epithelial transition
MIF	macrophage migration inhibitory factor
MMP	matrix metalloproteinase
MMT	mesothelial-mesenchymal transition
mRNA	messenger ribonucleic acid
mTOR	mammalian target of rapamycin
NAD	nicotinamide adenine dinucleotide
NADPH	nicotinamide adenine dinucleotide phosphate
NFκB	nuclear factor kappa-light-chain-enhancer of activated B cells
NO	nitric oxide
PARP	poly(ADP-ribose) polymerase
PBS	phosphate-buffered saline
PDGF	platelet-derived growth factor
PDGFR	platelet-derived growth factor receptor
PGI_2	prostacyclin
PROKR1/2	prokineticin receptor 1/2
RIPA	radio-immunoprecipitation assay
RNA	ribonucleic acid
RTK	receptor tyrosine kinase
RYK	receptor-like tyrosine kinase
SD	standard deviation
SDF-1	stromal cell-derived factor-1
STAT	signal transducer and activator of transcription
TF	tissue factor
TGF-β	transforming growth factor beta
TIMP	tissue inhibitor of matrix metalloproteinase
TNF-α	tumour necrosis factor alpha
tPA	tissue-type plasminogen activator
TSP-1/2	thrombospondin 1/2

TXA_2	thromboxane
uPA	urokinase-type plasminogen activator
VCAM-1	vascular cell adhesion molecule
VE-cadherin	vascular endothelial cadherin
VEGF	vascular endothelial growth factor
VEGFR	vascular endothelial growth factor receptor
VVO	vesiculo-vacuolar organelle
vWF	von Willebrand factor
WST8	water-soluble tetrazolium salt 8
ZO1	zonula occludens-1

Chapter 1. Introduction

Globally, cancer killed 10 million people in 2020,(1) and a great many of these deaths were related to metastatic spread of the primary tumour to distant sites. Metastasis drastically reduces prognosis due to the challenges faced in treating metastatic tumours.(2) This clinical complexity is clearly seen in ovarian cancer, a disease which has very poor rates of survival in advanced stages as described in the worldwide CONCORD-2 study.(2) In the UK, 5-year survival in ovarian cancer patients diagnosed with distant metastases (Stage 3) is 27% (3) and globally, the latest GLOBOCAN data indicate that deaths from ovarian cancer accounted for 65% of newly diagnosed cases (207,252 deaths of 313,959 new cases).(1)

Ovarian cancer usually arises in the ovaries or fallopian tubes and, due to the non-specific early symptoms, has frequently metastasised at diagnosis. The tumour initially spreads to other organs within the abdomen due to its anatomical location. This process is not only dependent on the ability of the ovarian cancer cells to invade and colonise these target organs, but also the microenvironment of the secondary site to support the enlarging metastasis. This process requires the growing tumour to induce new blood vessel formation (angiogenesis) to acquire nutrients and oxygen and once this is established the new tumour vasculature facilitates development of more distant metastases. Angiogenesis requires activation and proliferation of the endothelial cells (ECs) lining the blood vessels by factors present in the tumour microenvironment.

A major site of ovarian cancer metastasis is the omentum, an abdominal adipose tissue, and omentectomy is a frequent preventive or responsive surgical intervention for the disease. The high incidence of omental metastasis is probably the result of location and because the anatomical and cellular environment of the omentum provide a rich ‘soil’ for new tumour growth.

This thesis will examine the impact of the omental cellular environment on the ability of ovarian cancer cells to invade and induce angiogenic changes in the omentum that might support metastasis. Thus, this introduction chapter will discuss vascular ECs, ovarian cancer and its metastatic mechanisms, and the anatomy and cellular composition of the omentum.

1.1 The vascular system

The vascular system transports blood throughout the human body, through a range of vessel types. Specifically, in terms of flow direction, blood flows from the heart through the arteries, arterioles, capillaries, venules and then returns to the heart via the veins.(4) Broadly, the microvasculature refers to vessels less than 150 µm in diameter and consists of the arterioles, capillaries, and venules;(5, 6) while the macrovasculature refers to the large vessels (arteries and veins).(5)

Generally, blood vessels are composed of several layers, with different vessel types containing variable amounts of elastin and smooth muscle. The outermost layer provides vessel strength and is termed the tunica adventitia and is made up of connective tissue such as collagen and elastin fibres.(4) Beneath this layer is the tunica media, consisting of smooth muscle cells, elastin fibres, and a sublayer termed the external elastic lamina which provides structural support.(4) The innermost layer, which is exposed to the lumen of the vessel, is the tunica intima. This region consists of the endothelium (a layer of ECs) anchored to the basal lamina or basement membrane, and another sublayer termed the internal elastic lamina which stabilises the endothelium and provides flexibility.(4) Capillaries consist of the endothelium and basement membrane, with supporting pericytes wrapped around them.(4) Cross section diagrams of a blood vessel and a capillary depicting these layers are shown in **Figure 1**.

Due to the vastness of the vascular system, the surface area covered by the tunica intima may be up to 6000m^2 in humans.(6) ECs not only line the inner walls of the vascular system, but also the lymphatic system. Most tissues in the body require the vascular system for nutrient and oxygen supply, while the lymphatic system drains away interstitial fluids.(7) Further discussion will describe ECs in the vasculature since this is the focus of this thesis.

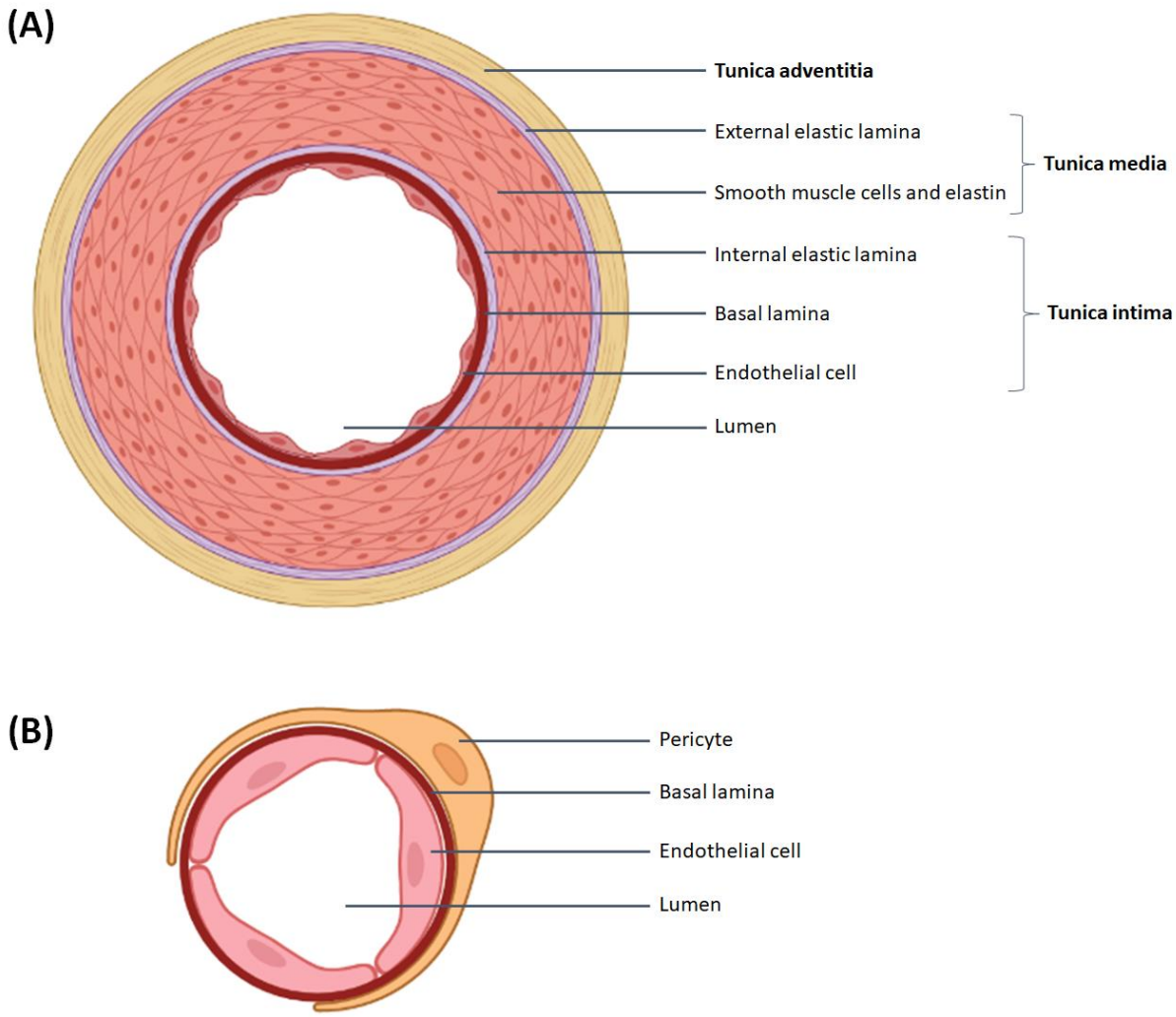

Figure 1. The structure of blood vessel walls. The walls of blood vessels generally consist of three main layers: the tunica adventitia (outermost), tunica media (middle) and tunica intima (innermost) (A). These layers are all not present in capillaries (B). Diagram created with BioRender.com.

The endothelium was previously thought to be an inert structural barrier separating blood components from surrounding tissue,(6) however EC biology is now a research area in its own right due to the myriad of functions attributed to the cells, both physiologically and pathologically. This greater understanding of EC biology has also highlighted the very great heterogeneity observed between ECs in different vascular beds and between the macrovasculature and microvasculature. EC structure, function and heterogeneity will be described in the following sections.

1.1.1 Structure and heterogeneity of endothelial cells

Generally, ECs are approximately 30–50 µm in length, 10–30 µm in width and 0.1–10 µm in depth; the range in dimensions reflects EC variation in different locations. Within the vascular system, arteries and veins have inherently distinctive functions (the former transport oxygen and nutrients, while the latter remove waste and deoxygenated blood) which translates to their distinctive local environments in terms of oxygen concentration, pH, blood pressure and flow rate.(6) Indeed, gene expression patterns between arterial and venous ECs are markedly different. Interestingly, these differences are not only influenced by environmental changes, but are established before fully functional blood vessels are formed.(8)

EC gene expression patterns are also tissue-specific, meaning that their morphology and function are suited to their microenvironment.(6, 8) For example, ECs are spindle-shaped in arterioles, irregular-shaped in capillaries, and elliptical-shaped in venules.(6, 9) In vivo, ECs are orientated according to the direction of blood flow to minimise shear stress. In in vitro culture, they form a cobblestone pattern in the absence of shear stress.(6)

Other EC structures, such as the surface glycocalyx, intercellular junctions and intracellular vesicles are discussed in the following subsections.

a) Endothelial glycocalyx

On the luminal surface of ECs, the surface which comes into contact with blood, is the glycocalyx layer with a thickness of approximately 20–3000 nm depending on tissue type.(5) The glycocalyx is a network of polysaccharides and proteins, comprised mostly of glycoproteins and proteoglycans.(5, 6) Glycosaminoglycan sidechains are attached to the proteoglycans, and are composed of molecules such as heparan-, chondroitin-, dermatan-, and keratan-sulfates.(6) Hyaluronic acid is another glycosaminoglycan which is not directly attached to the proteoglycans, but is ‘woven’ into the glycocalyx layer.(5)

The mesh-like structure of varying lengths and spacing allows the glycocalyx to function as a molecular sieve to exclude large molecules but allow water and other solutes through.(6, 10) It is also a protective barrier which reduces

physical contact between the blood components and the ECs.(5, 6) Surface interactions with leucocytes, erythrocytes, platelets, as well as plasma proteins is controlled by the glycocalyx, where they are repelled by the negative charge on this surface layer.(4, 6)

The glycocalyx also functions as a mechanotransducer to sense fluid shear stress which then translates to cellular signalling. Examples of biomolecular responses include the production of nitric oxide (NO) to increase blood flow (due to vessel dilation) and cytoskeleton reorganisation for the alignment of ECs to the direction of fluid flow.(10, 11)

b) Intercellular junctions

Intercellular junctions form attachment sites between adjacent ECs. Heterogeneity has been observed in the intercellular EC junctions across the vascular system. The EC junctions in large arteries are highly organised, which may be attributed to their function in transporting blood components at high pulsatile flow rates.(9) The structure is similar in the blood brain barrier whereby the intercellular junctions are densely organised in order to separate blood components from neural tissue.(9) Compared to capillaries in general, the intercellular junctions in arterioles are tighter while those in the venules are looser and appear disorganised. The latter's structure may be due to their role in inflammation, where leucocyte extravasation commonly occurs.(9)

Depending on the component protein type and their location, the intercellular junctions can be further classified as adherens junctions (zonula adherens) or tight junctions (zonula occludens). Within the intercellular cleft, the latter are often found nearer to the luminal EC surface compared to the adherens junctions.(9, 12)

Mechanically, these junction proteins act as barriers, in terms of paracellular transport (transport via the intercellular space between cells) and maintain the cell polarity between the luminal surface and the surface opposite (abluminal surface).(9) They also have roles in intracellular cell signalling due to their position on the cell membrane and being anchored to intracellular components.(12)

Vascular endothelial cadherin (VE-cadherin), an adherens junction protein, was reported to be involved in contact inhibition.(12) When cells are confluent,

contacts between cells are increased which in turn limits growth, possibly via cell cycle arrest, thus EC proliferation is regulated. Conversely, when the ECs are less confluent and the junctional proteins are not stabilised, the contact inhibition mechanism is not activated and cell proliferation occurs.(12) The stabilised junctions also communicate cell positioning in order to stabilise the endothelium.(12)

Junctional proteins also protect ECs from pro-apoptotic signals. In a confluent EC population, VE-cadherin-mediated signalling halts cell proliferation and promotes cell survival.(12) Signalling mediated by the platelet endothelial cell adhesion molecule-1 (or CD31), another junctional protein, has roles in suppressing mitochondria-dependent apoptosis.(13) Like the glycocalyx, VE-cadherin and PECAM-1 may function as mechanotransducers in response to blood-flow induced shear stress; this may lead to cytoskeleton reorganisation and subsequent cell shape alteration.(12)

c) Intracellular vesicles

ECs possess several types of vesicles which may be bound to the cell membrane or exist freely within the cytoplasm,(9) as depicted in **Figure 2**. Clathrin-coated vesicles are commonly involved in endocytosis and are commonly found in liver sinusoidal ECs.(9, 14) These vesicles are involved in the clearance of waste products and pathogens from the blood through the formation of lysosomes when endocytosed, and they are subsequently degraded within the cell.(9, 14)

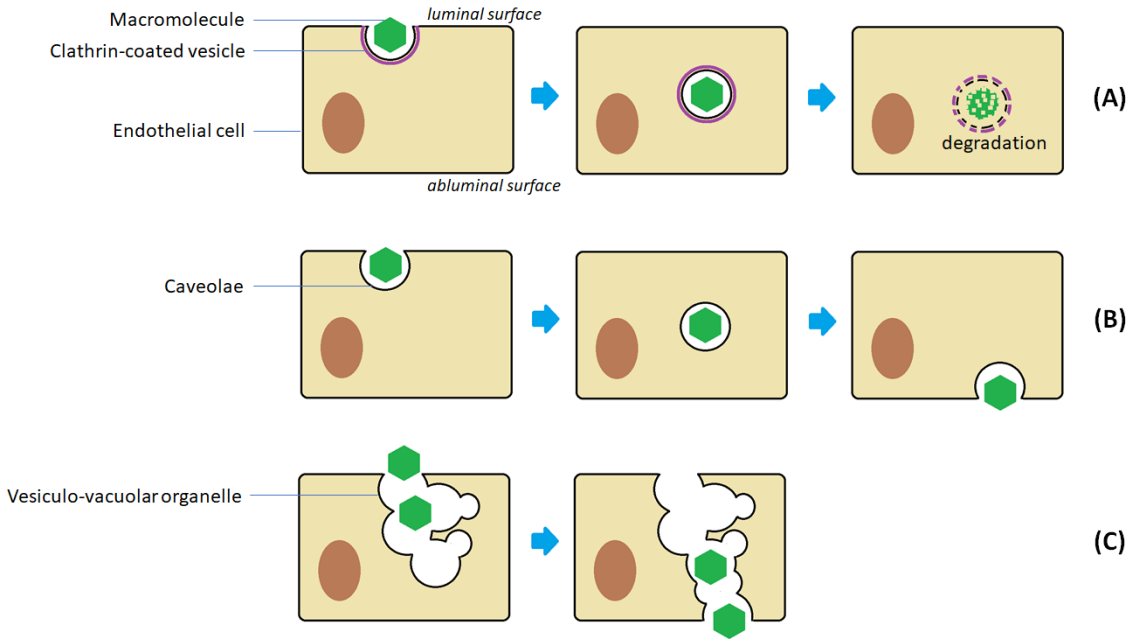

Figure 2. Types of intracellular vesicles in endothelial cells. Clathrin-coated vesicles (A) are involved in endocytosis and degradation of pathogens and waste products, while the caveolae (B) and vesiculo-vacuolar organelles (C) are involved in the transport of molecules (transcytosis) between the luminal and abluminal surfaces. Diagram adapted from Aird (2007)(9) and created with Microsoft Paint.

Caveolae mediate transcellular molecule transport (transcytosis), e.g. from the luminal EC surface to the abluminal surface, and are thought to regulate endothelium permeability.(15) Caveolin-1 is a protein commonly detected in the endothelium which regulates caveolae formation. It is also implicated in signalling pathways involved in cell permeability, such as those induced by vascular endothelial growth factor (VEGF), NO synthase and nuclear factor-kappa B (NFκB).(15) Examples of molecules transported by these vesicles include albumin, insulin, and lipoproteins.(15)

Similar to the caveolae, the vesiculo-vacuolar organelle (VVO) is also involved in transcytosis. This organelle is so named because it consists of conjoined vesicles and vacuoles forming a passage across the whole cell, from the luminal to the abluminal surface.(16) However, these vesicles and vacuoles are still bordered by their own membranes and interconnect with each other through stomata enclosed with thin diaphragms.(17) VVOs are implicated in the vascular hyperpermeability of tumour blood vessels.(17) It was postulated that

stomata opening can be regulated by tumour-secreted VEGF since VEGF was detected via immunocytochemistry in the stoma of VVOs. Inflammatory mediators, such as histamine, have also been detected in the stoma; hence, VVOs have also been implicated in vascular hyperpermeability during inflammation, facilitating plasma protein exit from the vessel lumen.(17)

1.1.2 Function and heterogeneity of endothelial cells

a) Maintenance of vascular tone

As part of the circulatory system, ECs regulate blood flow to tissues in partnership with the vascular smooth muscle cells present in the tunica media layer of blood vessels. The volume of blood reaching the tissues is determined by vascular tone, which is regulated by vasodilatory and vasoconstrictive factors, many of which are secreted by ECs.(18) An example of an endothelium-derived vasodilator is the gaseous mediator, NO, which is synthesised by the endothelial NO synthase through the conversion of the amino acid L-arginine. As a gas, NO diffuses into the surrounding smooth muscle cells to cause relaxation, thus maintaining the basal vasodilator tone of blood vessels.(18)

Cyclo-oxygenase (COX) enzymes are also detected in ECs. The two isoforms, COX-1 (see below) and COX-2 differ in action. Prostacyclin (PGI_2) is a vasodilator produced by ECs, via the COX-2 enzyme. PGI_2 acts on platelets to inhibit their aggregation, and relaxes the vascular smooth muscle leading to dilation similar to the effect of NO.(18) Interestingly, blocking PGI_2 synthesis does not affect vasodilation when NO is present, however, blocking NO synthase leads to increased PGI_2 production, inferring the latter's compensatory role in achieving vasodilation.(18)

Endothelium-derived hyperpolarising factor (EDHF) also causes vasodilation in blood vessels; interestingly however, its true identity is yet unknown. It is so named because it hyperpolarises the vascular smooth muscle resulting in a more negative cell membrane potential.(19) It was discovered that even when the effect of NO and PGI_2 were blocked, the hyperpolarised state persisted, which led to the hypothesis of an alternative activating molecule.(19) The

suggested entities of EDHF include carbon monoxide, hydrogen peroxide, endothelium-derived peptides, epoxyeicosatrienoic acids or even, endothelial-derived potassium.(19)

The COX-1 enzyme, mentioned above, catalyses thromboxane (TXA_2) production and has roles in platelet aggregation and vasoconstriction. Together, the PGI_2 and TXA_2 contribute to maintenance of homeostasis within the blood vessels.(18)

Endothelin-1 (ET-1) is another major vasoconstrictor secreted by ECs. Production is stimulated by inflammatory mediators such as interleukins and tumour necrosis factor alpha (TNF-α), and downregulated by NO and PGI_2. ET-1 action on smooth muscle cells causes vasoconstriction similar to TXA_2, but its autocrine action on ECs stimulates NO and PGI_2 to cause vasodilation.(18, 20)

b) Endothelial cells in haemostasis and thrombosis

In the regulation of blood coagulation, ECs secrete factors to maintain homeostasis. During vascular injury, ECs are activated and secrete tissue factor (TF). Within the coagulation cascade, TF binds to other coagulation factors to ultimately produce fibrin and form a stable clot to seal off the injury site. The role of TF may extend beyond coagulation as ECs also secrete TF in the presence of inflammatory mediators such as TNF-α, IL-1β and TXA_2.(21)

Platelet adhesion and aggregation is another feature of the coagulation system during vascular injury, with the formation of a haemostatic plug to contain the injury site and limit blood loss. Activated ECs release von Willebrand factor (vWF) which mediates the initial step in platelet adhesion to the injured site.(21, 22) At the same time, vWF is capable of binding to and depleting factor VIII, which is a coagulation factor present in the plasma.(21) Thus, the pro- and anti-coagulant roles of vWF contribute to vascular haemostasis. ECs also release platelet-activating factor which activates platelets, leading to their adhesion.(22) When the clot is no longer required, ECs cells release activating factors to aid clot dissolution and restore vessel patency. Tissue-type plasminogen activator (tPA) and urokinase-type plasminogen activator (uPA) convert plasminogen to the active plasmin enzyme, which degrades the fibrin mesh of blood clots.(22) Interestingly, the expression of these plasminogen activators differs between ECs originating from different tissues. For example, ECs from the vena cava

secrete four times the amount of tPA compared to the aorta, and 20 times more than the umbilical vessels.(6) A possible reason for the difference in tPA levels may related to the shear forces within the vessels and thus, the tendency to form clots.(6)

ECs further regulate the coagulation cascade through several methods. ECs express thrombomodulin, a receptor for thrombin, one of enzymes in the coagulation cascade. Thrombomodulin activation by thrombin induces the activation of protein C and protein S, which act as anticoagulants to dampen the coagulation cascade.(22) Additionally, the glycocalyx layer has anticoagulant properties by binding to mediators which can inactivate various pro-coagulant components within the coagulation cascade.(23) These mediators include thrombomodulin, antithrombin III and heparin cofactor II.(23)

In physiological conditions, in the absence of vascular injury and inflammation, ECs maintain an environment that prevents platelet adhesion and clot formation. Aside from their roles in vasomotor functions, NO and PGI_2 are constitutively secreted by ECs to prevent platelet aggregation and thus reduce the risk of thrombus formation.(22) This effect is compounded by enzymes (ectonucleotidases) at the EC luminal surface which hydrolyse ATP and ADP, which are secreted by platelets to promote platelet aggregation.(6) When the endothelium is damaged, this induces an inflammatory state which attracts platelets and leucocytes to the damaged area.

c) Endothelial cells and vascular permeability

The permeability of the vascular wall is dependent on the structure of the endothelium which differs across the vascular system and is broadly categorised to three main types: non-fenestrated continuous endothelium, fenestrated continuous endothelium and discontinuous endothelium (**Figure 3**). The term ‘continuous’ refers to the anchoring of the endothelium to a continuous basement membrane. Non-fenestrated continuous endothelium is found in the arteries, veins, and capillaries of major organs such as the brain, skin, heart and lung.(9, 22) In terms of permeability, water and solutes with <3nm radius pass in between cells, while macromolecules pass through transendothelial channels or through caveolae-mediated transcytosis.(9)

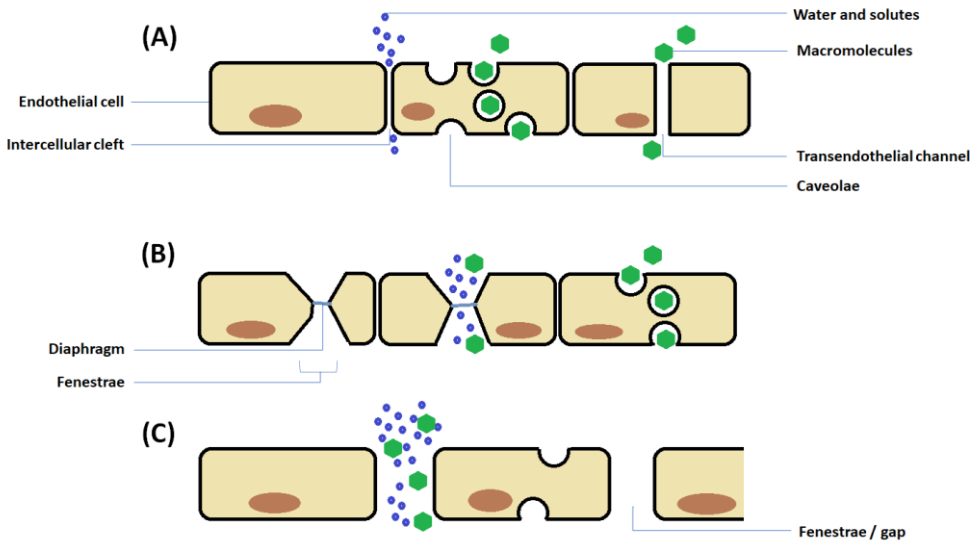

Figure 3. Heterogeneity of permeability of the endothelial layer. A) non-fenestrated continuous endothelium, where water and solutes (<3nm) pass through the intercellular cleft while macromolecules utilise transendothelial channels or caveolae-mediated transcytosis to permeate the endothelium; B) fenestrated continuous endothelium, where water and solutes pass through the fenestrae in larger quantities compared to the intercellular cleft in (A), while macromolecules are transported via transcytosis or filtered through the diaphragm of the fenestrae; C) discontinuous endothelium, where the fenestrae or intercellular gap is larger than that in (B), and macromolecules, water, and solutes are able to pass freely. Diagram adapted from Aird (2007)(9) and created on Microsoft Paint.

Fenestrated continuous endothelium is found in capillaries of exocrine and endocrine glands, the gastrointestinal mucosa and the renal glomeruli. In these locations, the transcellular pores or fenestrae (50-70nm diameter) allow transendothelial transport or filtration.(9, 22) Most fenestrae are covered with a thin diaphragm layer (5-6nm thickness) which confers size selective properties.(9, 22) Heterogeneity also exists in the density of the fenestrae, e.g. higher density in the intestinal capillaries compared with those in the pancreas. Expectedly, the fenestrations allow more water and solutes to permeate compared with non-fenestrated endothelium; however, macromolecule transcellular transport is similar between the two as the fenestral diaphragms function as molecular filters.(9)

Discontinuous or sinusoidal endothelium is characterised by larger fenestrae (100-200nm diameter) with no diaphragm and poorly formed basement membrane.(9, 22) Unlike the continuous endothelium, the discontinuous

endothelium does not have tight junctions between ECs.(22) The fenestrated gaps are large enough for whole cells, together with water, solutes and macromolecules, to pass through. They are often detected in the sinusoids (vascular structure similar to capillaries) of the liver, spleen and bone marrow.(9, 22)

d) Macrovascular and microvascular heterogeneity

It is clear from the discussion above that ECs display structural and functional heterogeneity according to tissue needs. Heterogeneity also exists between ECs of the macrovasculature and microvasculature.

For example, ECs from the microvasculature have an essential requirement for serum in their in vitro culture media which is not seen in macrovascular ECs. Serum is required for human microvascular ECs (HMECs) to maintain an intact monolayer. Without serum, the HMEC morphology was altered and more than 50% of the cells detached from their culture plate; contrastingly, human umbilical vein EC (HUVEC) growth appeared unaffected by the absence of serum.(24)

Using DNA microarrays, a study on 53 types of human ECs showed distinct gene expression profiles despite the cells being cultured in identical conditions.(8) The difference between ECs of macrovascular and microvascular origin was pronounced, which may be attributed to their location and thus, function. Macrovascular ECs preferentially expressed groups of genes involved in the production and remodelling of the extracellular matrix (ECM), in neuronal cell migration during development and maturation, as well as in lymphatic vessel proliferation and differentiation.(8) On the other hand, microvascular ECs preferentially expressed genes for basement membrane protein synthesis, cell trafficking, cytoskeleton remodelling and migration during angiogenesis, as well as lipid transport and metabolism.(8) It is possible that the macrovascular ECs have a larger role in the physical growth and maturation of the ‘circuitry’ networks (vascular, neuronal and lymphatic), whereas the microvascular ECs are mostly involved in function and homeostasis e.g. transport of molecules, pathogen docking and immune cell recruitment. Since the main site of angiogenesis is the microvasculature, many genes for the expression key

angiogenic proteins, such as angiopoietin 2 and ephrin-A1, were also specifically expressed in microvascular ECs.(8)

Other examples of macrovascular and microvascular heterogeneity in ECs include the response of cardiac ECs to oxidised low density lipoproteins in the formation of atherosclerotic lesions (macrovascular ECs were more susceptible to thrombus formation);(25) the production of prostacyclin upon serum stimulation (microvascular ECs produced the least);(26) cell-to-cell communication via coupling and connexin expression (junctional communication between the microvascular ECs was greater compared with macrovascular EC);(27) morphological changes in aged ECs (microvascular ECs showed actin cytoskeleton reorganisation not observed in macrovascular ECs).(28)

Thus, it is evident that considerable heterogeneity exists in EC structure and function across the vasculature, highlighting the need to study disease specific ECs when performing in vitro experiments.

1.1.3 Endothelial cells and angiogenesis

Angiogenesis is the development of new blood vessels from existing vessels and can be broadly divided into two types: intussusceptive or splitting angiogenesis, and sprouting angiogenesis.(29) In the former, the vessel wall reorganises itself and extends into the lumen to split the vessel in half. Intussusceptive angiogenesis occurs throughout life but is thought to have a larger role during embryonic development as during this time, rapid growth is required but at the same time resource conservation is a priority.(29) Thus, in intussusceptive angiogenesis, existing ECs in a vascularised tissue reorganise themselves to split the vessel, rather than relying on EC proliferation and migration to form or build up a new vessel.(29)

Sprouting angiogenesis is better understood as it was discovered earlier than intussusceptive angiogenesis.(29) As the name suggests, the process involves EC growth from an existing capillary by extension of a long pseudopodia (the ‘sprout’) to form a new capillary which then hollows out to form the luminal tube.(29, 30) Sprouting angiogenesis commonly occurs in areas of hypoxia

where new blood vessel formation is required to satisfy the nutrient and oxygen demands within the hypoxic tissue.(29, 30) Hence in contrast with intussusception, sprouting angiogenesis involves new vessel formation into areas without pre-existing blood vessels.

Sprouting angiogenesis is henceforth referred to as angiogenesis, as it is the more frequently studied process of the two and is implicated in cancer. The main site for angiogenesis is the microvascular network; indeed as discussed previously, many angiogenesis-related genes are expressed only in microvascular ECs. For example, these genes regulate the secretion and activation of necessary mediators, vessel plasticity to facilitate vessel remodelling during angiogenesis, and cytoskeletal reorganisation to facilitate migration.(8)

a) Mechanism of angiogenesis

Proliferatively, ECs are normally quiescent, with a low turnover rate; ranging from months in the liver and lungs, to years in the brain and muscle. When exposed to pro-angiogenic signals, e.g. during vascular damage or hypoxia, they become activated and proliferate rapidly, with a doubling time of days.(30) In the adult human, angiogenesis occurs physiologically during wound healing and the female menstrual cycle, and is a tightly controlled process.(30)

Structurally, quiescent ECs in the capillaries are surrounded by pericytes on the abluminal surface with their cytoplasmic processes wrapping around the ECs. The surface between the EC and pericyte is the common basement membrane. **Figure 4** depicts the steps in angiogenesis, broadly categorised into 4 steps: 1) tip cell selection, 2) stalk cell elongation and tip cell navigation, 3) tip cell fusion, and 4) stabilisation and resolution to quiescence.(29, 31) Upon pro-angiogenic activation in the first step, pericytes detach from ECs through the action of matrix metalloproteinases (MMPs) which degrade their common basement membrane. Intercellular spaces between the ECs become larger to allow the vessel to dilate. Vascular permeability also increases to allow the extravasation of plasma proteins, e.g. fibrinogen and fibronectin, which eventually form a provisional ECM surface for the EC to migrate to.(31)

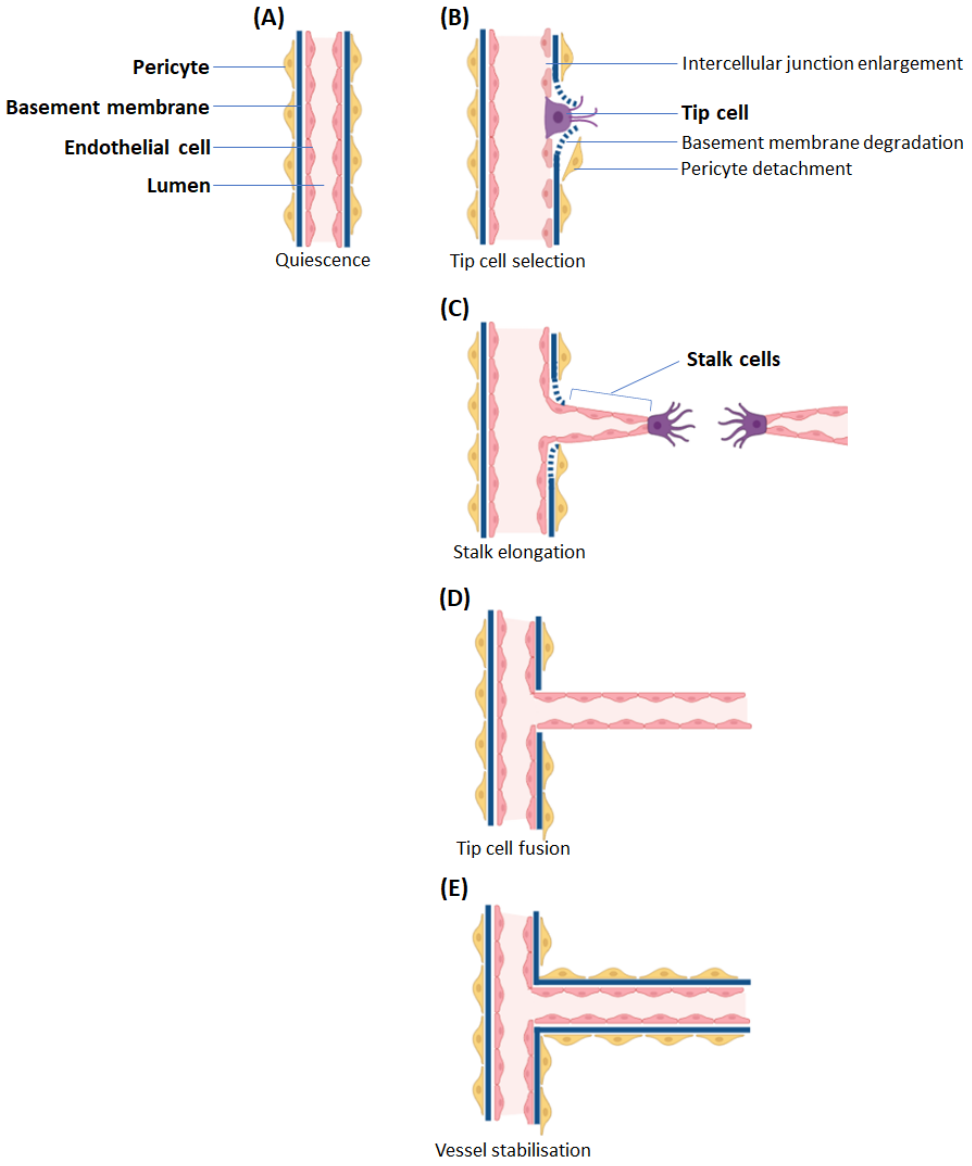

Figure 4. Steps in sprouting angiogenesis. In a quiescent vessel, the endothelial intercellular junctions are tight with pericyte coverage (A). Upon activation by pro-angiogenic factors, a tip cell is formed, which is associated with pericyte detachment, basement membrane degradation and endothelial cell junction enlargement (B). Trailing behind the tip cell are the endothelial stalk cells which elongate the stalk via proliferation (C). Opposing tip cells eventually fuse to form a new continuous lumen (D). The newly formed vessel is stabilised via pericyte recruitment, basement membrane formation and tightening of endothelial junctions (E). Diagram adapted from Carmeliet & Jain (2011)(31) and created with BioRender.com.

EC migration is led by a tip cell which possesses filopodia to navigate within the ECM. Adjacent to the tip cell are the stalk cells which proliferate to elongate the stalk. Both the tip and the stalk form the ‘sprout’ of sprouting angiogenesis. Within the stalk cells, vacuoles are formed to eventually develop the vessel lumen. Additionally, the tip cell secretes membrane type-1 MMP to degrade ECM and pave the way for the growing sprout.(29, 31, 32)

Eventually, tip cells from developing sprouts fuse together, or the tip cell fuses with an existing blood vessel to form a continuous lumen; this fusion is termed anastomosis. Stabilisation of this new capillary involves the establishment of EC intercellular junctions, pericyte recruitment and ECM deposition. The ECs then return to their quiescent state.(31, 33)

b) Mediators in angiogenesis

The key mediator of angiogenesis is VEGF, or also known as VEGF-A. Several isoforms of VEGF-A exist, which are a result of alternative splicing of the VEGFA gene.(34) Common isoforms are represented as $VEGF_{xxx}a$ and $VEGF_{xxx}b$ (xxx denotes the number of amino acids); the former was shown to be pro-angiogenic and the latter to be anti-angiogenic.(34, 35) The most studied isoform is the $VEGF_{165}a$, so much so that it is synonymous with the term VEGF.(34)

VEGF’s corresponding receptors are the VEGF receptor 2 (VEGFR2) and VEGF receptor 1 (VEGFR1), both of which have roles in angiogenesis.(31) A major regulator of VEGF is hypoxia. In a hypoxic environment, tissues upregulate the production of hypoxia-inducible factor 1 (HIF-1) which in turn increases their own VEGF production as an angiogenic stimulus.(30, 31) The filopodia of the EC tip cell possess VEGFR2 and thus are able to detect the VEGF gradient originating from hypoxic tissue areas and navigate towards it.(29, 31)

Delta-notch signalling drives sprout development and tip cell selection. The presence of VEGF guides the migration of the tip cell and stimulates proliferation in the stalk cells. VEGFR2 activation by VEGF stimulates delta-like ligand 4 (DLL4) expression in tip cells, which activates the notch receptor in the stalk cells.(29, 31) Notch activation results in VEGFR2 downregulation in the stalk cells, such that they do not acquire the migratory behaviour observed in

the tip cells. At the same time, notch signalling upregulates VEGFR1 in stalk cells, which functions as a ‘decoy’ to divert VEGF away from VEGFR2. Thus, the role of tip cells and stalk cells are a result of the ratio between VEGFR2 and VEGFR1 expression, i.e. a lower VEGFR2:VEGFR1 ratio leads to a stalk cell phenotype.(29, 31)

Accordingly, the EC exposed to the highest concentration of VEGF would be ‘selected’ as the tip cell; however, despite the high VEGF exposure, tip cell proliferation is less than that of stalk cells. Indeed, while VEGF deficiency leads to vascular defects, excess concentrations of VEGF lead to the overproduction of tip cells and disorganised vasculature; the latter is commonly observed in tumour angiogenesis where tumour cells secrete VEGF (refer to section 1.1.3d). In short, stalk cells are prevented from becoming tip cells and take on a proliferative phenotype; this allows for efficient angiogenesis by limiting the number of sprouts.(29, 31, 36) Additionally, increased vascular permeability to allow plasma protein extravasation during sprout formation is also attributed to VEGF.(31)

Tip cell navigation is not only guided by the VEGF gradient, but also by guidance molecules such as semaphorins and ephrins expressed within the surrounding tissue. Signalling downstream of semaphorin activation affects actin and microtubule dynamics to result in EC migration.(37, 38) Some subtypes of the ephrin family modulate VEGF signalling or induce cytoskeletal reorganisation in ECs to facilitate angiogenesis.(39)

To stabilise the newly formed vessel, ECs secrete platelet-derived growth factor (PDGF) as a chemoattractant for pericytes which possess the corresponding receptor, PDGF receptor-β (PDGFR-β). Pericyte coverage reinforces the vessel, prevents leakage and the pericytes secrete factors in concert with EC to maintain vascular homeostasis.(31) After the new vessel has formed, the previously hypoxic tissue is now perfused. The rise in oxygen concentration downregulates HIF-1 activity and VEGF secretion decreases accordingly, halting the angiogenic process.(30)

Aside from VEGF, other molecules are also implicated in the angiogenic process either directly or indirectly. For example, PDGF indirectly contributes to angiogenesis through the vessel stabilisation function of pericytes. Pericytes

produce VEGF and thus protect ECs from VEGF withdrawal or blockade.(30, 31) Other angiogenic-related molecules are the fibroblast growth factor (FGF) superfamily which can directly stimulate their receptors (FGFRs) on ECs or stimulate production of further angiogenic mediators from other cells.(31) These include the angiopoietin superfamily. Similar to PDGF, angiopoietins stimulate pericyte coverage of ECs and basement membrane deposition to stabilise vessels. Angiopoietins also contribute towards sprout formation during angiogenesis.(31)

Since ECs are normally quiescent, in physiological conditions anti-angiogenic mediators balance the effect of the pro-angiogenic mediators discussed earlier. Thrombospondin-1 (TSP-1) and -2 (TSP-2) are endogenously secreted by EC and are postulated to interfere with VEGF signal transduction by decreasing VEGFR2 activation.(40) Separately, TSP-1 and TSP-2 are implicated in the suppression of EC migration and cell cycle progression; mechanisms which are important in angiogenesis.(40)

Proteases such as MMPs regulate angiogenesis by cleaving and allowing the release of pro-angiogenic factors (e.g. FGF and VEGF) from the ECM.(31) The pro-angiogenic actions of MMPs are modulated by tissue inhibitor of MMP (TIMP), which is derived from the ECM and acts as a natural anti-angiogenesis factor.(31)

Endostatin is another ECM-derived factor with anti-angiogenic qualities. Endostatin is formed from the cleavage of collagen type XVIII by proteases (e.g. cathepsins and MMPs).(41) It inhibits angiogenesis by acting as a competitive inhibitor for VEGFR2 and thus disrupts the VEGF pro-angiogenic signalling.(41) It also upregulates TSP-1 expression, which also has anti-angiogenic properties.(41) In addition, endostatin binds to EC surface integrin receptors to inhibit EC migration.(41) Similar to endostatin, tumstatin is cleaved from collagen type IV in the ECM, and it has an anti-angiogenic role by stimulating EC apoptosis, as well as inhibiting EC proliferation and tube formation.(42)

c) Endothelial cell heterogeneity and angiogenesis

As discussed above, MMPs are crucial for angiogenesis. Jackson and Nguyen (1997) observed heterogeneity between human ECs obtained from the umbilical vein (HUVECs, to represent the macrovasculature) and from skin (HMECs, to

represent the microvasculature) in the secretory profiles of the different MMP subtypes and their inhibitor, TIMP.(24) For example, HUVECs secreted high levels of MMP-1, MMP-2 and TIMP-1 compared with HMECs in basal conditions. Treatment with phorbol myristate acetate, an angiogenic promoter which induces protease activity in ECs, stimulated at least ten-fold increase in the secretion of MMP-9 and TIMP-1 in HMECs compared with HUVECs.(24) These data implied that the microvascular ECs were more susceptible to pro-angiogenic stimulus compared with the macrovascular ECs, which is consistent with angiogenesis primarily occurring in capillaries.(8)

Another study compared HUVECs and human placental microvascular ECs (HPMECs), i.e. two types of ECs from the same anatomical structure.(43) Alongside VEGF and FGF-2, endocrine gland-derived VEGF (EG-VEGF, or prokineticin 1) is involved in angiogenesis in the human placenta. In vitro, VEGF and FGF-2 induced the proliferation and migration of both HUVECs and HPMECs. However, EG-VEGF induced proliferation and migration in HPMECs and inhibited these processes in HUVECs. This finding was attributed to the location of the corresponding receptors for EG-VEGF, prokineticin receptor 1 and 2 (PROKR1 and PROKR2), which were more abundantly expressed in HPMECs compared to HUVECs.(43) The study also reported differences in the signalling pathways of EC proliferation and migration. VEGF and FGF-2 activated the ERK1/2 and AKT1 signalling pathways in both HUVECs and HPMECs. With EG-VEGF treatment, the ERK1/2 pathway was activated in HPMECs and in HUVECs the AKT1 pathway was activated.(43) The expression of genes related to angiogenesis also varied between the two EC types; notably, the genes related to PROKR1 and PROKR2 were expectedly upregulated in the HPMECs. These data reinforced the functional differences of ECs in their respective cellular environments (macrovasculature versus microvasculature) despite originating from the same placental tissue.(43)

d) Tumour angiogenesis

EC proliferation and migration are two key functions required for angiogenesis and are highly regulated in physiological conditions. However, this highly controlled regulation is lost during angiogenesis in tumours. One of the hallmarks of cancer is angiogenesis.(44) As with non-malignant cells, tumour cells require nutrients and oxygen to survive which can initially be obtained by

diffusion from nearby vessels. The diffusion limit, however, is approximately 100-500 micron, beyond which the tumour requires its own vascular supply and initiates angiogenesis to achieve this.(45) This is a critical requirement for both primary tumour and metastasis development.(44, 45)

As mentioned previously, ECs are normally quiescent with a slow turnover rate. During this time, pro- and anti-angiogenic factors are in equilibrium as part of vascular homeostasis.(30, 33) In the development of cancer, the term ‘angiogenic switch’ refers to the process by which pro-angiogenic signals become dominant to give rise to new blood vessel formation and tumour progression.(33)

A possible trigger for this switch includes genetic alterations in the tumour cells themselves which leads to enhanced proliferation.(33) Oxygen consumption is increased in line with rapid proliferation of tumour cells, leading to hypoxia in the tumour tissue. As part of adapting to the hypoxic environment, genes responsible for pro-angiogenic mediators are also upregulated, leading to increased secretion of VEGF, PDGF and FGF from cancer cells.(46) The role of VEGF and PDGF in angiogenic activation (endothelial proliferation, sprouting, migration) and subsequent resolution (vessel stabilisation) were discussed previously (section 1.1.3b). Of the FGF family, specifically FGF-2, exerts pro-angiogenic activity by stimulating ECs to secrete proteases such as uPA to degrade vessel basement membrane in the first step of angiogenesis.(47) Additionally, ovarian cancer secreted FGF-2 stimulates uPA expression in an autocrine manner, as reported from an in vitro study.(48)

Another possible trigger for tumour angiogenesis is tumour-associated inflammation and the subsequent recruitment of immune cells such as macrophages, myeloid-derived suppressor cells (MDSCs) and neutrophils. The angiogenic role of macrophages is further discussed in section 1.4.3b. Tumour-associated macrophages induce EC sprouting and neovessel stabilisation through the secretion of angiogenic factors and enzymes.(33) MDSCs are immature myeloid cells recruited to tumour sites via inflammatory cytokines such as IL-1β and IL-6.(49) Their role in tumour angiogenesis is similar to macrophages, i.e. through the secretion of angiogenic factors, which not only stimulate angiogenesis but further recruit more MDSCs to the tumour site in a vicious cycle.(33) Tumour-induced STAT3 activation is thought to be

responsible for the production of angiogenic factors in immune cells; for example, in the secretion of VEGF, FGF-2, IL-8, TNF-α and hepatocyte growth factor (HGF).(50)

Neutrophils have VEGF-secretion properties in the physiological context (e.g. vascular repair), but this function becomes pathological in the context of tumorigenesis when they are recruited to the tumour site.(33) Aside from VEGF, and similar to ECs, the recruited neutrophils also secrete MMPs which are involved in the early steps of angiogenesis. Furthermore, these neutrophils lack the TIMPs, the physiological inhibitor of MMPs, which exacerbates their pro-angiogenic potential.(51)

In essence, the growing tumour initiates angiogenesis and to achieve this, the cancer cells secrete pro-angiogenic factors or stimulate other cells to do so. However, tumour angiogenesis is considered pathological angiogenesis; the angiogenic cascade is persistent, uncoordinated and is driven by the uncontrolled production of pro-angiogenic mediators, unlike physiological angiogenesis which resolves when perfusion between co-joined vessels is established.(52)

The aberrant tumour angiogenic process is evidenced by the leaky and convoluted (tortuous) architecture of the tumour vasculature.(53, 54) There is no clear distinction between the different types of vessels, e.g. arterioles and venules; blood flow direction is irregular and some vessels are blunt-ended.(53, 54) Tumour vessel diameter varies from very dilated, to the lumen being compressed.(53, 54) Compared to highly regulated physiological angiogenesis, tumour vessels have defective basement membrane (irregular thickness or even absent) and disrupted tight junctions between ECs. Vascular smooth muscle cells, which form part of the vessel wall, may be absent in tumour vessels and tumour cells may take their place.(53)

Pericytes normally provide mechanical support to the endothelium, induce tight junction formation between the ECs and limit angiogenic sprouting.(53) In tumour vessels, pericytes are detached or loosely wrapped around the tumour vessel or sometimes not present at all.(53, 54) This may result in uncontrolled sprouting leading to fragile vessels and vessel leakiness due to the lack of developed tight junctions between ECs.(53) The increased hyperpermeability of

the tumour vasculature also results in increased interstitial pressure within the tumour tissue, which impedes the delivery of anti-tumour drugs to deeper areas.(54) Detached pericytes may differentiate into cancer-associated fibroblasts and contribute towards tumour dissemination. For instance, freshly isolated pericytes from human tumours were injected into tumour xenografts in mice and these pericytes dissociated from the tumour vasculature and expressed fibroblast markers.(55).

Given the importance of tumour angiogenesis to both primary and secondary tumour growth it is perhaps not surprising that considerable effort has been expended to develop anti-tumour treatments that target the angiogenic process.(56)

1.2 Ovarian cancer

1.2.1 Epidemiology

Globally, ovarian cancer is the eighth most common cancer amongst females and coincidentally the eight most common cause of death. It is also the third most common gynaecologic cancer after cancers of the cervix and uterus.(1) The female reproductive system is shown in **Figure 5**.

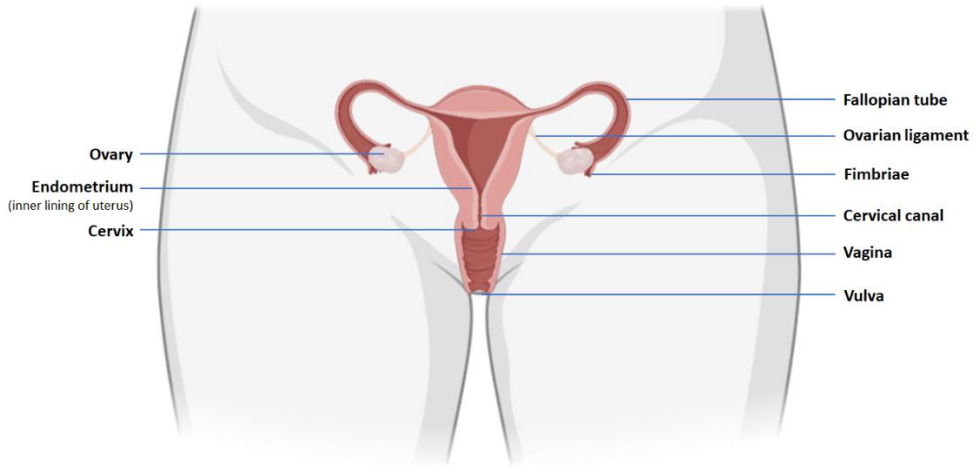

Figure 5. The female reproductive system. Diagram created with BioRender.com.

In the UK, ovarian cancer ranks sixth, both in incidence and common cause of cancer death; with the 70-79 age group having the highest incidence. In terms of cancer survival, the 5-year survival rate is less than half, at 43%, dropping further to 35% at ten years.(57) Expectedly, the survival rates are higher when the cancer is diagnosed at earlier stages: 93% at stage I, dropping to a paltry 13% when presented at stage IV (58) (staging of ovarian cancer is detailed in section 1.2.4). In earlier stages the cancer is limited to the ovaries, fallopian tubes and the pelvic area; while in later stages, the cancer has spread beyond the pelvis and to other distant sites.(59)

Unfortunately, most patients in the UK present at later stages (stages III and IV; 15,125 cases between 2013 and 2017) compared to stages I and II (10,614 cases).(58) The link between cancer stage at presentation and survival rates is not surprising; ovarian cancers detected at an early stage are mostly indolent or slow growing tumours with limited metastases and thus, have a good prognosis.(60)

A reason for the late presentation of ovarian cancer is the non-specific early symptoms which are often treated as gastrointestinal conditions or urinary tract-related disorders.(61, 62) Furthermore, in the UK, there is a lack of ovarian cancer symptom awareness, which in turn delays patients from seeking medical help.(63) The low positive predictive value of these vague symptoms, combined with the low frequency of an average general practitioner encountering a case of ovarian cancer (as infrequently as one case every 5 years) further compounds the issue.(61)

The lack of specific screening tools for ovarian cancer is another contributory factor for its late detection.(63) Other female cancers such as breast and cervical cancers have established procedures to detect pre-malignant or early abnormalities (mammogram and smear test, respectively), but none are available for ovarian cancer.

In short, the high mortality rate of ovarian cancer is linked to its late presentation; this can be attributed to the disease’s non-specific symptoms, the lack of awareness on the part of patients and heathcare providers, as well as, the unavailability of effective screening methods for early disease detection.

Alongside these factors, survival rates are also linked to the type of ovarian cancer.

1.2.2 Classification of ovarian cancer

Ovarian cancers are categorised based on where the tumour appears to originate from, mainly, from three different sites. The most common, consisting of more than 90% of all ovarian cancers, are epithelial tumours(64) (**Figure 6**). As the name suggests, they are thought to be derived from the epithelial surface of the ovaries. However, this is a misnomer as new findings suggest peri-ovarian origins, which will be elaborated later.

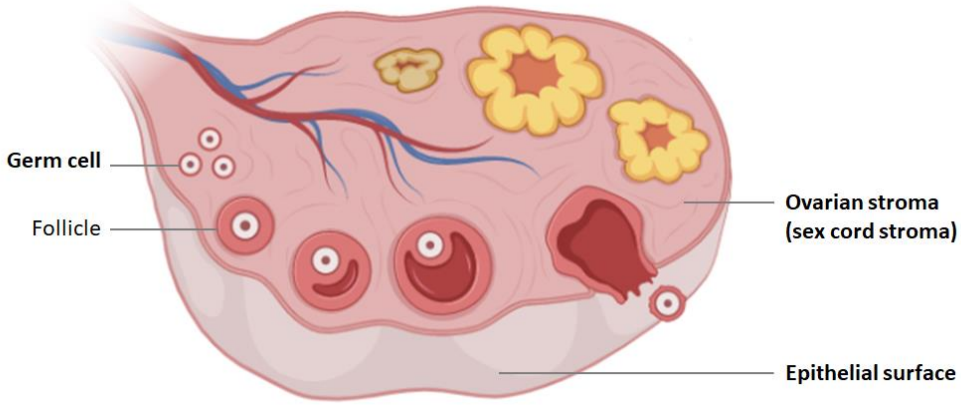

Figure 6. Cross section of an ovary. The sites which may give rise to ovarian cancers are the epithelial surface, the ovarian stroma, and the germ cells. Diagram created with BioRender.com.

The second type of ovarian cancer are germ cell tumours. They originate from the gonadal germ cells within the ovary and are less commonly encountered (3-5% of ovarian cancers). Compared to epithelial ovarian cancer (EOC), germ cell tumours tend to occur at a younger age (below 30 years of age; peak incidence between 15-19 years old). Although germ cell tumours tend to grow rapidly, and most patients present with a large abdominal mass accompanied by abdominal pain, they are highly curative. In early stage disease, cure rates can be up to

100% with chemotherapy; whereas in advanced stages, even in the presence of metastasis, cure rates reach as high as 75%.(64-67)

Sex-cord-stromal tumours are also rare (2-7% of ovarian cancers) and are derived from the ovarian stroma, the connective tissue which surrounds the ovarian follicles. These tumours are unique in that they are usually detected and managed in the early stages (due to the large abdominal mass sometimes accompanied by clinically visible hormonal changes such as menstrual dysfunction or hirsuitism), but their recurrence may occur up to 40 years from the initial diagnosis. Due to their rarity and lack of specific guidelines, the treatment for these tumours (mainly surgery and chemotherapy) is similar to that given in epithelial or germ cell tumours.(64, 65, 68, 69)

EOCs are divided to type I and type II. Histologically, type I tumours are classed as clear cell, endometrioid, mucinous or serous (low grade). Both the endometrioid and clear cell histology subtypes account for approximately 10-20% of EOCs. They tend to grow slowly and are genetically stable, thus, are usually detected in the early stages when the disease is still localised. Patients generally have good prognosis; the 5-year survival rate of both subtypes is at least 80%.(64, 70-72) The mucinous carcinoma subtype is the rarest of all EOCs, at 3% incidence. Most patients (80%) with this subtype are diagnosed early, which again leads to a good prognosis; with a 90% 5-year survival rate.(73)

Type II EOCs are aggressive and are genetically unstable. Because they grow and spread rapidly, they were often detected at an advanced stage. Type II tumours consist of serous (high grade), carcinosarcomatous, mixed morphology or undifferentiated morphology.(60, 64, 74, 75)

Approximately 70 to 80% of EOCs are high grade serous carcinomas (HGSC). Most women with HGSC (81-85%) present at advanced stages and subsequently, the ten-year mortality rate is as high as 70-75%.(60, 64) In practical terms, the HGSC is synonymous with the type II classification, as it is the most common and also the most lethal of ovarian cancers.

1.2.3 The origin of epithelial ovarian cancer

There are many theories as to how EOCs develop. The endometrium, fallopian tubes or ovarian surface epithelium have been proposed as the original tumour site and are discussed below. A representative diagram is shown in **Figure 7**.

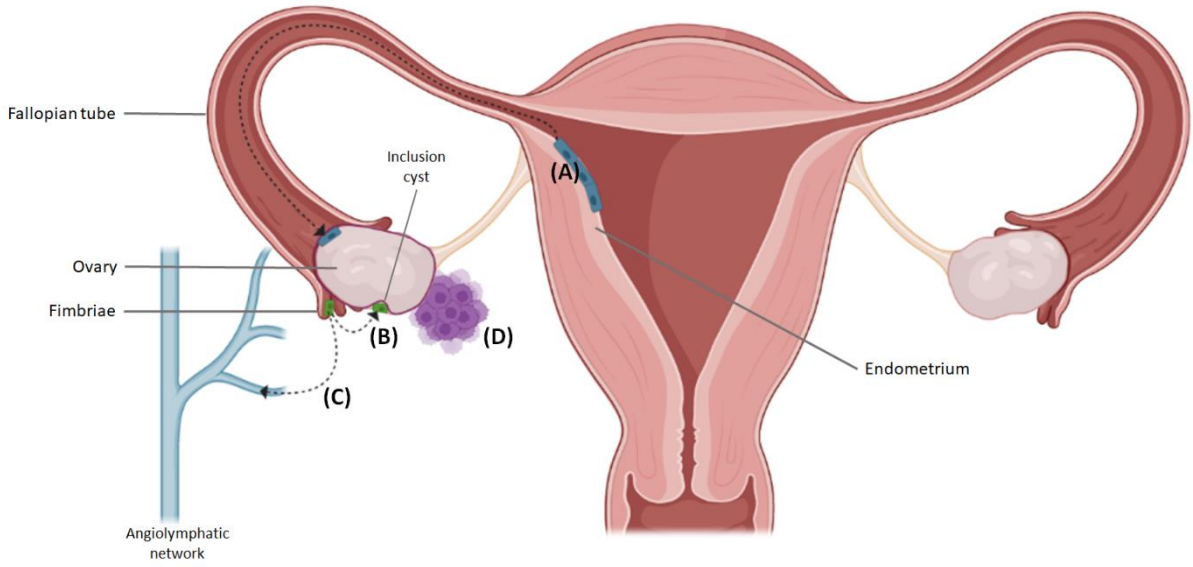

Figure 7. Ovarian cancer may originate from non-ovarian sources. Endometrial cells migrate outwards via the fallopian tube to implant onto the ovarian surface (A); tubal cells from the fimbriae implant onto the ovarian surface to form an inclusion cyst (B); they may migrate to distant sites via the angiolymphatic network (C); or tumour from nearby tissues may invade into the ovarian surface (D). Diagram created with BioRender.com.

a) The endometrium as the origin of ovarian cancer

The endometrioid and clear cell ovarian carcinomas are thought to arise from endometriotic lesions. The speculation that the endometrium could be implicated in ovarian cancer was derived from the concept of retrograde menstruation in endometriosis, where endometrial tissue ‘escapes’ via the fimbria end of the fallopian tubes, and implants outside of the uterus including onto the ovaries. The ability of the endometrial tissue to survive and invade outside of its original site was postulated to be due to intrinsic abnormalities within the cells themselves which can activate oncogenic pathways.(75-77)

This theory was supported by the finding that tubal ligation, a contraceptive procedure wherein fallopian tubes are surgically blocked, was associated with a lower risk of clear cell and endometrioid cancers, but not of the other histological types. The role of oestrogens in the development of oestrogen-responsive carcinomas, such as the clear cell and endometrioid type, has also been implicated. Tubal ligation or hysterectomies reduces oestrogen production in the ovaries, and thus, are associated with a lower risk of these cancers.(75-77) Furthermore, a gene profile study showed that endometrioid and clear cell tumours resembled the endometrium.(78)

b) The fallopian tube as the origin of ovarian cancer

The role of the fallopian tube was noted when pre-cancerous lesions were detected in women with a predisposition to ovarian cancer, e.g. those associated with inherited BRCA mutations (these mutations confer an average cumulated risk between 11% to 39% of being diagnosed with EOC by age 70). These lesions were not microscopically detected in the adjacent ovaries.(79-81) Additionally, a gene-profiling study found that the gene expression of serous tumours showed more resemblance to the fallopian tube than the epithelial surface of the ovaries.(78)

Another argument to support the role of the fallopian tube in ovarian cancer formation is the close proximity of the fimbria (ends of the fallopian tube) to the ovaries. Currently, there is evidence that up to 80% of HGSC originate from the fimbria.(82) Anatomically, the fimbria are in direct contact with the outer surface of the ovary. During ovulation, when the epithelial surface of the ovary is disrupted, epithelial cells from the tubal fimbria may be dislodged and implant onto the ovary to form an inclusion cyst. This hypothesis came from the observation that tubal epithelial cells are easily dislodged and collected via flushing of the fallopian tube, and also because of the incidence of endosalpingiosis whereby tubal-type epithelial cells are found on other pelvic and abdominal organs.(75, 83)

An interesting feature of the fimbria is its close proximity to the angiolymphatic network (which consists of both vascular and lymphatic circulation), where tubal epithelial carcinomas would have easy access to metastasise to distant sites.(75) This access to the angiolymphatic route means that distant

metastases may occur before the primary tumour grows large enough to be detected, which may contribute to late stage diagnosis.

Another theory has suggested that ovarian tumours can arise from tissues surrounding the ovaries (para-ovarian) or the fallopian tubes (para-tubal). When the tumour enlarges, it erodes into the nearby ovarian tissue, and can therefore appear as though it originated from the ovary.(75, 84)

c) The ovarian surface epithelium as the origin of ovarian cancer

Many ovarian cancers are thought to arise from the surface epithelium. A predominant theory for the development of EOC is the incessant ovulation hypothesis, first put forward in 1971.(85) Ovulation damages the ovarian surface leading to epithelial proliferation to repair the wound; when these events continually occur there is an increased chance of errors during cell replication, leading to cancer. When ovulation is suppressed and the proliferative processes are interrupted, for example in pregnancy, lactation or oral contraceptive use, the cancer risk is reduced. This is supported by the observed decreased risk of ovarian cancer in women of high parity and with oral contraceptive use.(85-87)

During ovulation, the damage to the ovarian epithelium may also initiate an inflammatory reaction. The epithelia initially proliferate to accommodate the growing follicle and then disintegrate via apoptosis to allow ovum release, which is a cycling process. Leucocyte infiltration and secretion of inflammatory cytokines are involved in this ovarian tissue remodelling and DNA repair. Thus, the repeated damage caused by inflammatory mediators may lead to the transformation of the surface epithelial cells into ovarian cancer cells.(86, 88)

Another theory for EOC development is related to excessive gonadotrophin hormone exposure, which stimulates the ovarian surface epithelium directly or via oestrogen stimulation. This over-stimulation then leads to malignant transformation, similar to that in breast cancer.(86, 89) Interestingly, levels of gonadotrophin increase with age; this is consistent with the older, often postmenopausal, age of ovarian cancer diagnosis.(86)

Aside from oestrogen and gonadotophins, androgens were also linked to ovarian cancer tumorigenesis. Androgen receptors are expressed in the different histological subtypes of EOC, especially in the serous subtype. The hypothesis that androgens are linked to ovarian cancer development coincides

with the observation that those with polycystic ovarian syndrome (a hyperandrogenic condition) have a higher risk of ovarian cancer, that the progestogen-only contraceptive (which suppresses ovarian androgen synthesis) has protective effects against ovarian cancer, and that androgen deprivation therapy offers some benefit in ovarian cancer.(90) Additionally, the growing follicles during the pre-ovulatory phase produce androgens. The proximity of these follicles to the ovarian surface epithelia mean that they are exposed to high levels of androgen, which may lead to their proliferation and subsequent transformation to a malignant state.(86)

1.2.4 Staging of ovarian cancer

The International Federation of Gynaecology and Obstetrics (FIGO) is widely accepted as an authority in matters of women's health, with their guidelines on gynaecologic cancer staging utilised globally. In 2014, a revised staging classification, which incorporated ovarian, fallopian tube and peritoneal cancer into one system, was released. Previously these three types of cancers were staged individually.(82)

The updated FIGO staging system is listed in **Table 1**, and is based on anatomical observations during surgery and also international consultation. While the three cancer types are staged under one system, the primary tumour site should be determined as much as possible, together with the histologic type when the cancer is staged.(82)

Table 1. The FIGO staging system for cancer of the ovary, fallopian tube, and peritoneum. The staging system was revised in 2014, adapted from Berek et al (2018).(82)

Stage	Description
I	**Tumour confined to ovaries or fallopian tube(s).**
IA	Tumour limited to one ovary (capsule intact) or fallopian tube; no tumour on ovarian or fallopian tube surface; no malignant cells in the ascites or peritoneal washings.
IB	Tumour limited to both ovaries (capsules intact) or fallopian tubes; no tumour on ovarian or fallopian tube surface; no malignant cells in the ascites or peritoneal washings.
IC *IC1* *IC2* *IC3*	Tumour limited to one or both ovaries or fallopian tubes, with any of the following: *Surgical spill* *Capsule ruptured before surgery or tumour on ovarian or fallopian tube surface* *Malignant cells in the ascites or peritoneal washings*
II	**Tumour involves one or both ovaries or fallopian tubes with pelvic extension (below pelvic brim) or peritoneal cancer.**
IIA	Extension and/or implants on uterus and/or fallopian tubes and/or ovaries.
IIB	Extension to other pelvic intraperitoneal tissues.
III	**Tumour involves one or both ovaries or fallopian tubes, or peritoneal cancer, with cytologically or histologically confirmed spread to the peritoneum outside the pelvis and/or metastasis to the retroperitoneal lymph nodes.**
IIIA1 *IIIA1(i)* *IIIA1(ii)*	Positive retroperitoneal lymph nodes only (cytologically or histologically proven): *Metastasis ≤ 10 mm in greatest dimension* *Metastasis > 10 mm in greatest dimension*
IIIA2	Microscopic extrapelvic (above the pelvic brim) peritoneal involvement with or without positive retroperitoneal lymph nodes.
IIIB	Macroscopic peritoneal metastasis beyond the pelvis ≤ 2 cm in greatest dimension, with or without metastasis to the retroperitoneal lymph nodes.
IIIC	Macroscopic peritoneal metastasis beyond the pelvis > 2 cm in greatest dimension, with or without metastasis to the retroperitoneal lymph nodes (includes extension of tumour to capsule of liver and spleen without parenchymal involvement of either organ)
IV	**Distant metastasis excluding peritoneal metastases**
IVA	Pleural effusion with positive cytology
IVB	Parenchymal metastases and metastases to extra-abdominal organs (including inguinal lymph nodes and lymph nodes outside of the abdominal cavity)

Ascites is the accumulation of fluid within the peritoneal cavity and is one of the hallmarks of ovarian cancer, so much so that it is specifically mentioned in the FIGO staging system. Ascitic fluid accumulation occurs when the inflow of the peritoneal fluid exceeds its outflow within the peritoneal cavity. This pathologic condition is also associated with poor prognosis, as ascites is usually present with HGSC or in advanced stages (91) and ascitic volume at diagnosis was observed to be inversely correlated with survival.(92) The mechanism for ascitic fluid build-up in ovarian cancer is thought to be due to the increased permeability of vessels within the abdomen (mostly driven by the increased VEGF expression from the growing tumour) and concomitant reduction in lymphatic drainage (blockage of lymphatic channels due to tumour invasion).(93) As a comparison, approximately 100 mL of peritoneal fluid is present in the peritoneal cavity under physiological conditions to reduce friction between tissue surfaces,(93) but in ovarian cancer ascitic volume can accumulate to more than 2 litres.(92)

1.2.5 Management of ovarian cancer

The two main modes of ovarian cancer management are surgery and chemotherapy, which are further discussed, together with targeted therapy.

a) Surgical management

As most patients present with advanced stage disease (stages III and IV), debulking or cytoreductive surgery is recommended, to reduce the volume of residual disease. Complete removal of macroscopic disease during surgery is a predictor of overall survival.(94) Debulking surgery involves the removal of the uterus, both ovaries and fallopian tubes, the omentum and other intra-abdominal tissues if obvious tumour sites are noted.(82) The location of the omentum within the abdomen and its involvement in ovarian cancer is further discussed in section 1.4.

Primary debulking surgery is performed prior to any chemotherapy, whereas interval debulking is performed after 3 to 4 cycles of chemotherapy.(82) The latter is applicable for patients who are not clinically fit (e.g. poor performance

status, significant co-morbidities) for primary debulking surgery at diagnosis, or if the primary debulking was deemed suboptimal.

Although, these initial treatments have a high response rate and initiate a period of remission, EOC has a very high rate of progression or recurrence.(95) In recurrent disease, secondary cytoreduction is currently being evaluated in clinical trials and is not standard practice.(82)

b) Chemotherapy

In advanced stage cancer, adjuvant chemotherapy follows primary debulking surgery. Current guidelines recommend 6 cycles of combination cytotoxic chemotherapy comprising of a platinum and a taxane drug. The same chemotherapy regime is given in combination with interval debulking to achieve the recommended total of 6 cycles.(82) Most chemotherapy is administered intravenously, although an intraperitoneal option is available. In early stage cancer, i.e. stage IA and IB, when prognosis is very good, chemotherapy is usually not recommended.(82)

Chemotherapy is also offered in recurrent ovarian cancer with the type of chemotherapy drug being dependent on the treatment-free interval. If the interval to recurrence is less than 6 months, the patient is considered platinum-resistant. Those with cancer progression during treatment or within 4 weeks of ceasing chemotherapy are considered as platinum-refractory. In both cases, patients are usually offered subsequent non-platinum-based chemotherapy. If the interval is more than 6 months, patients are considered platinum-sensitive and would be given platinum-based chemotherapy again.(82)

The combination of platinum and taxane as a standard for ovarian cancer chemotherapy was first established in the GOG111 study, published in 1996.(96) Up until now, ovarian cancer chemotherapy is still centred on this same platinum-taxane combination, but with amendments in the platinum or taxane drug type, drug dosages and/or duration of infusion.(95, 97) Addition of another class of chemotherapy drug to the platinum-taxane combination did not yield additional clinical benefits.(97)

c) Targeted therapy

Unlike the traditional cytotoxic chemotherapy used for most cancers, targeted therapy refers to the targeting of specific molecules involved in tumour growth. Due to their specific nature, targeted therapies are expected to be less harmful to non-cancerous cells compared with the indiscriminative conventional chemotherapy.

For instance, bevacizumab is an anti-VEGF monoclonal antibody therapy that inhibits angiogenesis by specifically targeting VEGF and thus angiogenesis, (discussed in section 1.1.3). It was originally used in the treatment of metastatic colorectal cancer, but its indication was later extended to ovarian cancer.(98) Bevacizumab is often given in combination with conventional chemotherapy in both the first-line setting and in disease recurrence.(98, 99) It may also be given on its own as treatment for malignant ascites, since increased levels of VEGF are associated with the enhanced vascular permeability which contributes to ascites.(100)

It is interesting to note that trials with bevacizumab have shown relatively little benefit to patient outcomes. For example, a gold-standard in clinical endpoint is overall survival, an aspect in which the costly addition of bevacizumab did not significantly improve in two landmark clinical trials, the GOG218 and ICON7.(101, 102) Progression-free survival, another important clinical endpoint, showed modest improvement of less than 4 months.(101-103)

Resistance to bevacizumab is also a clinical challenge.(98) In ovarian cancer cells in vitro, exposure to bevacizumab was linked to the upregulation of adaptive resistance genes resulting in HIF-1 (a pro-angiogenic stimulus described in section 1.1.3) degradation and downregulation, thus suppressing VEGF secretion from the cancer cells, leading to bevacizumab inaction.(104) In colon cancer cells resistant to bevacizumab, hypoxia tolerance was higher in cells resistant to bevacizumab compared to those which are sensitive. Contrasting to ovarian cancer cells, the HIF-VEGF-VEGFR autocrine signalling loop is upregulated as a resistance mechanism towards bevacizumab.(105)

This raises the possibly that angiogenesis induced in metastatic ovarian cancer tumours is not solely VEGF dependent and this suggestion is supported by previous work in this laboratory and other studies.(104, 106, 107) The activation

of receptors such as EphB4, or action of ligands such as IL-8 and HGF, have been put forward as potential angiogenic mediators.(104, 106, 107) The complex tumour microenvironment in the target organs for metastatic disease may therefore contribute to new tumour growth independently of VEGF and will be discussed in later sections. One of the aims of this thesis is to better understand the mechanisms underlying angiogenesis during EOC metastasis since without this knowledge, development of more successful therapies targeting angiogenesis is challenging.

Another class of drugs approved for use in ovarian cancer is the poly(ADP-ribose) polymerase (PARP) inhibitors. These drugs inhibit the action of PARP to disrupt the DNA repair pathways, which then leads to cancer cell apoptosis. PARP inhibitors are indicated for tumours with BRCA1/2 mutations, which are associated with the HGSC ovarian cancer subtype.(108) These drugs are used as maintenance therapy post-adjuvant chemotherapy, or in recurrent disease.(82) As a new class of drugs, PARP inhibitors were hailed as a new frontier in ovarian cancer treatment; however, treatment with PARP inhibitors does not improve overall survival,(109, 110) as a clinical endpoint in evaluating cancer treatment effectiveness.(111)

1.3 Ovarian cancer metastasis

The activation of invasion and metastasis is another one of the hallmarks of cancer.(44) For solid tumours to spread, cell migration from the primary site to secondary or distal sites must occur. The classical model of cancer metastasis, and the metastatic mechanisms of ovarian cancer spread are discussed in the following sections.

1.3.1 The metastatic cascade

In the classical or ‘traditional’ model of solid tumour metastasis, metastatic tumour cells journey to distal sites in 5 distinct steps, also termed the metastatic cascade: 1) infiltration of basement membrane and migration into adjacent tissue, 2) intravasation into the vascular or lymphatic circulatory system, 3) survival within the circulatory system, 4) extravasation from the circulation, 5) colonisation at the secondary tissue. With every step of the cascade, there is an

attrition in viable tumour cell numbers, hence metastasis is considered an inefficient process.(112) It has been postulated that only 0.01% of the circulating tumour cells are successful in forming distant colonies at secondary sites.(113)

In the first step, the cells need to survive being detached from the primary tumour since during detachment the usual cellular signals for growth and maintenance are disrupted. Cancer cells also require an ability to degrade ECM to journey towards the circulatory network. For the cancer cells to enter and exit the circulatory system in the second and fourth steps, they take advantage of available vasculature structures, e.g. valves within lymphatic drainage and fenestrations within the blood vessels, or they squeeze between the ECs lining the vasculature in response to a chemoattractant gradient, such as VEGF secreted by distant hypoxic tissue (previously discussed in section 1.1.3). Once in the circulation in step three, the cells must survive fluid movement-generated shear stress and immune cells. Upon arriving at a distant tissue in the final step, the cells adhere in a suitable niche which ensures their survival and subsequent growth.(112, 114, 115) A schematic of the metastatic cascade is depicted in **Figure 8**.

In the context of ovarian cancer, initial metastases are confined to the abdomen and the route of metastasis is unique compared with other types of solid tumour. Several potential mechanisms of ovarian cancer metastasis are discussed in the following subsections.

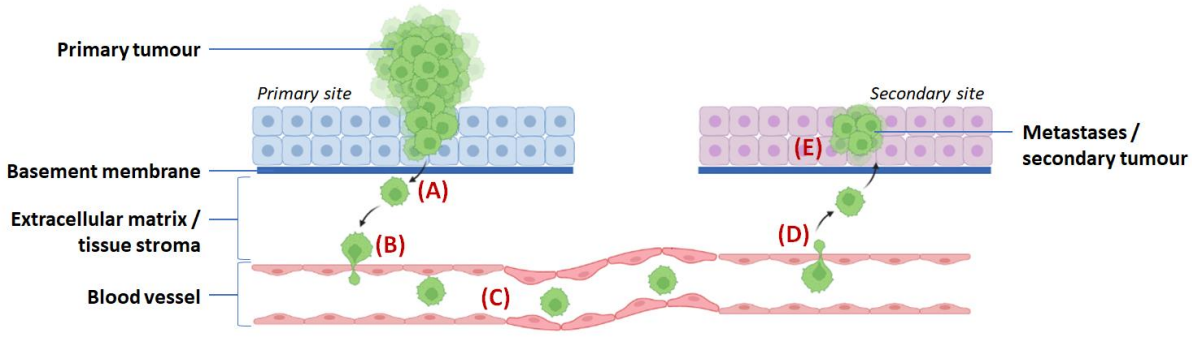

Figure 8. The metastatic cascade. Tumour cells dissociate from the primary tumour and migrate into adjacent tissue (A), before intravasating into the vascular (pictured) or lymphatic circulation (B). Tumour cells survive and travel via the circulation (C), before arresting and extravasating to the secondary site (D). Tumour cells invade into the new tissue to form metastases (E). Diagram adapted from Jiang et al (2015)(115) and created with BioRender.com.

1.3.2 Metastasis via direct extension

Patients with ovarian cancer often present with locally advanced disease with the cancer confined to the reproductive organs. Direct extension or spreading occurs when the ovarian capsule is breached and the tumour has grown beyond the boundaries of the ovary, commonly observed in the early stages, i.e. stage II onwards. This results in the cancer extending and even engulfing adjacent organs such as the ovary itself, uterus, fallopian tubes and occasionally the rectum and bladder.(116-118)

1.3.3 Metastasis via the lymphatic route

The lymphatic route in ovarian cancer metastasis is also of importance as pelvic and para-aortic nodal metastasis is frequently observed in advanced stages and/or in type II ovarian cancers; with 70-75% of stage III and IV EOC involving nodal metastasis.(119) Lymph node status is an important, but not the sole, prognostic factor in ovarian cancer. Indeed, survival rates are nearly three-fold lower in patients with lymph node metastases compared to those without, regardless of cancer histology. The risk of recurrent disease is also linked to nodal metastasis.(119, 120)

Considering the close proximity of the fallopian tube fimbria to the lymphatic network and the direction of lymphatic drainage from the ovary,(75, 121) nodal involvement is often anticipated in ovarian cancer, such that lymph node status is part of disease staging in the FIGO system (Table 1). As discussed in section 1.2.4, the formation of ascites may also be due to lymphatic invasion or obstruction by the metastatic tumour cells, which subsequently leads to decreased lymph resorption into the lymphatic circulation.(122)

1.3.4 Metastasis via the haematogenous route

The haematogenous spread of cancer is when the detached cancer cells from the primary tumour enter the blood circulation to be transported to other distant tissues, as described earlier (in section 1.3.1).(123) The haematogenous route in ovarian cancer metastasis was thought to be uncommon, since it was rarely

detected at diagnosis with the cancer mostly confined to the abdominal area.(118) Although circulating cancer cells were detected in the peripheral circulation, this did not translate to increased incidence of distant metastases. This finding was based on a study using peritoneovenous shunts, where abdominal pressure build up was alleviated using shunts to direct the ascitic fluid into the circulatory system. In this intervention, exfoliated cancer cells suspended in the ascites were continuously infused into the blood for up to 27 months; surprisingly, autopsy revealed no clinically significant metastatic lesions outside of the abdomen.(124)

However, more recent studies have showed that circulating cancer cells were associated with advanced tumour staging, poor treatment response and ultimately, poor prognosis and poor survival.(125-127) Thus, circulating cancer cells may be partly implicated in ovarian cancer metastases and there is potential in using these cells as a prognostic biomarker.(126, 127)

A recent animal study supports a haematogenous route for metastasis for ovarian cancer. In a parabiosis mouse model, where two mice were surgically joined such that they shared the same circulatory system, ovarian cancer cells injected into the ‘host’ mice resulted in metastasis in the omentum of both the conjoined mice.(128) This observation strengthened the notion of the omentum’s ‘receptivity’ towards colonisation by metastatic ovarian cancer cells. It is also possible that haematogenous spread to other parts of the body may occur when the metastatic cancer colony has been established in the omentum, which is a highly vascularised organ.(129)

1.3.5 Metastasis via the transcoelomic route

Transcoelomic metastasis refers to the dissemination of cancer cells throughout the peritoneal cavity by penetration of the peritoneal surface, which lines the abdominal and pelvic cavities.(118) The transcoelomic route of metastasis is commonly accepted as the predominant method of ovarian cancer spread. This is mostly attributed to the ease of cell movement from the primary tumour site to the peritoneal cavity due to the lack of anatomical barriers.(116, 122) The process of transcoelomic metastasis is divided into several steps: cells exfoliate

from the primary tumour and suspend in peritoneal fluid; acquire resistance to anoikis (apoptosis when detached from the ECM; explained in the following subsection); disperse within the peritoneal cavity via peritoneal fluid flow; attach onto peritoneal surfaces of organs such as the omentum (mainly composed of mesothelial cells); and finally, invade and grow at this secondary site.(116, 122, 130) As a result of this spread to the peritoneal area, malignant ascites formation is common and is a classical sign of ovarian cancer especially in the later stages.(116, 118, 122, 130)

The steps in transcoelomic metastasis are outlined in greater detail below.

a) Detachment from primary tumour and resistance to anoikis

The mechanism of cell detachment from the primary tumour may be due to the upregulation of integrin αvβ6 within the cancer cells. This upregulation is linked to the degradation ECM via the secretion of enzymes, uPA and MMPs, leading to tumour cell detachment from the ECM.(131) Aside from proteolytic roles, integrin αvβ6 also interacts with the uPA receptor, and separately, activates transforming growth factor beta (TGF-β, a factor upregulated in cancer cells); both these are associated with increased ovarian cancer cell proliferation and invasion.(132)

In addition, the cell adhesion molecule E-cadherin is downregulated in cancer cells. This membrane glycoprotein is detected in lower levels in the detached cancer cells compared with the original tumour.(116, 118) Downregulation of E-cadherin is associated with loss of cell-cell contact due to decreased anchorage and the cells undergo epithelial-mesenchymal transition (EMT). In EMT, the cells transform by losing their epithelial features and acquiring mesenchymal/stem cell phenotype such that they become less susceptible to apoptosis and are able to migrate efficiently to the new tissue site.(119) Thus, such transformation confers survival advantage on the metastatic cells. Low E-cadherin expression, from immunohistochemical studies in ovarian cancer tissue, is also linked to poor survival rates and invasive phenotype.(133, 134)

The invasiveness of the mesenchymal-like cells was evident in a xenograft mouse study whereby the cells were able to form tumours similar to the original human tumour.(135) Morphologically, mesenchymal-like cells aggregate as multicellular spheroids which have advantages in cancer compared to single

cell units – they are more resistant to chemotherapy and to anti-tumour antibodies (decreased exposure of the outer surface area and also expression of the anti-apoptotic protein, Bcl_{xL}) and are more invasive upon reaching the secondary site (better interaction with the peritoneal surface).(119, 135)

In a multifaceted manner, the EMT process is thought to be involved in resistance to anoikis, which is programmed cell death or apoptosis upon detachment from the ECM. The upregulation of several proteins are implicated. The overexpression of RAB25 is linked to chemotherapy resistance, tumour proliferation and aggressiveness, as well as, being associated with advanced disease and poor survival rates.(136) The surface protein B7-H4 is also implicated in the inhibition of anoikis, based on the observation that B7-H4 knockdown in cancer cells increased apoptosis.(137) The protein is detected in serous ovarian cancer cells but not in normal ovarian tissue, and its expression increases with higher cancer stages.(137, 138) In vitro studies on B7-H4-transfected ovarian cancer cells showed enhanced proliferation, adhesion, migration and invasion; while in vivo, tumorigenesis was observed in mouse models.(139)

b) Migration via the peritoneal fluid

The detached metastatic cells follow peritoneal fluid dynamics to be transported to the peritoneal cavity. This migration within the peritoneal fluid, or ascites, is influenced by the fluid volume: the greater the volume, the easier the dissemination within the cavity. High ascitic volume has been linked to worse survival rates.(91, 92) The ascitic fluid itself contains factors and other cells which promote tumour growth and invasion, e.g. growth factors, proteinases, CXC chemokine ligand 12 (CXCL12), cancer-associated fibroblasts, platelets.(91, 117) Thus, the ascites is considered to be a self-sustaining tumour microenvironment in its own right.

Due to the passive flow of the ascitic fluid, the shear stress generated by this fluid movement is thought to be negligible, as opposed to the high shear levels generated within blood vessels. However, a study showed that even the low shear stress (less than 0.1 dyne/cm^2) of the ascitic fluid promotes EMT and cancer cell ‘stemness,’ as observed by the increase in stem cell markers within the spheroid cells.(140) Example of stem cell markers include Oct-4 (regulates

tumorigenesis and metastasis), c-Kit (regulates tumorigenesis and increases chemoresistance) and P-gp (also involved in chemoresistance).(140) Considering their tumour-promoting characteristics, advanced cancer stages are often accompanied by these upregulated stem cell markers.(140) Additionally, an increase in ascitic volume with a corresponding decrease in shear stress (e.g. from 0.02 to 0.002 dyne/cm^2), further induces the expression of stem cell markers.(140)

c) Adhesion and invasion within the peritoneal cavity

The first step of secondary metastasis formation by cancer cells in the ascitic fluid is their adhesion to the mesothelial cells which line the surface of the omentum and the peritoneum. Upon reaching the secondary site, the cells undergo the reverse of EMT, i.e. the mesenchymal-epithelial transition (MET). E-cadherin expression is upregulated to facilitate attachment to the new site.(119) Both the EMT and MET events demonstrate the dynamics of E-cadherin expression for cancer cell detachment and reattachment. The transition to the epithelial phenotype also allows the cells to respond better to growth factors secreted from nearby cells,(117) thus advancing the metastatic colonisation process.

Several mechanisms that drive adhesion between the cancer cells and mesothelial cells have been put forward. ECM proteins such as collagen, laminin and fibronectin were detected on the outer surface of mesothelial cells. Consequently, the cancer cells may gravitate and bind to these proteins via integrins present on cancer cells. Some proposed interactions include the binding of α5β1-integrin with fibronectin, α6β1-integrin with laminin and α2β1-integrin with collagen type IV, although there is evidence that the integrins may interact with more than one type of ECM protein.(141-143) An in vitro study showed that the inhibition of the β1 subunit, which is common to the integrins aforementioned, abolished ovarian cancer cell migration towards the ECM proteins.(143)

Aside from integrins, the interaction between the CD44 receptor on the cancer cells and hyaluronan on the mesothelial cells may be partly implicated in the metastatic adhesion process.(144) A recent study suggested that the role of CD44 in metastasis was not merely binding between receptor and ligand or

surface-level adhesion; but rather, the cancer cells transport exosomes of CD44 to the mesothelial cells. The mesothelial cells internalise these exosomes, transform into a mesenchymal phenotype, and secrete MMP to enzymatically clear the mesothelial layer and thus lead to cancer cell invasion.(145)

After the initial adhesion to the peritoneal surface, the cancer cells then invade through the mesothelial cell layer. This could occur by induction of mesothelial cell apoptosis through the binding of the CD95 receptor on mesothelial cells to the Fas ligand secreted by the cancer cells, as observed in an in vitro study using a colon cancer cell line and human peritoneal mesothelial cells.(146) This ligand-receptor binding interaction also induces tumour growth.(147) When mesothelial cells are cleared, the metastatic tumour cells have access to, and can thus invade, deeper layers.

Another molecule of interest is lysophosphatidic acid, which is secreted from ovarian cancer cells and mesothelial cells.(148) and is found in malignant ascites, but is not detected in non-malignant ovarian cells or in the peritoneal fluid in health.(149) Lysophosphatidic acid activation of the Ras/MEK kinase 1 pathway within the ovarian cancer cells is related to cell migration.(119) Lysophosphatidic acid also induces the secretion of proteases, uPA and MMPs, by the ovarian cancer cells which degrade ECM leading to enhanced tumour invasion, and also EMT.(148, 150)

The mesothelial cells themselves, being the first point of contact for the metastatic cancer cells, are thought to affect the behaviour of the attached cancer cells. For example, the mesothelial cells stimulate changes in the gene expression profiles of the cancer cells, leading to increased invasiveness and proliferation – qualities which promote the establishment of cancer at the new site. An example is the downregulation of a tumour suppressor micro RNA, miR-193b, upon ovarian cancer cell interaction with peritoneal mesothelial cells in vitro and also with human omental tissue ex vivo.(151) The observed increased invasion of the ovarian cancer cells was attributed to the induction of uPA when miR-193b was downregulated.(151)

Conversely, the adhesion of the cancer cells induces inflammation of the mesothelial cells, which in turn increases their cytokine secretion (e.g. interleukin-1,-6,-8), and subsequently VEGF secretion leading to tumour

angiogenesis and the formation of ascites.(119) This interplay of events at the microenvironment level renders the peritoneal cavity suitable for cancer invasion and growth.

Within the peritoneal cavity and lined by mesothelial cells, both the omentum and the peritoneum are the most common sites for initial metastasis in EOC.(117, 152) Indeed, debulking surgery usually involves omentectomy to treat or prevent secondary spread.(153) Although listed as two separate entities, developmentally, the omentum is derived from the peritoneum (via a peritoneal fold), and the mesothelial cell layer is the common outer surface of these structures. Considering the structure and myriad functions of the omentum, it is considered as an organ in its own right as opposed to the peritoneum, which is a membrane lining the entire peritoneal cavity.(154) Thus, moving forward, cancer metastasis specific to the omentum is further discussed.

1.4 The omentum

The preference of metastatic ovarian cancer cells for the omentum is not a chance event and is termed ‘organ tropism.’ This concept is also referred to as the ‘seed and soil’ theory, which was proposed by a surgeon, Stephen Paget, in his work on breast cancer using post-mortem data.(155) In this theory, the metastatic cancer cells are considered the ’seeds’ which require a suitable microenvironment (the ‘soil’) for metastatic colonisation to occur. The focus of this theory is the role of the microenvironment in determining the success of the ‘seedlings,’ i.e. the metastatic tumour cells, and not so much on the location of the primary tumour.(112, 155)

1.4.1 Structure of the omentum

The omentum is a large adipose tissue organ in the peritoneal cavity, formed by folds of the peritoneum to give rise to the greater omentum and the lesser omentum. The latter is smaller in size and is connected to the lesser curvature of the stomach, the duodenum and the liver. Structurally, the lesser omentum

supports the blood and lymph circulation between the liver and the stomach.(156)

The greater omentum forms the majority of the organ and is connected to the greater curvature of the stomach and the transverse colon. It appears as a 'hanging' sheet from the stomach which extends to the large colon and intestines, similar to a hanging apron (**Figure 9**).(156) The bulk of research on the omentum's diverse physiological functions, as well as its role in ovarian cancer metastasis is concentrated on the greater omentum, which is henceforth simply referred to as the omentum.

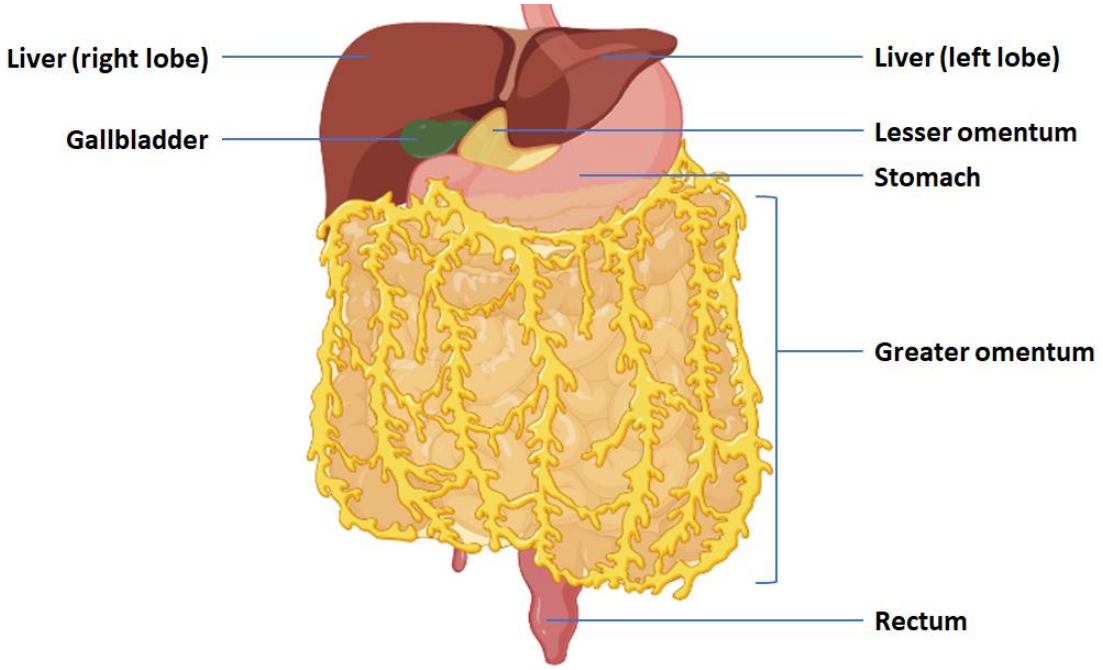

Figure 9. Location of the omentum within the abdomen. The lesser omentum is connected to the lesser curvature of the stomach, the duodenum and the liver. The greater omentum is connected to the greater curvature of the stomach and the transverse colon and extends over the small intestine and large colon. Diagram created with BioRender.com.

The omentum may weigh up to 2kg, and has a large surface area, up to 1500cm^2. The outer surface of the omentum consists of mesothelial cells, which envelope the visceral adipose tissue underneath. The omentum is mostly composed of adipocytes and due to its size, it is a major storage site for abdominal fat.(157, 158) Grossly, the omentum appears yellow in colour due to

the high lipid content of the adipocytes, and was initially thought of as an inert organ solely for fat storage or energy reserve.(159) Over time, especially after the era of microscopy when its intricate structures were visualised, the omentum's role in peritoneal immunity was duly recognised.(160)

The omentum is highly vascularised, with capillary beds running underneath the outer mesothelial cell layers. The vascular network is dotted with knot-like structures similar to renal glomeruli which are termed the omental glomeruli. Leucocytes aggregate to these glomeruli to form lymphoid structure-like areas termed as 'milky spots,' so named due to the white-coloured appearance of the leucocytes embedded in the yellow-coloured background of adipocytes.(157, 158)

The various functions of the omentum, in tissue repair and in immune regulation, are explored in subsequent sections, as well as, how the structure and composition of the omentum contributes to the 'seed and soil' theory of ovarian cancer metastasis.

1.4.2 The omentum in tissue regeneration and mechanical defence

The omentum plays a major role in the repair of peritoneal injury and in immune defence. In response to inflammation (due to injury, contamination or infection), in rat models, the omentum switches to an activated state and the omental volume increases drastically, more than 20-fold increase.(161, 162) For perspective, adipocytes usually make up 95% of the omentum in the native state but only 30% in the activated state.(161) The increase in volume is a result of new tissue production, consisting of mesenchymal stromal cells, as well as blood and lymphatic vessels.(161, 162) The 'milky spot' areas are also expanded in the activated omentum.(162)

In tissue injury and inflammation, the omentum functions as a 'bandage.' In rat studies, the activated omentum mechanically adhered to and wrapped around foreign particles such as polydextran beads or a polyvinyl chloride rod.(161, 162) The expanded mesenchymal stromal cell population in the activated omentum may contribute to this regenerative process since they express stem cell markers and pluripotent embryonic markers (e.g. SDF-1α, Oct-4,

Nanog).(161, 162) Increased density of blood and lymphatic vessels accompanied the volume expansion of the omentum, possibly due to the increased VEGF detected in the media cultured with the omental samples.(161, 162) These findings thus support the role of the omentum in tissue repair.

Infection or contamination within the peritoneal cavity initiates a similar early sequence of events. In a rat study, the activated omentum adhered to the affected site to seal it off and thus contain spread to the rest of the peritoneal cavity. Fibrin secreted by the omentum adheres to the affected area and then progressively, new blood vessels, fibroblasts and collagen are laid down to form dense adhesions. This is achieved through the secretion of similar factors, e.g. VEGF to increase blood flow to the affected area.(156, 163)

Concurrently at the site of inflammation, any pathogens or necrotic tissues are absorbed by the omentum and degraded. This is achieved by the activation of macrophages located in the milky spots, which phagocytose the offending particles.(156)

1.4.3 The omentum in immune regulation

Omental ‘milky spots,’ as mentioned above, play a key role in peritoneal immune defence. Structurally, they lie in close proximity to the omental glomeruli, and possess fenestrated or discontinuous capillaries. Above this vascular network, the mesothelial cells have intercellular pores between them (stomata) and an absent basal membrane underneath them.(157) A schematic of the omental milky spot is depicted in **Figure 10**.

When peritoneal inflammation occurs, the milky spots increase in size and number with the increased recruitment of lymphocytes and macrophages. This observation supports the hypothesis that the omentum functions as a secondary lymphoid structure and thus, has immunological roles.(164, 165) Fluid from the peritoneal cavity, together with any foreign particulates, is drained via the omental lymphatics and ‘filtered’ into the milky spots.(156) The population of immune cells in the milky spots then detect and inactivate these pathogens. The fenestrated capillaries facilitate the transmigration of immune cells.(156, 158, 166)

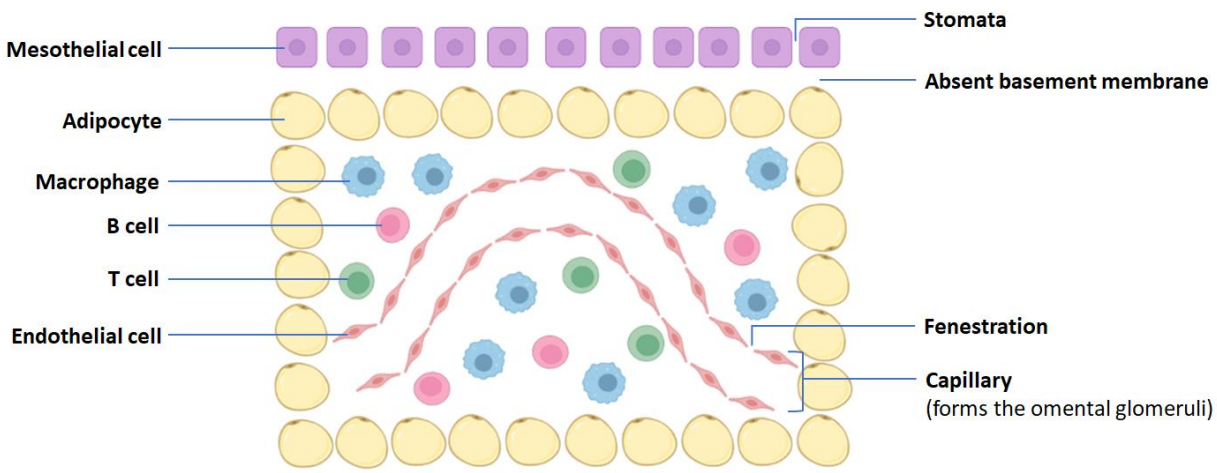

Figure 10. Schematic of the omental milky spot. The outermost layer of the omentum consists of mesothelial cells. Underneath this layer is the omental stroma consisting mostly of adipocytes, with capillary beds termed the omental glomeruli. Resident immune cells such as B cells, T cells and macrophages are present in the surroundings of the glomeruli. The structure of the milky spot (mesothelial cell stomata, absent basement membrane, fenestrated capillary wall), and the presence of immune cells allows for peritoneal immune surveillance and induction of immune response. Diagram adapted from Di Nicola (2019)(156) and created with BioRender.com.

Many types of immune cells are found in the environs of the milky spots, although the majority are B cells. The chemokine CXCL13, constitutively expressed in the omentum and also in peritoneal macrophages, is thought to be the main attractant for B cells to home towards the milky spots.(166) The B1 subclass of B cells are considered permanent residents within the omentum and the peritoneal cavity, but the B2 subclass circulates between the omentum and other lymphoid tissues.(158, 166) Additionally, the milky spots themselves are a main development site of a unique subtype of B cells, the CD5+ B cell, which mature in the milky spots independently from the bone marrow, where conventional B cells are developed.(156) It is postulated that the contribution of B cells to local immunity is to stimulate natural antibody production in response to intercepted foreign pathogens.(166)

T cells have also been detected within the omentum and may be involved in the inactivation of foreign pathogens.(158) Memory T cells generated from other sites, e.g. from the gastrointestinal and respiratory systems, have also been shown to home to the omentum,(165) strengthening the role of the omentum as part of the larger lymphoid system. Additionally, inhibitor and knockout studies

in mice indicated that the adipose tissue-associated T cells may have roles in regulating metabolism and inflammation, e.g. relating to weight gain and insulin resistance.(158)

As part of peritoneal defence, macrophages play an important role. Aside from their role in secreting CXCL13 to attract B cells,(166) they also engulf and lyse invading pathogens and execute antigen-presenting functions to stimulate the adaptive immune response.(167) Macrophages are resident within the omentum and peritoneal cavity, with macrophage colony-stimulating factor being produced within the milky spots to stimulate macrophage proliferation.(168) Inflammation within the peritoneal cavity rapidly stimulates the influx of macrophages and other cells to the omentum resulting in an increase in size and number of the milky spots.(158, 169, 170) This is not limited to cells already present in the peritoneal cavity but is also from the circulatory system, e.g. neutrophils, which jointly phagocytose and overcome invading pathogens.(171)

Despite its peritoneal defence capability, the omentum is still susceptible to tumour metastases. It was observed that in early stage ovarian cancer patients, microscopic metastases were not detected in the omental adipose tissue but only limited to the milky spots.(172) It is possible that the features designed for immune regulation, especially the milky spots, inadvertently render the omentum to become the ‘soil’ for the metastatic tumour ‘seeds.’ This is further elaborated in terms of the peritoneal fluid flow, the characteristic of the macrophages, as well as the properties of the mesothelial cells.

a) Peritoneal fluid flow through the milky spots facilitates tumour metastasis

Rat studies have shown that metastatic colon cancer cells suspended in the peritoneal fluid, which also have the propensity to metastasise to the omentum, are passively flowed through the omentum and inevitably encounter the milky spots first.(169, 173) In the first 8 to 72 hours, cancer cell numbers in the peritoneal fluid decreased which led to conclusion that the invading cancer cells were successfully eliminated by the macrophages already concentrated at the milky spots.(169, 173) However, parts of the omentum outside of the milky spots showed increased tumour proliferation.(170, 173) In a pseudo-positive

feedback loop, new milky spots are formed on parts of the omentum with adhered tumour clusters as a result of macrophage influx to the infiltrated tumour area, part of the immunological response to tumour cell invasion.(169, 170)

Eventually, after as few as 7 days, the milky spots were overrun with tumour cells and were indiscernible from other parts of the omentum.(169, 170) After overwhelming the omentum's defence mechanism, omental metastases had formed.(170) The enlargement of the metastases can then cause lymphatic obstruction, resulting in the accumulation of peritoneal fluid or ascites.(174)

b) Macrophage characteristics facilitate tumour metastasis

Like a double-edged sword, it has been reported that the omental macrophages may also enhance metastasis as well as providing peritoneal defence. Studies using murine and human ovarian cancer cell lines showed that omental colonisation was independent of other immune cells such as B- and T-cells.(175) However, in a mouse study, macrophage depletion prior to the intraperitoneal injection of ovarian tumour cells was associated with an 11-fold decrease in omental metastatic colonisation when compared to no macrophage depletion.(172) This observation was not replicated when the macrophage depletion procedure was performed after the introduction of tumour cells intraperitoneally, suggesting a role for macrophages in the early metastatic process.(172)

It was postulated that the resident omental macrophages secrete CCL23, a chemokine ligand which binds to the CCR1 receptor found on ovarian tumour cells, thus promoting tumour colonisation in the milky spots.(172) CCL23 was found to increase the proliferation of other cells that express CCR1, such as ECs.(176) Thus, the CCL23-CCR1 interaction may also be implicated in tumour angiogenesis.

The 'fluidness' or plasticity of macrophages is an inherent characteristic of their response to their environment. Macrophages can differentiate to different functional forms, with the two extreme phenotypes termed the M1 macrophage (inhibit/kill type) or the M2 macrophage (heal/growth type). The purpose of this M1/M2 balance is for tissue homeostasis and to provide primary host defense.(167)

Tumour-associated macrophages were observed to skew towards the M2 phenotype, possibly due to interactions with the tumour itself.(177) The M2 phenotype macrophages have immunosuppression functions (reduced antigen-presenting abilities, as well as secreting immune suppressor factors and tumour growth factors).(177, 178) Additionally, they have pro-angiogenic functions (migration to hypoxic areas to stimulate angiogenesis, which includes ECM degradation and EC proliferation) and also contribute towards stromal tissue transformation (mesenchymal cells differentiate into cancer-associated fibroblasts, as well as ECM and basement membrane degradation to allow tumour growth).(178) These functions allow the metastatic tumour cells to avoid immunological destruction and gain a stronger foothold in the invaded tissue.

c) Mesothelial cells at the milky spots facilitate tumour metastasis

The role of the mesothelial cells in the milky spot areas is also relevant to the omental metastasis event. Structurally, the lack of basement membrane underneath the mesothelial cells means that the connective tissues of the omental stroma are in direct contact with these surface mesothelial cells.(179) Additionally, through the gaps in between the mesothelial cells, there is direct communication between the underlying connective tissue and the peritoneal cavity itself.(179) Thus, tumour cells suspended in peritoneal fluid can easily access, and later invade, the omental stroma.

Furthermore, the mesothelial cells at the milky spot express adhesion molecules such as ICAM-1 and VCAM-1. As part of the peritoneal defence mechanism, the expression of these adhesion molecules is upregulated in peritoneal inflammation, in a bid to increase macrophage numbers at the milky spots, since macrophages express receptors which bind to these adhesion molecules.(179)

However, this feature of mesothelial cells may be their Achilles heel, as tumour cells can also express ICAM-1. In some cancers, e.g. breast and gastric cancers, ICAM-1 expression is linked to tumour aggressiveness and metastatic potential.(180, 181) In breast cancer, the homophilic interaction between ICAM-1 molecules of the tumour cells and that in the bone marrow facilitates metastasis.(182) It is possible then that ovarian cancer metastasis may occur in

a similar manner, since the expression of ICAM-1 in HGSC is linked to poor prognosis.(183)

1.5 Adipocytes in tumour metastasis to the omentum

Due to the high adipose tissue content, adipocytes are the most abundant type of cells within the omentum. The omentum's role as a fat depot was easily presumed due to the adipocyte's large cellular lipid droplet, or fat reservoir, which takes up most of the cell volume. However, recent findings revealed the endocrine function of adipocytes, in that they secrete a range of factors, e.g. cytokines, hormones, growth factors; these factors are collectively termed adipokines.(159, 184) Adipokines regulate a range of normal physiological processes, e.g. insulin sensitivity, blood flow, energy metabolism.(185)

Given the propensity of EOC to metastasise to the omentum it is also possible that the high density of adipocytes in the omentum inadvertently creates a microenvironment that supports cancer progression. Some of the proposed mechanisms include low grade inflammation within the adipose tissue environment in obesity, promotion of cancer cell EMT, phenotypic alteration of adipocytes to fibroblasts, supplying fatty acids as an energy source, as well as roles in cancer anti-apoptosis, chemoresistance and angiogenesis.(159, 186)

1.5.1 Possible link between obesity and cancer

The role of adipocytes or the adipose tissue in cancer progression has been highlighted by the association between obesity and increased risk of several female cancers (e.g. endometrium, breast) and gastrointestinal cancers (e.g. oesophagus, gallbladder, pancreas, liver).(184) Poor treatment outcomes and poor survival are also associated with obesity, which may also be explained by co-morbidities arising from obesity, such as cardiovascular disease, renal disease, or metabolic syndrome.(187)

The evidence to support an association between ovarian cancer incidence and obesity is inconsistent.(188) However, obesity is associated with poorer ovarian

cancer survival,(189, 190) with a 5-unit increment in body mass index (BMI) conferring a 10% increment in mortality.(189) It is possible that the larger omental mass associated with obesity may partly contribute to enhanced metastatic growth and thus poorer outcomes in these individuals. Compared to individuals with normal body weight, being obese also increases the risk of postoperative complications (e.g. bleeding, infection, venous blood clots) and is linked to poorer survival rates in ovarian cancer;(190) this is pertinent as surgical management is usually the primary treatment for ovarian cancers (discussed in section 1.2.5a).

Despite this, the mechanisms underlying the link between obesity and cancer are not well understood and it is likely that the highly complex adipose tissue microenvironment supports tumour growth in both individuals with healthy and overweight BMI.

1.5.2 Adipocytes in transcoelomic metastasis

When ovarian cancer cells detach from the primary tumour they undergo EMT to form spheroids, a phenotype which is more resistant towards anoikis, and allowing the metastatic cells to survive before reaching the omentum. In EMT, the cell adhesion protein E-cadherin is downregulated, a process driven by growth factors and cytokines within the tumour microenvironment.(191) A possible source of these factors are the omental adipocytes.(192, 193)

IL-8 is a cytokine associated with the reduction of E-cadherin expression in ovarian cancer cells,(194) and higher levels of IL-8 have been detected in the serum and ascitic fluid of patients with ovarian cancer compared with those with non-ovarian cancer.(195, 196) Similarly, IL-6 was detected in ascites of ovarian cancer patients (195) and was secreted by adipocytes.(193) E-cadherin downregulation is also induced by IL-6 via the activation of the intracellular STAT3 pathway.(197) Both IL-8 and IL-6 were notably higher in malignant ascites compared with non-malignant ascites, which supports their potential role as ovarian cancer markers.(195)

IL-11 is another cytokine secreted by adipocytes, with a corresponding receptor expressed on the ovarian cancer cells. As IL-11 belongs to the IL-6 family, its

action in downregulating E-cadherin is similar to that of IL-6, i.e. via the activation of STAT3.(198, 199) Aside from the STAT3 pathway, the ERK pathway has also been implicated in the regulation of E-cadherin during EMT. This was most likely achieved by IL-33, expressed in ovarian cancer as well as adipocytes.(200, 201)

Insulin-like growth factor 1 (IGF-1) secretion by adipocytes is another possible contributor to the resistance of cancer cells to anoikis, through the activation of the Src/Akt/ERK pathway.(202, 203) Hence, the activation of STAT3 and ERK pathways, by driving the EMT process, enhances metastatic cell survival.

As previously mentioned, ovarian cancer is often associated with build-up of ascites and this can play an important role in transporting the metastasising cells to the omentum. The development of malignant ascites is thought to be linked to increased VEGF levels, for example, VEGF levels were higher in malignant ascites than in ascites associated with cirrhosis and tuberculosis.(204) While VEGF is commonly secreted by ovarian cancer cells, adipocytes themselves also secrete VEGF (205, 206) and stimulate ovarian cancer cells to do so by activating the STAT3 pathway via IL-6 secretion.(207)

The omental adhesion of the ascites-suspended metastatic cancer cells is not a random event. Adipocytes, being a major constituent of the omentum, may attract these cells to the omentum, possibly through the secretion of attractant adipokines. In vitro studies showed the migration of ovarian cancer cells toward adipocytes and also adipocyte-conditioned media.(193) Using antibody-based inhibitors, the adipokines IL-6 and IL-8 were shown to be responsible for these observations.(193)

The mesothelial cells on the outer surface of the omentum are the first point of contact for metastatic cancer cell adhesion. A proposed mechanism of adhesion is the interaction between the hyaluronan on the mesothelial cells and the CD44 receptor on the ovarian cancer cells (in section 1.3.5c).(144) Adipocytes may contribute to this through the secretion of TNF-α into the tumour microenvironment which increases CD44 expression, thus facilitating cancer cell adhesion to the mesothelial cells.(208, 209) Indeed in ovarian cancer, increased expression of CD44 is associated with chemoresistance, formation of spheroids in the EMT process, tumour growth and recurrence;(210) metastatic-

related events linked to the STAT3 pathway.(211) Additionally, CD44 has been investigated as a prognostic marker for ovarian cancer as its expression on tumour cells correlates with a worse clinical outcome and poorer 5-year survival rate.(212)

Another adipokine which may contribute to CD44 upregulation is HGF, also secreted by adipocytes.(213) HGF was associated with CD44 signalling in breast, pancreatic and colorectal cancers;(214) thus, it is possible that HGF may have a role in ovarian cancer, which requires further study.

1.5.3 Adipocytes as an energy source for cancer cells

Due to the large surface area of the omentum, the adipose tissue within it is a major energy storage depot.(157, 158) Adipocytes possess intracellular lipid droplets containing triglycerides which can be broken down to form free fatty acids as an energy source. Interestingly, to fuel themselves, ovarian cancer cells can induce lipolysis in the adipocytes and the fatty acids released can then be taken up by the tumour cells.(193) This was observed at the adipocyte-tumour cell interface in omental metastasis, where tumour cells in contact with adipocytes contained more intracellular lipids compared with those without adipocyte interaction; similar observations were noted at the interface between breast and colon cancers with adipocytes.(193) Additionally, co-culture of human breast cancer cells and murine adipocytes resulted in adipocytes with an altered phenotype, seen as reduced number and size of lipid droplet.(215) These phenotypically-altered adipocytes are referred to as cancer-associated adipocytes.(215) Interestingly, culturing ovarian cancer cells with adipocytes from the omentum or the peritoneum resulted in more lipid accumulation in the cancer cells, compared to when co-culturing with subcutaneous or mesenteric adipocytes;(193) suggesting a specific affinity of ovarian cancer towards the omentum or peritoneum.

The uptake of fatty acids into cancer cells fuels metastatic tumour growth. Co-culturing adipocytes and ovarian cancer cell lines induced cancer cell proliferation.(193) In mice, subcutaneous injection of ovarian cancer cells together with omental adipocytes resulted in tumours three-fold larger than if

ovarian cancer cells were injected alone.(193) Knockout mice and inhibitor studies pinpointed the fatty acid–binding protein 4 (FABP4) as a main mediator in this cancer cell-adipocyte interaction. FABP4, which transports fatty acids, was upregulated in the ovarian cancer cells only in the presence of omental adipocytes.(193) This finding was substantiated in a study on human breast cancer cells where treatment with exogenous FABP4 increased the expression of fatty acid transport proteins.(216)

The transfer of fatty acids from adipocytes to the cancer cells suggests changes in lipid metabolism. Activation of lipolysis is normally induced by stimulation of the β-adrenergic receptor, leading to activation of lipolytic enzymes (hormone-sensitive lipase, HSL, and perilipin A) and triglyceride breakdown, with a resulting increase in free fatty acids.(193) In an in vitro study, in the presence of ovarian cancer cells these lipolytic enzymes were activated in human omental adipocytes (observed as phosphorylated HSL and increased mRNA levels of perilipin A), leading to the increased fatty acid release from the adipocytes. In addition, β-adrenergic receptor inhibition partially reversed HSL phosphorylation.(193) These observations inferred that adipocyte lipid metabolism is altered by the presence of the cancer cells. Interestingly, in prostate cancer cells, altered lipid metabolism resulted in lipogenesis where excess lipids were stored intracellularly as lipid droplets.(217)

Metabolism within the ovarian cancer cells is also affected by this interaction with adipocytes. Co-culture of ovarian cancer cells and adipocytes resulted in the activation of AMP-activated protein kinase (AMPK) in the former. This leads to the deactivation of enzymes involved in lipogenesis and activation of catabolic processes such as fatty acid β-oxidation.(193, 218) This finding was supported by the increased mRNA levels of carnitine palmitoyltransferase-1, an enzyme downstream of this AMPK pathway, whose function is to regulate mitochondrial transfer of fatty acids for subsequent β-oxidation.(193)

1.5.4 Phenotypic transition of adipocytes to fibroblasts

As mentioned previously, the interaction between adipocytes and cancer cells can result in phenotypically-altered adipocytes, known as cancer-associated

adipocytes. This transition has been primarily studied in breast cancer where these host adipocytes acquire fibroblast-like features and are termed adipocyte-derived fibroblasts.(219) These cells are thought to contribute towards the pool of cancer-associated fibroblasts,(219) which are also postulated to originate from resident fibroblasts, progenitor cells from the bone marrow or even ECs through endothelial-mesenchymal transition.(220)

Dissimilar to fibroblasts which are normally quiescent, cancer-associated fibroblasts are considered ‘activated’ and they promote tumour progression by secreting mediators which can promote chemoresistance within the cancer cells (e.g. the secreted HGF in lung cancer tissue confers resistance to tyrosine kinase inhibitor therapy).(220, 221) They also promote angiogenesis (e.g. the secreted SDF-1 in pancreatic cancer mobilises endothelial precursor cells to form new blood vessels) and modulate ECM (e.g. the secreted MMPs degrade ECM to provide space for tumour growth, to release VEGF for angiogenesis, and to detach cancer cells for EMT).(220)

The transition of omental adipocytes into fibroblasts has only been recently reported. Iyoshi et al (2021) showed that in vitro, human omental adipocytes dedifferentiate into fibroblasts when incubated with ascites from ovarian cancer.(222)

1.5.5 Adipocytes and chronic low-grade inflammation within the adipose tissue

In obesity, lipid accumulation from the weight gain causes the enlargement of adipocytes and growth of adipose tissue which may outstrip its blood supply. This leads to hypoxia and eventually adipocyte death.(223) Infiltrating macrophages surround the dead adipocytes and release inflammatory cytokines such as TNF-α, IL-1β and IL-6.(159, 223) This inflammatory microenvironment within the adipose tissue is then able to support the growth of metastatic ovarian cancer leading to tumour progression.(159) Interestingly, a mouse study reported that the inflammation associated with ovarian cancer metastasis is mostly mediated by macrophages. The depletion of peritoneal macrophages decreased levels of VEGF detected in the ascites, which is a

reflection of amount of tumour present, implying that macrophage depletion was partly responsible for reduced tumour dissemination.(224)

1.5.6 Adipocytes and cancer chemoresistance

The adipocyte microenvironment also promotes anti-apoptosis of ovarian cancer cells. This occurs via the mitochondrial apoptotic pathway, which is regulated by the B-cell lymphoma/leukemia 2 family of proteins. Anti-apoptotic proteins, Bcl_2 and Bcl_{XL}, are upregulated in ovarian cancer cells, and regulate the caspase enzymes responsible for cell death.(225) Upregulation of these anti-apoptotic proteins was associated with the presence of IL-6 and IL-8,(225-227) adipokines which may originate from nearby adipocytes.

Adipocytes can also contribute to tumour progression by inactivating chemotherapeutic agents. A proof-of-principle finding by Sheng et al (2017)(228) reported that adipocytes absorb and enzymatically metabolise daunorubicin, an anthracycline chemotherapy drug. This has implications, especially in adipocyte-rich tissues such as the omentum. Cytotoxic activity may be decreased in these areas, potentially leading to drug-resistant cancer cells and subsequent treatment failure.

1.5.7 Adipocytes in tumour angiogenesis

Once metastatic cancer cells have adhered to the omentum, they proliferate and eventually invade into the omental stroma. In the early steps, cancer cells obtain nutrients from nearby cells via diffusion; the transfer of fatty acids directly from the adipocytes is an example.(117, 193) Tumour growth then requires angiogenesis (section 1.1.3d). Adipocytes are known to release angiogenesis-associated factors and the most studied of these factors is VEGF.

Aside from its role in EMT formation and as a chemoattractant for ovarian cancer cells to home towards the omentum, IL-6 has also been shown to stimulate EC migration, proliferation and formation of new blood vessels(229, 230) to levels similar to that induced by VEGF stimulation.(230) Correspondingly, the receptor for IL-6, IL-6R, was expressed in ECs of the

human ovary.(229) In mice, increased expression of IL-6 by adipocytes and macrophages in the tumour microenvironment was also implicated in resistance to anti-angiogenic treatment.(231) Furthermore, serum IL-6 levels in overweight breast cancer patients treated with anti-angiogenic therapy correlated with poor outcomes e.g. less response to treatment and larger tumour size.(231)

Several other adipokines which have also been implicated in tumour angiogenesis, such as HGF and PDGF, are also secreted from adipocytes.(213, 232) Individually, HGF and PDGF stimulate the proliferation and migration of ECs.(106, 233, 234) Additionally, receptors for HGF and PDGF were detected in HOMECs (106, 234) thus supporting their role in tumour angiogenesis and progression.

1.6 Mesothelial cells

Mesothelial cells line the body's cavities and their internal organs, mainly the pleural, pericardial and peritoneal cavities. Morphological and histochemical studies of the mesothelium show that mesothelial cells are generally similar across many mammalian species and across anatomical sites.(235)

In the context of ovarian cancer metastasis, the focus is on the mesothelial cells of the peritoneal cavity and especially of the omentum. As the outer layer of the omentum, they are the first point of contact for metastasising ovarian cancer cells; the possible mechanisms of interaction between the omental mesothelial cells and the cancer cells were previously outlined in section 1.3.5c.

The structure and functions of mesothelial cells, and also their role in cancer metastasis, are discussed in the following sections.

1.6.1 Structure of the mesothelial cell

Structurally, mesothelial cells appear flat and squamous-like, similar to epithelial cells. In this quiescent state, at any one time, fewer than 0.5% of mesothelial cells are undergoing mitosis.(236) Additionally, cuboidal mesothelial cells have

been observed. The cuboidal cells were assumed to be mesothelial cells in an activated state, as their cytoplasmic components contained a larger nucleus, as well as higher numbers of mitochondria, endoplasmic reticulum, microfilaments and other organelles, compared with the squamous-like cells.(235) It is possible that the flat resting mesothelial cells are involved in membrane transport whereas the cuboidal cells are involved in several metabolic activities.(235) The flat mesothelial cell is also capable of transforming into the cuboidal morphology in situations requiring high metabolic activity, such as in wound healing.(237) Notably, cuboidal cells were detected on the milky spots of the omentum,(235) which may be expected in an area with high immune activity (discussed in section 1.4.3).

Mesothelial cells are situated atop a basement membrane layer, with microvilli on their exposed luminal surface.(235, 238) The density of microvilli fluctuates in response to, or in adaptation with, their environment.(235) Alteration in mesothelial surface membrane charge is related to these changes in the microvilli, through changes in the composition of the mesothelial glycocalyx (a negatively charged surface layer) and also the charged molecules trapped within the microvilli.(235)

The role of hyaluronan was earlier discussed in section 1.3.5c in relation to its adhesion with the CD44 receptor expressed by cancer cells. Hyaluronan is a major constituent of the mesothelial glycocalyx,(239) and has been implicated in peritoneal homeostasis. Some proposed functions of hyaluronan include microvilli formation and preservation;(240) maintenance of water balance to provide a hydrated environment for cell division and migration;(239) regulation of cell surface adhesivity, as well as maintenance of cell structure and integrity during proliferation and migration.(241, 242) Hyaluronan is also involved in inter- and intracellular signalling; in the context of cancer, hyaluronan interacts with CD44 and receptor for hyaluronan-mediated motility to regulate tumour cell motility, proliferation and angiogenesis.(243)

Mesothelial cells also play a key role in material transport across the mesothelium as evidenced by their system of vesicles and vacuoles, often located near the peritoneal cell surface.(235)

1.6.2 Mesothelial cells and mechanical protection

The mesothelium has protective functions against physical injury and invading pathogens due to the tight junctions between the mesothelial cells, as well as the secretion of hyaluronan on the outer peritoneal surface.(235) This presence of hyaluronan, together with the increased surface area from the microvilli and the secretion of phosphatidylcholine (a lubricant similar to the surfactant found in lungs), confers mesothelial cells with a non-adhesive surface to reduce friction between organs and tissues.(236) The microvilli protrusions on the mesothelial cells may also physically entrap pathogens.(240)

1.6.3 Mesothelial cells in host defence mechanisms

Situated on outer surfaces of organs, mesothelial cells are the first line of defence against pathogens, or other chemical or physical insult. This is achieved by the secretion of relevant mediators such as cytokines, growth factors, and adhesion molecules. The secretion is usually induced by the inflammation which follows the initial infection or the exposure to foreign particulates.(235) The immunological functions of mesothelial cells were mostly studied in the lung (pleural mesothelial cells). In the case of peritoneal mesothelial cells, many studies have focused on peritonitis, which is a frequent consequence of peritoneal dialysis.

Although mesothelial cells phagocytose bacteria, it is the subsequent release of IL-8, leading to neutrophil influx, which forms the main mechanism of defense.(244) Exposure to asbestos in rat pleural mesothelial cells,(245) and exposure to talc in human pleural mesothelial cells(246) stimulated an inflammatory response evidenced by release of proinflammatory cytokines such as IL-8 and monocyte chemoattractant protein-1 (MCP-1).(245, 246)

Other inflammatory cytokines released by mesothelial cells include stromal cell-derived factor-1 (SDF-1, or CXCL12) which is involved in the migration and proliferation of B cell precursors;(247) eotaxin which is a chemoattractant for eosinophils;(248) and IL-6 which is able to stimulate lymphocytes and has antiviral properties.(249)

Mesothelial cells induce leucocyte migration to the site of inflammation, through the secretion of granulocyte colony-stimulating factor (G-CSF) and granulocyte-monocyte-CSF (GM-CSF).(249) Lymphocyte function-associated antigen-1 (LFA-1/ αLβ2) and Mac-1 (αMβ2) are integrins found on macrophages and lymphocytes which bind to the ICAM-1 expressed on mesothelial cells, leading to macrophage and lymphocyte migration.(179) Activated mesothelial cells, as a result of bacterial lipopolysaccharide stimulation, express higher amounts of VCAM-1 which then binds to the VLA-4 integrin of macrophages and lymphocytes and stimulate their migration across the mesothelial cells.(179)

1.6.4 Mesothelial cells in tissue repair

Mesothelial cells are involved in several aspects of tissue repair following injury. Sites of tissue injury are associated with inflammation, and activated mesothelial cells release mediators such as cytokines, growth factors, and adhesion molecules to modulate the inflammatory response.(235) As part of tissue repair, mesothelial cells secrete ECM components such as collagens, fibronectin and laminin. They also regulate the turnover of ECM via the secretion of MMPs and TIMPs.(250)

The hyaluronan on the surface of mesothelial cells may play a role in tissue repair. At sites of injury, hyaluronan synthesis is increased to form cross-linked intercellular cables to retain the migrated leucocytes.(251) The hyaluronan-bound leucocytes secrete growth factors, which may contribute to the healing process.(251) The hyaluronan cross-links also serve as a physical barrier to prevent the loss of ECM components.(251)

Following an injury, the fibrin deposition is one of the first steps in wound healing; but without eventual degradation, the wound area becomes overloaded with fibrin which later leads to fibrosis.(250) Mesothelial cells regulate fibrin deposition by the secretion of tissue factor (a procoagulant involved in the coagulation cascade which ultimately forms fibrin) and fibrinolytic enzymes (e.g. tPA and uPA). The balance between these pro- and anti-fibrinolytic mediators is regulated by other inflammatory-related factors such as TNF-α, IL-1, and TGF-β.(250) Thus, a disruption in the mesothelium can lead to fibrin accumulation

and the laying down of ECM, eventually leading to fibrous tissue formation and adhesion between tissue surfaces.(250) This is often observed in peritoneal dialysis, where frequent injury and inflammation on the peritoneal mesothelial cells can lead to peritoneal thickening and fibrosis.(252)

1.6.5 Mesothelial cells in tumour progression

In previous sections, the properties of mesothelial cells which aid tumour adhesion and invasion were described. The interaction between mesothelial cells and metastatic cancer cells is the first step of cancer invasion, resulting in alteration of the invading cancer's genetic profile to increase invasiveness and was discussed in section 1.3.5. The presence of mesothelial cells in the milky spots of the omentum also contributes to ovarian cancer metastasis, as discussed in section 1.4.3c. Other mechanisms by which mesothelial cells may contribute towards tumour progression are discussed below.

a) Injury and inflammation

The inflammatory repair processes induced by mesothelium injury generate leucocyte chemoattractants and growth factors. However, this mechanism inadvertently creates a suitable microenvironment for tumour cell growth.(253, 254) A study on rats showed that adhesion of colon cancer cells within the peritoneal cavity was greater following conventional surgery compared with a laparoscopic procedure, suggesting that tumour growth was increased with greater surgical wounding, and by extension, mesothelium damage.(253) The authors concluded that the inflammatory response post-surgical trauma upregulated adhesion molecules on the mesothelial cells, which enhanced tumour cell adhesion. At the same time, mesothelium-secreted growth factors could also inadvertently contribute to tumour growth.(253)

Separately, a mouse study showed that fewer numbers of injected melanoma cancer cells were required to cause tumour growth at a surgical injury wounded site compared to a non-wounded site.(255) However, eventually tumours also occurred at sites distant to the wound. The authors concluded that the growth factors released at the wounded site eventually affected the non-wounded site. They linked these observations to tumour recurrence, both local and distant,

which often occurs after surgical removal of the primary tumour.(255) The findings of both these studies are highly applicable in ovarian cancer, where surgery is the primary treatment and the subsequent recurrence rate is still high.(256)

The same mouse study also tested the ability of TGF-β or FGF-2 (individually or in combination) to promote tumour growth in mice.(255) Increased tumour growth was induced when the hind limb surgery site was injected with melanoma cells plus a combination of TGF-β and FGF-2, which suggested a tumour-promotion role of TGF-β and FGF-2.(255) In the context of ovarian cancer, both TGF-β and FGF-2 were detected in the tumour microenvironment, secreted by the cancer cells themselves, and also by the omental adipocytes and mesothelial cells.(257-263)

In vitro studies also showed the role of inflammatory cytokines and growth factors in tumour adhesion to the mesothelium. Pre-treating rat mesothelial cells with IL-1β increased colon cancer cell adhesion, possibly through the upregulation of mesothelial adhesion molecules such as ICAM-1 and VCAM-1.(254) Mesothelial cell pre-treatment with epidermal growth factor (EGF), a known growth factor for mesothelial cells, increased their proliferation and also tumour adhesion.(254) These data suggest that the increased tumour adhesion may be attributed to the increase in adhesion molecule expression (with IL-1β pre-treatment), or increased cell numbers available for adhesion (with EGF pre-treatment).(254)

Physiologically, the upregulation of adhesion molecules on mesothelial cells may have similar functions to that in ECs. In the latter, inflammatory cytokines upregulate adhesion molecules to allow leucocyte rolling and migration via the interaction with these molecules.(254) Likewise, in their immune defence role, mesothelial cells are also involved in leucocyte adhesion and movement. Metastatic tumour cells take advantage of this inflammation-induced expression of adhesion molecules in order to implant onto mesothelial cells.(254)

b) Secretion of tumour-promoting mediators

Mesothelial cells also secrete other mediators which can interact with cancer cells. An example is the CXCL12-CXCR4 axis; CXCL12 is a chemokine secreted by both mesothelial and ovarian cancer cells, with the corresponding

CXCR4 receptor expressed in the cancer cells.(264) An in vitro study showed that the activation of this CXCL12-CXCR4 axis was associated with the proliferation and migration of ovarian cancer cells, as well as, their adherence and invasion through a mesothelial cell layer.(264) In immunohistochemical studies on malignant and non-malignant ovarian samples, the expression of CXCR4 was inversely associated with both progression-free and overall survival, and was a potential prognostic factor. Furthermore, CXCR4 expression positively correlated with lymph node metastasis and CXCL12 expression positively correlated with ascites volume.(265)

Fibrin deposition during mesothelial tissue repair may trap the metastatic tumour cells facilitating binding of the cancer integrins to the ECM components of the submesothelial tissue.(250) Although, metastatic cancer cells may bind to ECM already present in the submesothelial region, it has also been reported that they can stimulate the mesothelial cells to produce more fibronectin, a component of the ECM, via TGF-β signalling, aiding metastasis.(263) This is supported by the observation that inhibition of fibronectin secretion from mesothelial cells reduced cancer migration, adhesion and invasion.(263) Mesothelial cells are also capable of secreting and remodelling collagen type I in the presence of ovarian cancer cells, creating a suitable environment for metastatic initiation.(266) The deposition of collagen also promotes angiogenesis by supplying pro-angiogenic factors and mediating EC migration.(267)

c) Ovarian cancer and mesothelial-associated molecules

As previously mentioned, the hyaluronan on the mesothelial cell surface was proposed as a target which binds to the CD44 receptor of metastatic ovarian cancer cells leading to cancer cell adhesion in the study by Cannistra et al (1993) (section 1.3.5c).(144) Contrastingly, a study by Jones et al (1995) reported that an intact hyaluronan coating in mesothelial cells is protective against ovarian tumour adhesion, as treating mesothelial cells with hyaluronidase disrupted hyaluronan, leading to increased cancer cell adhesion.(268) The presence of exogenously added hyaluronan or mesothelial cell conditioned media (containing free-floating hyaluronan) reduced cancer cell adhesion to mesothelial cells in in vitro experiments,(268) possibly because the free hyaluronan functioned as a ‘decoy’ for the ovarian cancer cell to bind to.

However, this protective effect was not as extensive as that observed in the presence of constitutive hyaluronan on mesothelial cell surface.(268) The authors then proposed that the hyaluronan coating contributes to the protection of mesothelial cells against cancer cell adhesion.(268)

The seemingly contradictory findings that the mesothelial hyaluronan promotes or inhibits cancer adhesion may be explained by the different CD44 variants present on ovarian cancer cells. Specifically, hyaluronan binds to the CD44H variant and different ovarian cancer cell lines have been shown to express different variants of CD44, which give rise to different levels of mesothelial adhesion.(269) The ovarian cancer cell lines used in the Jones et al and Cannistra et al studies were different, thus resulting in different observations.

In the study by Jones et al, it was possible that the hyaluronan coat refers to the mesothelial glycocalyx, where other molecules alongside the hyaluronan may also be protective against cancer cell adhesion, as they reported that the constitutive hyaluronan better protected mesothelial cells from cancer cell adhesion compared to exogenous hyaluronan. Additionally, this finding has implications during surgical resection of peritoneal tumours. At the end of such surgery, peritoneal lavage is performed to remove surgical debris. This step may inadvertently flush away the protective coating on the mesothelial cell surface and thus pave the way for residual tumour cells to adhere to the exposed surface.(235)

The integrins present on ovarian cancer cells can interact with ECM molecules such as fibronectin, collagen type IV and laminin (discussed in section 1.3.5c) which are present in the submesothelial region. An in vitro study showed that treating the ovarian cancer cells with antibodies against the integrins inhibited cancer cell migration towards these ECM molecules.(143) Interestingly, when the ovarian cancer cells were treated with a CD44 antibody, their migration towards these ECM molecules also showed a 60% reduction which the authors attributed to the different variants of the CD44 receptor which are able to bind to the ECM molecules.(143) These data suggest that both the integrins and CD44 present on the ovarian cancer cells are responsible for their adhesion to mesothelial cells.

Another possible role of mesothelial cells in ovarian cancer adhesion is the expression of another cell membrane surface molecule, mesothelin, on both the mesothelial and cancer cells.(270) It was reported that CA125, a glycoprotein highly detected in ovarian cancer and often used as a marker for diagnosis and treatment monitoring, binds to mesothelin.(270) This was postulated as a first step in ovarian cancer implantation within the peritoneal cavity in transcoelomic metastasis.

d) Clearance of the mesothelial cell layer

Another method by which ovarian cancer cells can access submesothelial tissue is via the physical clearance of the mesothelium layer. After adhering to the fibronectin on the mesothelium via the α5β1 integrin (previously mentioned in section 1.3.5c), the cancer cells use traction force to physically displace the mesothelial cells from their monolayer (mesothelial clearance).(271)

A study on ovarian cancer cell lines showed that those expressing more mesenchymal markers generally have greater mesothelial clearance ability.(272) Considering the EMT process when cancer cells dissociate from the primary tumour, the resulting mesenchymal phenotype is thus related to cancer invasiveness.

e) Mesothelial-mesenchymal transition

Similar to the EMT process where cancer cells convert to a mesenchymal phenotype during metastasis (discussed in section 1.3.5), mesothelial-mesenchymal transition (MMT) can be induced in mesothelial cells by the ovarian cancer cells. This process has been reported to be mediated by TGF-β1, IGF-1 and HGF secreted from the cancer cells.(273, 274) In MMT, the mesothelial cells acquire a fibroblast-like shape (as opposed to a cobblestone appearance), have decreased E-cadherin expression (similar to EMT) and increased vimentin expression (an intracellular marker for fibroblasts).(274)

When ovarian cancer cells were added to a collagen matrix layer seeded with mesothelial cells of the mesenchymal phenotype, the cancer cells invaded to a deeper layer compared with non-transitioned mesothelial cells (of the epithelial-like phenotype) indicting that the mesenchymal phenotype enhances cancer invasion.(273) Scanning electron microscopy confirmed that the cancer invasion

occurs through interaction between the cancer and mesothelial cells, and not the adhesion of cancer cells to the underlying ECM.(273)

In a mouse model, the MMT process contributed to the pool of cancer-associated fibroblasts,(273) which are associated with tumour proliferation, survival and invasion. Indeed, immunohistochemical studies on tissue samples of peritoneal metastases of ovarian, endometrial and colon cancers showed the dual nature (mesothelial and fibroblast-like) of the cells surrounding the tumour; suggesting the mesothelial origin of the cancer-associated fibroblasts.(273) Furthermore, the mesenchymal-type mesothelial cells secrete high levels of pro-angiogenic VEGF.(275) Increased angiogenesis was confirmed by greater CD34-positive staining in tissue samples (from ovarian, pancreatic, colorectal cancers) with micro-metastases present, than staining in tumour-free areas of the same tissue sample.(273) CD34 is a marker of angiogenesis, commonly detected in the tip cells of angiogenic sprouts.(276)

1.7 Chapter summary and research aims

It is clear that patients with ovarian cancer often present with advanced metastatic disease and that current treatments are relatively ineffective. Globally, the overall 5-year survival for ovarian cancer is relatively unchanged since 1995 (<4% increase) and still remains below 50%.(277) Clearly new therapies are urgently needed and thus it is critical that the mechanisms involved in the metastasis and growth of secondary tumours are better understood. Only then can better therapies be developed. Thus, this thesis aims to better understand, using relevant human cells, the mechanism of ovarian cancer metastasis to the omentum – a major site for secondary tumour formation.

Ovarian cancer cells metastasising to the omentum via the transcoelomic route initially adhere to the mesothelium surface, which consists of mesothelial cells.(117) Varied mechanisms support this including the release of mediators which act as chemoattractants for tumour cells to migrate towards the mesothelial cells, clearance of the mesothelial layer for tumour cells to invade submesothelial tissues, as well as expression of adhesion molecules or ECM secretion by mesothelial cells for tumour cells to bind to.

Once the tumour cells have invaded the omental stroma beneath the mesothelial cell layer, the metastatic cells proliferate, induce angiogenesis and establish a secondary tumour. The initiation of angiogenesis in the local microvasculature requires EC activation by pro-angiogenic factors derived from omental mesothelial cells, tumour cells themselves, and the resident cells within the omentum such as the omental adipocytes. Indeed, adipocytes have a complex cross talk with the growing tumour via secretion of a range of adipokines. Thus, the omentum provides an ideal ‘soil’ for the metastatic tumour to establish and grow, although the mechanisms by which the omentum supports metastasis growth and angiogenesis are poorly understood.

Support for an interaction between the omental adipose tissue and tumour growth can be found in other cancers where adipokines contribute to cancer progression, e.g. breast cancer. Indeed, the omentum is increasingly recognised as an ‘active’ secretory organ, hence it seems plausible that the secreted adipokines influence cells in the vicinity such as the ECs and the

mesothelial cells. Yet, there is a paucity of literature investigating the effect of omental-secreted adipokines in inducing angiogenesis of human omental ECs and in facilitating the adhesion of metastatic ovarian cancer cells to the omental mesothelium. Human omental ECs are not commercially available, which could explain why most studies on angiogenesis are performed on non-disease relevant ECs.

Therefore, the **hypothesis** behind the work presented of this thesis is that:

Adipokines secreted from omental adipocytes support metastasis of EOC to the omentum.

The **overall aim** is to examine, using disease-relevant human cells, whether adipokines secreted from omental adipocytes enhance (a) initial binding of EOC to the mesothelium and (b) pro-angiogenic phenotypic changes in the local omental microvascular ECs. It is hoped that a greater understanding of the mechanisms involved in these processes will identify potential future therapeutic targets that may ultimately improve the current poor prognosis or women presenting with advanced EOC.

The specific objectives are to:

a) develop an improved method to isolate primary microvascular ECs from the human omentum (chapter 3)
b) investigate the pro-angiogenic effects of omental adipokines on human omental microvascular endothelial cells (HOMECs) (chapters 3 and 4);
c) develop a method to isolate and culture primary human omental mesothelial cells (chapter 5);
d) investigate the effect of omental adipokines on adhesion of EOCs to a mesothelial layer (chapter 6)

Chapter 2. Materials and Methods

2.1 Sources of materials by manufacturer

Abcam plc, Cambridge, UK: Human adiponectin ELISA kit; anti-vimentin mouse monoclonal antibody; anti-cytokeratin 18 rabbit monoclonal antibody; anti-ZO1 rabbit monoclonal antibody; recombinant human adiponectin; recombinant human leptin; recombinant human lipocalin-2; recombinant human MIF.

Bio-Rad Laboratories Ltd, Watford, UK: Cell-counting slides.

Corning, New York, USA: Phosphate buffered saline (PBS) 1x without calcium and magnesium; PBS 1x with calcium and magnesium; multichannel pipette reservoir; multiwell plates – 6-well, 24-well, 96-well.

Enzo Life Sciences Ltd, Exeter, UK: Collagen I rat tail.

Fisher Scientific UK Ltd., Loughborough, UK: Calcium chloride solution; Nunc® cryovial 1.8mL; D(+)-glucose anhydrous; sodium chloride powder; microcentrifuge tubes – 0.6mL, 1.5mL, 2mL, 5mL; paraformaldehyde 4% solution; pipette tips - 10µL, 200µL, 1000µL.

Invitrogen (part of Thermo Fisher Scientific Inc, Waltham, USA): Dynabeads™ CD31 endothelial cell; eBioscience™ calcein-AM viability dye; goat anti-rabbit Alexa Fluor 594 secondary antibody; goat anti-mouse Alexa Fluor 488 secondary antibody; ProLong™ Diamond antifade mountant; human cathepsin L ELISA kit; human NGAL ELISA kit; human leptin ELISA kit.

Life Technologies (part of Thermo Fisher Scientific Inc, Waltham, USA): Collagenase type I and type II; gentamicin 50mg/mL;

Merck Life Science UK Limited, Gillingham, UK: BrdU cell proliferation assay kit; cathepsin L from human liver; human MIF ELISA kit; Millicell EZ 8-well glass chamber slide; nylon net 30µm filter; phosphatase inhibitor cocktail 2 and 3; potassium chloride powder; protease inhibitor cocktail; syringe filter unit 0.22µm.

Miltenyi Biotec, Surrey, UK: Anti-fibroblast microbeads; LS+ positive selection column.

PromoCell GmbH, Heidelberg, Germany: Endothelial cell basal medium MV2; supplement pack endothelial cell growth medium MV2.

Premier Healthcare & Hygiene Ltd, Tyne & Wear, UK: Sterile non-woven swabs; Swann Morton disposable scalpel size 10.

R&D Systems Inc, Minneapolis, USA: Human adipokine array kit; human phospho-RTK array kit; human phospho-kinase array kit; human FGF basic DuoSet ELISA, human TGF-beta 1 DuoSet ELISA, human VEGF DuoSet ELISA; human VEGFR3 monoclonal antibody; DuoSet ELISA ancillary reagent kit 1 & 2; sample activation kit 1.

Sarstedt AG & Co. AG, Nümbrecht, Germany: Pipettes – 25mL, 10mL, 5mL, 2mL; tissue culture flasks – T75, T25; petri dish 60x15mm; 12-well Cell+ plate.

Scientific Laboratory Supplies, Nottingham, UK: Coverslips – 10mm diameter, 22x50mm.

Sigma-Aldrich (part of Merck Life Science UK Limited, Gillingham, UK): Amphotericin B solution; anti-CD31 mouse monoclonal antibody; anti-von Willebrand Factor rabbit monoclonal antibody; anti-occludin monoclonal mouse antibody; bovine serum albumin (BSA); cell counting kit-8; collagen type IV from human placenta; Dulbecco's Modified Eagle's Medium/Ham's Nutrient Mixture F-12 (DMEM/F12); Dulbecco's Modified Eagle's medium (DMEM) low glucose; dimethyl sulfoxide (DMSO) solution; ethylenediaminetetraacetic acid (EDTA) powder; foetal bovine serum (FBS); gelatin from bovine skin; goat serum; Hanks' balanced salt solution 10x; HEPES powder; HEPES 1M solution; hydrogen peroxide 30% w/w solution; L-glutamine 200mM solution; trypan blue solution; trypsin-EDTA 1x solution.

Thermo Fisher Scientific Inc, Waltham, US: Pierce™ bicinchoninic acid (BCA) protein assay kit; Sterilin™ polystyrene 7mL container.

2.2 Equipment and software packages

Equipment	Manufacturer	Function
Azure 500	Azure Biosystems Inc.	Chemiluminescence imaging
EVOS Fluo	Life Technologies (part of Thermo Fisher Scientific Inc)	Fluorescence microscopy
EVOS XL Core	Life Technologies (part of Thermo Fisher Scientific Inc)	Phase contrast microscopy
ImageJ v1.51j8	National Institutes of Health, USA	Image and data analysis
JuLI™ Stage Real-Time Cell History Recorder	NanoEnTek Inc	Cell migration imaging
JuLI™ Stat Cell Analysis Software	NanoEnTek Inc	Image and data analysis
Leica DM4000 B LED	Leica Microsystems (UK) Ltd	Fluorescence microscopy
Prism v7.03 & v8	GraphPad Software Inc	Data analysis and graphing
SpectraMax® M2e Microplate Reader	Molecular Devices LLC	Absorbance and fluorescence reading of multiwell plates

2.3 Cell culture buffers and solutions

2.3.1 Human omental tissue samples

Sample collection medium

Hanks' balanced salt solution (HBSS) 10x	50mL
HEPES 1M	5mL
Amphotericin B 250µg/mL	5mL
Gentamicin 50mg/mL	500µL
Autoclaved distilled water	440mL

2.3.2 Human microvascular omental endothelial cells (HOMECs)

Complete growth medium

Endothelial cell basal medium MV2	500mL
Gentamicin 50mg/mL	500µL

Supplement pack endothelial cell growth media MV2 comprising:

Foetal bovine serum (FBS)	25mL
Ascorbic acid 1mg/mL	500µL
Basic fibroblast growth factor 10µg/mL	500µL
Epidermal growth factor 5µg/mL	500µL
Hydrocortisone 200µg/mL	500µL
Insulin-like growth factor 20µg/mL	500µL
$VEGF_{165}$ 0.5µg/mL	500µL

Starvation medium

Endothelial cell basal medium MV2	500mL
FBS	5mL
Gentamicin 50mg/mL	500µL

HOMEC freezing solution

FBS	7mL
Complete HOMEC growth medium	2mL
DMSO	1mL

Enzyme solution for HOMEC isolation procedure

BSA	7.5g
Calcium chloride 1M	500µL
Collagenase type I or II	0.75g
D-glucose	0.45g
HEPES	2.98g
Potassium chloride	1.87g
Sodium chloride	3.5g
Distilled water	to 500mL

Adjusted to pH 7.4, then sterile-filtered (0.22µm) into 50mL aliquots and stored at -20°C.

BSA in PBS (10% w/v) for HOMEC isolation procedure

BSA	10g
PBS 1x without calcium, magnesium	to 100mL

Adjusted to pH 7.4, then sterile-filtered (0.22µm) into 10mL aliquots and stored at -20°C.

BSA in PBS (0.1% w/v) for HOMEC isolation procedure

BSA	100mg
PBS 1x without calcium, magnesium	to 100mL

Adjusted to pH 7.4, then sterile-filtered (0.22µm) into 5mL aliquots and stored at -20°C.

Lysis buffer for HOMEC lysate collection

RIPA buffer	4365µL
Protease inhibitor cocktail	45µL
Phosphatase inhibitor cocktail 2	45µL
Phosphatase inhibitor cocktail 3	45µL

2.3.3 Human omental mesothelial cells

Complete growth medium

Dulbecco's Modified Eagle Medium (DMEM)	500mL
FBS	100mL
L-Glutamine 200mM	5mL
Gentamicin 50mg/mL	500µL

Modified PBS for mesothelial cell isolation procedure

BSA	5g
Calcium chloride 1M	100µL
PBS 1x without calcium, magnesium	to 100mL

Adjusted to pH 7.4, then sterile-filtered (0.22µm) into 10mL aliquots and stored at -20°C.

Anti-fibroblast microbead buffer

BSA	0.5g
EDTA	0.744g
PBS 1x without calcium, magnesium	100mL

Adjusted to pH 7.4, then sterile-filtered (0.22µm) and stored at 2-8°C.

Mesothelial cell freezing solution

FBS	7mL
Complete mesothelial cell growth medium	2mL
DMSO	1mL

2.3.4 Ovarian cancer cell lines (SKOV3, A2780)

Complete growth medium

DMEM/F12	500mL
FBS	50mL
Gentamicin 50mg/mL	500µL

2.3.5 Serum-free basal medium for collection of conditioned medium

Endothelial cell basal medium MV2	500mL
Gentamicin 50mg/mL	500µL

2.3.6 Coating of tissue culture plasticware

All plasticware (culture flasks, multiwell plates, multiwell slides) were coated with at least 50 µL/cm^2 of coating solution and left for at least 2 hours in 37°C, prior to removal by aspiration.

Gelatin 2% w/v

Bovine gelatin powder	2g
Distilled water	100mL

Mixture autoclaved, then stored in 50mL aliquots at 2-8°C.

Gelatin 0.2% w/v

Bovine gelatin powder	0.2g
Distilled water	100mL

Mixture autoclaved, then stored in 50mL aliquots at 2-8°C.

Collagen I 3.33 µg/mL or 0.00025% (w/v)

Collagen type I (from rat tail) 100µg/mL	1mL
PBS without calcium, magnesium	30mL

Mixture made immediately before use.

Collagen IV 5µg/mL or 0.0005% (w/v)

Collagen type IV (from human placenta) 1mg/mL	100µL
Autoclaved distilled water	20mL

Mixture stored in 50mL aliquots at 2-8°C.

2.4 Isolation of human omental microvascular endothelial cells (HOMECs)

Two protocols were employed in the isolation of HOMECs. The initial isolation procedure was adapted from Winiarski et al (2011),(278) and this was later amended to produce the final protocol (further detail in section 3.2.1).

Human omental samples were obtained from adult female patients undergoing elective surgical procedures within the gynaeoncology department at the Centre for Women's Health, Royal Devon and Exeter NHS Foundation Trust. All patients gave their written informed consent for use of their omental tissue (ethical approval 2003/2/26; South West LREC). Only healthy (non-diseased) omental tissue was collected and all tissue was received anonymised. The samples were collected in sample collection media (section 2.3.1) and processed within 24 hours of collection.

2.4.1 Isolation of HOMECs (initial protocol)

Visible blood vessels and fibrotic portions of the tissue sample were dissected and removed, and the remaining tissue was dissected to approximately 1 cm^3 pieces. These were mixed with pre-warmed enzyme solution (containing collagenase type II), at a tissue : enzyme solution ratio of 1 : 1.5 v/v, and placed on a rotary mixer at 37°C for 25 minutes.

At the end of the digestion, the tissue pieces were manually removed and washed multiple times in cold PBS until the washings were clear. The tissue pieces were further minced until a porridge-like consistency was obtained, before being mixed with pre-warmed enzyme solution (containing collagenase type I), at the same ratio of 1 : 1.5 v/v. The mixture was placed on a rotary mixer at 37°C for 2 hours.

At the end of this second digestion, the mixture was strained and compressed through two layers of gauze swab in order to remove the undigested tissue. The filtrate was collected and centrifuged at 350*g* at 4°C for 5 minutes. The cell pellet was washed in cold BSA in PBS (10% w/v), and then in cold PBS (both times centrifuged at 600*g* at 4°C for 3 minutes). The cells were then suspended in cold 5mL serum-free endothelial cell medium and syringe-filtered in a Swinnex filter holder with a 30µm nylon filter within. The nylon filter was removed and agitated in a petri dish filled with cold serum-free endothelial cell medium to remove any cell clumps. The filter was fitted back into the Swinnex filter holder and the filtration procedure repeated thrice. The cells in the petri dish were transferred to a centrifuge tube and centrifuged at 600*g* at 4°C for 3 minutes.

For the immunoselection procedure, the cell pellet was resuspended in 500µL cold BSA in PBS (0.1% w/v) solution, and 5µL of anti-CD31 antibody-coated Dynabeads (washed beforehand with the BSA in PBS (0.1% w/v) solution) was added to the suspension. The Dynabead mixture was placed on a roller mixer at 4°C for 20 minutes. The 'magnetised' HOMECs were selected using a magnetic particle concentrator (MPC-E magrack 1) four times, with BSA in PBS (0.1% w/v) washes in between. The final pellet was suspended in complete growth medium and cultured in a gelatin (2% w/v)-coated well of a 6-well plate.

2.4.2 Isolation of HOMECs (final protocol)

Visible blood vessels and fibrotic portions of the tissue sample were dissected away, and the remaining tissue was dissected to approximately 1 cm^3 pieces. These were mixed with pre-warmed enzyme solution (containing collagenase type II), at a tissue : enzyme solution ratio of 1 : 1.5 v/v, and placed on a rotary mixer at 37°C for 25 minutes.

At the end of the digestion (digestion 1), FBS was added to the mixture at 1:10 v/v to neutralise the enzyme solution. The tissue pieces were manually removed and washed twice in cold PBS. The remaining neutralised enzyme solution was kept aside for mesothelial cell isolation (refer to section 2.5). The tissue pieces were further minced until a porridge-like consistency was obtained, before being

mixed with pre-warmed enzyme solution (containing collagenase type I), at the same ratio of 1 : 1.5 v/v. The mixture was placed on a rotary mixer at 37°C for 5 hours.

At the end of this second digestion (digestion 2), the mixture was strained through two layers of gauze swab in order to remove the undigested tissue. The filtrate was collected and centrifuged at 350*g* at 4°C for 5 minutes, resulting in multiple layers of oil, adipocytes, enzyme solution and cell pellet (**Figure 11**). The adipocyte layer was removed at this point for conditioned media collection if required (refer to section 2.7.2). The cell pellet was washed in cold 10% w/v BSA in PBS, and then in cold PBS (both times centrifuged at 600*g* at 4°C for 3 minutes) to remove any residual enzyme solution.

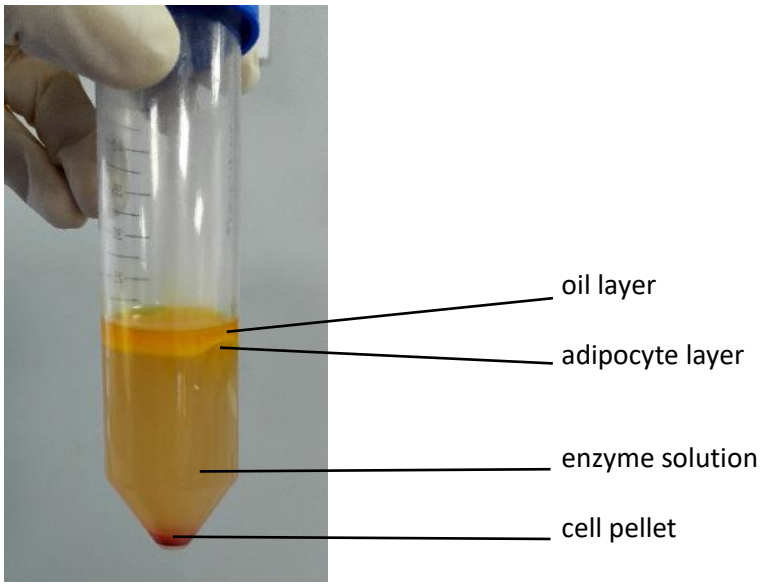

Figure 11. A photograph showing the layers of oil, adipocytes, enzyme solution and cell pellet. This was observed after digestion of omental tissue with collagenase I followed by centrifugation.

For the immunoselection procedure, the cell pellet was resuspended in 1mL cold BSA in PBS (0.1% w/v) solution, and then split into two microcentrifuge tubes (500µL each) containing 3µL of anti-CD31 antibody-coated Dynabeads. The Dynabeads were washed beforehand with the BSA in PBS (0.1% w/v) solution. The Dynabead mixture was placed on a roller mixer at 4°C for 30

minutes. The ‘magnetised’ HOMECs were selected using a magnetic particle concentrator (MPC-E magrack 1) four times, with BSA in PBS (0.1% w/v) washes in between. The final pellet in both microcentrifuge tubes were each cultured into a gelatin (2% w/v)-coated well of a 6-well plate filled with complete growth medium.

When the wells were confluent, the cells were trypsinised (refer to section 2.6), pelleted and resuspended in 500µL BSA in PBS (0.1% w/v). To purify the HOMEC population, the cells were subjected to another round of Dynabead immunoselection with 5µL Dynabeads added to the cell suspension in a microcentrifuge tube. The mixture was incubated on a roller mixer at 4°C for 30 minutes and subjected to a magnetic particle concentrator as described previously. The final pellet was cultured in complete growth medium in a T25 flask pre-coated with gelatin 2% w/v.

To expand the HOMEC population, subsequent passaging was capped at a maximum split ratio of 1:5. For experiments, the HOMECs were utilised between passages 4 and 7.

2.5 Isolation of human omental mesothelial cells (final protocol)

The neutralised enzyme solution from digestion 1 (section 2.4.2) was processed to isolate mesothelial cells using a method modified from that of Takahashi et al (1991).(279) The solution was passed through one layer of gauze swab to remove any undigested tissue, and then centrifuged at 300*g* at 4°C for 10 minutes. The resultant cell pellet was resuspended in 1mL of mesothelial complete growth medium, and then gently layered onto 10mL cold modified PBS and allowed to separate at room temperature. After 10 minutes, this top layer seeped downwards into the modified PBS. The top and bottom 1mL ‘layers’ were discarded, and the middle 9mL portion was centrifuged at 300*g* at 4°C for 10 minutes.

The cell pellet was resuspended and layered again in the same manner. Again, the middle 9mL portion was retained and centrifuged at 300*g* at 4°C for 10 minutes. The final cell pellet (consisting mostly of erythrocytes and mesothelial cells) was resuspended in 1mL of complete medium and seeded into a collagen

IV-coated well of a 6-well plate. After 2 to 3 days, the medium was changed to fresh growth medium to remove any erythrocytes.

When the wells were confluent, the cells were trypsinised (refer to section 2.6) and transferred to T25 flasks. To expand the mesothelial cell population, subsequent passaging was capped at a maximum split ratio of 1:5. For experiments, the cells were utilised between passages 2 and 5.

2.6 Trypsinisation and passaging of cells

When cells reached at least 90% confluency within their flasks or multiwell plates, the media was aspirated and cells were washed twice with warmed PBS. Warmed trypsin/EDTA (0.05%/0.02% w/v) solution was added to the cells (1.5mL in a T75 flask, or 1mL in a T25 flask, or 500µL in a 6-well plate) and incubated at 37°C between 1 to 5 minutes. Cell detachment was confirmed by microscope and the trypsin was neutralised with warmed complete media (at least 8.5mL for a T75 flask, or 4mL for a T25 flask, or 2mL for a 6-well plate). The cell suspension was centrifuged at 200*g* for 5 minutes, and the supernatant aspirated off. The cell pellet was resuspended in warmed complete media and seeded into fresh flasks or multiwell plates.

2.7 Collection of conditioned media

2.7.1 Omental adipose tissue conditioned medium

In earlier procedures, the dissected adipose tissue pieces (approximately 1 cm^3) were washed twice in cold PBS and placed into 7mL polystyrene containers pre-filled with 1 to 2mL serum-free basal medium. The tissue pieces were added or removed, weighing each time, to obtain a tissue-volume concentration of 1g/mL. However, it was difficult to fit the forceps through the narrow opening of the container.

The method of collecting conditioned medium was amended. Instead of polystyrene containers, the washed and dissected omental adipose tissue pieces (approximately 1 cm^3) were placed into previously-weighed petri dishes (10cm diameter) and weighed. The net weight of the tissue pieces determined

the volume of serum-free basal medium to be added in order to obtain a tissue-volume concentration of 1g/mL. Petri dishes were incubated at 37°C/5% CO_2 for 24 hours. The conditioned medium was filtered through a syringe-driven 0.22µm filter into labelled microcentrifuge tubes. Each filter was only used for a maximum of 10mL conditioned media volume, as larger volumes would clog the filter. The tubes were stored at -80°C for future use.

As a control, serum-free basal medium which was not exposed to the omental tissue was placed in a separate petri dish and also incubated. This medium was also syringe-driven 0.22µm filtered and frozen at -80°C. This method for collection of control media was also applied for the following conditioned media collection (section 2.7.2 and 2.7.3).

2.7.2 Omental adipocyte conditioned medium collection

Omental adipocytes, obtained after digestion 2 during the isolation of HOMECs (described in section 2.4.2), were washed twice in PBS and then placed into 7mL polystyrene containers containing serum-free basal medium (**Figure 12**). As it was not possible to quantify adipocytes by cell number (as they float due to their high fat content and are very adhesive), they were weighed together with the medium; the amount of adipocytes ranged from 2 to 4g per mL of medium. After gently swirling them, the containers were incubated at 37°C/5% CO_2 for 24 hours. As it was not possible to separate the adipocytes from the medium, the whole suspension was pipetted into a 10mL syringe fitted with a 0.22µm filter. The filtered conditioned medium was aliquoted into labelled microcentrifuge tubes and stored at -80°C for future use.

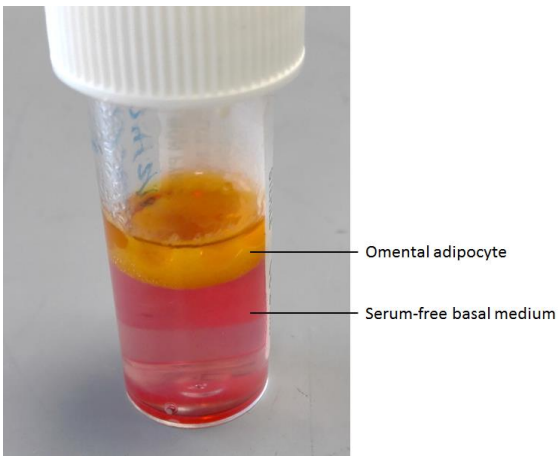

Figure 12. A photograph showing the method used to collect omental adipocyte conditioned medium. Washed adipocytes clump together and float on top of the medium.

2.7.3 Adherent cell conditioned medium collection

Ovarian cancer cell lines (SKOV3, A2780) and omental mesothelial cells were cultured in T75 flasks until a confluent monolayer was observed. Cells were washed twice with PBS and then incubated at 37°C/5% CO_2 for 24 hours with 10mL serum-free basal medium. The conditioned medium was syringe-driven 0.22µm filtered into labelled microcentrifuge tubes and stored at -80°C for future use.

2.8 Freezing and thawing of cells

After the cells were trypsinised and pelleted (section 2.6), they were suspended in freezing medium and placed in labelled cryovials. Each T75 flask of cells was split 1:3 into 3 separate cryovials for HOMECs, 1:2 for mesothelial cells and 1:6 for ovarian cancer cell lines; with a minimum cell density of 500,000 cells per 500µL freezing medium per cryovial. The cryovials were placed in a controlled-rate freezing container at -80°C at least overnight, and then moved to long term storage in liquid nitrogen or the -150°C cryofreezer.

When thawing cells, each cryovial was thawed rapidly at 37°C, filled with 1 to 2mL warmed complete media and pipetted gently up and down. The whole mixture was then transferred to a fresh flask filled with warmed complete media.

After 24 hours, the media was exchanged with fresh complete media to remove the initial freezing media.

For cells isolated from omental tissue, namely the HOMECs and mesothelial cells, the cell population were expanded prior to freezing them; thus, they were commonly frozen at the 3rd or 4th passages.

2.9 Immunocytochemistry

All incubations and washes were performed at room temperature, unless otherwise specified. The treatment volume was 150µL per well or dish, or 250µL in 24-well plates.

Cells were cultured in glass-bottomed culture dishes, 8-well chamber slides or 24-well plates; cell seeding densities are indicated in later chapters. When confluent, media was aspirated and the cells were fixed with paraformaldehyde 4% (w/v) in PBS for 20 minutes. The paraformaldehyde was washed away with PBS, and the cells rinsed with PBS four times. If the protocol required staining of intracellular components, then a permeation step was performed: the cells were treated with methanol at -20°C for 10 minutes. The methanol was also washed away with PBS four times.

To block non-specific binding sites, the fixed cells were treated with a mixture of 5% (v/v) goat serum and 2% (w/v) bovine serum albumin in PBS for 30 minutes. Thereafter, primary antibodies (diluted in PBS) were applied and the cells were incubated for one hour at room temperature, or overnight at 2-8°C. Primary antibody was substituted with PBS only for the negative control well or dish. Before the addition of secondary antibodies, cells were washed four times with PBS. Depending on the animal species of the primary antibody, the cells were incubated with either fluorescently labelled goat anti-mouse or goat anti-rabbit IgG secondary antibody for 30 minutes, before another round of four PBS washes. All antibodies were diluted in PBS according to manufacturer guidelines, detailed in **Table 2**.

Nuclei staining was performed using DAPI (1µg/mL) which was added for 10 minutes after the secondary antibody staining, and then removed with two PBS washes, followed by a final wash with distilled water, and air dried. Cells were

mounted with coverslips and mounting media, and then imaged on a fluorescence microscope.

Table 2. Details of the antibodies used for immunocytochemistry, their species of origin and their dilution factor. All antibodies were monoclonal. Primary antibodies were of mouse or rabbit origin; while secondary antibodies were only of goat origin to ease sample preparation as goat serum was used to block non-specific binding sites.

Antibody Type	Antibody	Species of origin	Brand and product code	Dilution with PBS (v/v)
Primary antibodies	Anti-CD31	Mouse	Sigma-Aldrich (P8590)	1:100
	Anti-cytokeratin 18	Rabbit	Abcam (ab133272)	1:500
	Anti-occludin	Mouse	Sigma-Aldrich (CB1044)	1:250
	Anti-vimentin	Mouse	Abcam (ab8069)	1:200
	Anti-VEGFR3	Mouse	R&D Systems (MAB3491)	1:50
	Anti-von Willebrand factor	Rabbit	Sigma-Aldrich (F3520)	1:200
	Anti-ZO1	Rabbit	Abcam (ab276131)	1:50
Secondary antibodies	Anti-rabbit with Alexa Fluor 594	Goat	Invitrogen (A-11012)	1:1000
	Anti-mouse with Alexa Fluor 488	Goat	Invitrogen (A-11001)	1:1000

2.10 Cell seeding and treatment

Cells were plated into 96-well flat-bottomed plates coated with gelatin (2% w/v) at 10,000 cells per well. The cells were incubated in complete growth media (100µL per well) at 37°C/5% CO_2 for at least 24 hours. For wells designated as the complete media control, media in the experimental wells was substituted for starvation media (100µL per well) and then incubated overnight. For consistency with the starvation step, the complete media control wells were replaced with fresh complete growth media.

The next day, the starvation media in the experimental wells was exchanged for fresh media with different treatment conditions depending on the experimental procedure. Treatment (100µL per well) consisted of CM from adipose tissue and/or ovarian cancer cells (collected as described in section 2.7), or of exogenous compounds (adiponectin, cathepsin L, leptin, lipocalin-2, or MIF)

reconstituted in starvation media; all treatments were diluted to required concentrations. Again, for consistency with the treatment addition step, complete media control wells were replaced with fresh complete growth media. Cells were then incubated for 24 to 72 hours as indicated.

2.11 Bromodeoxyuridine assay to assess cell proliferation

The bromodeoxyuridine (BrdU) proliferation assay kit, which is a colorimetric-based assay, was utilised to determine HOMEC and mesothelial cell proliferation. In principle, the BrdU reagent, a thymidine analogue, added to cells would be integrated into the DNA of proliferating cells. Anti-BrdU antibodies detect and bind to this incorporated BrdU. Due to the peroxidase enzyme attached to the antibody, a blue colour was observed after substrate addition. The more BrdU present, the more antibody would be bound, hence the stronger the blue colour observed. Stop solution was added to halt the enzymatic reaction and the absorbance of the resultant yellow colour was measured at 450nm wavelength. The absorbance values correlate with DNA synthesis; thus, a greater measured absorbance value implied greater proliferative activity.

In the experiments, cells were seeded in 96-well plates and treated as described in their relevant sections. Some wells were designated as blanks (media only, with no cells) and background wells (see below). The BrdU reagent (diluted according to manufacturer's recommendation) was added to all wells, except those designated as background wells, after 24 hours of treatment incubation. The duration of BrdU incubation differed between experiments and is described in later chapters. All media were then aspirated, and cells fixed with the given fixing solution (200µL per well, incubated for 30 minutes). As per manufacturer's protocol, the subsequent steps of anti-BrdU antibody addition (100µL per well, incubated for one hour), plate washes and substrate addition (100µL per well, incubated for 20 minutes), as well as absorbance value measurements (at 450nm wavelength) were performed immediately or within a week of cell fixation.

As for the controls, the blank wells indicate the non-specific binding of the BrdU reagent to the plastic surface of the plate, while the background wells provide

information on the non-specific binding of the anti-BrdU antibody to the cells without the BrdU reagent. Both these controls should have absorbance values below 0.1 according to manufacturer's protocol, to infer that the procedure is valid. During results analysis, the mean readings from the background wells were subtracted from that of the corresponding treatment wells. This is to indicate the 'net' amount of BrdU incorporated within the cells, based on the binding of the anti-BrdU antibody. The readings from the blank wells were not utilised in results analysis.

2.12 Water-soluble tetrazolium salt 8 assay to assess cell proliferation

To complement the BrdU assay, the water-soluble tetrazolium salt 8 (WST8) assay was also utilised to assess cell proliferation. In principle, the WST8 reagent does not enter the cells but stays in the culture media. Via an electron mediator, 1-methoxy-5-methylphenazium methylsulfate (1-mPMS),(280) the WST8 reagent (tetrazolium) is reduced by cellular dehydrogenases to produce a yellow-orange formazan dye (**Figure 13**). The greater the cell number, the more cellular dehydrogenases are present, the more WST8 reagent is reduced to form the coloured dye. Thus, the intensity of this yellow-orange colour, by which the absorbance was measured at 450nm wavelength, is proportional to the number of living (and thus, metabolising) cells in culture.

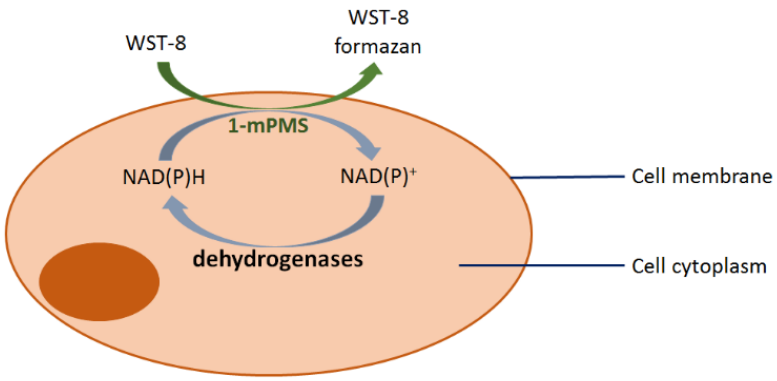

Figure 13. Principle of the WST8 assay. The conversion of the WST8 reagent into its formazan dye is achieved through the action of the electron mediator 1-mPMS. The amount of the yellow-orange formazan dye generated is proportional to the cellular dehydrogenases within the cells. 1-mPMS: 1-methoxy-5-methylphenazium methylsulfate; NADP+/NADPH: nicotinamide adenine dinucleotide phosphate. Diagram based on information from Chamchoy et al (2019) (280) and created on Microsoft Powerpoint.

In the experiments, cells were seeded in 96-well plates and incubated with treatment media for varying duration, as indicated in their relevant sections. As this is a colorimetric assay, several empty wells were designated as blanks (i.e. media only with no cells) to account for the spontaneous absorbance of the WST8 reagent and for the phenol red present in the media. To run the assay, 10µL/well of the WST8 reagent was added into every well and the plate incubated for at least 90 minutes in 37°C/5% CO_2, prior to absorbance measurement on a spectrophotometer set to 450nm. During data analysis, the average reading from the blank wells was subtracted from that of the corresponding treatment wells; thus, the absorbance values of the reagent itself and of the phenol red within the media were removed.

2.13 Scratch wound healing assay to assess cell migration

Alongside cell proliferation, endothelial cell migration is another indicator of angiogenesis. Hence, HOMEC migration was assessed via a scratch wound healing assay.

HOMECs were seeded in 96-well plates at 10,000 cells/well. After at least 24 hours incubation at 37°C/5% CO_2, the media was exchanged for starvation media and cells incubated overnight. As with the proliferation experiments, some wells were designated as the complete media controls. For consistency with the starvation step, the complete media control wells were replaced with fresh complete growth media.

A scratch wound was etched across the well diameter using a 200µL pipette tip (P200) and the starvation media aspirated to remove cell debris as a result of wounding. Treatment media were added into wells (100µL per well), with complete media control wells replaced with fresh complete growth media.

The 96-well plate was incubated at 37°C/5% CO_2 in the JuLI™ Stage Real-Time Cell History Recorder. Using the 4x objective lens, the focal point of each well's etch was adjusted and positioned. Images of each well were taken at 15-minute intervals for at least 20 hours to follow cell migration and subsequent closure of the wound.

The area of the scratch wound was calculated in square pixels using ImageJ. Images obtained at the 12- and 20-hour timepoints were compared with the images from the 0-hour timepoint, and expressed as a percentage of scratch closure. The 0-hour scratch gaps were interpreted as 0%, while a fully closed gap is considered 100%.

2.14 Bicinchoninic acid protein assay to determine total protein concentration

The Pierce™ Bicinchoninic acid (BCA) Protein Assay Kit was utilised to determine the concentration of proteins (adipokines) secreted by the adipose tissue and adipocytes, as well as, the concentration of HOMEC lysates. This colorimetric-based assay quantifies total protein through the reduction of cupric (Cu^{2+}) to the cuprous ion (Cu^{+}) by the proteins. The intensity of the colour, as a result of BCA and cuprous binding together, corresponds to total protein concentration.

The assay was performed with slight modification to the manufacturer's protocol. The albumin standard or BSA ampoule was diluted with serum-free basal medium to give final BSA concentrations, for a standard curve, between 5µg/mL to 2000µg/mL. These were prepared in labelled centrifuge tubes. The basal medium on its own was used as a blank. A 25µL volume of each BSA standard and of the samples were pipetted into three separate wells (triplicate) of a 96-well plate. To prepare the working reagent, Reagent B (containing 4% w/v cupric sulfate) was added to Reagent A (containing bicinchoninic acid) at a ratio of 1:25 v/v. The working reagent was freshly diluted each time for the assay. The working reagent (200µL per well) was pipetted into wells containing albumin standards and samples, and the plate was incubated at 37°C for a maximum of 5 hours.

Absorbance was measured at the 562nm wavelength, at intervals of 30 minutes for a duration of 5 hours initially. In later experiments, absorbance measurements were taken at 2 hours only as further colour development (and the corresponding calculated protein concentration) beyond 2 hours did not differ substantially (average reads were ±5% of the reads at the 2-hour time point). The average absorbance of the blank wells (basal medium only) was

subtracted from each individual absorbance value to give the net absorbance. The net absorbance of the BSA standards were plotted to form a standard curve (**Figure 14**) and the total protein concentration of each sample was interpolated from this curve using GraphPad Prism. The albumin standards were freshly prepared for each experiment, and the corresponding standard curve was utilised only for samples within the same plate.

The assay was repeated several times if the absorbance values of the samples were beyond the standard curve. In such cases, the samples were subsequently diluted with basal medium to achieve a concentration between 1:2 to 1:100 v/v.

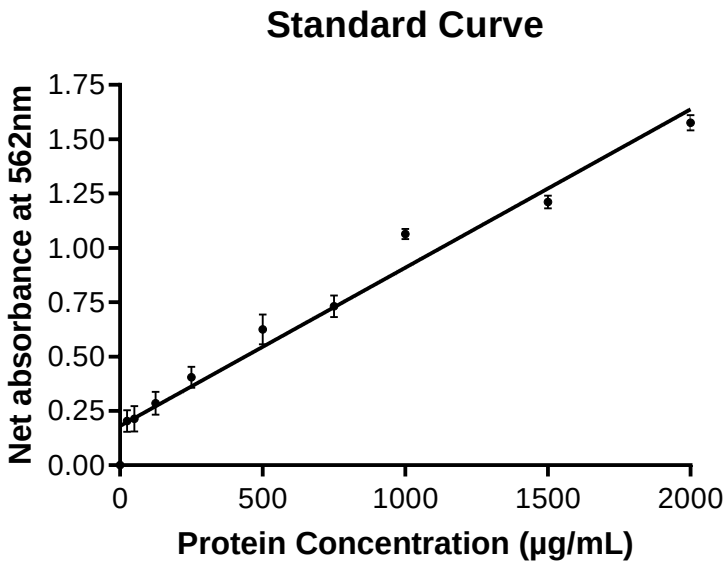

Figure 14. A representative bovine serum albumin (BSA) standard curve. BSA was diluted with media to form a range of known concentrations, including a blank sample (basal media only). Triplicate samples of the standards were mixed with the BCA working reagent in a 96-well plate and absorbance measured at 562nm wavelength after incubation at 37°C. Blank absorbance values were subtracted from each absorbance value before plotting into the standard curve. Values shown are mean ± SD.

2.15 Enzyme-linked immunosorbent assay (ELISA) to determine concentration of secreted factors

Commercial ELISA kits were utilised to measure the concentration of adipokines secreted by human omental adipose tissue, as well as, factors secreted by ovarian cancer cells after adipokine treatment. **Table 3** details the ELISA kits utilised in the study.

Table 3. Commercial ELISA kits used to quantify analytes in conditioned media from omental adipose tissue or adipokine-incubated ovarian cancer cells.

Sample tested	Analyte tested	Brand and product code
Conditioned media from omental adipose tissue	Adiponectin	Abcam (ab99968)
	Cathepsin L	Invitrogen (BMS257)
	Leptin	Invitrogen (KAC2281)
	MIF	Sigma-Aldrich (RAB0360)
	NGAL	Invitrogen (BMS2202)
Conditioned media from ovarian cancer cells pre-incubated with adipokines	FGF2	R&D Systems (DY233)
	TGF-β1	R&D Systems (DY240)
	VEGF	R&D Systems (DY293B)

The ELISA kits used for the adipose tissue conditioned media contained 12 x 8-well strip plates pre-coated with capture antibodies for the intended analyte; samples were added directly into the plates. However, the kits used to test the conditioned media from ovarian cancer cells required more preparation. Adhering to manufacturer's instructions, the capture antibodies were incubated in 8-well strip plates overnight and then blocked for an hour prior to sample addition.

After the sample incubation step, a biotinylated detection antibody was added to bind with the captured analyte. Streptavidin-HRP was then added to bind with the biotin. In the presence of HRP, the addition of substrate resulted in a blue

colour development; the more analyte bound, the stronger the colour. Addition of stop solution halted the HRP enzymatic reaction and the resultant yellow colour was measured with a spectrophotometer.

The analyte standards, supplied in the kit, were diluted to a range of concentrations as recommended by the manufacturer, with the plain diluent buffer as a zero standard (blank). As the amount of targeted analyte in the conditioned media was unknown, the conditioned media were diluted between 1:10 to 1:10,000 v/v with the supplied diluent buffer. The standards and the diluted conditioned media were applied to the wells in triplicate and treated according to the manufacturers' protocol, with the absorbance measured at 450nm. A minimum of three separate conditioned media samples were tested in each experimental run ($n \geqslant 3$).

The average absorbance values of the blank wells were subtracted from each of the analyte standard absorbance values before plotting into a standard curve on GraphPad's Prism. The absorbance of the conditioned media samples, after subtracting the average blank absorbance values, were interpolated from this standard curve to determine the analyte concentration. The analyte standards were freshly prepared for each experiment, and the resultant standard curve were utilised only for samples within the same plate.

Several repeats of this ELISA procedure were performed when the absorbance values of the conditioned media fell outside of the standard curve due to under- or over-dilution with the diluent buffer. In such cases, the dilution ratio was adjusted accordingly.

2.16 Antibody arrays to detect adipokines or phosphorylated cellular targets

Three different commercial antibody arrays were utilised in this study; all arrays were sourced from R&D Systems. The adipokine array kit (ARY024) were used to detect the adipokines secreted by omental adipocytes and omental adipose tissue. The phospho-kinase array kit (ARY003B and ARY003C) and the phospho-receptor tyrosine kinase (phospho-RTK) kit (ARY001B) were used to

examine kinase targets activated within HOMEC lysates after treatment with conditioned media.

The main component of these kits are the nitrocellulose membranes with pre-spotted control and capture antibodies for the defined target molecule (e.g. adipokines, kinases). Each type of antibody was spotted in duplicate. Ultimately, the relative amount of target analyte bound to these antibodies were quantified by chemiluminescence.

Unless otherwise noted, all reagents were supplied in the kit and the manufacturer's protocol was adhered to. Methods of sample preparation are explained in their relevant sections in chapters 3 and 4. Prior to use, the nitrocellulose membranes were incubated with a blocking buffer on a plate rocker for an hour. Thereafter, the membranes were incubated with their samples (conditioned media/ cell lysate) overnight on a plate rocker at 2-8°C.

In between multiple washing steps to eliminate any unbound material, biotinylated detection antibodies, streptavidin-HRP and chemiluminescent reagents were applied. The chemiluminescence emitted was captured using an Azure c500 Imaging System at varying exposures ranging from 2 to 10 minutes. The ImageJ programme was used to determine the chemiluminescent signal intensity by measuring the pixel density of each spot. Depending on the array type and after preliminary testing, it was determined that a chemiluminescence exposure time between 5 to 20 minutes was optimal for pixel density analysis. The desired membrane images should have clear contrast between the spots and membrane background (i.e. not underexposed), and the spots should not overlap each other (i.e. not overexposed).

To analyse the data, the images were first converted to 32-bit, which is the highest setting for non-colour images within ImageJ. The images were digitally magnified to 600% of its original size to better visualise the spots. A circular region of interest approximately 50% smaller than each spot, was drawn to define the boundaries of the measured pixel density. To account for background signal, the average pixel density values of the negative control spots were subtracted from each individual pixel density value. The reference spots on the membrane indicated that the streptavidin-HRP was correctly applied during the procedure as well as denoting the orientation of the membrane. An example of

the membrane coordinates and the chemiluminescent image of an antibody array is shown in **Figure 15**.

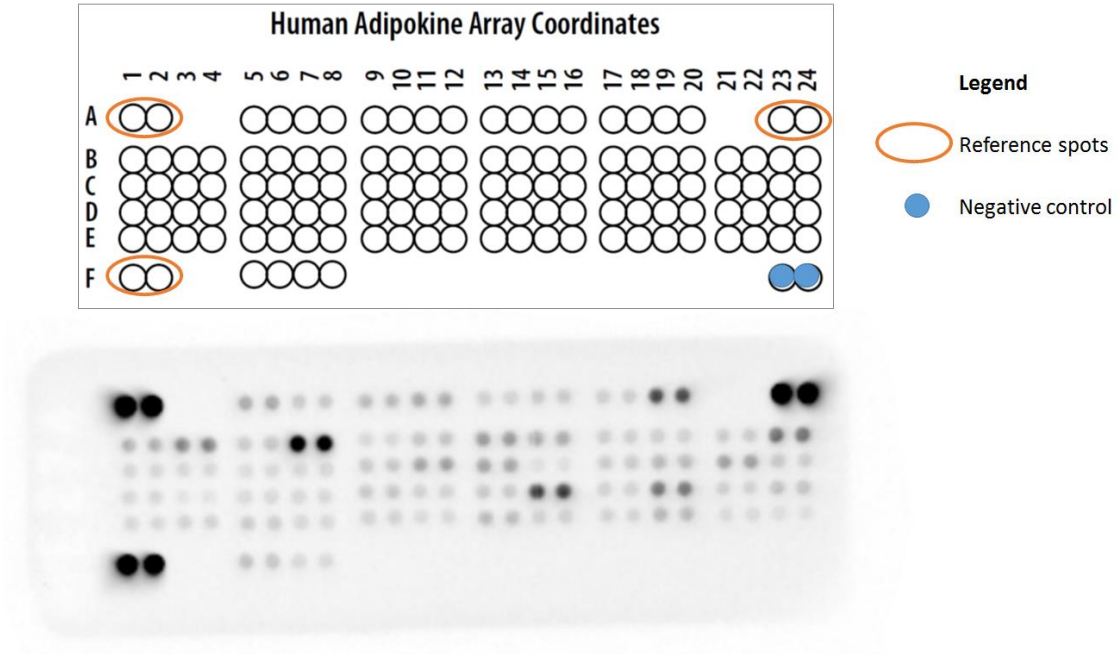

Figure 15. A sample chemiluminescent image of the adipokine antibody array membrane (bottom) with its corresponding coordinate grid (top). Each pair of spots represents a specific adipokine as indicated by the co-ordinates. The reference spots indicated the correct application of reagents and also orientated the membrane to match the coordinate grid. The negative control spots denoted background signal.

2.17 Experimental conduct and statistical analysis

In all experiments, each treatment condition was conducted in triplicate as a minimum (intra-experimental n ≥ 3). Experiments were conducted at least 3 times (inter-experimental n ≥ 3) unless otherwise noted. For example, the individual wells on a multiwell plate represent the intra-experimental n, and the multiwell plate itself represents the inter-experimental n. Unless indicated, all n numbers in the thesis refer to the inter-experimental n.

Data were entered into the Prism (GraphPad Inc) software. Only data with inter-experimental n of 3 and above were subjected to analysis using the Mann-Whitney U test. This non-parametric test was chosen as the experimental data

were in general not normally distributed; for instance, due to the relatively low inter-experimental n. A p-value of less than 0.05 ($p<0.05$) was considered statistically significant.

Chapter 3. An investigation into the pro-angiogenic effects of adipokines on human omental microvascular endothelial cells

3.1 Introduction

The major component of the omentum, a prime site of ovarian cancer metastasis, is the adipocytes. As discussed in section 1.5, adipocytes have multiple roles in tumour progression through the actions of their secreted adipokines. Therefore, metastatic tumour angiogenesis within the omentum may be driven, in part, by adipokine action on ECs.

Due to the heterogeneity in ECs mentioned in section 1.1.3c, especially in terms of their macrovascular versus microvascular origin, as well as their structure and function in different vascular beds, it is pertinent to utilise the appropriate ECs in in vitro experiments to resemble in vivo conditions more closely. Hence, disease-relevant ECs were required to study ovarian cancer metastasis and angiogenesis within the human omentum, specifically, human omental microvascular endothelial cells (HOMECs). In investigating angiogenesis, EC activation can be characterised by cell proliferation and migration.

This chapter investigates the crosstalk between ovarian cancer cells, adipokines and disease relevant ECs, and is divided into sections aimed at:

a) developing a more consistently reliable HOMEC isolation protocol (section 3.2.8);
b) assessing HOMEC proliferation when treated with omental adipose tissue and ovarian cancer conditioned media (section 3.3.3);
c) identifying and quantifying the adipokines secreted from omental adipocytes (section 3.3.4);
d) assessing HOMEC proliferation when treated with identified adipokines from (c) (section 3.3.5); and
e) assessing HOMEC migration in response to adipose tissue conditioned media and identified adipokines (section 3.3.6).

3.2 Methods

3.2.1 Developing a more consistently reliable human omental microvascular endothelial cell (HOMEC) isolation protocol

To obtain disease relevant ECs for further experiments, cells were isolated from human omentum samples. Although an existing protocol was in place in the laboratories, it was not found to be consistently reliable. Therefore, this section outlines the improvements made to the previous HOMEC isolation protocol.

The initial isolation protocol was that of Winiarski et al (2011),(278) which consisted of two digestion steps, filtration and then immunoselection. This protocol is summarised in **Figure 16** and described in section 2.4.1. Using this procedure, only one omental tissue sample out of 18 (6%) successfully yielded HOMECs; this prompted some adjustments to the protocol.

Several observations were noted of the initial isolation protocol:

- After the two-hour digestion with collagenase type I (step C, **Figure 16**), the enzyme-tissue mixture was strained through gauze swab layers in order to separate the undigested tissue from the digest solution which contained the HOMECs (step D, **Figure 16**). It could be seen that the undigested tissue was not substantially reduced in size when compared to pre-digestion, and the swab required manual compression to maximise the collection of the digest solution.
- After subjecting the cells to filtration with a 30µm nylon filter (step E, **Figure 16**), there were relatively few cells collected in the filter-wash medium. This was evident in the final culture post-immunoselection, where the anti-CD31 magnetic beads mostly appeared scattered rather than being aggregated. This implied that there were few ECs for the beads to adhere to.
- During the immunoselection step (step F, **Figure 16**), the magnetic beads were incubated with the cell suspension for 20 minutes. After multiple washings to remove cells which did not adhere to the beads, the selected cells were cultured in a well of a 6-well plate. The well appeared dense with magnetic beads and generally, more beads were observed than the actual number of cells.

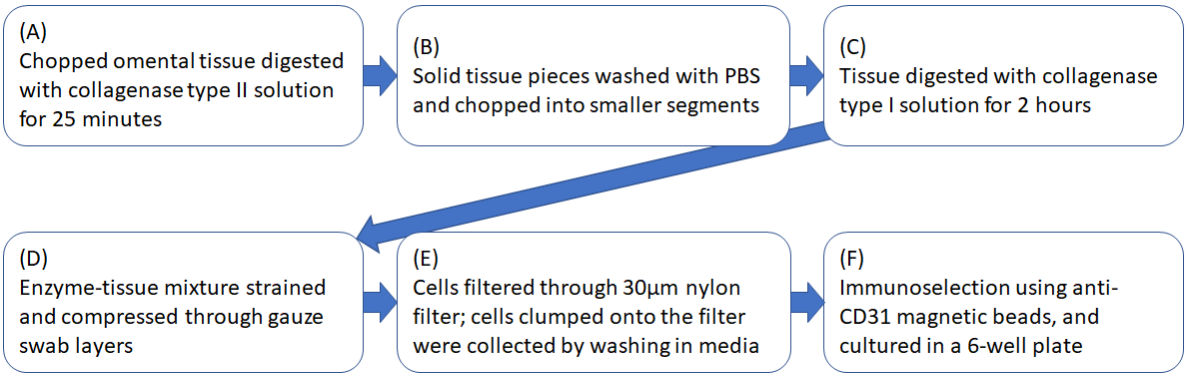

Figure 16. A schematic of the initial HOMEC isolation protocol. The protocol, adapted from Winiarski et al (2011),(278) consisted of two enzymatic digestion steps (A & C), filtration steps (D & E) and finally an immunoselection step (F) before culturing the isolated cells.

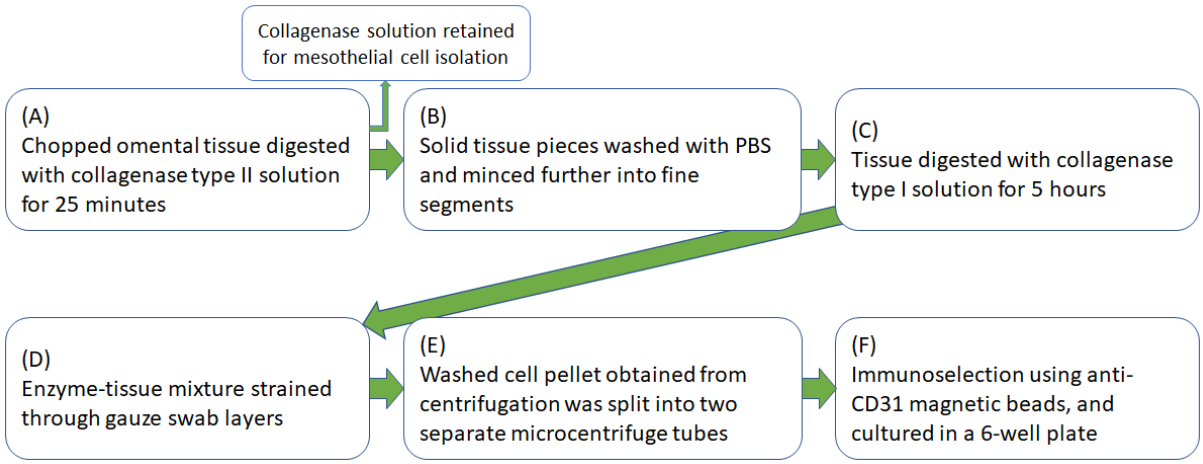

Figure 17. A schematic of the amended HOMEC isolation protocol. As with the initial protocol, this protocol also consisted of two enzymatic digestions (A & C), a filtration step (D) and an immunoselection step (F); however, the duration of enzymatic digestion was extended (C) and some filtration steps were omitted. Mesothelial cell isolation is detailed in chapter 5.

Based on these observations, the HOMEC isolation protocol was amended as follows (summarised in **Figure 17**):

- The duration of collagenase I digestion was extended to 5 hours (step C, **Figure 17**). Previous findings from the laboratory showed that the prolonged digestion did not significantly alter surface detection of the extracellular CD31 marker, which was essential to select ECs cells from

other cell types. The enhanced digestion resulted in less wastage of undigested tissue and in turn, a larger cell pellet for easier handling of subsequent steps. Additionally, with less volume of undigested tissue, the enzyme mixture strained easier through the gauze swab, without the need for compression (step D, **Figure 17**).

- The filtration through the 30µm nylon filter step was omitted to reduce cell loss via reduced handling.
- To optimise the immunoselection procedure, and to better process the larger cell pellet obtained, the pellet was split into two microcentrifuge tubes prior to addition of the magnetic beads (step E, **Figure 17**). Each tube was mixed with 3µL of anti-CD31 bead suspension, and allowed to mix for 40 minutes at 4°C. As the cell : bead ratio was greater than that from the earlier protocol, the duration of mixing was increased to enhance antibody binding. Ultimately each tube was cultured in a well of a 6-well plate. The advantage is twofold; fewer magnetic beads were used per well, and with two wells there were higher number of cells to expand the population.

The final protocol used for the isolation of HOMECs from omental tissue is described in section 2.4.2.

3.2.2 Immunocytochemistry

Due to the changes to the initial protocol, it was necessary to confirm that the isolated cells were of an EC phenotype. The cells were therefore stained for cell membrane markers (CD31, occludin), as well as, intracellular markers (von Willebrand factor, vimentin)(278, 281, 282) and visualised with immunocytochemistry using methods detailed in section 2.9.

3.2.3 General experimental methods

HOMEC seeding and treatment were performed as described in section 2.10. Conditioned medium (CM) was collected as described in section 2.7. To assess cell proliferation, BrdU and WST8 assays were performed as described in

sections 2.11 and 2.12 respectively. To assess cell migration, a scratch wound healing assay was performed as described in 2.13.

3.2.4 Method development - assessment of HOMEC proliferation using the bromodeoxyuridine (BrdU) assay

The principle of the BrdU assay was described in section 2.11. In initial experiments, after the treatment media were added to the HOMECs (section 2.10), the BrdU reagent was added two hours later to all wells except those designated as background wells. The cells were then incubated at 37°C/5% CO_2 for a further 20 to 22 hours (manufacturer's protocol states 2 to 24 hours).

With this BrdU incubation duration, the BrdU incorporation was similar for cells treated with complete growth medium and those treated with starvation medium (<20% difference). However, cells in complete growth medium were expected to show greater proliferation compared to the latter, since starvation media would be expected to arrest or impede cell growth. It was possible that this observation was due to the prolonged BrdU incubation time; i.e. allowed enough time, cells in the starvation medium may incorporate nearly the same total level of BrdU into their DNA as those in the complete growth medium.

Therefore, an experiment to determine the optimum BrdU incubation duration was performed. The BrdU reagent was added at various time points after the start of treatment, and the cells were incubated with BrdU for varying lengths of time (**Table 4**). It was observed (**Figure 18**) that the addition of BrdU after at least 24 hours of cell growth allowed for a greater differentiation between cells grown in starvation and complete growth media. Based on these data, in subsequent experiments on HOMECs, BrdU was applied after 24 hours of treatment, with a minimum BrdU incubation time of 6 hours.

The final BrdU protocol used for determining cell proliferation is described in section 2.11.

Table 4. Design of an experiment to determine optimum timing for BrdU addition. The experimental design of Plate 1 was the same as that previously described, while Plates 2 to 4 examine BrdU incorporation in HOMECs at different time points and with varying incubation duration.

Plate	Time period between treatment addition and BrdU addition	BrdU incubation time prior to cell fixation
Plate 1	2 hours	21 hours
Plate 2	8.5 hours	14.5 hours
Plate 3	24 hours	6 hours
Plate 4	26 hours	21 hours

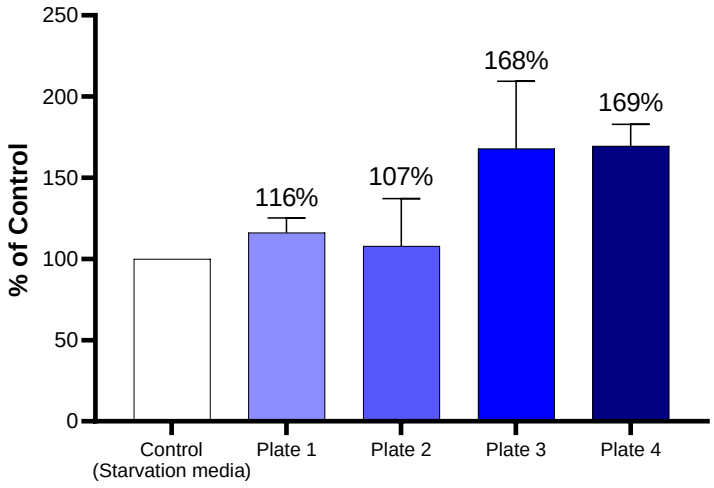

Figure 18. Addition of BrdU after 24 hours of cell growth is optimum for assessment of HOMEC proliferation. HOMECs were seeded in complete growth medium (10,000 cells/well) in 96-well plates and cultured for at least 24 hours prior to overnight serum starvation in 1% (v/v) FBS media. Freshly prepared starvation media (control) and complete growth media (Plates 1-4) were used as treatments. BrdU was applied after 2 hours (Plate 1), 8.5 hours (Plate 2), 24 hours (Plate 3) or 26 hours (Plate 4); and cells fixed after 21 hours (Plate 1 and Plate 4), 14.5 hours (Plate 2) or 6 hours (Plate 3) after BrdU application. Results shown are mean ± SD and expressed as percentage of the control; intra-experimental n=3-6.

3.2.5 Method development - assessment of HOMEC migration using the scratch wound healing assay

EC migration is also a hallmark of angiogenesis and thus migration of HOMECs in response to adipose tissue CM was investigated. Although initial studies were carried out as described in section 2.13, it was found that the analysis methodology needed to be improved.

Initially, all the time-lapse images from the scratch assay were analysed with the wound healing application on the JuLI™ Stat Cell Analysis Software. In setting up this application to measure scratch closure, measurement thresholds (background and sensitivity) were individually adjusted for each well. In all experiments, the background and sensitivity settings ranged from levels 1 to 4, and 7 to 10, respectively. The resultant analyses were generated as a percentage of wound closure over time. However, using this method, it was found that the boundaries of the scratch wound were not accurate, as detailed in **Figure 19**, and this affected the closure percentage calculations.

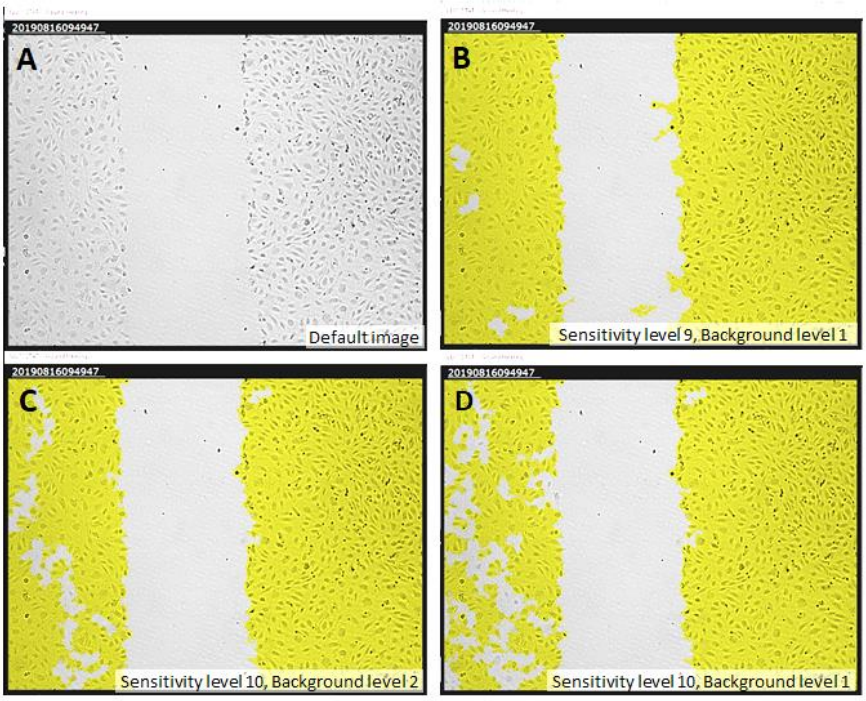

Figure 19. Representative images showing the difficulty in setting the measurement thresholds to define the scratch wound boundary. The yellow-shaded regions depict the presence of cells, while the non-coloured regions depict the scratch wound. It can be seen that when the default image (A) was subjected to different sensitivity and background settings (B-D) on the JuLI™ Stat Cell Analysis Software, the software-generated boundaries differed substantially and were not accurate.

Therefore, an analysis methodology with the ImageJ software was developed as an alternative. As all the time-lapse images were taken on the same device, the specifications of each image were set to 8-bit with dimensions of 1936 x 1456 pixels. The area of the scratch wound was manually selected using the 'freeform selection tool' (example in **Figure 20**) and then measured in square pixels. This method of measurement is more accurate than the default analysis software. In further experiments to measure HOMEC migration, all images at the 0, 12 and 20 hour time points were analysed in this manner and compared.

The final protocol used for determining cell migration is described in section 2.13.

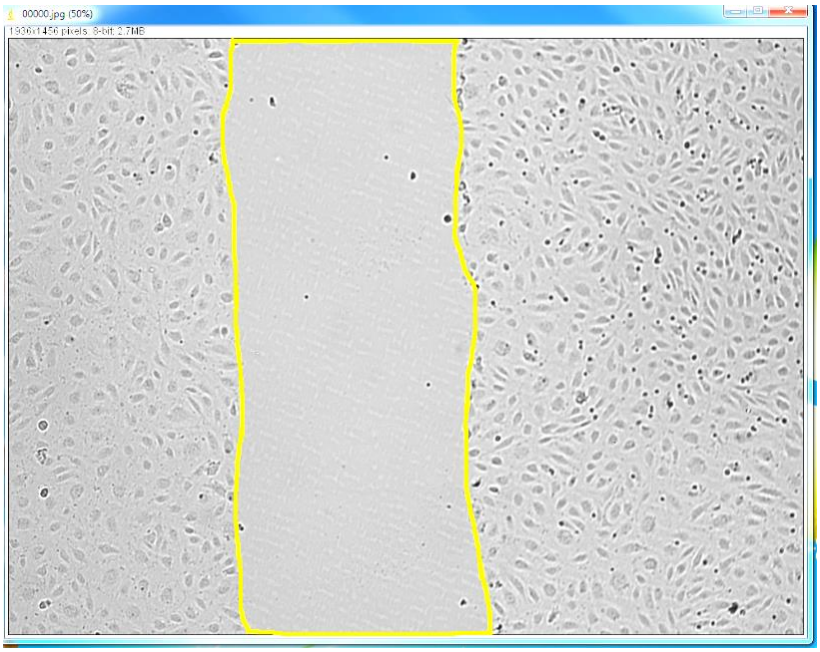

Figure 20. Representative image shows how the scratch wound boundary was manually selected. The freeform selection tool in the ImageJ software was utilised to select the region of interest. The selected yellow-edged region was determined as the scratch wound and the area measured in square pixels.

3.2.6 Determination of protein concentration in omental adipocyte and adipose tissue conditioned media

Secreted adipokines present in the omental adipocyte and adipose tissue CM (collected as described in section 2.7) were identified using a commercially available adipokine antibody array. Since this required a fixed amount of proteins/adipokines (200µg) per sample, the protein concentration in the CM was determined using the BCA assay as described in section 2.14.

Both adipocyte and adipose tissue CM were examined due to the difficulty of handling and quantifying the omental adipocytes compared to the adipose tissue samples. The latter could be easily weighed, and the CM collection was standardised at 1g/mL (detailed in section 2.7.1); such standardisation was not possible with the isolated adipocytes due to their adhesiveness and low density.

3.2.7 Identification of adipokines using an antibody array

A commercial adipokine array kit (ARY024, R&D Systems) was utilised to identify secreted adipokines. The array consists of nitrocellulose membranes with antibodies specific for 58 different human adipokines, and functions as a screening tool to detect adipokines present in a sample.

For sample preparation, a volume of CM corresponding to 200µg of protein, as determined by the BCA protein assay, was diluted to 1mL with the supplied blocking buffer. The same volume of basal media served as control and was diluted in the same manner. The samples were loaded onto the membranes supplied in the kit and processed according to the manufacturer's instructions. The signal intensity of the adipokine spots in the control (basal media only) and the adipocyte or adipose tissue CM samples were then compared (detailed in section 2.16).

A diagram of the array membrane and the corresponding adipokine coordinates are shown in **Figure 21**.

(A)

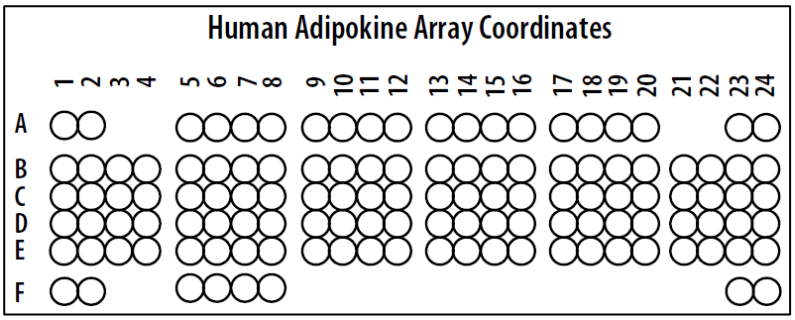

(B)

Membrane coordinates	Adipokine	Membrane coordinates	Adipokine
A1, A2, A23, A24, F1, F2	Reference spots	F23, F24	Negative controls
A5, A6	Adiponectin	C19, C20	IL-6
A7, A8	Angiopoietin-1	C21, C22	IL-8
A9, A10	Angiopoietin-2	C23, C24	IL-10
A11, A12	Angiopoietin-like 2	D1, D2	IL-11
A13, A14	Angiopoietin-like 3	D3, D4	Transforming growth factor beta 1 (TGF-β1)
A15, A16	B-cell activating factor/ CD257	D5, D6	Leptin
A17, A18	Bone morphogenic protein 4 (BMP4)	D7, D8	Leukaemia inhibitory factor (LIF)
A19, A20	Cathepsin D	D9, D10	Lipocalin-2/ NGAL
B1, B2	Cathepsin L	D11, D12	Monocyte Chemoattractant Protein-1 (MCP-1)
B3, B4	Cathepsin S	D13, D14	Colony stimulating factor 1 (CSF1)
B5, B6	Chemerin	D15, D16	Macrophage migration inhibitory factor (MIF)
B7, B8	Complement factor D (CFD)	D17, D18	Myeloperoxidase
B9, B10	C-reactive protein (CRP)	D19, D20	Nidogen-1/ Entactin
B11, B12	Dipeptidyl peptidase-4 (DPP-IV)/ CD26	D21, D22	Oncostatin M
B13, B14	Endocan	D23, D24	Pappalysin-1
B15, B16	Calgranulin C	E1, E2	Visfatin
B17, B18	Fetuin B	E3, D4	Pentraxin-3
B19, B20	Prostatropin/ FGF-2	E5, E6	Preadipocyte factor 1 (Pref1)
B21, B22	FGF-19	E7, E8	Proprotein Convertase 9
B23, B24	Fibrinogen	E9, E10	RAGE
C1, C2	Somatotropin	E11, E12	CCL5/ RANTES
C3, C4	Hepatopoietin A/ HGF	E13, E14	Resistin
C5, C6	Intercellular Adhesion Molecule 1 (ICAM-1)/ CD54	E15, E16	Angiotensinogen/ serpin A8
C7, C8	Insulin-like growth factor-binding protein 2 (IGFBP-2)	E17, E18	Serpin A12
C9, C10	IGFBP-3	E19, E20	Serpin E1
C11, C12	IGFBP-4	E21, E22	TIMP metallopeptidase inhibitor 1 (TIMP-1)
C13, C14	IGFBP-6	E23, E24	TIMP-3
C15, C16	IGFBP-7	F5, F6	TNF-α
C17, C18	Interleukin-1 beta (IL-1β)	F7, F8	Vascular endothelial growth factor (VEGF)

Figure 21. A diagram of the adipokine array membrane (A) and the coordinates of the 58 adipokines analysed (B). Information adapted from the package insert of the Proteome Profiler™ Array (R&D Systems, ARY024)

3.2.8 Quantification of adipokines using ELISA

Adipose tissue CM from at least 3 different omental samples were examined in each ELISA kit (adiponectin, cathepsin L, leptin, lipocalin-2, and MIF). The ELISA protocol is detailed section 2.15, and the resultant standard curves of the tested adipokines are shown in **Figure 22**.

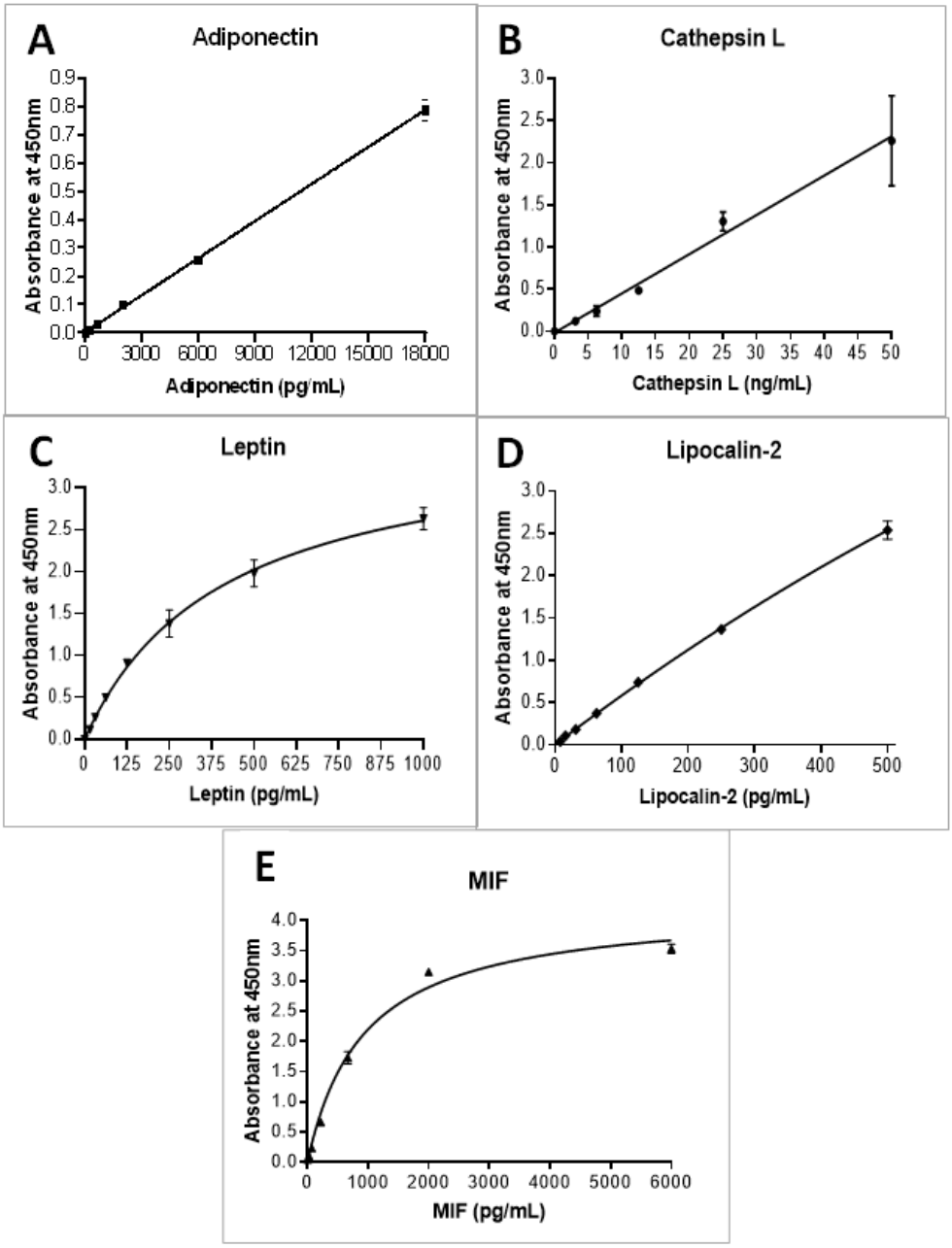

Figure 22. Representative ELISA standard curves for adiponectin (A), cathepsin L (B), leptin (C), lipocalin-2 (D) and MIF (E). The protein concentration of the conditioned media samples were interpolated from these standard curves based on their absorbance values. For each kit, the supplied protein standards were diluted to the recommended range of concentrations, assayed by ELISA on 96-well plates and the absorbance was then read at 450nm. Absorbance values shown are mean ± SD (n=2).

3.2.9 Investigating proliferation in HOMECs incubated with conditioned media from adipokine-incubated ovarian cancer cells

Ovarian cancer cells were seeded in 12-well plates in complete growth media (7000 cells/well for SKOV3, 15000 cells/well for A2780) and cultured for 5 days until 70-80% confluent. For both the cancer cell lines to achieve similar levels of confluence, a higher number of A2780 cells was required at seeding since the latter are smaller cells; by eye, A2780 cells have a cell diameter approximately half that of SKOV3 cells. Once confluent, each well was rinsed once with warmed PBS prior to addition of treatment media at 1200µL/well. Treatment consisted of the individual adipokines diluted in starvation media, at a mid-range concentration detected via ELISA (section 3.2.6); i.e. adiponectin 5µg/mL, cathepsin 6ng/mL, MIF 1 µg/mL, leptin 3ng/mL, and lipocalin-2 3ng/mL. The ovarian cancer cells were incubated at 37°C/5% CO_2 with the adipokine treatment for 24 or 48 hours. As a control, starvation media alone were used to treat the ovarian cancer cells in place of the adipokines.

The CM from treated SKOV3 or A2780 were collected and centrifuged at 437*g* for 5 minutes to remove any cell debris, before being transferred to fresh microcentrifuge tubes. The CM were then added as treatments onto HOMECs f(which were processed beforehand according to section 2.10) for a duration of 24 hours, and HOMEC proliferation was assessed using WST8 and BrdU assays. A schematic of the experiment design is shown in **Figure 23**.

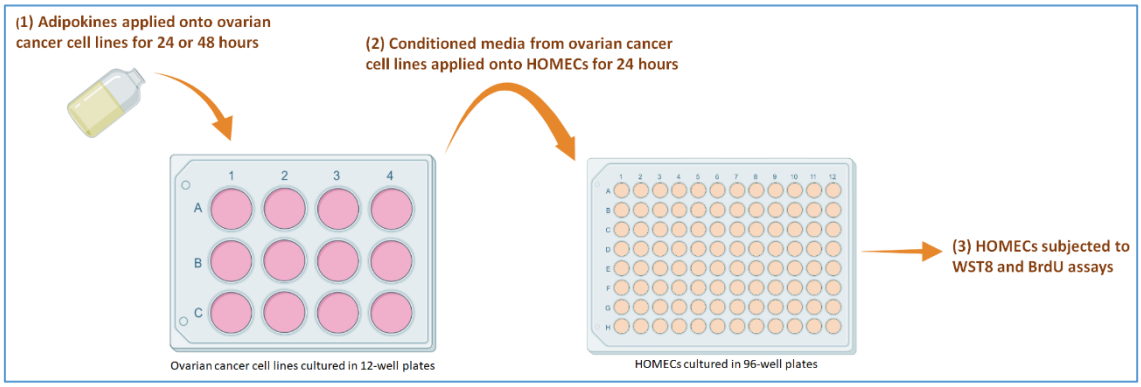

Figure 23. The experiment protocol for assessing proliferation in HOMECs incubated with conditioned media from adipokine-incubated ovarian cancer. Adipokines diluted in starvation media were applied onto ovarian cancer cells; cancer cells treated with starvation media alone acted as a control. After 24 or 48 hours of incubation, this media was collected from the cancer cells and applied onto the HOMECs. Proliferation was assessed after 24 hours using WST8 and BrdU assays. Figure created with BioRender.com.

3.3 Results

3.3.1 Cell isolation using the amended HOMEC isolation protocol

With the amended protocol described in section 3.2.1, the HOMEC yield was improved. The cell pellet obtained was visibly larger, which necessitated its apportionment into two microcentrifuge tubes for the immunoselection step. The selected cells were seeded in a larger growth area (in two wells of a 6-well plate, as opposed to one well in the earlier protocol) and the higher cell numbers allowed for successful first passage. When transferring or expanding the cell population, if other cell contaminants were observed under microscope e.g. fibroblasts most commonly, another magnetic immunoselection was performed to purify the HOMEC population.

Using this improved protocol, 7 of 12 omental tissue samples successfully yielded HOMECs i.e. a success rate of nearly 60%. Representative photographs of successfully isolated cells are shown in **Figure 24**. For subsequent experiments, HOMECs were used up until the seventh passage. This was based on a previous finding that their endothelial morphology was retained at passage 7;(283) and immunocytochemistry performed showed similar patterns of staining to HOMECs at lower passages.

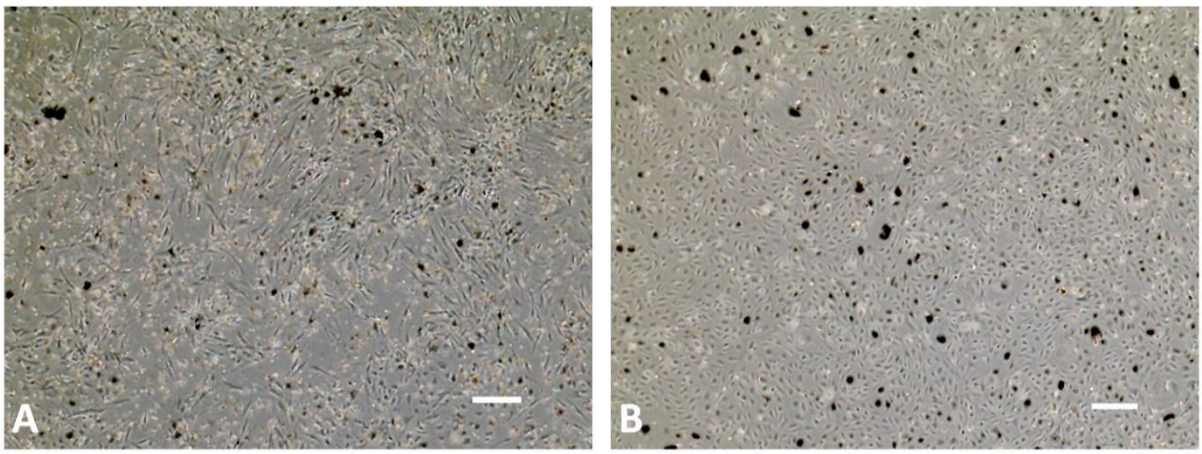

Figure 24. Images of HOMECs isolated using the amended protocol. Images, captured at 4x magnification with EVOS XL Core, show isolated HOMECs with magnetic anti-CD31 beads seen as black dots. Isolated HOMECs after 10 days in culture (A) and first passage HOMECs after a second immunoselection step (B). Scale bar 200µm.

3.3.2 Characterisation of the isolated cells via immunocytochemistry

Immunocytochemistry confirmed the endothelial phenotype of the cells isolated from the omentum, as depicted in **Figure 25** and **Figure 26**. The isolated cells expressed CD31, occludin, von Willebrand factor (vWF) and vimentin.

Immunocytochemistry performed on previously frozen and thawed HOMECs, as well as HOMECs at passage 7 showed similar results to **Figure 25 and Figure 26**.

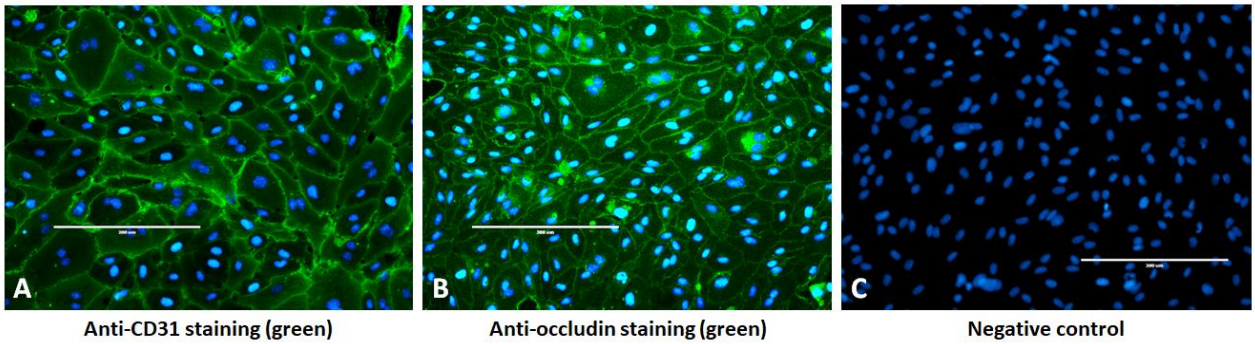

Figure 25. Isolated HOMECs expressed CD31 and occludin. HOMECs were seeded at 10,000 cells/well in 8-well chamberslides and cultured to confluence. Cells were fixed with 4% (v/v) paraformaldehyde and incubated overnight with primary antibodies (anti-CD31, A, and anti-occludin, B), or PBS for control; followed by incubation with fluorescent-conjugated secondary antibodies (green). Cell nuclei were stained blue with DAPI. After mounting with coverslips, slides were visualised via fluorescence microscopy. The negative control (C) shows background level of staining with PBS in place of anti-CD31 primary antibody (identical results were seen with PBS instead of anti-occludin antibody). Data show representative images, captured at 10x magnification with EVOS Fluo, of one experiment which was repeated twice on different HOMEC populations with similar results. Scale bar 200µm.

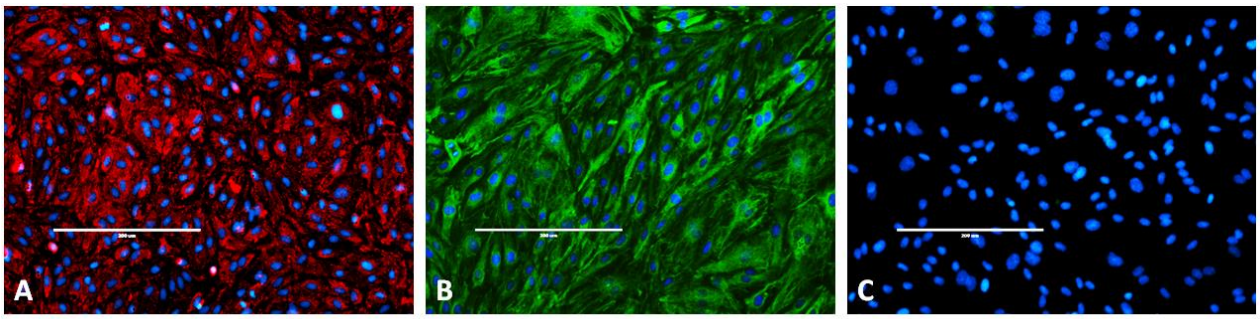

Figure 26. Isolated HOMECs expressed von Willebrand factor (vWF) and vimentin. HOMECs were seeded at 10,000 cells/well in 8-well chamberslides and cultured to confluence. Cells were fixed with 4% (v/v) paraformaldehyde at room temperature and then permeabilised with methanol at -20°C. Cells were incubated overnight with primary antibodies (anti-vWF, A, and anti-vimentin, B), or PBS for control; followed by incubation with fluorescent-conjugated secondary antibodies. Cell nuclei were stained blue with DAPI. After mounting with coverslips, slides were visualised via fluorescence microscopy. The negative control (C) shows background level of staining with PBS in place of anti-vWF primary antibody (identical results were seen with PBS instead of anti-vimentin antibody). Data show representative images, captured at 10x magnification with EVOS Fluo, of one experiment which was repeated twice on different HOMEC populations with similar results. Scale bar 200µm.

3.3.3 The effect of conditioned media on HOMEC proliferation

The improved isolation protocol provided a reliable source of HOMECs for use in subsequent experiments. Initial studies aimed to assess whether secreted mediators from adipocytes and ovarian cancer cells induced ECs responses associated with angiogenesis, specifically proliferation, in HOMECs.

a) The effect of conditioned media from adipose tissue on HOMEC proliferation

To test the hypothesis that factors secreted from the adipose tissue promoted HOMEC activation, BrdU and WST8 proliferation assays were performed. The HOMECs were seeded and treated according to section 2.10. The adipose tissue CM was diluted to 1:2, 1:5 and 1:10 with starvation media prior to HOMEC treatment; the control received starvation media alone. The dilutions were necessary because in early experiments, adding the undiluted CM resulted in HOMEC death, as assessed by microscopy.

The effects of adipose CM on HOMEC proliferation assessed by BrdU assay are shown in **Figure 27**. Incubation with 1:2 and 1:5 diluted adipose tissue CM significantly increased HOMEC proliferation by more than 120% compared to the control (100%), $p<0.05$. Although not statistically significant, HOMEC proliferation was also increased by 88% when treated with the 1:10 diluted CM.

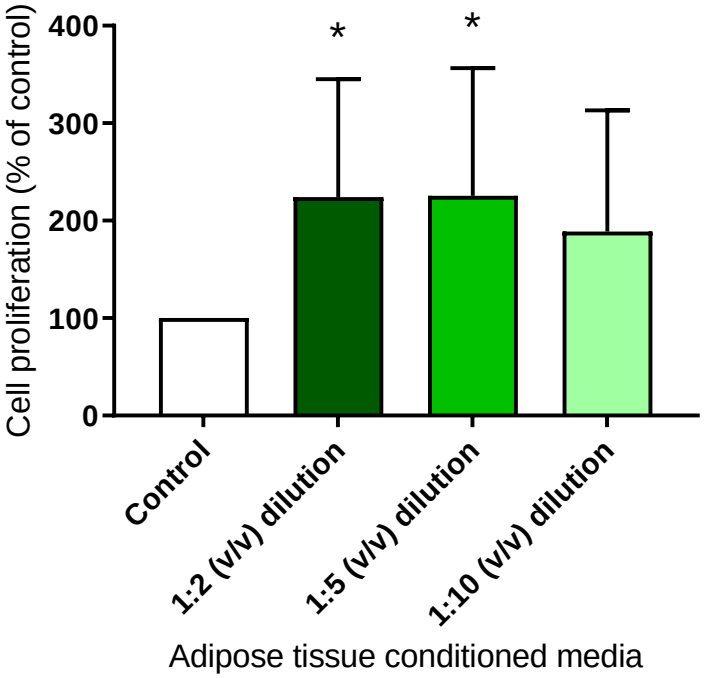

Figure 27. Omental adipose tissue conditioned media enhanced HOMEC proliferation as assessed by BrdU assay. HOMECs were seeded at 10,000 cells/well in 96-well plates and cultured for at least 24 hours before overnight serum starvation. Diluted adipose tissue conditioned media was added to the cells and the BrdU reagent added after 24 hours. Cells were fixed after 6 hours; plates were read at 450nm. Results shown are mean ± SD and expressed as percentage of the control; data were analysed with Mann-Whitney U tests. n=6-12; *$p<0.05$ vs control.

To complement the BrdU assay, the WST8 proliferation assay was also performed whereby the HOMECs were treated with diluted CM for 24, 48 or 72 hours. The results of the WST8 assays are shown in **Figure 28**. HOMEC proliferation was increased by at least 5% compared to control (100%) when treated with adipose tissue CM at all timepoints. At the 24- and 48-hour timepoints, the increase in HOMEC proliferation was statistically significant after treatment with 1:10 diluted CM (increases of 8% at 24 hours and 11% at 48

hours, compared to their respective controls, p<0.05). At the 72-hour timepoint, all concentrations of CM induced statistically significant increases in HOMEC proliferation; the 1:2 dilution induced a 23% increase in proliferation, 1:5 dilution a 17% increase, and the 1:10 dilution a 13% increase; all p<0.05.

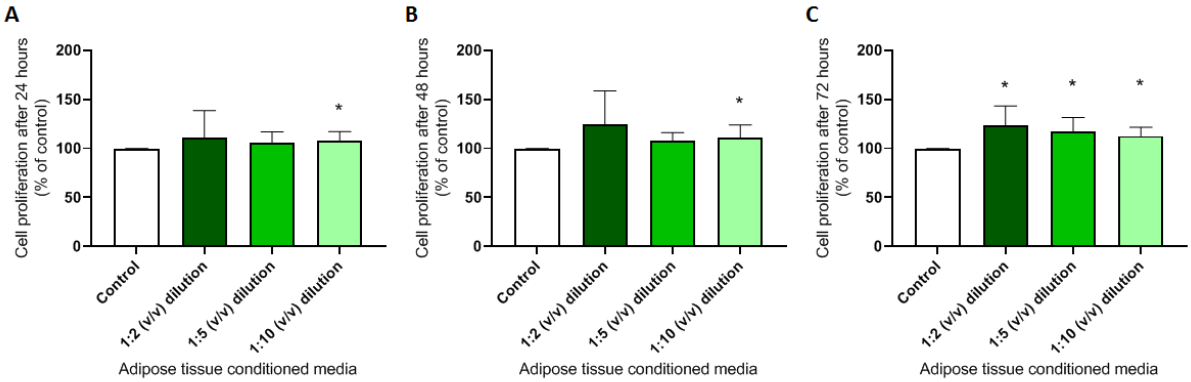

Figure 28. Omental adipose tissue conditioned media enhanced HOMEC proliferation as assessed by WST8 assay. HOMECs were seeded at 10,000 cells/well in 96-well plates and cultured for at least 24 hours before overnight serum starvation. Diluted adipose tissue conditioned media was then added to the cells and WST8 reagent added after treatment incubation for 24 (A), 48 (B) or 72 (C) hours. Plates were then read at 450nm after 2 hours. Results shown are mean ± SD and expressed as percentage of the control; data were analysed with Mann-Whitney U tests. n=8; *p<0.05 vs control.

These data indicate that factors secreted from omental adipose tissue induced HOMEC proliferation as assessed by two different assay protocols. At 24 hours, the 1:2 and 1:5 dilution of CM significantly increased the rate of DNA synthesis of the HOMECs (based on the BrdU assay), while after 72 hours of treatment all three dilutions significantly increased proliferation as assessed by cell metabolism (based on the WST8 assay). Therefore, the secreted factors responsible were investigated further in section 3.3.4.

b) The effect of adipose tissue conditioned media plus conditioned media from ovarian cancer cells on HOMEC proliferation

The data described in the previous subsection indicate that factors secreted from omental adipocytes induced proliferation of HOMECs, which suggests that the omental environment contributes to a switch to a more activated and pro-angiogenic endothelial phenotype. In vivo, during ovarian cancer cell metastasis to the omentum it is possible that this phenotype is also induced by factors secreted from the cancer cells themselves as previously discussed in section 1.3.5.

Therefore, HOMEC proliferation was also assessed after treatment of cells with ovarian cancer CM. CM were collected from two different ovarian cancer cell lines (section 2.7.3). The SKOV3 cell line was originally derived from the ascitic fluid of ovarian adenocarcinoma,(284) and represents metastatic cells; while the A2780 cell line was derived from an adenocarcinoma tumour in untreated ovarian cancer.(285)

To assess HOMEC proliferation, cells were seeded and treated as described in section 2.10. Ovarian cancer CM were diluted with starvation media to a 1:2, 1:5 and 1:10 concentration. Additionally, in some treatments, CM from the ovarian cancer cells and the adipose tissue were mixed prior to treating the HOMECs. For all treatments, proliferation was assessed by BrdU and WST8 assays, and the results shown in **Figure 29**, **Figure 30** and **Figure 31**.

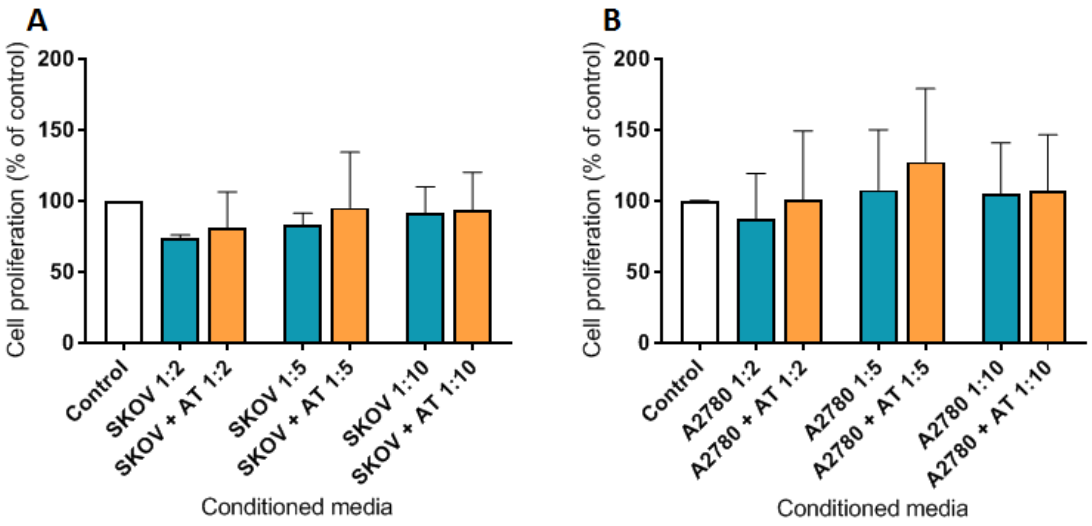

Figure 29. SKOV3 and A2780 conditioned media, alone or in combination with adipose tissue conditioned media did not enhance HOMEC proliferation as assessed by BrdU assay. HOMECs were seeded at 10,000 cells/well in 96-well plates and cultured for at least 24 hours before overnight serum starvation. The diluted conditioned media from SKOV3 (A) and A2780 (B) were applied onto cells as indicated, and the BrdU reagent added after 24 hours. Cells were fixed after 6 hours; plates were read at 450nm. Results shown are mean ± SD and expressed as percentage of the control; data were analysed with Mann-Whitney U tests, n=3. SKOV: SKOV3 conditioned media; A2780: A2780 conditioned media; AT: adipose tissue conditioned media.

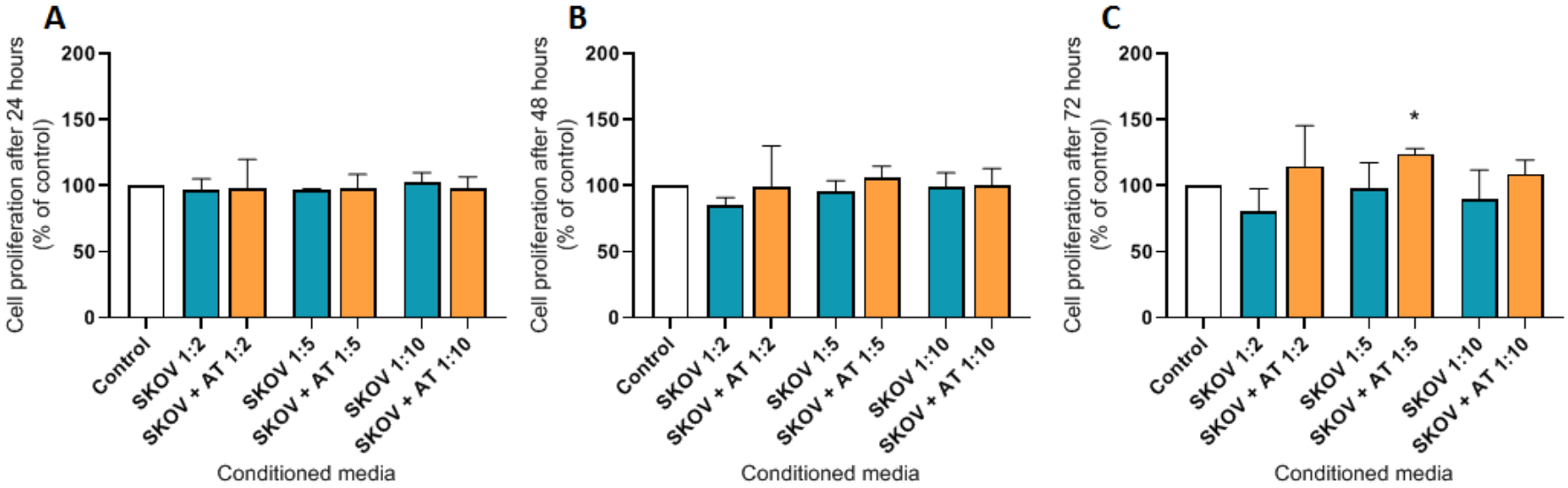

Figure 30. SKOV3 conditioned media alone or in combination with adipose tissue conditioned media did not enhance HOMEC proliferation as assessed by WST8 assay. HOMECs were seeded at 10,000 cells/well in 96-well plates and cultured for at least 24 hours before overnight serum starvation. Cells were then treated with conditioned media as indicated. WST8 reagent was added after treatment incubation for 24 (A), 48 (B) or 72 (C) hours, and plates were read at 450nm after 2 hours. Results shown are mean ± SD and expressed as percentage of the control; data were analysed with Mann-Whitney U tests, n=3; *p<0.05 vs control. SKOV: SKOV3 conditioned media; AT: adipose tissue conditioned media.

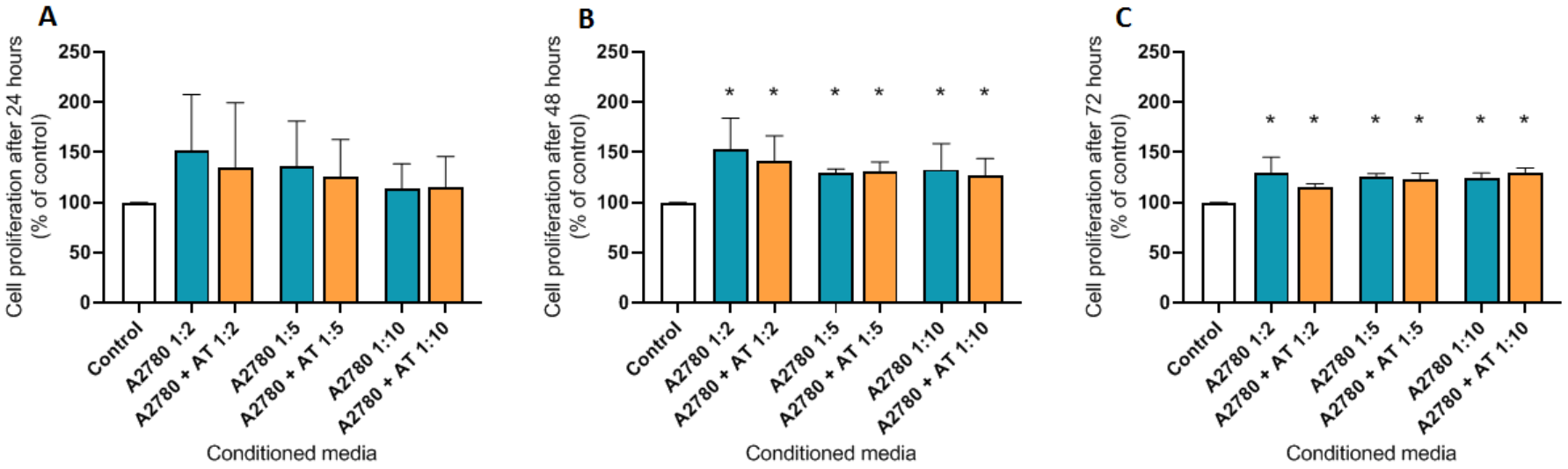

Figure 31. A2780 conditioned media alone or in combination with adipose tissue conditioned media enhanced HOMEC proliferation after 48 and 72 hours as assessed by WST8 assay. HOMECs were seeded at 10,000 cells/well in 96-well plates and cultured for at least 24 hours before overnight serum starvation. Cells were then treated with conditioned media as indicated. WST8 reagent was added after treatment incubation for 24 (A), 48 (B) or 72 (C) hours, and plates were read at 450nm after 2 hours. Results shown are mean ± SD and expressed as percentage of the control; data were analysed with Mann-Whitney U tests, n=3; *p<0.05 vs control. A2780: A2780 conditioned media; AT: adipose tissue conditioned media.

At 24 hours, the CM from neither ovarian cancer cell line significantly increased HOMEC proliferation in either assay (**Figure 30** and **Figure 31**). In fact, data from the BrdU assay indicate that SKOV3 CM treatment appeared to reduce HOMEC proliferation compared to control (**Figure 29A**), although this was not statistically significant. For example, treatment with the 1:2 dilution of SKOV3 CM reduced HOMEC proliferation to 73% compared to the control, treatment with the 1:5 dilution was 83% and treatment with the 1:10 dilution was 91%; all $p>0.05$.

Interestingly, CM from SKOV3 cells, which are derived from a metastatic tumour, also had no effect on HOMEC proliferation at the later time points (48 and 72 hours) studied by WST8 (**Figure 30B** and **Figure 30C**). In contrast, treatment with CM from A2780, a cell line derived from the primary ovarian tumour, significantly increased HOMEC proliferation after 48 and 72 hours in the WST8 assay (**Figure 31B** and **Figure 31C**). HOMEC proliferation was enhanced by up to 52% (1:2 dilution) compared with control after 48 hours, and up to 30% (1:2 dilution) after 72 hours, all $p<0.05$. At the 24-hour timepoint in the WST8 assay, none of the dilutions of CM from A2780 significantly enhanced HOMEC proliferation.

To better recreate the in vivo environment cells were treated with both adipose and cancer cell CM. In general, the combination of CM did not enhance proliferation above that observed with just cancer cell CM alone. The only exception was at the 72-hour timepoint in the WST8 assay (**Figure 30C**) when a combination of SKOV3 and adipose tissue CM increased HOMEC proliferation by 19 to 34 percentage points vs SKOV3 CM treatment alone at the different dilutions. Of these, only the combination CM at 1:5 dilution was significant (a 24% increase vs control 100%, $p<0.05$).

These results suggest that there are differences between the factors secreted into the CM of SKOV3 and A2780, which are discussed in section 3.4.4b.

3.3.4 Identification and quantification of adipokines in omental adipose tissue conditioned media

Since the data demonstrated that omental adipose tissue CM induced HOMEC proliferation, an investigation was carried out to elucidate which of the factors/ adipokines secreted into the CM caused this effect. This was initially investigated using adipokine antibody arrays and confirmed by ELISA (methods described in sections 3.2.7 and 3.2.8).

a) Protein concentration in omental adipocyte and adipose tissue conditioned media

Prior to testing the omental and adipose tissue conditioned media in the adipokine antibody array, the total secreted protein concentration in the CM was determined using the BCA assay (section 3.2.6).

From the BCA assay, the concentration of total protein secreted into adipose tissue CM (from 1g/mL, i.e. tissue weight per media volume) varied between donor samples, ranging from 1800µg/mL to 3800µg/mL (n=4). Total protein secreted from adipocytes (when standardised to 1g/mL of adipocyte weight per media volume), ranged from 5100µg/mL to 8800µg/mL (n=2).

Weight for weight, the amount of protein secreted from the adipocytes appeared higher than that of the adipose tissue; possibly because an isolated population of adipocytes is more densely packed compared to the adipose tissue due to the absence of connective tissue, and that adipose tissue is mostly composed of adipocytes (286) (this was supported by results obtained in the subsequent section).

b) Adipokines detected in omental adipocytes and adipose tissue conditioned media as assessed by adipokine array

A range of proteins were secreted from both the omental adipose tissue and the isolated adipocytes (**Figure 32** and **Figure 33**). These included growth factors, hormones, enzymes and other cell signalling molecules. The results are shown in **Figure 33**, presented in average pixel density values as a percentage of the control.

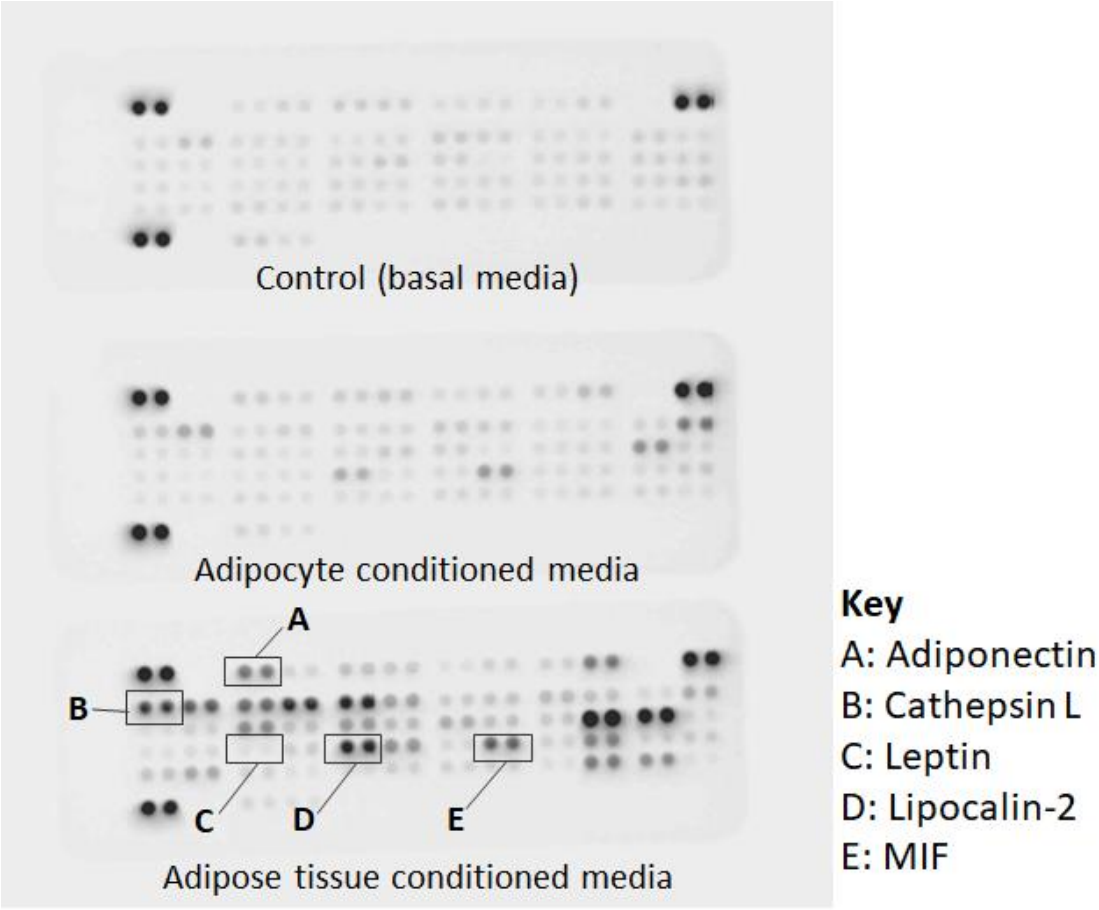

Figure 32. Sample membrane images obtained using an adipokine array with a ten-minute exposure time. Conditioned media and basal media were incubated with the antibody-spotted adipokine array membrane overnight. Detection antibodies, streptavidin-HRP and chemiluminescent reagents were applied in between multiple washings, and the membranes imaged on the Azure 500 imager. The membrane incubated with adipose tissue conditioned media showed more contrasting spots compared to that incubated with adipocyte conditioned media and basal media (control). Key adipokines are labelled to show their position on the membrane.

.

A

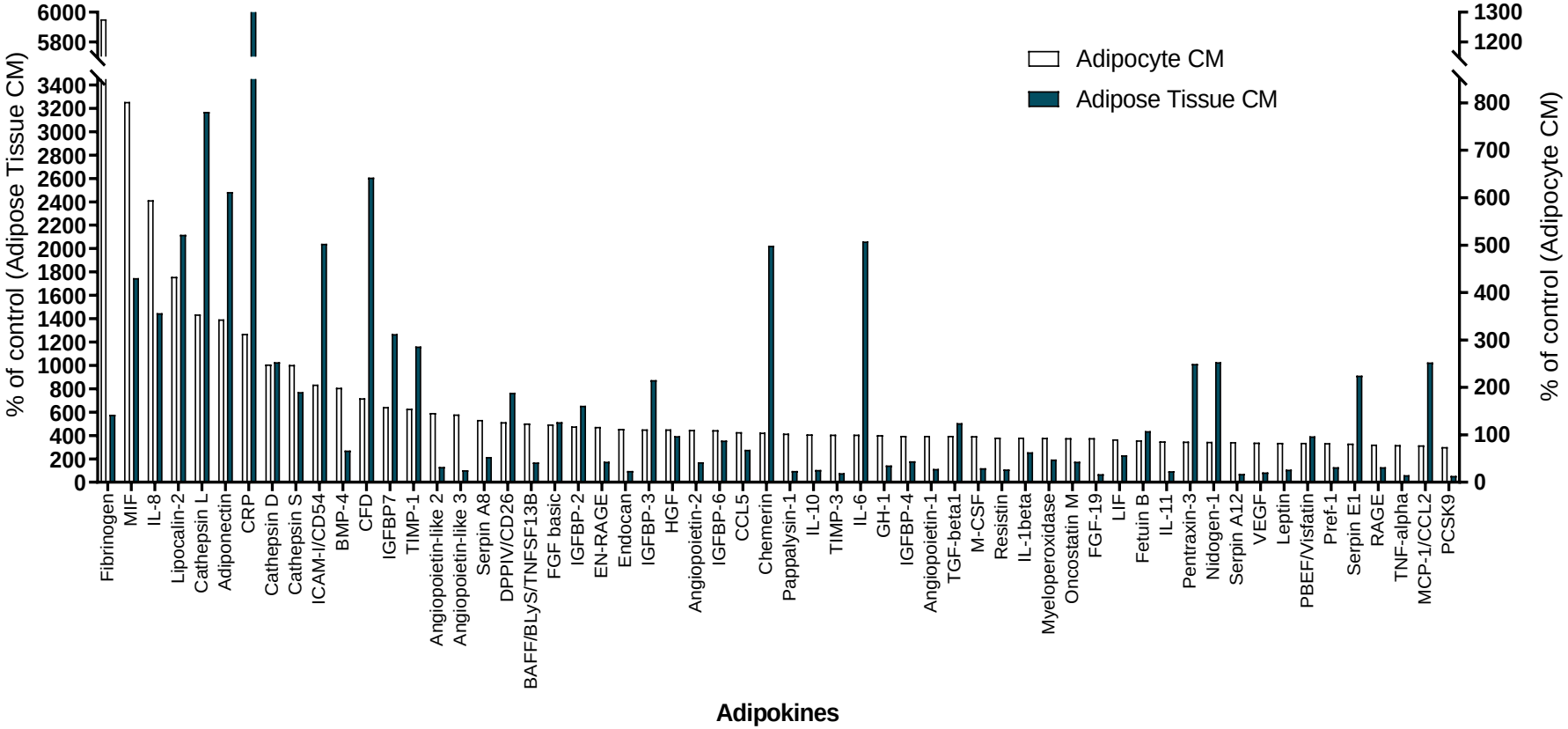
% of control (Adipose Tissue CM)
% of control (Adipocyte CM)
Adipocyte CM
Adipose Tissue CM
Adipokines
Fibrinogen
MIF
IL-8
Lipocalin-2
Cathepsin L
Adiponectin
CRP
Cathepsin D
Cathepsin S
ICAM-I/CD54
BMP-4
CFD
IGFBP7
TIMP-1
Angiopoietin-like 2
Angiopoietin-like 3
Serpin A8
DPPIV/CD26
BAFF/BLyS/TNFSF13B
FGF basic
IGFBP-2
EN-RAGE
Endocan
IGFBP-3
HGF
Angiopoietin-2
IGFBP-6
CCL5
Chemerin
Pappalysin-1
IL-10
TIMP-3
IL-6
GH-1
IGFBP-4
Angiopoietin-1
TGF-beta1
M-CSF
Resistin
IL-1beta
Myeloperoxidase
Oncostatin M
FGF-19
LIF
Fetuin B
IL-11
Pentraxin-3
Nidogen-1
Serpin A12
VEGF
Leptin
PBEF/Visfatin
Pref-1
Serpin E1
RAGE
TNF-alpha
MCP-1/CCL2
PCSK9

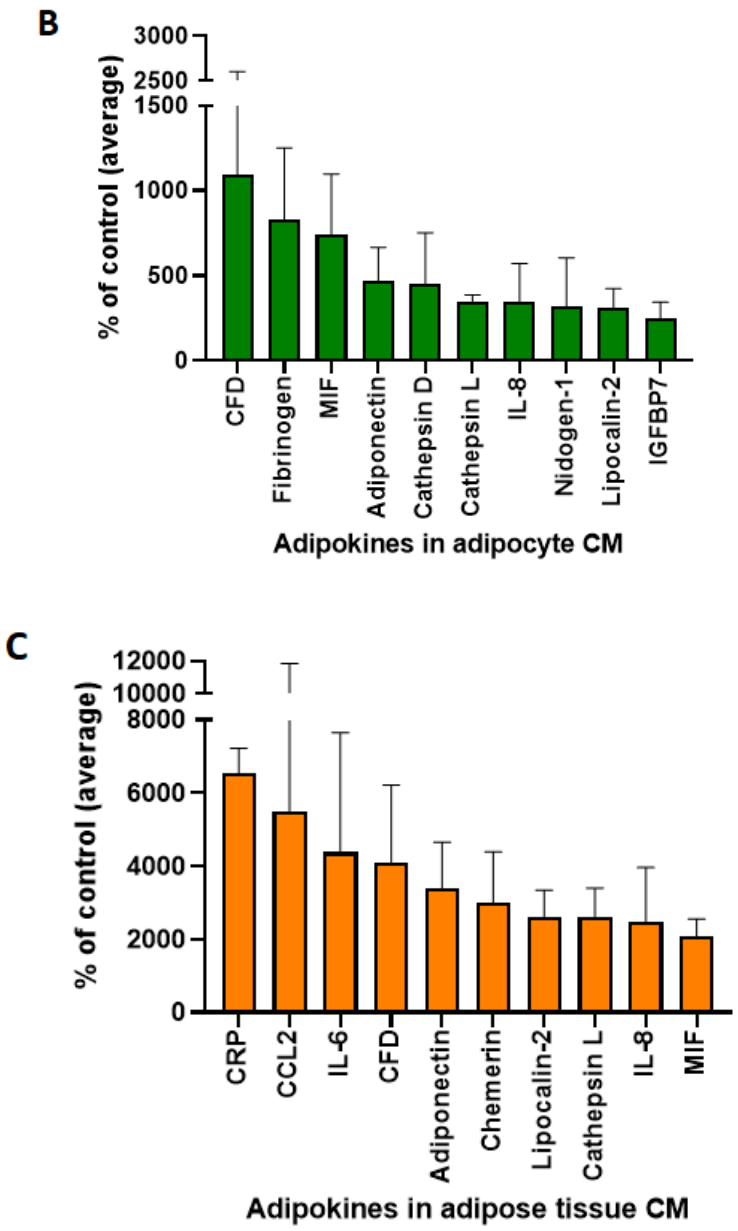

Figure 33. Omental adipose tissue and adipocytes secrete a range of proteins. Using conditioned media collected from the adipocytes and adipose tissue from the same omental sample donor, the relative abundance of all 58 adipokines tested are shown in (A). The ten most abundant adipokines secreted in adipocyte CM (n=3) is shown in (B), while (C) shows the most abundant adipokines secreted from adipose tissue (n=2). Conditioned media containing 200µg of total protein, and equivalent volume of basal media as matched control, were incubated overnight on nitrocellulose membranes pre-spotted with capture antibodies for various adipokines. Following multiple washings, chemiluminescent reagents were applied prior to imaging the membranes on the Azure 500 imager. After subtracting the negative control, the abundance of each adipokine was calculated as a percentage of the basal media's (control) pixel density. CM: conditioned media, CFD: complement factor D, MIF: macrophage migration inhibitory factor, IL: interleukin, IGFBP: insulin-like growth factor-binding protein, CRP: C-reactive protein, MCP: monocyte chemoattractant protein.

Figure 33A shows the relative intensities of all 58 adipokines tested from one omental tissue sample, using both the adipocyte and the adipose tissue CM. **Figure 33B** shows the top ten adipokines (as determined by % increment above control levels) detected in adipocyte CM, while **Figure 33C** shows the top ten in adipose tissue CM. Interestingly, although the conditioned media loaded onto the arrays were standardised to 200µg of total protein, the pixel density values of the adipokines were higher in the adipose tissue CM than in the adipocyte CM. For example, the average pixel density of adiponectin was 3385% of the control (100%) in the adipose tissue CM but was 468% in the adipocyte CM, approximately seven times less.

The ten most highly secreted proteins in adipose tissue were CRP, MCP-1, IL-6, CFD, adiponectin, chemerin, lipocalin-2, cathepsin L, IL-8, MIF and in adipocytes were CFD, fibrinogen, MIF, adiponectin, cathepsin D, cathepsin L, IL-8, nidogen-1, lipocalin-2, IGFBP-7. This experiment also showed that the adipokines identified in the adipose tissue were mostly similar to those in the adipocytes, which strengthened the assumption that the adipocytes form the bulk of the cells in the adipose tissue.

Highly secreted adipokines with pro-angiogenic effects based on previous literature and identified in both the adipocytes and adipose tissue were selected for further study. These were adiponectin, cathepsin L, lipocalin-2 and MIF, which were initially selected for subsequent experiments. The adipokine leptin was later investigated as it was often associated with adiponectin in the context of adipose tissue.(286, 287)

c) Quantification of adipokines in omental adipose tissue conditioned media

The adipokine antibody array served as a screening tool to identify the most abundant adipokines secreted from the omental adipose tissue. Before testing the pro-proliferative activity of selected adipokines (adiponection, cathepsin L, lipocalin-2, MIF and leptin), it was necessary to confirm their identity and determine the concentrations of each secreted by the adipose tissue. This was achieved using their respective commercial ELISA kits (methods described in section 3.2.8).

From ELISA, the measured adipokine concentrations are listed in **Table 5**, and they provided the approximate concentrations for use in later experiments. Of the 5 adipokines, both the leptin and lipocalin-2 were secreted in the ng/mL range at no more than 5ng/mL per 1g of adipose tissue. The adiponectin, cathepsin L and MIF were secreted in the µg/mL range from the same quantity of adipose tissue mass. The concentration of adiponectin was the highest, up to 12.6µg/mL from 1g of tissue. Cathepsin L was detected up to 9.90µg/mL, and MIF up to 2.18 µg/mL.

Table 5. Concentration of adipokines detected in omental adipose tissue conditioned media using ELISA. For each ELISA kit, the adipose tissue conditioned media were diluted between 1:10 to 1:1000 (v/v), assayed in triplicate by ELISA on 96-well plates and the absorbance read at 450nm. The absorbance values, after subtracting the blank controls, were interpolated on the standard curve to determine the adipokine concentration. The range of values obtained were based on at least three different adipose tissue samples.

Adipokine	Concentration detected per 1g of adipose tissue
Adiponectin	2.5 – 12.6 µg/mL
Cathepsin L	3.35 – 9.90 µg/mL
Leptin	0.4 – 4.92 ng/mL
Lipocalin-2	2.014 – 4.05 ng/mL
MIF	0.28 – 2.18 µg/mL

3.3.5 The effect of the selected adipokines on HOMEC proliferation

It was previously shown that treatment with omental adipose tissue CM induced proliferation in HOMECs. To elucidate which secreted adipokines might be responsible for this, the selected adipokines were tested individually for their ability to induce proliferation at a range of concentrations as guided by the concentrations detected by the ELISA.

Initially, HOMEC proliferation was examined when cells were directly treated with adipokines individually. HOMEC proliferation was subsequently also assessed when treated with a combination of adipokines to better mimic the adipose tissue CM, or with ovarian cancer CM post-adipokine treatment. These are elaborated in the following subsections.

a) The effect of individual adipokines at a range of concentrations on HOMEC proliferation

The effect of the selected adipokines (adiponectin, cathepsin L, leptin, lipocalin-2, and MIF) on HOMEC proliferation was tested using the BrdU and WST8 assays. All the adipokines utilised were recombinant human in origin and were diluted in starvation media prior to treating the HOMECs.

The results of the BrdU and WST8 assays are shown in **Figure 34** and **Figure 35** respectively. The results of the WST8 assay at 24 hours and the BrdU assay complemented each other as none of the adipokines enhanced HOMEC proliferation. Furthermore, selected concentrations of some adipokines reduced HOMEC proliferation, e.g. adiponectin at 0.625 and 5µg/mL (BrdU), and 0.3125µg/mL (WST8 at 24 hours). At later timepoints (WST8 at 48 and 72 hours), there was also no significant change in HOMEC proliferation.

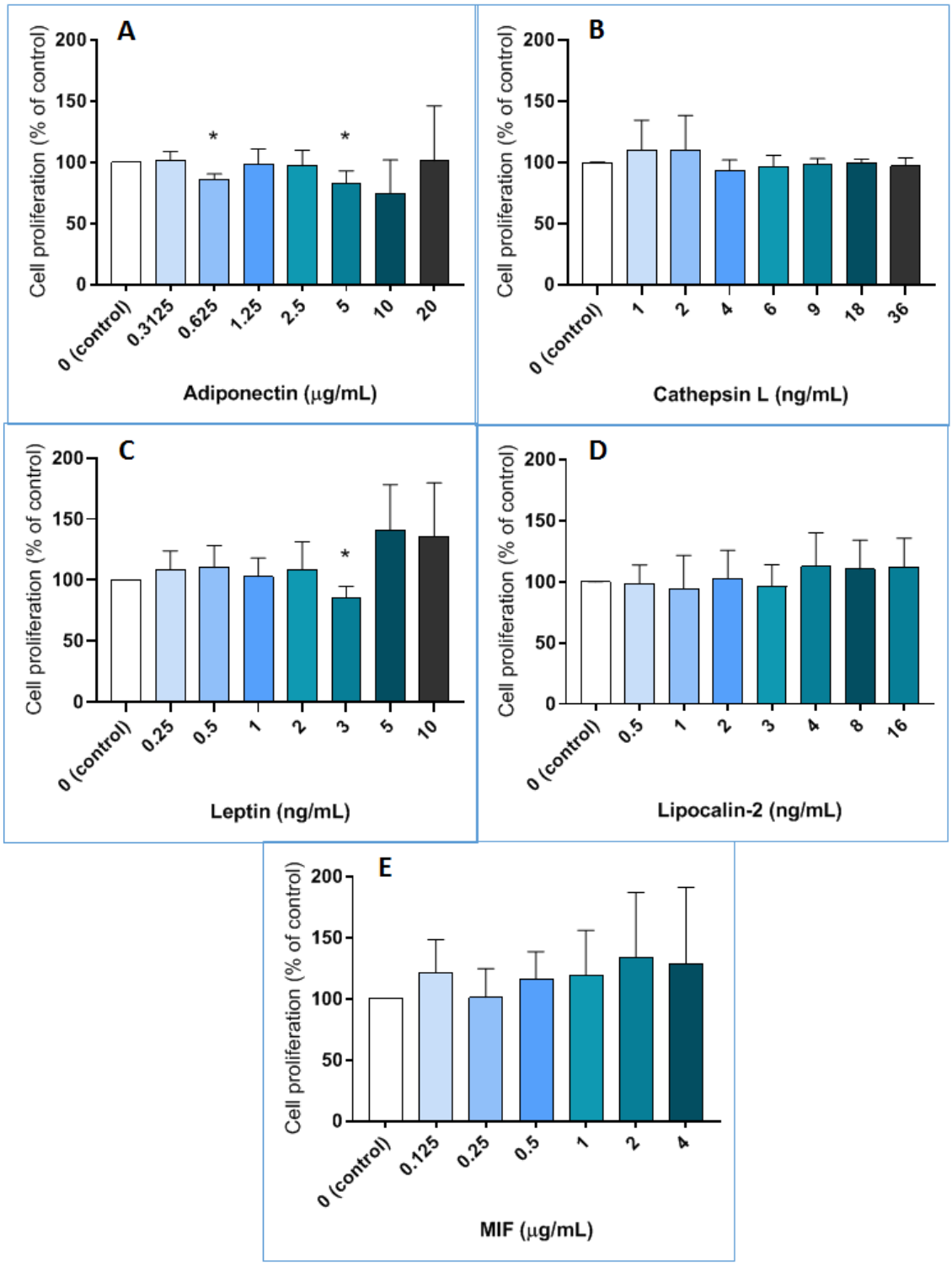

Figure 34. Individually, the adipokines did not induce HOMEC proliferation as assessed by the BrdU assay. HOMECs were seeded at 10,000 cells/well in 96-well plates and cultured for at least 24 hours before overnight serum starvation. Adipokines diluted in starvation media were applied onto cells and the BrdU reagent added after 24 hours. Cells were fixed after 6 hours; plates were read at 450nm. Results shown are mean ± SD and expressed as percentage of the control. Data were analysed with Mann-Whitney U tests, n=3-6; *p<0.05 vs control.

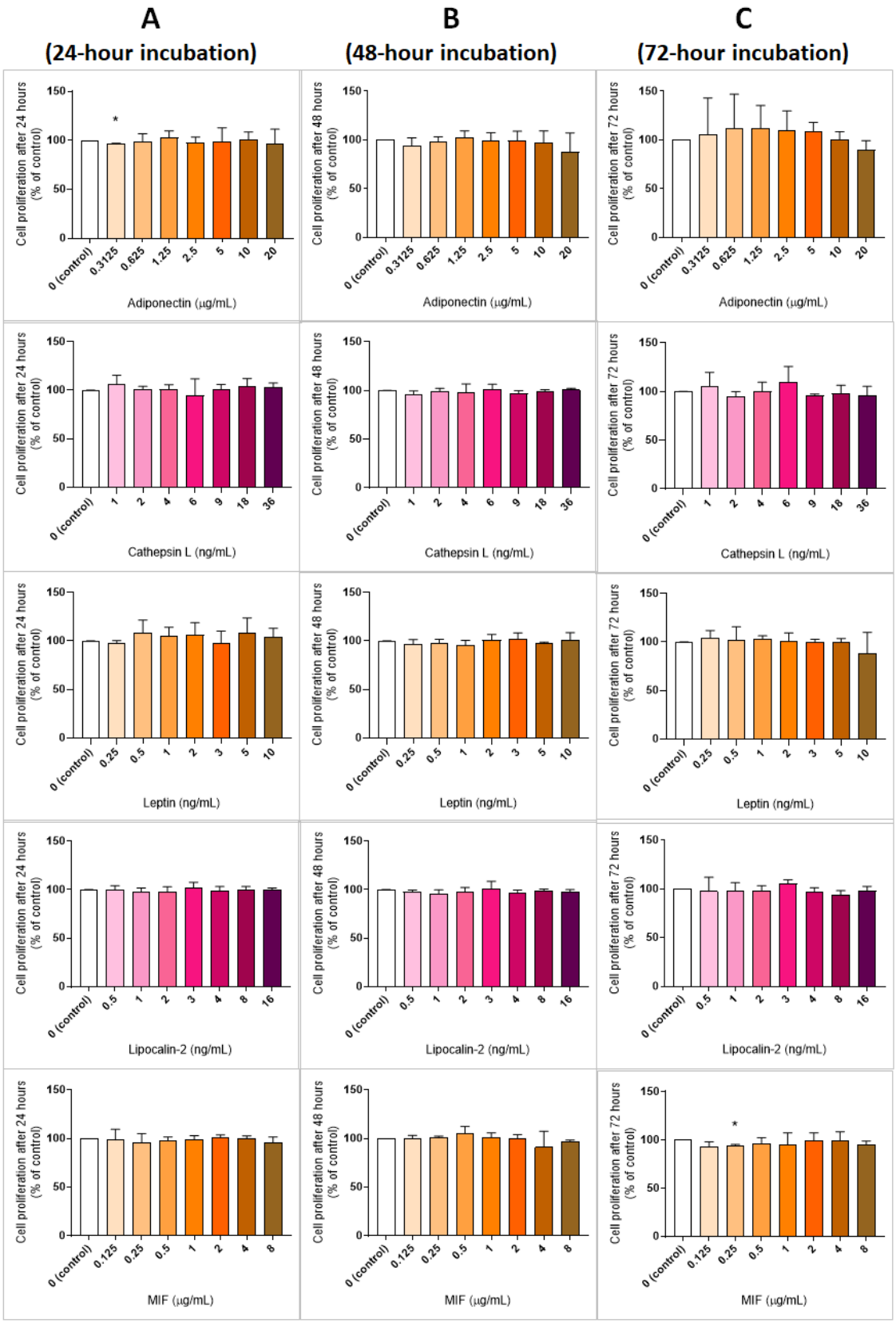

Figure 35. Individually, the adipokines did not induce HOMEC proliferation after 24, 48 or 72 hours of incubation as assessed by the WST8 assay. HOMECs were seeded 10,000 cells/well in 96-well plates and cultured for at least 24 hours before overnight serum starvation. Adipokines diluted in starvation media were applied onto cells. WST8 reagent was added after treatment incubation for 24 (A), 48 (B) or 72 (C) hours; plates were read at 450nm after 2 hours. Results shown are mean ± SD and expressed as percentage of the control. Data were analysed with Mann-Whitney U tests, n=3-6; *p<0.05 vs control.

b) The effect of applying combinations of adipokines on HOMEC proliferation

HOMEC proliferation was not induced by the individual adipokines selected. It was possible that a mixture of adipokines, to mimic the original composition of the adipose tissue CM, was required to induce HOMEC proliferation.

To test this hypothesis proliferation assays were performed using adipokine cocktails: the selected adipokines were diluted in starvation media to a final concentration of 10µg/mL for adiponectin, 9ng/mL for cathepsin L, 5ng/mL for leptin, 4ng/mL for lipocalin-2 and 2µg/mL for MIF. The concentrations selected were on the upper range from the ELISA results (section 3.3.4c). Starvation media was designated as the control. The HOMECs were processed according to section 2.10, and their proliferation tested using the BrdU and WST8 assays. The WST8 assay was only performed at 48 and 72 hours, since data from past WST8 assays at 24 hours were similar to that of the BrdU.

Data from the BrdU assay showed that none of the adipokine combinations studied enhanced HOMEC proliferation (**Figure 36**). Notably, at 24 hours all combinations which contained adiponectin had a significant reduction of proliferation of at least 20% compared with control, all $p<0.05$. For example, HOMEC proliferation in cells treated with the 5-adipokine combination (labelled A in **Figure 36**) was 66% of control (100%), the 4-adipokine combination (labelled B) was 77% and the 3-adipokine combination (labelled D) was 70%. A combination of MIF and lipocalin-2 only (labelled G on **Figure 36**, at 89%), or with leptin (labelled E, 94%) or cathepsin L (labelled F, 87%), also caused slight reduction in HOMEC proliferation compared with the control; all $p<0.05$.

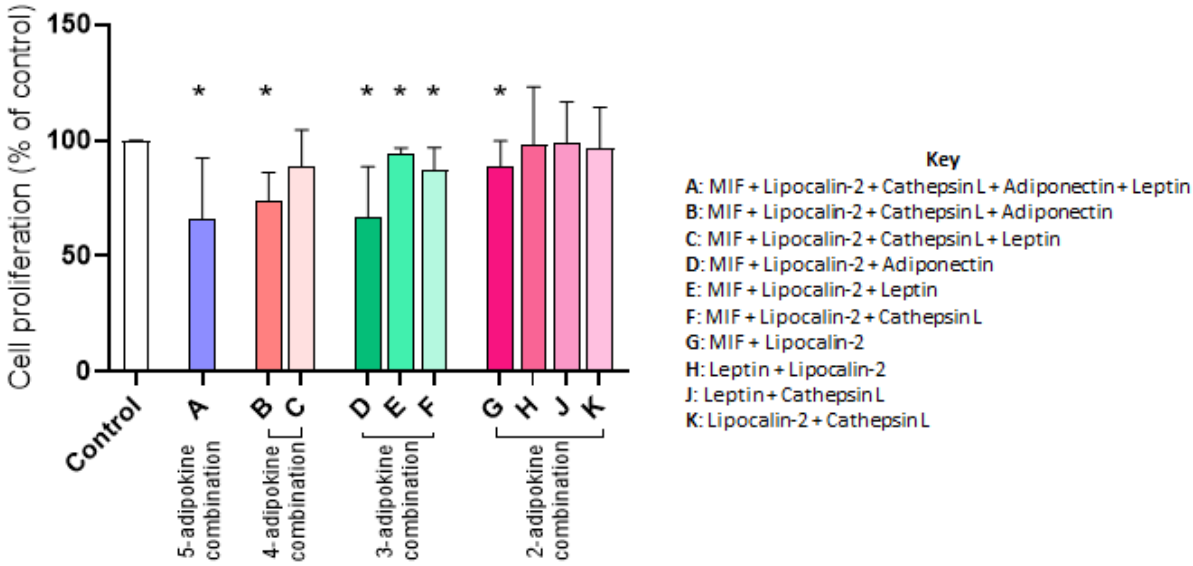

Figure 36. Various combinations of adipokines did not induce HOMEC proliferation as assessed by BrdU assay. HOMECs were seeded at 10,000 cells/well in 96-well plates and cultured for at least 24 hours before overnight serum starvation. Adipokines diluted in starvation media were applied as indicated, and the BrdU reagent was added after 24 hours. Cells were fixed after 6 hours; plates were read at 450nm. Results shown are mean ± SD and expressed as percentage of the control. Data were analysed with Mann-Whitney U tests, n=3; *p<0.05 vs control.

The WST8 assay results are shown in **Figure 37**. Again, none of the adipokine combinations enhanced HOMEC proliferation. At both the 48- and 72-hour timepoints, HOMEC proliferation was lowest when cells were treated with a combination of 5 adipokines (labelled A) i.e. it was significantly reduced to 85% at 48 hours and 82% at 72 hours when compared with the control (100%); $p<0.05$. The combination of MIF, lipocalin-2 and leptin (labelled E) also caused a slight reduction in proliferation at both timepoints, to 97% at 48 hours and 96% at 72 hours compared with the control; $p<0.05$.

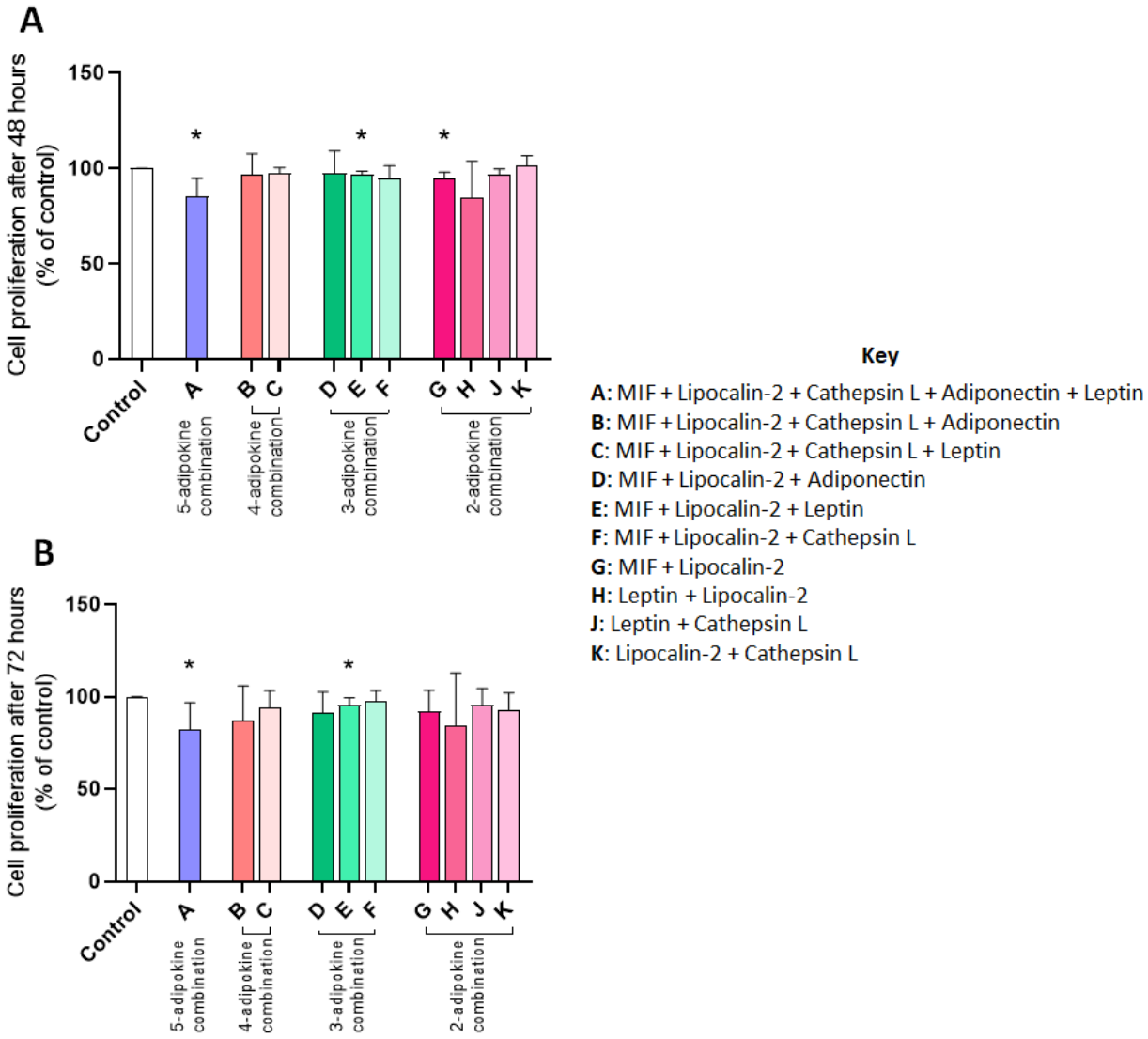

Figure 37. Various combination of adipokines did not induce HOMEC proliferation after 48 or 72 hours as assessed by the WST8 assay.
HOMECs were seeded at 10,000 cells/well in 96-well plates and cultured for at least 24 hours before overnight serum starvation. Adipokines diluted in starvation media were applied as indicated. WST8 reagent was added after treatment incubation for 48 (A) or 72 (B) hours and plates were read at 450nm after 2 hours. Results shown are mean ± SD and expressed as percentage of the control. Data were analysed with Mann-Whitney U tests, n=3-4; *p<0.05 vs control.

c) The effect of factors secreted from adipokine-incubated ovarian cancer cells on HOMEC proliferation

The previous data showed that treatment with omental adipose tissue CM significantly increased HOMEC proliferation (section 3.3.3a), but that selected adipokines (adiponectin, cathepsin L, leptin, lipocalin-2, and MIF), present in the CM individually or in combination had no significant effect on HOMEC proliferation. These adipokines were selected based on previous studies indicating that they induced EC proliferation and/or migration, which are hallmarks of angiogenesis. However, these data indicate that there are yet unidentified adipokine(s) or combinations of adipokines which induced HOMEC proliferation. Time did not allow this to be investigated further in the present study, although the data presented in chapter 4 may provide a starting point.

It was interesting to note that, unexpectedly, 24-hour treatment with CM from A2870 and SKOV3 cells did not induce proliferation of HOMEC (section 3.3.3b). Additionally, longer treatment with CM from SKOV3 cells, which as mentioned previously are considered to represent metastatic EOC cells, had no effect on HOMEC proliferation. Since the omental adipocytes clearly did secrete a range of adipokines that have been reported to be pro-tumorigenic, these data raised the possibility that complex interactions within the tumour microenvironment contribute to the frequent incidence of omental metastases. Specifically, the adipokines secreted by the omental adipocytes may interact with the metastatic ovarian cancer cells to induce angiogenesis.

This possibility was investigated further by examining whether incubating ovarian cancer cells with the adipokines identified could induce their secretion of a pro-proliferative factor for HOMECs. This study was conducted as described in section 3.2.9. Briefly, cancer cells were incubated with the adipokines for 24 or 48 hours. Their conditioned medium was then collected and added to HOMECs. Both ovarian cancer cell lines, SKOV3 (of ascitic origin) and A2780 (of primary origin), were utilised to compare if there were differences due to cancer cell origin.

Strikingly, treatment with CM derived from SKOV3 cells incubated with either leptin or lipocalin-2 for 24 hours, enhanced HOMEC proliferation assessed by both WST8 and BrdU assays (**Figure 38** and **Figure 39** respectively). Both

leptin- and lipocalin-2-incubated CM increased proliferation by 24% ($p<0.05$) compared with the control (100%) as assessed by WST8 assay (**Figure 38A**). This contrasts with the data obtained when HOMECs were treated with adipokines alone, where no effect on proliferation was observed, and also the data from ovarian cancer CM alone where no proliferative effect of the SKOV3 CM was observed even up to 72 hours. These data suggest that the adipokines induce secretion of intermediary pro-proliferative factors from the cancer cells. Interestingly, when the CM was collected from SKOV3 cells incubated with the same adipokines for 48 hours, the pro-proliferative effect of the CM was not observed (**Figure 38B**).

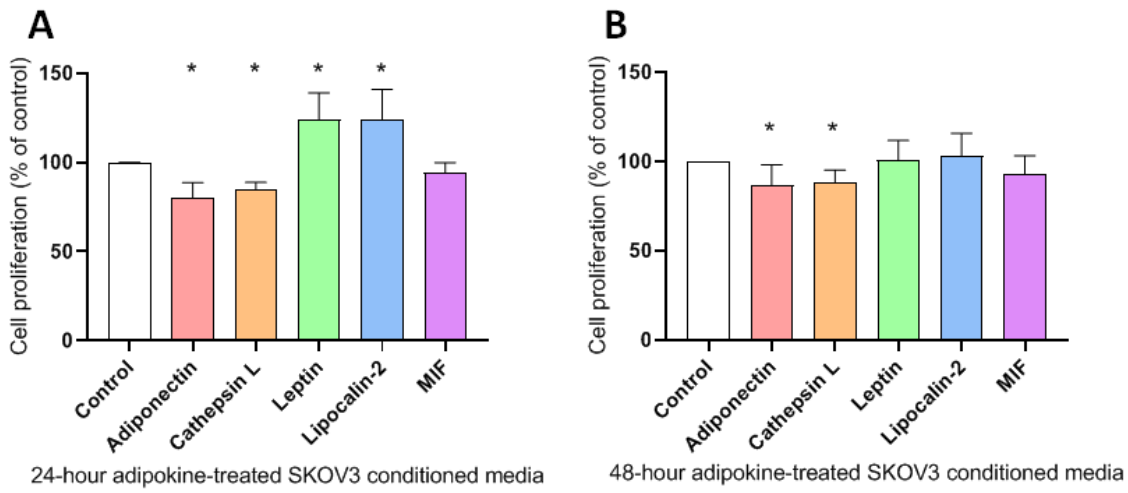

Figure 38. Conditioned media collected from SKOV3 incubated with leptin or lipocalin-2 for 24 hours enhanced HOMEC proliferation as assessed by WST8 assay. HOMECs were seeded at 10,000 cells/well in 96-well plates and cultured for at least 24 hours before overnight serum starvation. Conditioned media, collected from SKOV3 cells incubated with individual adipokines for 24 (A) or 48 (B) hours, was then applied to the HOMECs. WST8 reagent was added 24 hours after treatment application, and plates were read at 450nm after 2 hours. Results shown are mean ± SD and expressed as percentage of the control; data were analysed with Mann-Whitney U tests. n=3-4; *$p<0.05$ vs control.

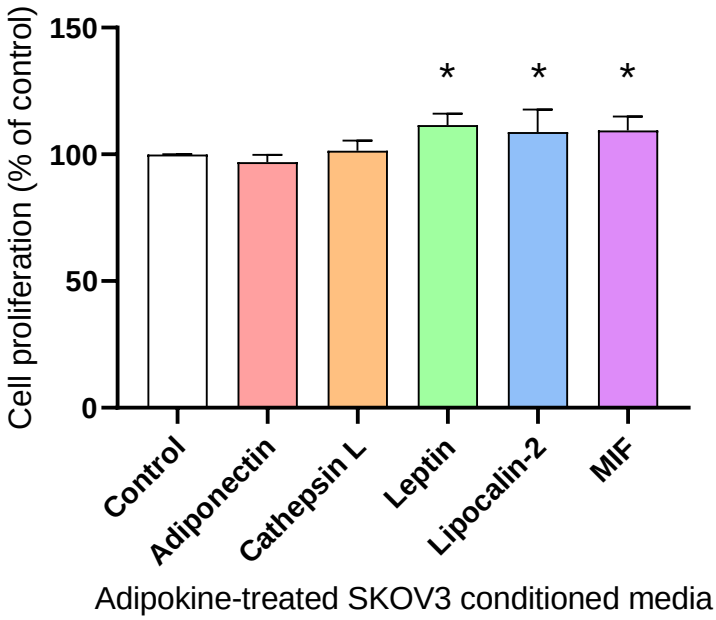

Figure 39. Conditioned media collected from SKOV3 cells incubated with leptin, lipocalin-2 or MIF enhanced HOMEC proliferation as assessed by BrdU assay. HOMECs were seeded at 10,000 cells/well in 96-well plates and cultured for at least 24 hours before overnight serum starvation. Conditioned media, collected from SKOV3 cells incubated with individual adipokines for 24 hours, was then applied to the HOMECs. The BrdU reagent was added after 24 hours and cells were fixed after 6 hours; plates were read at 450nm. Results shown are mean ± SD and expressed as percentage of the control; data were analysed with Mann-Whitney U tests. n=3; *p<0.05 vs control.

These observations were confirmed with the BrdU assay (**Figure 39**). HOMEC proliferation was increased by cancer CM obtained after incubating the SKOV3 cells with leptin, lipocalin-2 or MIF for 24 hours. Specifically, incubation with leptin yielded SKOV3 CM which increased HOMEC proliferation by 12%, incubation with lipocalin-2 by 9% and incubation with MIF also by 9%; all $p<0.05$.

When assessed by WST8 assay, none of the adipokines induced the secretion of HOMEC pro-proliferative factors from A2780 cells (**Figure 40**). However, in the BrdU assay, HOMEC proliferation was induced by CM from A2780 cells previously incubated with leptin (16% increase), lipocalin-2 (21% increase) and MIF (18% increase); all $p<0.05$ (**Figure 41**).

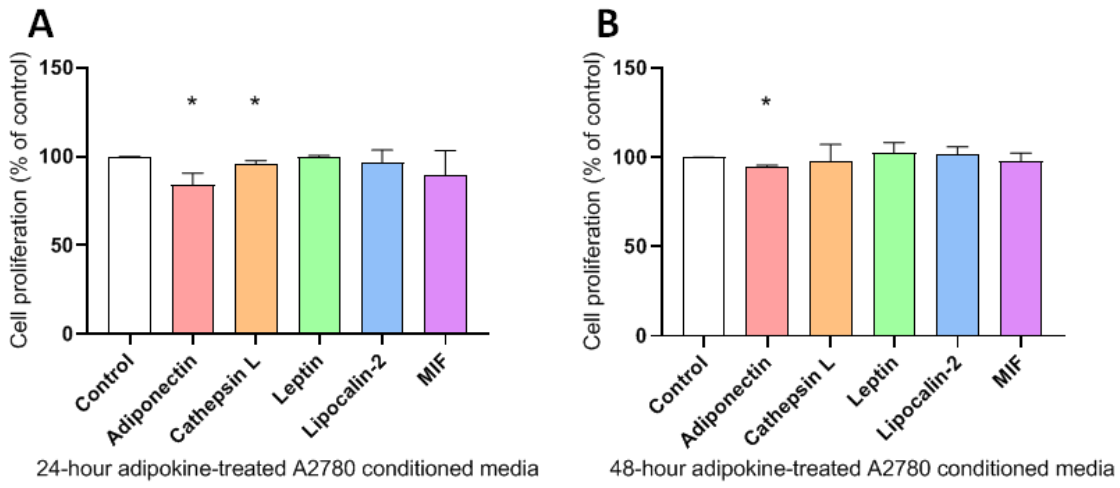

Figure 40. Conditioned media collected from A2780 cells incubated with individual adipokines did not enhance HOMEC proliferation as assessed by WST8 assay. HOMECs were seeded at 10,000 cells/well in 96-well plates and cultured for at least 24 hours before overnight serum starvation. Conditioned media, collected from A2780 cells incubated with individual adipokines for 24 (A) or 48 (B) hours, was then applied to the HOMECs. WST8 reagent was added 24 hours after treatment application, and plates were read at 450nm after 2 hours. Results shown are mean ± SD and expressed as percentage of the control; data were analysed with Mann-Whitney U tests. n=3-4; *p<0.05 vs control.

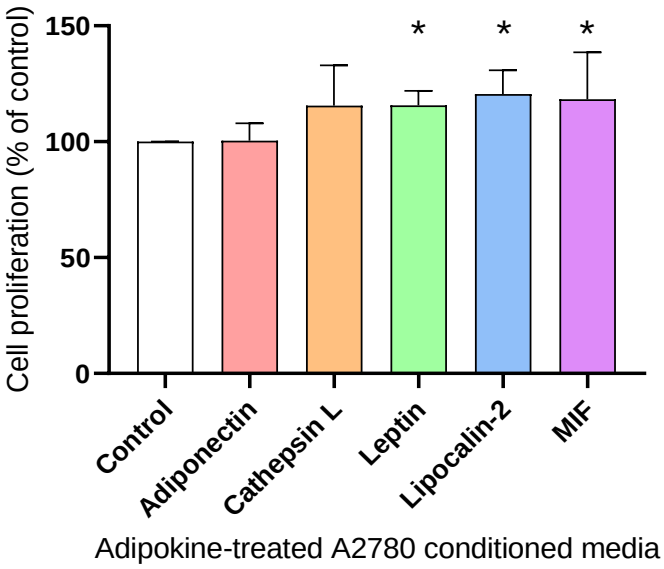

Figure 41. Conditioned media collected from A2780 cells incubated with leptin, lipocalin-2 or MIF enhanced HOMEC proliferation as assessed by BrdU assay. HOMECs were seeded at 10,000 cells/well in 96-well plates and cultured for at least 24 hours before overnight serum starvation. Conditioned media, collected from A2780 cells incubated with individual adipokines for 24 hours, was then applied onto cells. The BrdU reagent was added after 24 hours and cells were fixed after 6 hours; plates were read at 450nm. Results shown are mean ± SD and expressed as percentage of the control; data were analysed with Mann-Whitney U tests. n=3; *p<0.05 vs control.

Interestingly, incubation of tumour cells with adiponectin for both 24 and 48 hours yielded CM which subsequently reduced HOMEC proliferation compared with the control. Treatment with SKOV3 CM collected after adiponectin incubation showed decreased proliferation to 80% of control (100%) levels (CM collected after adiponectin incubation for 24 hours) and to 87% of control levels (incubation for 48 hours); both $p<0.05$ (**Figure 38**). The same effect was observed when CM from adiponectin-incubated A2780 cells was applied onto HOMECs; 84% (incubation for 24 hours) and 95% (incubation for 48 hours) of the control; both $p<0.05$ (**Figure 40**).

Similar results were obtained using CM collected from SKOV3 cells incubated with cathepsin L prior to addition to HOMECs. CM collected from SKOV3 cells incubated with cathepsin L for 24 and 48 hours subsequently reduced HOMEC proliferation to 85% and 87% respectively vs control (100%) (both $p<0.05$) as assessed by WST8 assay (**Figure 38**). Reduced HOMEC proliferation (96% of control, $p<0.05$) was also observed when cells were incubated with CM collected from A2780 incubated with cathepsin L for 24 hours (**Figure 40**).

A summary of the effect of CM from adipokine-incubated ovarian cancer cells on HOMEC proliferation are collated in **Table 6**. It can be seen that CM collected from ovarian cancer cells pre-incubated with leptin or lipocalin-2 for 24 hours was the most consistent in inducing HOMEC proliferation. The actions of these two adipokines were further investigated in chapter 4.

Table 6. The effect of conditioned media derived from ovarian cancer cells incubated with adipokines on HOMEC proliferation. HOMECs were seeded at 10,000 cells/well in 96-well plates and cultured for at least 24 hours before overnight serum starvation. Conditioned media, collected from ovarian cancer cells incubated with individual adipokines for 24 or 48 hours, was then applied to the HOMECs. HOMEC proliferation was assessed by WST8 or BrdU assays after 24 hours of conditioned media treatment. Significant increase in HOMEC proliferation is marked with an upward arrow (↑), a significant decrease with a downward arrow (↓), and dashed line (--) indicated no significant change in proliferation.

		Adipokine				
		Adiponectin	Cathepsin L	Leptin	Lipocalin-2	MIF
	Duration of adipokine incubation with ovarian cancer cells	**Effect on HOMEC proliferation**				
Proliferation assessed by WST8 assay	24-hour incubation / SKOV3 cells	↓	↓	↑	↑	--
	48-hour incubation / SKOV3 cells	↓	↓	--	--	--
	24-hour incubation / A2780 cells	↓	↓	--	--	--
	48-hour incubation / A2780 cells	↓	--	--	--	--
Proliferation assessed by BrdU assay	24-hour incubation / SKOV3 cells	--	--	↑	↑	↑
	24-hour incubation / A2780 cells	--	--	↑	↑	↑

Legend:

↑ increased HOMEC proliferation;

↓ decreased HOMEC proliferation;

-- no significant change in HOMEC proliferation.

3.3.6 The effect of omental adipose tissue and ovarian cancer cell CM on HOMEC migration

Alongside cell proliferation, migration is also a functional response to EC activation in angiogenesis. To assess if secreted mediators from omental adipocytes and ovarian cancer cells affected HOMEC migration, scratch wound healing assays were performed as described in section 2.13. Representative images from the scratch wound healing assays are shown in **Figure 42**.

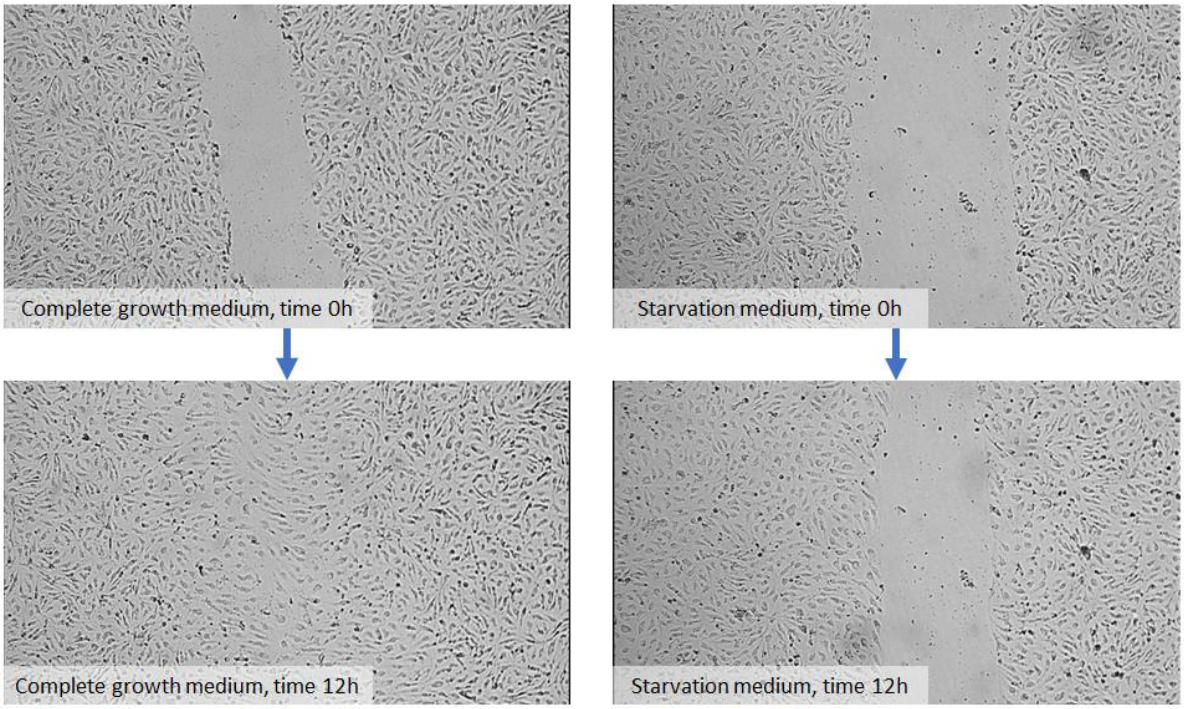

Figure 42. HOMEC migration after 12 hours in the scratch wound healing assay. HOMECs were seeded at 10,000 cells/well in 96-well plates and cultured for at least 24 hours before overnight serum starvation. Each well was scratched with a P200 pipette tip prior to treatment with respective media. Wells were imaged using the JuLI™ Stage Real-Time Cell History Recorder. Representative images show scratch wound closure of 100% and 30% at the 12-hour timepoint when HOMECs were incubated with complete growth medium and starvation medium respectively.

a) HOMEC migration with conditioned media from adipose tissue

Migration of HOMECs treated with adipose tissue CM was examined. CM was diluted to 1:2, 1:5 and 1:10 with starvation media, and the control wells received starvation media alone.

Results of the scratch wound healing assay are shown in **Figure 43**. At both time points, 12 and 20 hours, all dilutions of the adipose tissue CM increased HOMEC migration but none of these increases were statistically significant (all $p>0.05$) compared with their respective controls. At 12 hours, the increase in cell migration compared with control was only 5% and 6% with the 1:2 and 1:5 dilutions of CM respectively. At 20 hours, the CM enhanced wound closure by 10% (1:2 dilution) and 7% (1:5 dilution) compared with the control. With the 1:10 dilution, the difference between treated and control was only 2% and 1%, at the 12- and 20-hour timepoints respectively.

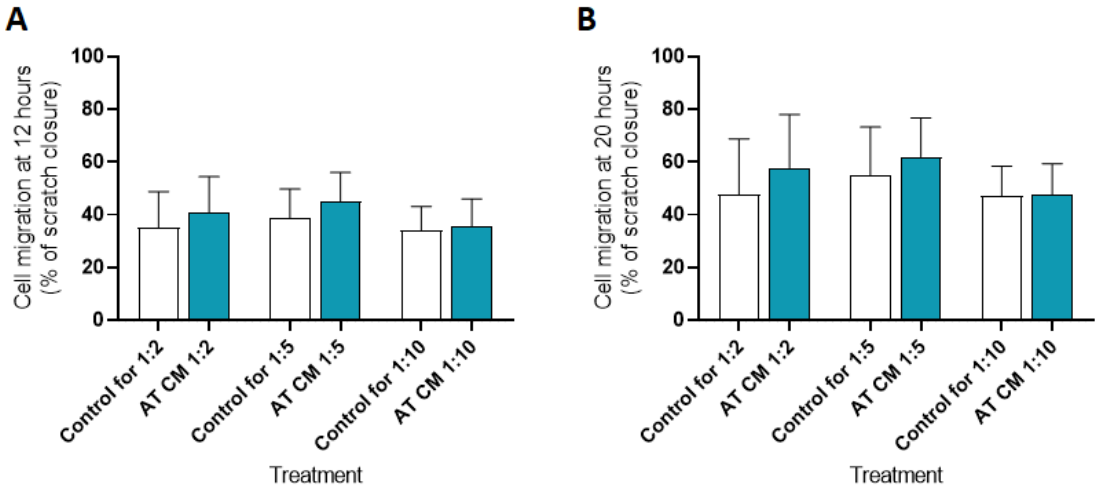

Figure 43. Adipose tissue conditioned media did not significantly enhance HOMEC migration after 12 or 20 hours as assessed by a scratch wound healing assay. HOMECs were seeded at 10,000 cells/well in 96-well plates and cultured for at least 24 hours before overnight serum starvation. Each well was scratched with a P200 pipette tip prior to treatment with conditioned media as indicated. Wells were imaged using the JuLI™ Stage Real-Time Cell History Recorder. The scratch gap at 12 (A) and 20 (B) hours was calculated as a percentage of scratch closure from time 0. Results shown are mean ± SD. Data were analysed with Mann-Whitney U tests, n=10-12. AT: adipose tissue; CM: conditioned media; 1:2, 1:5, 1:10: dilution factor.

b) HOMEC migration with adipose tissue conditioned media combined with from ovarian cancer conditioned media

To complement the proliferation data in HOMECs treated with ovarian cancer CM, the impact of cancer cell CM on HOMEC migration was also examined. The ovarian cancer CM were diluted with starvation media to a 1:2, 1:5 and 1:10 concentration. In some treatments, CM from the ovarian cancer cells and the adipose tissue were mixed prior to treating the HOMECs.

Similar to the proliferation data, SKOV3 CM alone or in combination with adipose tissue CM did not enhance HOMEC migration (**Figure 44**). Interestingly, treatment with SKOV3 CM alone decreased HOMEC migration compared to control, although this was not statistically significant (all $p>0.05$). Using the 1:5 dilution of SKOV3 CM as an example, at the 12-hour timepoint, scratch closure was 31% after treatment compared with 39% in the control (**Figure 44A**); while at the 20-hour timepoint, scratch closure in treated cells was 45% compared with 57% in the control (**Figure 44B**).

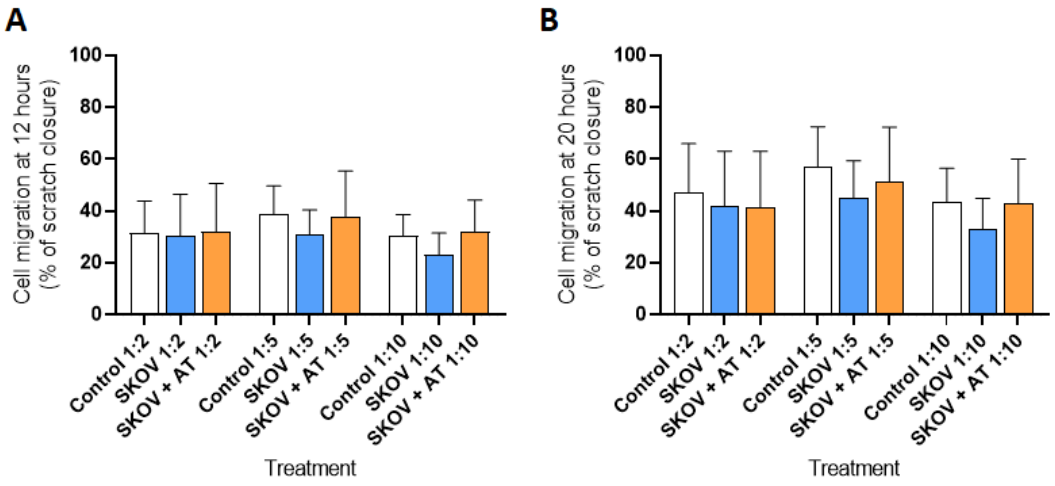

Figure 44. SKOV3 conditioned media alone or in combination with adipose tissue conditioned media did not enhance HOMEC migration as assessed by a scratch wound healing assay. HOMECs were seeded at 10,000 cells/well in 96-well plates and cultured for at least 24 hours before overnight serum starvation. Each well was scratched with a P200 pipette tip prior to treatment with conditioned media as indicated. Wells were imaged using the JuLI™ Stage Real-Time Cell History Recorder. The scratch gap at 12 (A) and 20 (B) hours was calculated as a percentage of scratch closure from time 0. Results shown are mean ± SD. Data were analysed with Mann-Whitney U tests, n=5-6. AT: adipose tissue conditioned media; SKOV: SKOV3 conditioned media; 1:2, 1:5, 1:10: dilution factor.

HOMEC migration was, however, increased when cells were treated with A2780 CM alone and in combination with adipose tissue CM. With the 1:5 dilution at the 12-hour timepoint (**Figure 45A**), scratch closure was 52% with A2780 CM treatment alone and 55% with combination CM treatment compared with 34% in the control; both $p<0.05$. At 20 hours (**Figure 45B**), the scratch closure was significantly increased for the 1:5 dilution: 70% with A2780 CM treatment alone and 75% with combination CM treatment as opposed to 44% in the control; both $p<0.05$. No differences were observed, however, between scratch closure induced by A2780 CM alone and A2780 CM plus adipose tissue CM.

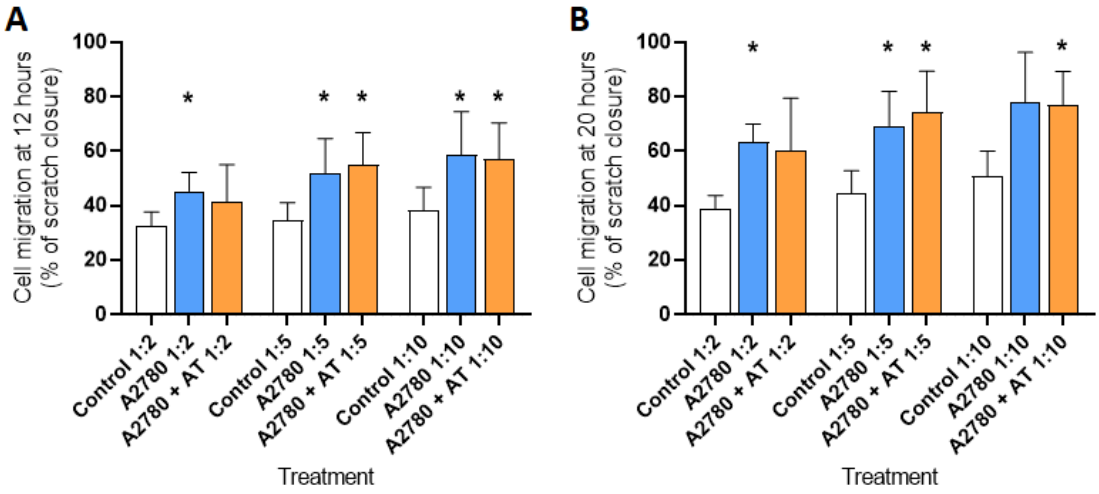

Figure 45. A2780 conditioned media alone or in combination with adipose tissue conditioned media enhanced HOMEC migration as assessed by a scratch wound healing assay. HOMECs were seeded at 10,000 cells/well in 96-well plates and cultured for at least 24 hours before overnight serum starvation. Each well was scratched with a P200 pipette tip prior to treatment with conditioned media as indicated. Wells were imaged using the JuLI™ Stage Real-Time Cell History Recorder. The scratch gap at 12 (A) and 20 (B) hours was calculated as a percentage of scratch closure from time 0. Results shown are mean ± SD. Data were analysed with Mann-Whitney U tests, n=5. *$p<0.05$ vs corresponding control. AT: adipose tissue conditioned media; A2780: A2780 conditioned media; 1:2, 1:5, 1:10: dilution factor.

c) HOMEC migration with individual adipokines at a range of concentrations

Although not statistically significant, treatment with adipose tissue CM did enhance HOMEC migration compared with the control (**Figure 43**). To complement the HOMEC proliferation data from section 3.3.5a, the scratch wound healing assay to assess HOMEC migration was therefore performed using the same selected adipokines (adiponectin, cathepsin L, leptin, lipocalin-2, and MIF) at increasing concentrations as previously.

Similar to the proliferation data, the individual adipokines did not enhance HOMEC migration after 12 or 20 hours (**Figure 46**). As expected, the percentage of scratch closure was higher at the 20-hour timepoint compared to the 12-hour timepoint. For example, scratch closure in the adiponectin control was 60% at 12 hours, which rose to 80% at 20 hours; or the increase from 54% (12 hours) to 82% (20 hours) when treated with 0.25µg/mL of MIF. But none of these were statistically different to the control; all $p>0.05$.

Subsequent experiments focussed on HOMEC proliferation as factors secreted by omental adipose tissue did not have a significant effect on HOMEC migration.

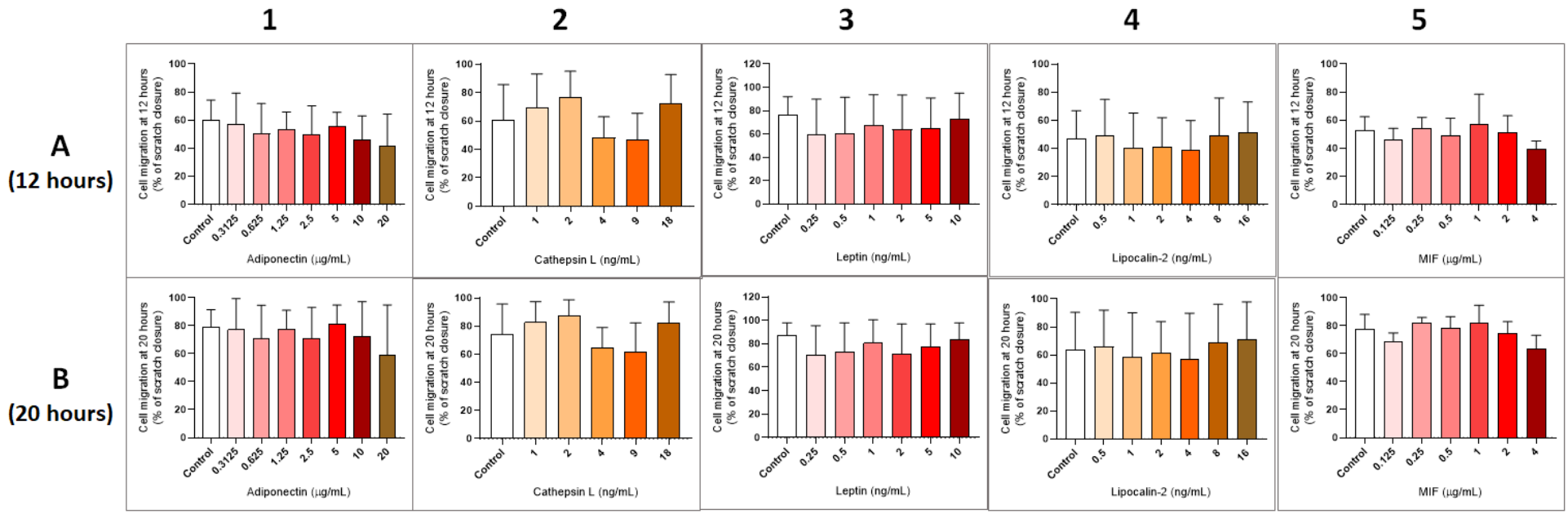

Figure 46. Individual adipokines did not induce HOMEC migration after 12 and 20 hours as assessed by a scratch wound healing assay. HOMECs were seeded at 10,000 cells/well in 96-well plates and cultured for at least 24 hours before overnight serum starvation. Each well was scratched with a P200 pipette tip prior to treatment with adipokines (adiponectin (1), cathepsin L (2), leptin (3), lipocalin-2 (4) and MIF (5)) diluted in starvation media to the concentrations indicated. Wells were imaged using the JuLI™ Stage Real-Time Cell History Recorder. The scratch gap at 12 (row A) and 20 (row B) hours were calculated as a percentage of scratch closure from time 0. Results shown are mean ± SD, and compare the percentage of scratch closure with adipokine treatment at a range of concentrations against the control. Data were analysed with Mann-Whitney U tests, n=3-5.

3.4 Discussion

This chapter initially described the development of an improved protocol to isolate disease-relevant HOMECs. These cells were then utilised to investigate the effect of factors secreted from omental adipocytes on pro-angiogenic responses of HOMECs, specifically proliferation and migration, in order to better understand the role of the omental tissue in supporting ovarian cancer metastases.

The data show, for the first time, that the secretome of omental adipose tissue stimulates HOMEC proliferation. However, even though key secreted adipokines with potential roles in angiogenesis were identified and quantified, none of the selected proteins alone or in combination stimulated HOMEC proliferation, suggesting that the adipokines selected were not responsible for the proliferation induced by the CM.

It was possible, however, that these adipokines could play a role in supporting ovarian cancer metastasis within the complex microenvironment of the developing secondary tumour in the omentum where cross-talk between ECs, adipocytes and ovarian cancer cells may occur. The data showed, for the first time, that incubation of ovarian cancer cells with the adipokines leptin and lipocalin-2 induced secretion of factors that stimulate HOMEC proliferation i.e. the adipokines acted on the cancer cells to indirectly stimulate pro-angiogenic responses. This was particularly observed in the SKOV3 cell line, where the basal cancer cell CM did not enhance EC responses, but the CM from adipokine-incubated cancer cells had robust effects on the same responses.

3.4.1 Improvements to the HOMEC isolation protocol

When investigating ovarian cancer metastases and angiogenesis into the omentum, disease specific ECs were required. The development of an improved HOMEC isolation protocol was instrumental in obtaining sufficient numbers for subsequent investigations. There are very few reports in the literature of the use of HOMECs when studying EOC metastasis. Many studies of angiogenesis were performed in HUVECs, possibly due to the ease of obtaining and culturing these cells. However, they are not representative of

tumour angiogenesis since HUVECs originate from a location (umbilical vein) where tumours rarely occur. Furthermore, HUVECs are derived from the macrovasculature, whereas the process of angiogenesis usually occurs in the microvasculature. Hence, the isolated HOMECs would be better suited to study EOC metastasis especially to the omentum.

With the amended isolation protocol, the HOMEC yield at passage 0 was visibly better than the original procedure. This subsequently allowed successful cell population expansion as evidenced by the increased proportion of successful isolations. The most significant amendment to the initial protocol of Winiarski et al (2011)(278) was the duration of collagenase type I digestion, which was increased from 2 hours to 5 hours to allow more of the tissue to be enzymatically broken down, thus 'releasing' more cells. Importantly, previous work in the lab showed that the increased digestion duration with collagenase type I did not significantly reduce the number of viable HOMECs and that CD31 was still present on the isolated cells post extended digestion.(288) The presence of CD31 on the target cells was crucial as the final immunoselection step was reliant on this extracellular marker.

The increased duration of collagenase type I digestion resulted in a lower undigested tissue volume. This then led to the elimination of several downstream steps which were no longer necessary: the need to forcefully compress the undigested tissue through swab layers, the 30µm nylon filtration and the filter wash. The elimination of these steps minimised cell losses due to reduced handling.

In the initial protocol, the ratio of the anti-CD31 magnetic beads to the cell suspension volume was 5µL : 500µL of suspension containing the entire cell pellet obtained from the whole omental tissue sample. In the amended protocol, the final cell pellet was divided into 2 x 500µL aliquots to accommodate the larger cell pellet obtained and the bead/cell suspension ratio was amended to 3µL : 500µL. Thus, the number of beads utilised in the amended protocol was only 20% higher than the initial protocol, 6µL versus 5µL total per whole tissue. Since the pellet was larger the resulting bead/cell ratio was reduced. This strategy was adopted because the cell yield from the initial protocol was so low that often more beads were observed in the passage 0 culture than the intended cells.

In the manufacturer's manual (Dynabeads® CD31 Endothelial Cell by Invitrogen), the prescribed ratio was 25µL beads to 1mL of suspension consisting of 1 x 10^8 cells. This ratio was not followed in either protocol since a cell counting step was not performed prior to the selection. However, back-calculating from what is known about the number of HOMECs/cm^2 in a confluent monolayer (approximately 2.5 x 10^6 cells in a T75 flask), and estimating confluency in the 6-well plates the day after isolation (approximately 20% confluence per well i.e. approximately 60,000 cells per well), it is clear that the number of beads used is more than enough to capture all of the HOMECs in the isolated cell pellet. For future isolation work, a cell counting step could be added prior to bead addition to ensure a consistent bead/cell ratio.

3.4.2 HOMEC serum starvation

In setting up the HOMECs for experiments, a serum starvation step was performed prior to treatment addition. This starvation step i.e. treatment with media devoid of growth factors and with reduced FBS, was performed to synchronise the HOMECs to the same cell cycle phase (G_0/G_1 phase) and thus minimise the impact of cell cycle towards treatment response.(289, 290) When observed under microscope post-overnight starvation, HOMEC morphology appeared unchanged. This starvation step is routinely performed in our lab when working with HOMECs,(106, 291) and also in other labs.(292)

Furthermore, treatments were diluted in starvation media instead of complete growth media to reduce possible confounding factors which may arise from interaction with the growth factors supplemented in the complete media. A source of growth factors is the FBS, present in higher concentrations in the complete growth media (5% v/v) compared with the starvation media (1% v/v). Being a naturally derived product, FBS is subjected to batch-to-batch variation, which in turn may affect growth factor constituents.(293) To eliminate this confounder in experiments, the use of serum-free basal media was initially attempted as starvation media. This basal media was devoid of growth factors and resulted in HOMEC death after overnight incubation, which was observed under microscopy as changed morphology or detachment from cultureware surface. Thus, a nominal amount of FBS is required for the viability of HOMECs.

3.4.3 Comparison between cell proliferation assay methodologies

When assessing HOMEC proliferation, two different methods were utilised – the BrdU and WST8 assays. The BrdU assay measures the incorporation of the added BrdU reagent into the DNA of replicating cells. The BrdU assay is deemed more sensitive because it measures the direct incorporation of the added BrdU reagent into the DNA of replicating cells; thus, the BrdU assay measures the rate of DNA synthesis (previously outlined in section 2.11), which is an element of cell proliferation.

The WST8 assay is an indirect assessment based on the metabolic activity of the cells, utilising cellular dehydrogenases to reduce the WST8 reagent (a tetrazolium salt) to its coloured formazan dye; thus, the greater the cell number, the stronger the colour intensity and higher spectrophotometer absorbance readings. In measuring cell proliferation inferred from cell metabolism levels, many factors may result in the under- or over-reporting of WST8 assay absorbance measurements (i.e. lower or higher cell viability, respectively, than the actual numbers) compared to other methods of measuring cell proliferation, e.g. BrdU incorporation.

An example of under-reporting may explain the difference observed in **Figure 27** where adipose tissue CM treatment increased cell numbers based on BrdU incorporation into the DNA, and in **Figure 28A** where the same treatment conditions did not appear to increase cell numbers assessed by changes cell metabolism in the WST8 assay. HOMEC numbers may have increased in the 24 hours of treatment incubation, however the limited size of the culture well may have led to contact inhibition and subsequent cell cycle arrest.(294) Thus, the positive correlation between cell number and absorbance measurements are obliterated: when the WST8 reagent was added after 24 hours, the cell metabolism had reduced leading to less reduction of the reagent and a low absorbance reading. To circumvent any impacts of contact inhibition future experiments could use lower seeding densities of HOMECs.

Another possibility for the low absorbance reading may be due to the depletion of cellular NAD+. As a precursor of NADP (NADP is involved in the mechanism of WST8 reagent reduction, as previously shown in **Figure 13**), NAD+ functions as a co-substrate in DNA repair mechanisms,(295) thus may be involved in the

increased DNA synthesis associated with cell proliferation. NAD+, and subsequently NADP, depletion may have led to less WST8 reagent being reduced to the formazan dye. To examine if this was the case for under-reporting in the WST8 assay results in future experiments, commercial kits to detect NAD+ levels are available. These kits utilise alcohol dehydrogenase to convert NAD+ to NADH, which in turn converts back to NAD+ by diaphorase enzyme; interestingly, the action of diaphorase is detected by the reduction of a tetrazolium salt into a formazan dye,(296) thus the level of NAD+ is indirectly detected by an assay similar to the WST8.

An example of over-reporting of the WST8 assay compared with the BrdU assay can be seen in **Figure 38A** where CM from SKOV3 cells incubated with leptin or lipocalin-2 induced HOMEC proliferation by 124% (for each adipokine) compared with the control when assessed by WST8 assay, and in **Figure 39** where the same treatment induced proliferation to a lesser magnitude (112% and 109% respectively) when assessed by BrdU assay. Since the principle of the WST8 assay is based on reduction of the tetrazolium reagent, the presence of other reducing molecules may thus affect the absorbance readings.

It was possible that the cancer-derived CM treatment applied onto HOMECs contained reducing agents. Reactive oxygen species (ROS) are possible candidates, as exogenous compounds added to ovarian cancer cells triggered ROS induction,(297, 298) which was thought to be one of the mechanisms in which cancer cells acquire resistance to therapeutic drugs.(299) Thus, future work could test the treatment media for the presence of ROS; for example, using fluorescent or chemiluminescent probes, spectrophotometry or chromatography.(300, 301)

Tetrazolium-based assays, such as the WST8 assay, are quick tools to determine numbers of viable cells and are commonly used in labs. However, there are pitfalls to their use as described above, and based on previous comparison studies.(302, 303) It is thus good practice to utilise at least two mechanistically different assays to confirm findings; in the present study, the BrdU assay was also performed alongside the WST8 assay.

3.4.4 HOMEC proliferation in conditioned media from omental adipose tissue and ovarian cancer cells

a) Treating HOMECs with omental adipose tissue conditioned media

Early experiments using undiluted adipose tissue CM to treat the HOMECs resulted in cell death; the normally adherent HOMECs detached from the cultureware surface, as observed under microscopy. Since the CM was collected over 24 hours, a possible explanation for this may be that the CM was too ‘concentrated’ with adipokines at levels higher than what is normally encountered by ECs in vivo, which becomes detrimental to the HOMECs. Thus, in subsequent experiments, the adipose tissue CM was diluted using starvation media.

From the results of the BrdU assay, all three dilutions of adipose tissue CM increased HOMEC proliferation, however only the increment observed in the 1:2 and 1:5 dilution were statistically significant. Likewise, in the WST8 assay, all dilutions at all three timepoints showed increased HOMEC proliferation but only a few of these increments were statistically significant. The explanation for the difference in the results of these proliferation studies were described in section 3.4.3. Importantly, treatment with adipose tissue CM increased HOMEC proliferation using both methodologies.

Likewise, HOMEC migration was also increased with adipose tissue CM treatment when compared to the control, although the results were not statistically significant (**Figure 43**). Taken together, these data suggested that the omental adipose tissue CM contained secreted factors which induce HOMEC pro-angiogenic responses observed as proliferation and migration. This is the first demonstration of this in HOMECs, although as discussed in section 1.5, these findings might have been expected as adipocytes secrete a range of factors involved in angiogenesis.

b) Treating HOMECs with ovarian cancer cell conditioned media

HOMEC proliferation was also tested with CM collected from two different ovarian cancer cell lines, SKOV3 and A2780. The SKOV3 cell line was originally derived from the ascites of a patient with ovarian adenocarcinoma, which is a type of epithelial ovarian cancer;(284, 304) thus, the SKOV3

represents metastatic cancer cells. On the other hand, the A2780 cell line was derived from the tumour tissue itself from an untreated patient diagnosed with ovarian endometroid adenocarcinoma;(285, 304) thus the A2780 represents primary ovarian tumour cells. In a mice study, both these cell lines were injected subcutaneously and intraperitoneally, and both locations showed tumour formation, characterised by gross and microscopic lesions.(305) This implied the high tumorigenicity of both cell lines and suggested that both are representative of metastatic ovarian cancer; thus suitable as ovarian cancer models in the present study.

It was initially postulated that factors secreted by the ovarian cancer would induce HOMEC activation and thus, proliferation, since it is widely accepted that cancer cells activate angiogenesis in order to sustain tumour growth (discussed in section 1.1.3d). However, this was not the case. When the ovarian cancer CM were tested on the HOMECs, HOMEC proliferation was not significantly increased by the treatments as assessed by BrdU assay (**Figure 29**). In the WST8 assay, the SKOV3 CM did not increase HOMEC proliferation at 24, 48 or 72 hours (**Figure 30**). The A2780 CM did however increase HOMEC proliferation at 48 and 72 hours, but not at 24 hours (**Figure 31**). These results contrasted with a previous study by Winiarski et al which showed that both SKOV3 and A2780 CM induced EC proliferation, with greater proliferation recorded at later timepoints (up to 72 hours).(106) SKOV3 CM treatment increased EC proliferation at 24 hours by at least 120%, while A2780 CM treatment increased proliferation at 24 hours by at least 150%.(106) However, there were differences in the methodology used for assessing HOMEC proliferation. In the Winiarski et al study, HOMEC proliferation was assessed by a different tetrazolium-based assay (WST1) and the ovarian cancer CM was presumably applied undiluted to the HOMECs at 150µL per well.(106) The different assay type (WST1, as opposed to WST8 or BrdU), together with a higher concentration of ovarian cancer secreted factors in the CM (undiluted CM and larger volume per well) may have resulted in enhanced HOMEC proliferation in the study by Winiarski et al. Alternatively, it is possible that the undiluted ovarian cancer CM in their study may have contained high levels of reducing factors such as reactive oxygen species (outlined in section 3.4.3),

which may have given rise to higher than actual cell viability values, when assayed using a tetrazolium reduction method.

The observation that only the 48- and 72-hour timepoints in the WST8 assay showed a significant increase in HOMEC proliferation when treated with A2780 CM, suggested that pro-angiogenic factors within the A2780 CM required time to manifest their proliferative action. Interestingly, factors secreted from the A2780 cells enhanced HOMEC proliferation but those from SKOV3 did not. Cancer cells are known to secrete a range of molecules, including growth factors. Since they are different ovarian cancer cell subtypes, the secretome of A2780 and SKOV3 may elicit different effects on the HOMECs; with the A2780 cells secreting more pro-proliferative factors than the SKOV3. Winiarski et al identified and compared the levels of a range of proteins in the secretomes of SKOV3 and A2780 cells and noted distinct differences. Notably, CXCL16 and HGF were detected in CM from A2780 at levels at least 20 times higher than in CM from SKOV3.(106) In vitro experiments in immortalised umbilical ECs showed that HGF treatment induced EC migration and tubule formation, which are characteristics of angiogenesis.(306) CXCR6 was detected in HMECs and served as a specific receptor for CXCL16;(307) similar to HGF, treatment with CXCL16 induced HMEC migration and tubule formation in vitro.(307) Thus, HGF and CXCL16 are possible candidates which may have induced HOMEC proliferation when treated with CM from A2780. Future work could elucidate other proliferative factors secreted from A2780 and investigate their effect on ECs.

The difference between the A2780 and SKOV3 secretome may be due to their cell origin. It was thought that A2780 cells, classed as the less aggressive non-serous cancer subtype and originally derived from the primary ovarian tumour, would be less inherently metastatic compared to SKOV3 cells.(308) The latter is classed as HGSC, deemed as the more aggressive and lethal subtype of ovarian cancers (described in section 1.2.2). An in vitro study, however, reported that A2780 cells displayed greater invasion activity (i.e. more aggressive characteristic) into collagen matrix (which resembles the ECM) compared to SKOV3 cells.(308) The authors of this study gave a possible explanation. They suggested that since the SKOV3 cells are of ascitic origin, able to grow in suspension and do not require invasion to survive, they do not

secrete factors to induce angiogenesis and invasion. In contrast A2780 cells are from the primary tumour and thus possess invasive characteristics expected of cancer cells, including secreting factors to induce angiogenesis.(308)

An alternative explanation relates to how immortalised cell lines are formed, since using primary cells to establish cell lines is difficult and most cell lines are derived from late stage tumours.(308) The presence of ascites, where SKOV3 cells were derived from, indicates advanced cancer stage, thus such cells possess metastatic potential due to the multiple genetic mutations which occurred from early to advanced cancer stage.(308) The primary tumour-derived A2780 cells may have undergone different genetic mutations to become an immortalised cell line and these mutations may have resulted in a different secretome and also incidentally bestowed metastatic potential. Since metastatic tumour growth was reported when both these ovarian cancer cell lines were injected into mice,(305) the latter explanation is possible. Interestingly, the invasive potential of A2780 cells may be demonstrated by the higher levels of MMP9 secretion by A2780 cells (at least 5-fold higher) compared to SKOV3 cells in the study by Winiarski et al;(106) in vitro invasion assays reported increased invasion with increased MMP9 levels, detected by Western blot analysis.(309)

c) Treating HOMECs with a combination of adipose tissue and ovarian cancer conditioned media.

The effect of the combination of both adipose tissue and ovarian cancer CM was studied to better mimic the in vivo environment. It was hypothesised that the omentum is such a rich environment for metastatic tumour growth because the secretome of the adipocytes enhance the effects of factors secreted from the metastasising cancer cells.

However, HOMEC proliferation when cells were treated with a combination of adipose tissue and ovarian cancer CM was similar to levels in HOMECs treated with ovarian cancer CM alone (**Figure 30** and **Figure 31**); and was lower than when HOMECs were treated with adipose tissue CM alone, as assessed by BrdU assay. This suggested an attenuation in proliferative effect when the CM were combined; however, the reason for this is unclear. It is possible that factor(s) secreted by the ovarian cancer cells may actually be anti-proliferative

in certain conditions and counteracted the proliferative effect of the adipose tissue CM. A possible candidate may be serpin E1 or also known as plasminogen activator inhibitor-1 (PAI-1).

PAI-1 was found to be highly secreted by both A2780 and SKOV3 cells,(106) and exerts pro- and anti-angiogenic capabilities depending on its concentration levels.(310, 311) Its pro-angiogenic effects were evident at lower, physiological concentrations while supraphysiological concentrations revealed its anti-angiogenic effect, as assessed by vessel outgrowth in a mouse aortic ring assay when treated with a range of PAI-1 concentrations.(310) Indeed, in an in vivo chicken chorioallantoic membrane angiogenesis assay, increasing PAI-1 concentrations inhibited angiogenesis induced by FGF-2, which is a known pro-angiogenic mediator.(311) Thus, from this finding, it is possible that the HOMEC proliferation induced by adipose tissue CM may have been lessened by PAI-1 in the ovarian cancer CM. Similarly, it was also possible that the cancer-secreted PAI-1 may have contributed to the lack or low levels of proliferation in HOMECs treated with CM from A2780 and SKOV3 cells. Additionally, PAI-1 was also detected in adipose tissue CM (**Figure 97** in the appendix), but its level was nowhere near as high as other secreted adipokines which are possibly pro-proliferative. Future work could examine the extent of the anti-proliferative effect of PAI-1 or other mediators secreted by cancer cells.

3.4.5 HOMEC migration

Aside from proliferation, HOMEC migration is an indicator of EC activation. Similar to the proliferation data, treatment with adipose tissue CM increased HOMEC migration (indicated by scratch closure) compared with the control, but the results did not achieve statistical significance. ECs are normally quiescent in both proliferation and migration;(312) in such conditions, the factors which promote or inhibit their migration are in equilibrium. It is possible that the combination of adipokines within the adipose tissue CM (in the absence of inhibitory mediators derived from other cell types) tips this equilibrium towards a pro-migratory state, while the individual adipokines tested (adiponectin, cathepsin L, lipocalin-2 and MIF) were not sufficient to disrupt this quiescent equilibrium.

It was also possible that the numerous adipokines secreted by adipose tissue have a larger role in activating signalling pathways related to HOMEC proliferation than signalling pathways involved in cell migration. This can be exemplified by FGF-2 and VEGF, two known pro-angiogenic factors which were shown in an in vitro study to have differential effects on EC proliferation and migration.(313) At the same concentrations, treatment with FGF-2 induced greater levels of HUVEC proliferation (4-fold higher) than VEGF, whereas VEGF induced greater HUVEC migration (2-fold higher) than FGF-2.(313) However, combination treatment consisting of both FGF-2 and VEGF did not synergistically increase cell proliferation and migration.(313)

Treatment with SKOV3 CM alone or in combination with adipose tissue CM did not increase HOMEC migration. However, treatment with A2780 CM alone or in combination with adipose tissue CM increased HOMEC migration. Similar to the results of HOMEC proliferation, this suggests that factor(s) secreted by A2780, and not SKOV3, induced cell migration. As discussed in the previous subsection, secreted factors such as HGF and CXCL16 may be implicated. A study using a similar scratch wound assay conducted in umbilical ECs reported that treatment with HGF increased EC migration rate.(306) In a study by Isozaki et al (2013) HMEC migration was assessed using a chemotaxis assay (modified Boyden chamber) and showed that HMEC migration towards CXCL16 was dose-dependent.(307) Thus, HGF and CXCL16 are possible candidates for future work examining HOMEC migration. Future experiments could also investigate the mechanism of HOMEC migration, e.g. in terms of protrusion formation and forward movement,(312, 314) in response to stimulating factors secreted by adipose tissue and ovarian cancer cells.

3.4.6 Adipokine identification and quantification

Since the adipose tissue CM clearly had pro-angiogenic effects in the HOMECs, an adipokine array was utilised to identify the adipokines secreted into the adipocyte and adipose tissue CM that might promote these effects. The overlap of the identified adipokines in the adipocyte and adipose tissue CM (**Figure 33A**) supported the assumption that the adipose tissue was primarily composed of adipocytes. Although the array was not specifically designed for quantitative

detection of adipokines, the pixel density measurements were clearly higher when the membrane was treated with adipose tissue CM compared to adipocyte CM (**Figure 33**).

It could be seen that a very wide range of proteins were secreted from omental adipocytes in varying amounts. From the most abundantly secreted adipokines, four were initially chosen for further investigation based on their reported involvement in angiogenesis: adiponectin, cathepsin L, lipocalin-2 and MIF. Adiponectin is the most abundantly secreted adipokine from adipocytes,(315) hence its detection in the adipokine array was expected. Past studies reported adiponectin involvement in angiogenesis. For example, in a mouse in vivo study, adiponectin stimulated angiogenesis and restored vascular circulation in ischaemia.(316) In vitro, adiponectin increased migration of human umbilical vein ECs (HUVECs) and their differentiation into capillary-like structures.(317) Indirectly, adiponectin may also stimulate angiogenesis via the expression of VEGF.(318)

The role of adiponectin is commonly associated with another adipokine, leptin. The amount of secreted adiponectin is inversely proportional to body fat mass, whereas circulating leptin levels are proportional to body fat mass.(315) The concept of the leptin-adiponectin ratio, as opposed to either adipokine alone, better encapsulates adipose tissue dysfunction and associated conditions such as type 2 diabetes and cardiovascular diseases.(287, 319) Furthermore, the increase in this ratio was associated with the risk or prognosis of some cancers, such as breast, colorectal, endometrial and ovarian cancers.(320-323) On its own, leptin induced proliferation in ovarian cancer cell lines based on in vitro experiments.(324) Leptin is also involved in angiogenesis; leptin receptors were detected in HUVECs and leptin treatment induced tube formation in vitro.(325, 326) Based on these observations, and since secreted leptin was detected in the adipokine array, it was also selected for further investigation.

Cathepsin L, a type of cysteine protease enzyme, is associated with tumour angiogenesis and is secreted by various types of tumours. Studies in human lung microvascular endothelial cells, HUVECs and HOMECs reported that treatment with cathepsin L induces cell sprouting, migration and proliferation.(106, 327, 328)

Lipocalin-2, also known as neutrophil gelatinase-associated lipocalin, is a glycoprotein whose upregulation is associated with some cancers, e.g. breast, pancreatic, thyroid and ovarian cancers.(329-332) Lipocalin-2 showed direct pro-angiogenic effects in rat brain ECs,(333) and indirectly in HUVECs via altered VEGF expression in breast cancer cells,(332) and thus lipocalin-2 was selected for further investigation.

When MIF was discovered, its role was initially thought to be limited to immune function. Subsequently, increased levels of MIF were found to be associated with some types of cancers, e.g. bladder, hepatocellular, prostate and breast cancers.(334-337) In vitro studies in human dermal microvascular ECs (HDMECs) and HUVECs reported increased cell migration and tube formation with MIF treatment.(335, 338) Similar to adiponectin and lipocalin-2, MIF treatment increased angiogenesis in breast cancer through the upregulation of other pro-angiogenic factors, e.g. VEGF and IL-8.(337) With a role in angiogenesis, MIF was thus also selected for further investigation.

After the 5 adipokines were selected, ELISAs were performed to determine their individual concentrations within the adipose tissue CM. This was necessary as the ELISA provided an estimate of the physiological concentrations of these adipokines, whereas the adipokine array only provided the rank order of the adipokines and not their specific concentrations. When the adipokines were tested on the HOMECs, the concentration range used was based on the levels detected by the ELISA.

3.4.7 HOMEC activation with adipokines

Interestingly, individually, the selected adipokines did not increase HOMEC proliferation or migration at any of the concentrations tested. At this juncture, there were two possible assumptions: the selected adipokines were not the main pro-angiogenic components of the adipose tissue CM, or the adipokines did not manifest their angiogenic functions individually. Considering that the selected adipokines showed pro-angiogenic effects from past studies and that the adipose tissue CM consisted of various adipokines, the latter hypothesis was tested.

To test this, treatment consisting of adipokine mixtures or cocktails were tested on HOMECs. When preparing the adipokine cocktail, only one concentration per adipokine was chosen to reduce the number of permutations which invariably arises with 5 separate adipokines. A value in the upper range of the ELISA results was chosen to maximise the adipokine effect on the HOMECs. However, treatment with adipokine cocktails did not enhance HOMEC proliferation as assessed by either BrdU or WST8 assays.

Interestingly, treatment with cocktails containing adiponectin showed the lowest levels of proliferation in the BrdU assay (**Figure 36**). The 5-adipokine cocktail, containing adiponectin, resulted in lowest proliferation in the WST8 assay (**Figure 37**). This observation may be attributed to the protective effects of adiponectin on the vasculature. For instance, in studies related to metabolic disorders, low circulating adiponectin levels were found to be associated with conditions such as atherosclerosis and diabetes, which are conditions that exemplify vascular dysfunction.(339)

Adiponectin also has direct effects on ECs. An in vitro study by Bråkenhielm et al (2004) found that that adiponectin treatment reduced both the proliferative and migrative effect induced by FGF-2 and VEGF in ECs; and that the anti-angiogenic activity of adiponectin was achieved via EC apoptosis.(340) This was not observed via microscopy in the current study, i.e. the HOMECs did not become unadhered from the culture surface. Additionally, both BrdU and WST8 data (**Figure 34** and **Figure 35**) inferred that cell numbers and viability when treated with adiponectin alone were similar to the control, untreated cells. The ECs used in the study by Bråkenhielm et al were derived from bovine and porcine sources (i.e. non-human derived EC), and the magnitude of proliferation and migration inhibition positively correlated with the concentration of adiponectin applied.(340) The maximum concentration of adiponectin used in their study was 2µg/mL;(340) by extrapolation, and since the maximum concentration of adiponectin used in the treatment cocktail was 10µg/mL it was possible that these levels suppressed proliferation of HOMECs. Inconsistently, when the authors of the previous study concluded that the reduction in EC proliferation and migration was due to apoptosis, the experiment was conducted in bovine ECs and HMECs using adiponectin concentrations between 10-20µg/mL; i.e. up to 10-fold more than the maximal concentration tested in EC

proliferation and migration, which was originally tested in bovine and porcine ECs.(340)

The protective effect of adiponectin is also supported by studies of pathological conditions. Adiponectin has been reported to restore endothelial function in pathologies such as diabetic nephropathy and atherosclerosis.(341, 342) For example, in an in vitro model of atherosclerosis, treatment with oxidised low density lipoprotein (ox-LDL) was found to induce proliferation of human aortic ECs, an early step in atherosclerosis development. Treatment with both ox-LDL and adiponectin, or with adiponectin alone, resulted in EC numbers similar to the control, as assessed by tetrazolium-based and deoxyuridine-based assays (similar to WST8 and BrdU assays respectively). The authors concluded that adiponectin has no effect on EC proliferation on its own, but its protective effect (by reducing EC proliferation) only manifests in the presence of a noxious stimulant such as ox-LDL. Similarly, to model a diabetic nephropathy state, rat glomerular ECs treated with high glucose significantly decreased cell viability in a WST8 assay.(341) Treating the ECs with both high glucose and adiponectin (up to 25µg/mL) resulted in cell viability levels similar to the control.(341) Thus, the study authors concluded that adiponectin is protective against glucose-induced damage to ECs.(341)

Consistent with this, it was possible that the experimental conditions were not fully representative of physiological conditions, e.g. the selective combination of adipokines in the adipokine cocktails represents only a subset of the adipose tissue CM. In this deviation from physiological conditions, adiponectin may have exerted its protective effects; thus, treatment with adiponectin-containing cocktails resulted in reduced HOMEC proliferation.

EC quiescence is a result of the balance between pro- and anti-proliferative factors and their associated signalling pathways;(343) of the factors secreted by omental adipocytes, it is possible that adiponectin exerts an anti-angiogenic role. In the same study by Bråkenhielm et al, mentioned previously, adiponectin was injected into fibrosarcoma tumours in mice and the authors demonstrated tumour size reduction attributed to apoptosis and reduction in vessel growth.(340) At the same time, direct application of adiponectin (up to 30µg/mL) onto the tumour cells in vitro did not show changes in cell numbers. These findings, together with the earlier observation that adiponectin causes EC

apoptosis, led the authors to conclude that adiponectin is a negative regulator of angiogenesis.(340)

One possibility as to why no significant increase in HOMEC proliferation was observed with individual adipokines could be the very nature of the cell culture experiments. In vivo, ECs are normally quiescent in terms of proliferation (section 1.1.3). In vitro, they are more actively proliferating (292) and this phenotype thus served as a baseline (control). Additional proliferative activity as a result of treatment media (e.g. treatment with individual adipokines or with a combination of adipokines) may not be easily distinguished from the control. Thus, for the treatment media to show significant difference compared with the control, the proliferative effect must be several orders of magnitude greater to achieve statistical significance. By this reasoning, it was possible that the adipose tissue conditioned media (consisting of a larger range of adipokines) is more effective than the individual adipokines in eliciting proliferation in HOMECs. Although cell culture has many benefits for researchers, such discrepancies between the in vitro and in vivo environments have been noted previously as a potential disadvantage.(344)

3.4.8 The effects of CM from adipokine-incubated ovarian cancer cells

Given the multifaceted role of adipocytes in tumour metastasis (discussed in section 1.5), interaction between the omental adipocytes and the metastatic ovarian cancer cells is possible. It was hypothesised that a complex secretory profile within the tumour microenvironment, formed by factors secreted from the adipokines and the cancer cells, may be conducive in activating angiogenesis. To test this, ovarian cancer cells were incubated with selected adipokines, and the CM collected after 24 or 48 hours of incubation. These CM were then applied onto HOMECs, and their proliferation assessed.

It was observed that HOMECs treated with CM from SKOV3 or A2780 cells, pre-incubated for 24 hours with leptin or lipocalin-2, showed significant proliferation when assessed using the BrdU assay (**Figure 39** and **Figure 41**). The BrdU assay is deemed more sensitive in measuring cell proliferation, as

discussed in section 3.4.3. The data clearly suggest that the adipokines induce release of pro-proliferative factors from the cancer cells.

To date there are no past studies which showed that cancer cells secrete factors which activate ECs after the exogenous application of lipocalin-2. Immunohistochemical and serum studies in breast, endometrial and colorectal cancers reported increased expression of lipocalin-2 on the cancer cells themselves; and this observation was positively correlated with VEGF expression.(332, 345-347) This increased VEGF concentration then induced angiogenesis, leading to cancer invasion and metastasis.(332, 345) Additionally in ovarian cancer, the expression of lipocalin-2 was shown to be significantly higher than in normal ovarian tissue (348, 349) and the protein was also detected in the SKOV3 cell line.(349) Based on the past studies mentioned, VEGF may be a possible candidate secreted by the ovarian cancer cells incubated with lipocalin-2 in the present study.

Likewise, no past studies reported that ovarian cancer cells secrete factors which induce EC proliferation after the exogenous application of leptin. Several studies in animal models reported the secretion of VEGF from cancer cells after treatment with leptin. For example, mouse mammary cancer cells incubated for 24 hours with leptin at various concentrations resulted in VEGF secretion in a dose-dependent manner;(350, 351) however, the minimum concentration of leptin used was 10ng/mL,(350, 351) which was least 3 times more than that utilised in the present study (3ng/mL). Furthermore, the cancer cell CM collected was frozen prior to ELISA,(350) which may yield inconsistent results (discussed in section 4.2.3 in chapter 4). In another study, incubating leptin with mouse pre-neoplastic colon epithelial cells yielded CM which induced proliferation when treated on HUVECs; VEGF was identified as the pro-angiogenic factor in the CM.(352)

Other factors were also secreted when cancer cells were incubated with leptin. Mouse mammary cancer cells secrete the pro-inflammatory mediator, IL-1, which partially mediates the upregulation of VEGF expression in the cancer cells.(351) Increased MMP7 expression was detected when ovarian cancer cells, including SKOV3, were incubated with leptin.(353) The enzyme MMP7 has an indirect pro-angiogenic role, by degrading VEGF inhibitors secreted by ECs such that the inhibitor-bound VEGF is released and able to exert its pro-

angiogenic effects; this was evidenced by cell migration and tube formation in HUVECs.(354) From these past studies, VEGF appeared to be a common secreted factor when cancer cells were treated with lipocalin-2 or leptin; thus, VEGF was further investigated in the following chapter.

Enhanced proliferation was not observed when the HOMECs were treated with CM from SKOV3 or A2780 cells pre-incubated for 48 hours with the same adipokines (**Figure 38B** and **Figure 40B**). A possible explanation is that the proliferative factor(s) secreted after 24-hour incubation may no longer be active if left in incubation for 48-hours. Furthermore, the incubations with adipokines were performed with starvation media. Nutrients within the media may be fully exhausted by 48 hours and conditions may no longer be conducive for the cancer cells to secrete this factor, or for the HOMECs to respond to it.

To further explore these possibilities, a similar experiment was performed using complete growth media instead of starvation media when incubating the SKOV3 cells with the adipokines. Strikingly, treatment with CM after 24-hour incubation with leptin or lipocalin-2 did not enhance HOMEC proliferation as significantly as treatment with CM obtained after 48-hour incubation (**Figure 98** in the appendix). In the latter, HOMEC proliferation was 121% and 126% vs control (100%) after treatment with CM from SKOV3 cells incubated with leptin and lipocalin-2 respectively.

It is therefore possible that after 24 hours of incubation, the CM (composed of growth media) may still contain sufficient nutrients to allow HOMEC proliferation with or without the presence of adipokines. After 48 hours of incubation, the nutrients within the media may be exhausted and created conditions similar to that in starvation media; i.e. the secreted factors, not the growth media, supported HOMEC proliferation. Thus, the conditions in the 48-hour incubation with growth media may resemble those in the 24-hour incubation with starvation media, since the CM from both these enhanced HOMEC proliferation when leptin or lipocalin-2 were incubated with the SKOV3.

Interestingly, treatment with CM from ovarian cancer cells pre-incubated with adiponectin showed reduced HOMEC proliferation compared to control, which was in contrast with a study by Ouh et al (2019). They showed that CM from SKOV3 cells, incubated with adiponectin for 48 hours, induced angiogenesis in

HUVECs.(355) This discrepancy may be due to the EC type; HUVECs are derived from the macrovasculature while HOMECs from the microvasculature, with the latter being more relevant in angiogenesis and to EOC metastasis, as discussed in section 1.1.2d. Furthermore, the method of measuring EC activation was different. The previous study looked at tube formation, while the current study assessed proliferation via DNA synthesis (BrdU assay) and cell metabolism (WST8 assay); thus, adiponectin action on ECs may manifest differently depending on which pathways are involved. Additionally, the adiponectin concentration utilised in the previous study was 80ng/mL for tube formation, whereas in the current study the ovarian cancer cells were incubated with 5µg/mL of adiponectin, which was the average concentration detected in the omental adipose tissue CM via ELISA (section 3.3.4c). It is possible that a 60-fold difference in adiponectin concentration may influence the types of factors secreted by cancer cells. As previously discussed, treating HOMECs with adiponectin in combination with other adipokines resulted in reduced proliferation (section 3.3.5b, and discussed in section 3.4.7). The CM collected from the ovarian cancer cells may have contained the initial incubated adiponectin together with other factors secreted by the cancer cells; thus the combination of these factors may then yield similar results when treated on HOMECs.

3.8 Chapter summary

The microenvironment of an EOC metastasis developing in the omentum is highly complex, with multiple cell types present. Many of these cells have the potential to secrete factors able to switch the resident omental microvascular ECs (HOMECs) to the pro-angiogenic phenotype required to support the new vessel growth needed for tumour development. These cells include the adipocytes, the major cell type present in the omentum, and the tumour cells themselves. This chapter examined the effect of CM from both cell types on the angiogenic phenotype of HOMECs, specifically proliferation and migration.

Importantly, the whole secretome (i.e. CM) of the omental adipose tissue enhanced HOMEC proliferation; but after identifying and quantifying highly secreted pro-angiogenic factors (adipokines) and testing potential pro-

angiogenic adipokines individually and in combination, no increase in HOMEC proliferation was observed.

SKOV3 and A2780 cells are human ovarian cancer cell lines representing metastatic and primary cancer cells respectively. Factors secreted from A2780, but not SKOV3 cells, induced proliferation in HOMECs only after prolonged incubation (48 and 72 hours). Considering the tumorigenicity of these ovarian cancer cell lines, this was unexpected as inducing angiogenesis, achieved through the secretion of pro-proliferative factors, is a hallmark of cancer.

To better simulate the tumour microenvironment during cancer metastasis to the omentum, the ovarian cancer cells were incubated with adipokines to investigate if the adipocyte-secreted factors enhance the effects of cancer-secreted factors. Incubating SKOV3 and A2780 cells with leptin and lipocalin-2 yielded CM which when added to HOMECs, induced their proliferation. This adipokine action and how it affects the intracellular pathways involved in HOMEC proliferation are explored in the following chapter.

This observation implied that the combination of factors secreted from the cancer cells and that of the omental adipocytes provided suitable conditions, or ‘soil’, for cancer metastasis to the omentum. The combination of proliferative factors supports angiogenesis, which in turn encourages tumour growth. Future work could focus on the synergy between the omental adipocytes and the metastasising cancer cells. A suitable starting point may be to assess the proliferation of HOMECs when treated with a combination of CM from ovarian cancer cells previously incubated with leptin or lipocalin-2, and with CM from adipose tissue. On that note, HOMEC migration studies could also be investigated using CM from cancer cells incubated with adipokines.

Chapter 4. An investigation into the intracellular pathways in involved in the proliferation of human omental microvascular endothelial cells

4.1 Introduction

In the previous chapter, data presented showed that HOMEC proliferation was significantly enhanced when cells were treated with CM from SKOV3 cells previously incubated with leptin or lipocalin-2 as assessed by WST8 and BrdU assays, and also when treated with CM from A2780 cells as assessed by BrdU assay. Separately, HOMEC proliferation was also observed with omental adipose tissue CM treatment. The latter observation may represent in vivo conditions due to the proximity between HOMECs and adipocytes within the omentum, while the former may be a result of the interaction between omental adipokines and the ovarian cancer cells leading to HOMEC activation and subsequently tumour angiogenesis. Thus, it is possible that the adipokines were either (a) inducing enhanced secretion of pro-proliferative factors from the cancer cells, or (b) inducing a secretion of a different range of pro-proliferative factors from the cancer cells.

Therefore, a series of experiments were carried out to investigate what components of the adipokine-induced cancer cell secretome could be responsible for the enhanced HOMEC proliferation. This type of investigation could potentially be carried out using two approaches; to directly investigate the changes in the components of the cancer cell secretome, or to investigate the signalling pathways activated in the HOMECS and interrogate the secretome specifically for pro-proliferative proteins known to activate these pathways. Due to logistical reasons, the latter approach was taken.

In the regulation of cell proliferation, signalling pathways activated by growth factor are characterised both the surface receptor involved, and intracellular signalling proteins activated. Since many growth factors act via surface tyrosine kinase receptors and phosphorylation is a key regulatory mechanism of many signalling molecules, activation of both can be studied by changes in their phosphorylation levels.(356, 357) Thus, this chapter investigates the intracellular signalling pathways involved in HOMEC proliferation induced by adipose tissue CM and CM from adipokine-incubated ovarian cancer cells, and

proposes the potential signalling pathways activated upstream of HOMEC proliferation. Experiments were also conducted to determine if the proliferative factor(s) in these two CM types are the same.

This chapter is divided into sections aimed at:

a) identifying the receptors activated when HOMECs are treated with CM from ovarian cancer cells pre-treated with leptin or lipocalin-2, or with CM from omental adipose tissue (sections 4.3.1 and 4.3.6);
b) identifying and quantifying the ligands secreted from ovarian cancer cells pre-treated with leptin or lipocalin-2 that may activate these receptors (section 4.3.2);
c) assessing HOMEC proliferation in cells co-treated with inhibitors of identified receptors in the presence of ovarian cancer CM (section 4.3.4); and
d) identifying the intracellular targets (kinases) activated when HOMECs are treated with CM from ovarian cancer cells pre-treated with leptin or lipocalin-2, or with CM from omental adipose tissue (sections 4.3.5 and 4.3.7)

4.2 Methods

4.2.1 Collection of HOMEC lysate

To elucidate the intracellular signalling mechanisms by which cell proliferation occurs, the CM-treated HOMECs were lysed to obtain their intracellular components. To maximise the concentration of lysate collected, the experimental setup described in section 3.2.9 was proportionally scaled upwards based on the growth area of lab plasticware. Ovarian cancer cells were seeded in 6cm diameter dishes (42,000 cells/dish for SKOV3; 89,000 cells/dish for A2780), with an adipokine incubation volume of 7mL/dish; their CM were collected as described in section 3.2.9.

HOMECs were seeded in 10cm diameter dishes at 1.5 million cells/dish, cultured for at least 24 hours and then subjected to serum starvation overnight before the application of the fresh ovarian cancer cell CM (15mL/dish), similar to the procedure described in section 3.2.9. The treatment conditions studied CM

from SKOV3 cells incubated with leptin or lipocalin-2, and CM from A2780 cells incubated with leptin or lipocalin-2, with their respective controls. In a separate protocol, the serum-starved HOMECs were treated with omental adipose tissue CM diluted 1:2 with starvation media. The corresponding control was starvation media alone in place of the diluted adipose tissue CM.

The CM treatments were applied onto the HOMECs for 5 minutes, then aspirated off and the cells were rinsed twice with ice cold PBS to halt cellular reactions. The purpose of this short treatment duration (5 minutes) is to examine the initial receptor activation and cellular signalling which eventually leads to cell proliferation, i.e. the 'spark' which initiates downstream signalling. The activation (phosphorylation) of several key cellular targets are known to be maximum at 5 minutes.(358, 359) This method was also commonly practised in the lab.(360)

600µL of cold lysis buffer (components detailed in section 2.3.2) was applied per dish before the HOMECs were scraped off using a cell scraper. To maximise the protein concentration within the lysate, 3 dishes of HOMECs were used per treatment and this same volume of lysis buffer (600µL) was shared between the 3 dishes. The cell suspension was transferred to microcentrifuge tubes and allowed to lyse on a rotary mixer at 2-8°C for 30 minutes. The tubes were then centrifuged at 20,000*g* at 4°C for 15 minutes to separate the supernatant from the cell debris. The supernatants were transferred to fresh microcentrifuge tubes and stored at -80°C for later use.

4.2.2 Screening of HOMEC lysate for phosphorylated receptor tyrosine kinase and phosphorylated kinase targets

Commercial antibody array kits were used to identify both the receptor tyrosine kinases (phospho-RTK array) and intracellular kinases (phospho-kinase array) activated in HOMECs treated with adipose tissue and ovarian cancer CM. The main component of the kits are the nitrocellulose membranes containing control and capture antibodies for specific targets. The phospho-RTK array kit (R&D Systems, ARY001B) detects phosphorylated (activated) receptor tyrosine kinases (RTK), while the phospho-kinase array kit (R&D Systems, ARY003B

and ARY003C) detects phosphorylated intracellular protein kinases in a given sample.

Two versions of the phospho-kinase array kit were utilised (ARY003B and ARY003C). The manufacturer's handling instructions were identical between the two versions, however, the targets imprinted on the membranes were different. ARY003B contained more kinase targets compared to ARY003C: 45 and 39 targets respectively. Only targets which were common to both versions were analysed. The phospho-RTK array contained 49 targets.

Lysates collected from HOMEC treated as indicated were prepared as described in section 4.2.1. The frozen lysate supernatant was thawed at room temperature and were used only as sample for the arrays; any thawed balance was discarded. In preparing the samples, the volume of HOMEC lysate supernatant corresponding to 200-400µg of protein (as determined by the BCA protein assay, section 2.14) was diluted to 1.5mL (phospho-RTK array) or 2mL (phospho-kinase array) with the supplied blocking buffer. The samples were then loaded onto the nitrocellulose membranes supplied in the kit based on protein amount.

The array membranes were processed according to the manufacturer's instructions (section 2.16). After calculating the pixel density of each spot and subtracting the negative control values, the membranes treated with the control lysate were compared with the membranes treated with lysate from adipokine-incubated ovarian cancer CM, or from adipose tissue CM. The difference between pixel densities were expressed as a percentage of the control.

Diagrams of the phospho-RTK array and phospho-kinase array membranes, and their corresponding target coordinates are shown in **Figure 47** and **Figure 48** respectively.

(A)

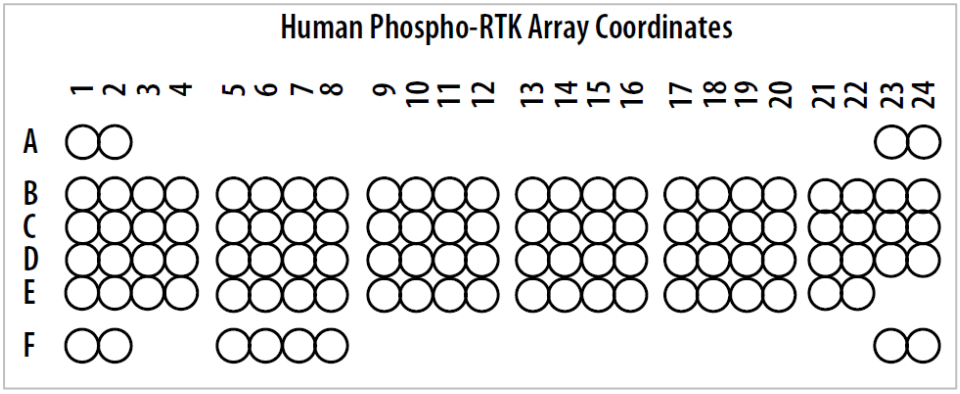

(B)

Membrane coordinates	Receptor Tyrosine Kinase	Membrane coordinates	Receptor Tyrosine Kinase
A1, A2, A23, A24, F1, F2	Reference spots	F23, F24	Negative controls
B1, B2	EGFR	D1, D2	Tie-2
B3, B4	ErbB2	D3, D4	TrkA
B5, B6	ErbB3	D5, D6	TrkB
B7, B8	ErbB4	D7, D8	TrkC
B9, B10	FGFR1	D9, D10	VEGFR1
B11, B12	FGFR2α	D11, D12	VEGFR2
B13, B14	FGFR3	D13, D14	VEGFR3
B15, B16	FGFR4	D15, D16	MuSK
B17, B18	Insulin R	D17, D18	EphA1
B19, B20	IGF-1R	D19, D20	EphA2
B21, B22	Axl	D21, D22	EphA3
B23, B24	Dtk	D23, D24	Eph A4
C1, C2	Mer	E1, E2	EphA6
C3, C4	HGFR	E3, D4	EphA7
C5, C6	MSPR	E5, E6	EphB1
C7, C8	PDGFRα	E7, E8	EphB2
C9, C10	PDGFRβ	E9, E10	EphB4
C11, C12	SCFR	E11, E12	EphB6
C13, C14	Flt-3	E13, E14	ALK
C15, C16	M-CSFR	E15, E16	DDR1
C17, C18	c-Ret	E17, E18	DDR2
C19, C20	ROR1	E19, E20	EphA5
C21, C22	ROR2	E21, E22	EphA10
C23, C24	Tie-1	F5, F6	EphB3
		F7, F8	RYK

Figure 47. The receptors assessed in the phospho-RTK array kit. Location of receptors on the membrane (A) and the coordinates of the 49 receptor tyrosine kinase targets (B). Adapted from the package insert of the Proteome Profiler™ Array (R&D Systems, ARY001B).

(A)

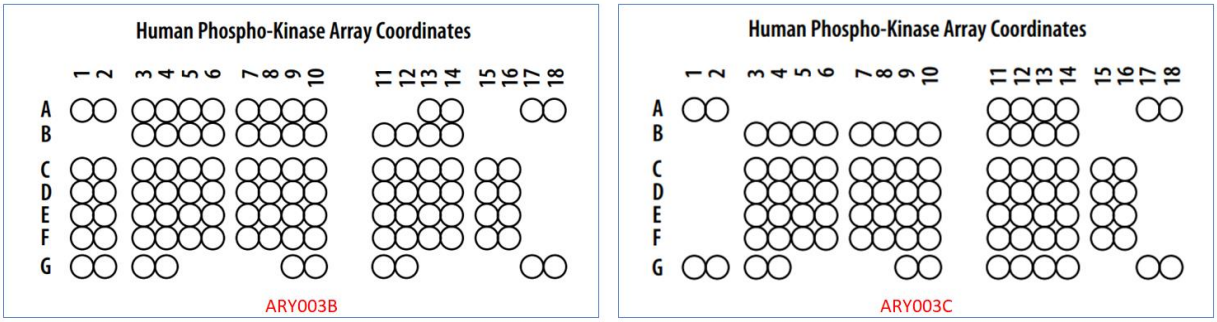

(B)

Membrane coordinates (ARY003B)	Membrane coordinates (ARY003C)	Kinase (Phosphorylation site, if available)	Membrane coordinates (ARY003B)	Membrane coordinates (ARY003C)	Kinase (Phosphorylation site, if available)
A1, A2, A17, A18, G1, G2	A1, A2, A17, A18, G1, G2	Reference spots	G9, G10, G17, G18	G9, G10, G17, G18	Negative controls
B11, B12	A11, A12	AKT1/2/3 (T308)	-	D7, D8	Lyn (Y397)
B9, B10	A13, A14	AKT1/2/3 (S473)	B5, B6	D9, D10	MSK1/2 (S376/S360)
B7, B8	-	AMPKα1 (T183)	E13, E14	-	p27 (T198)
C7, C8	-	AMPKα2 (T172)	-	D11, D12	p70 S6 kinase (T389)
-	B3, B4	CREB (S133)	D11, D12	D13, D14	p70 S6 kinase (T421/S424)
B3, B4	B5, B6	EGFR (Y1086)	-	D15, D16	PRAS40 (T246)
D15, D16	B7, B8	eNOS (S1177)	A3, A4	E3, E4	p38α (T180/Y182)
A5, A6	B9, B10	ERK1/2 (T202/Y204, T185/Y187)	F7, F8	E5, E6	PDGFRβ (Y751)
F3, F4	B11, B12	Chk-2 (T68)	E15, E16	E7, E8	PLC-γ1 (Y783)
-	B13, B14	c-Jun (S63)	-	E9, E10	Src (Y419)
C3, C4	-	CREB (S133)	F15, F16	E11, E12	PYK2 (Y402)
F5, F6	-	FAK (Y397)	-	E13, E14	RSK1/2 (S221/S227)
E5, E6	C3, C4	Fgr (Y412)	D13, D14	E15, E16	RSK1/2/3 (S380/S386/S377)
E1, E2	-	Fyn (Y420)	-	F3, F4	STAT2 (Y689)
A9, A10	C5, C6	GSK-3α/β (S21/S9)	F9, F10	F5, F6	STAT5a/b (Y694/Y699)
-	C7, C8	GSK-3β (S9)	C1, C2	-	TOR (S2448)
F1, F2	-	Hck (Y411)	F13, F14	F7, F8	WNK1 (T60)
C5, C6	C9, C10	HSP27 (S78/S82)	E3, E4	F9, F10	Yes (Y426)
G11, G12	G13, G14	HSP60	-	F11, F12	STAT1 (Y701)
-	C11, C12	p53 (S15)	E11, E12	F13, F14	STAT3 (Y705)
B13, B14	C13, C14	p53 (S46)	F11, F12	F15, F16	STAT3 (S727)
A13, A14	C15, C16	p53 (S392)	C9, C10	G3, G4	B-Catenin
A7, A8	D3, D4	JNK1/2/3 (T183/Y185, T221, Y223)	E9, E10	-	STAT5b
-	D5, D6	Lck (Y394)	E7, E8	G11, G12	STAT6 (Y641)

Figure 48. The protein kinases assessed in the phospho-kinase array kit. Location of kinases on the membranes (A) and the coordinates of the kinase targets (B). Adapted from the package insert of the Proteome ProfilerTM Array (R&D Systems, ARY003B and ARY003C).

4.2.3 Quantification of identified secreted ligands using ELISA

To determine the concentration of FGF-2, TGF-β1 and VEGF secreted into CM from ovarian cancers pre-incubated with lipocalin-2 or leptin CM, the ELISA protocol detailed section 2.15 was utilised. The CM were collected based on the method elaborated in section 3.2.9 and were tested by ELISA as fresh samples. This was because in preliminary experiments, -80°C frozen and thawed CM samples did not yield reliable results on ELISA. The resultant standard curves are shown in **Figure 49**.

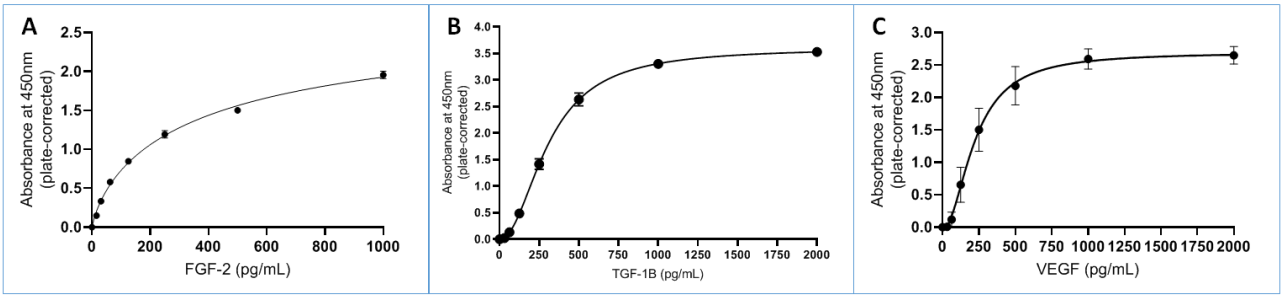

Figure 49. Representative ELISA standard curves for FGF-2, TGF-β1 and VEGF. The concentration of individual ligands detected in the conditioned media samples were interpolated from these standard curves based on their absorbance values. For each kit, the supplied standards (FGF-2 (A), TGF-β1 (B), VEGF (C)) were diluted to the recommended range of concentrations, assayed by ELISA on 96-well plates and the absorbance was then read at 450nm. Absorbance values shown are mean ± SD; n=3-4.

4.2.4 Establishing the maximal non-toxic concentration of receptor inhibitors in HOMECs using the WST8 assay

To examine the involvement of identified ligands or receptors in HOMEC proliferation, specific inhibitors of the receptors were used. However, prior to their use it was necessary to establish a non-toxic working concentration range.

Alectinib, SAR131675 and AZD4547 (inhibitors of ALK, VEGFR3 and FGFR1/2/3 respectively) were dissolved in DMSO to form a stock solution. The stock solution was then diluted in starvation medium to concentrations between 1nM to 100μM, based on concentrations used in the literature. DMSO at the

highest concentration used for each inhibitor was included as the vehicle control.

The HOMECs were seeded at 10,000 cells/well in 96-well flat-bottomed plates coated with gelatin (2% w/v). The cells were incubated in complete growth media (100µL/well) at 37°C/5% CO_2 for at least 24 hours before substituting the media for the inhibitor treatment at various concentrations. After overnight incubation, the wells were replenished with the same inhibitor treatment for another 24 hours. The purpose of this overnight followed by a 24-hour incubation with the inhibitor was to simulate previous experimental conditions, whereby HOMECs were serum-starved overnight prior to treatment application (also diluted in starvation media) for 24-hours, as described in section 2.10.

The WST8 assay was performed according to section 2.12. As this was a preliminary dose-finding experiment, the procedure was only performed twice with HOMECs isolated from two separate omental samples. Statistical tests were not performed due to the small number of repeats (n=2).

4.2.5 An investigation into the effect of inhibitors of identified receptors on proliferation induced by conditioned media from adipokine treated ovarian cancer cells.

The ovarian cancer cells, A2780 and SKOV3, were processed according to section 3.2.9 to obtain fresh CM. The HOMECs were seeded and overnight pre-treated with the inhibitors as described in section 4.2.4.

The next day, inhibitors were freshly diluted into the CM obtained from ovarian cancer cells before applying this treatment mixture to the HOMECs (note: the stock solutions of the inhibitors were at least 10,000-fold more concentrated than the concentration applied onto the HOMECs). An equivolume of DMSO was diluted in the same conditioned media to form the DMSO control. Ovarian cancer cell CM alone, without inhibitor, was also included to examine any effects of DMSO. After 24 hours of incubation in 37°C/5% CO_2, HOMEC proliferation was assessed using BrdU assay.

4.3 Results

4.3.1 Receptor tyrosine kinase activation by conditioned media from ovarian cancer cells incubated with leptin or lipocalin-2

The identification of activated surface receptors is a first step in determining the signalling pathways involved in HOMEC proliferation induced by treatment with various CM from adipokine-incubated ovarian cancer cells. To examine this, lysates from CM-treated HOMECs were screened using antibody arrays designed to detect phosphorylated (activated) receptor tyrosine kinases, which are receptors regulating cell processes such as proliferation. The method of collecting HOMEC lysate is described in section 4.2.1, while screening the lysate with antibody arrays is described in section 4.2.2. CM from both SKOV3 and A2780 were tested.

Multiple receptor tyrosine kinase sites were activated in HOMECs treated with CM from SKOV3 or A2780 pre-incubated with leptin or lipocalin-2. Only those with a calculated pixel density increase of 20% above the control were included to better focus on the receptor targets which showed the highest magnitude of activation. No statistical analysis was performed as the array was only performed twice for each CM (n=2). Sample array images generated from HOMEC lysate after treatment of cells with SKOV3 CM and A2780 CM are shown in **Figure 50** and **Figure 51** respectively. The intensities of selected receptor tyrosine kinase are shown in **Figure 52**. The full results from the phospho-RTK arrays are shown in **Table 9** and **Table 10** in the appendix.

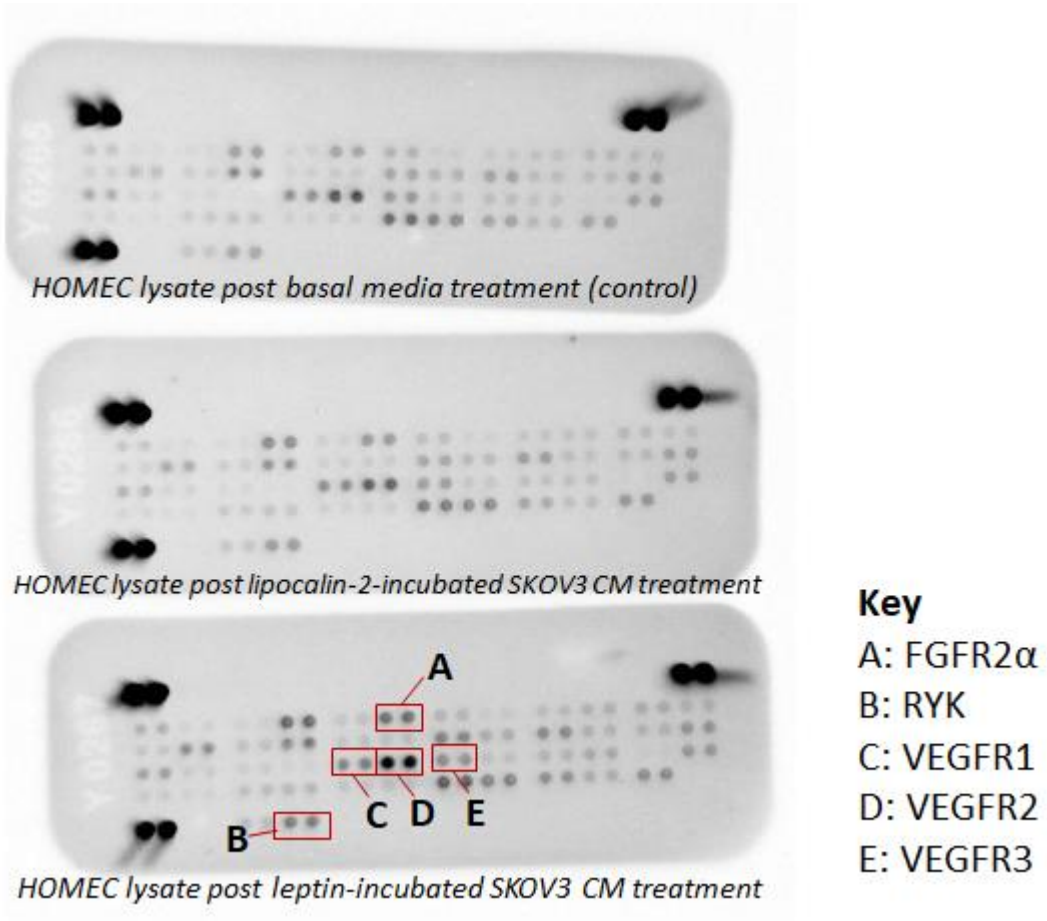

Figure 50. Conditioned media from adipokine-incubated SKOV3 cells induced phosphorylation of multiple receptor tyrosine kinases in HOMECs. HOMECs were treated with basal media, and CM from lipocalin-2-incubated SKOV3 cells and leptin-incubated SKOV3 cells for 5 minutes. HOMECs were then lysed, and lysate was incubated overnight with nitrocellulose membranes pre-spotted with capture antibodies for various phosphorylated receptor tyrosine kinases. Detection antibodies, streptavidin-HRP and chemiluminescent reagents were applied in between multiple washings, and the membranes imaged on the Azure 500 imager. Representative images are shown from n=2. Key activated receptor tyrosine kinases are labelled to show their position on the membrane. FGFR2α: fibroblast growth factor receptor-2-alpha; VEGFR1/2/3: vascular endothelial growth factor receptor-1, -2, -3; RYK: receptor-like tyrosine kinase; CM: conditioned media.

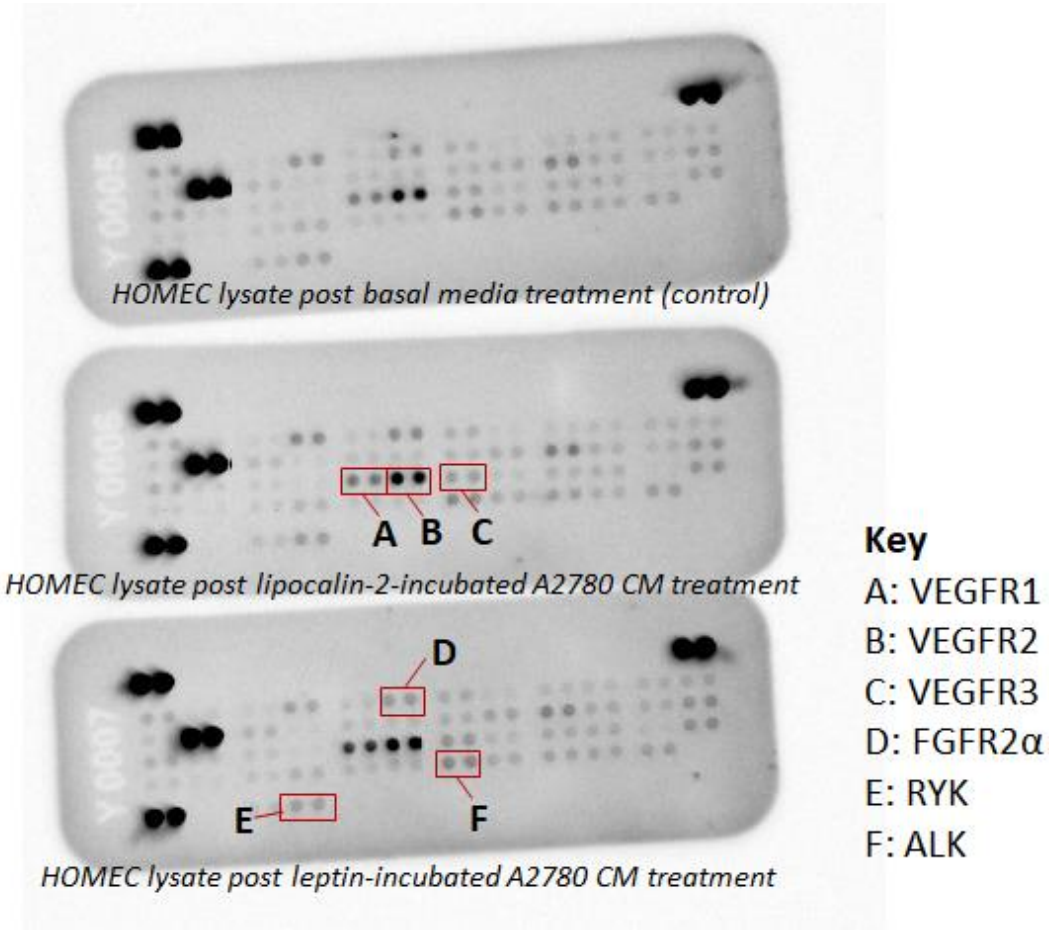

Figure 51. Conditioned media from adipokine-incubated A2780 cells induced phosphorylation of multiple receptor tyrosine kinases in HOMECs. HOMECs were treated with basal media, and CM from lipocalin-2-incubated A2780 cells and leptin-incubated A2780 cells for 5 minutes. HOMECs were then lysed, and lysate was incubated overnight with nitrocellulose membranes pre-spotted with capture antibodies for various phosphorylated receptor tyrosine kinase. Detection antibodies, streptavidin-HRP and chemiluminescent reagents were applied in between multiple washings, and the membranes imaged on the Azure 500 imager. Representative images are shown from n=2. Key activated receptor tyrosine kinases are labelled to show their position on the membrane. FGFR2α: fibroblast growth factor receptor-2-alpha; VEGFR1/2/3: vascular endothelial growth factor receptor-1, -2, -3; RYK: receptor-like tyrosine kinase; ALK: anaplastic lymphoma kinase; CM: conditioned media.

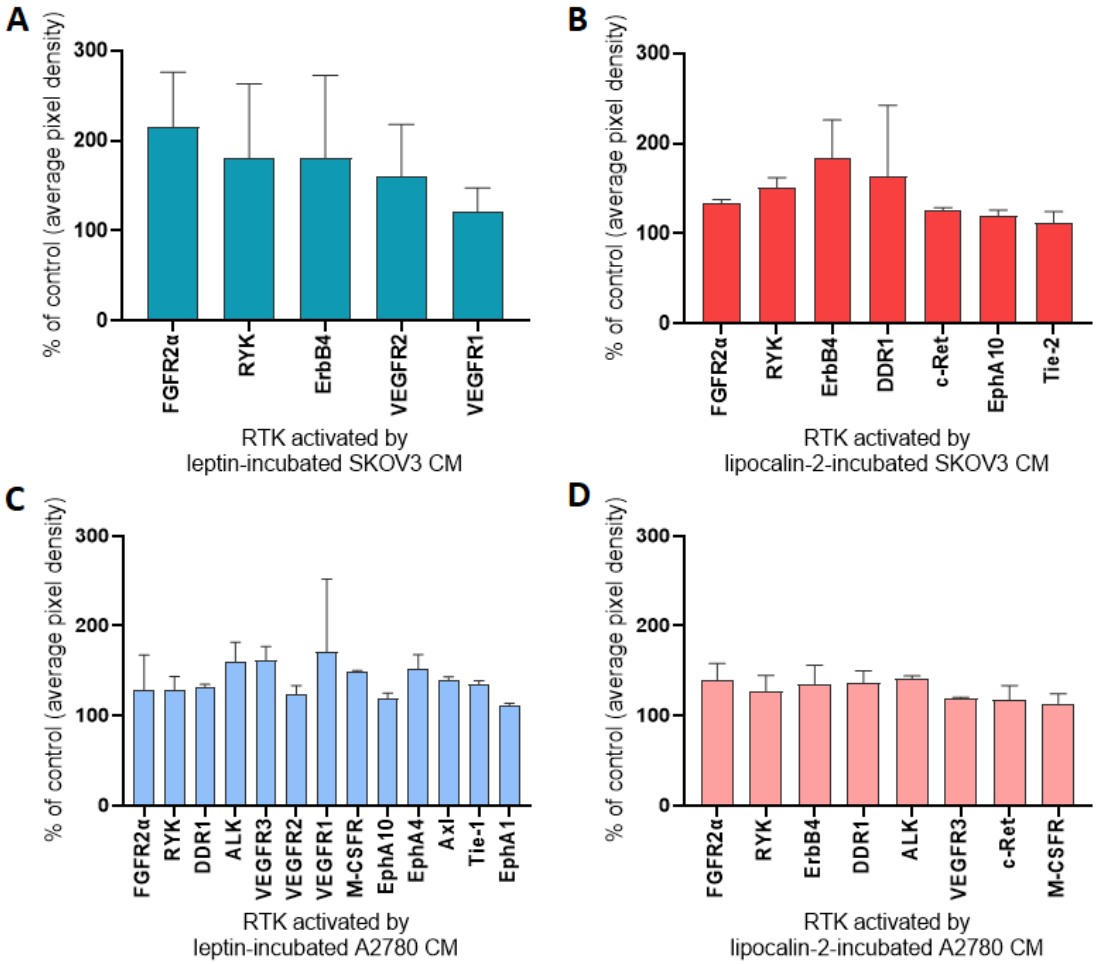

Figure 52. Multiple receptor tyrosine kinase targets were activated (phosphorylated) in HOMECs treated with conditioned media collected from adipokine-incubated ovarian cancer cells. HOMECs were treated for 5 minutes with CM from leptin-incubated SKOV3 cells (A), lipocalin-2-incubated SKOV3 cells (B), leptin-incubated A2780 cells (C) and lipocalin-2-incubated A2780 cells (D). HOMECs were then lysed, and lysate samples containing 200-300µg of total proteins were incubated overnight with nitrocellulose membranes pre-spotted with capture antibodies for various phosphorylated receptor tyrosine kinases. Following multiple washings, chemiluminescent reagents were applied prior to imaging the membranes. After subtracting negative control, the abundance of each target was calculated as a percentage of the corresponding control pixel density. Only receptor targets with average increase in pixel density and activation ≥20% compared with control (100%) are shown. n=2 for each conditioned media type. CM: conditioned media; RTK: receptor tyrosine kinase.

It can be seen that the fibroblast growth factor receptor substrate 2-alpha (FGFR2α) and the receptor-like tyrosine kinase (RYK) were activated when HOMECs were treated with all 4 types of ovarian cancer CM. For FGFR2α, leptin-incubated SKOV3 CM induced the greatest increase in activation (phosphorylation) with a 115% increase above the control (100%). This was followed by the lipocalin-2-incubated A2780 CM (40% increase), lipocalin-2-incubated SKOV3 CM (33% increase) and leptin-incubated A2780 CM (29% increase). Treatment with leptin- incubated SKOV3 CM enhanced RYK activation by 81%, followed by lipocalin-2-incubated SKOV3 CM (51%), leptin-incubated A2780 CM (29%) and lipocalin-2-incubated A2780 CM (27%).

Increased activation of anaplastic lymphoma kinase (ALK) was observed when HOMECS were treated with CM from leptin- and lipocalin-2-incubated A2780 (increases of 60% and 41% respectively); but this was not observed when treated with CM from leptin and lipocalin-2-incubated SKOV3.

Similarly, increased VEGFR3 activation was observed when HOMECs were treated with CM from leptin- and lipocalin-2-incubated A2780 cells (increases of 61% and 20% respectively), but not observed when treated with CM from SKOV3 cell incubated with leptin or lipocalin-2. Interestingly, VEGFR1 and VEGFR2 activation was only observed in HOMECs treated with CM from leptin-incubated ovarian cancer cells. Treatment with CM from leptin-incubated SKOV3 cells increased VEGFR1 activation by 21% and VEGFR2 by 60% compared with control, while treatment with CM from leptin-incubated A2780 cells increased VEGFR1 activation by 71% and VEGFR2 by 23%.

From the results of the RTK arrays, it can be seen that some of the activated receptors were common to all CM types (e.g. FGFR2α and RYK). However, ALK was activated only when HOMECs were treated with leptin- and lipocalin-2-incubated A2780 CM, but not with SKOV3 CM; while the variable activation of VEGFR1, VEGFR2 and VEGFR3 depended on the CM type (adipokine pre-treatment, or the ovarian cancer cell origin).

Thus, from these findings and those of previous studies from the literature,(361-367) several candidate ligands and receptor targets involved in HOMEC proliferation by factors secreted into the CM were chosen for further study. Specifically, the receptors VEGFR2, VEGFR3, FGFRs and ALK were studied.

Extrapolating backwards from the identified receptors, it was hypothesised that the CM contained FGF-2 and VEGF, and so the CM were screened for the presence of these growth factors. Additionally, it was hypothesised that TGF-β1 was also secreted into the CM since based on previous literature, TGF-β1 was implicated in tumour growth and metastasis (discussed in sections 1.3.5 and 1.6.5). Co-incidentally, these three ligands (FGF-2, VEGF and TGF-β1) were also detected in omental adipocyte and adipose tissue CM.

In the following sections, a series of experiments were performed to investigate the possible involvement of these ligands and receptors.

4.3.2 Quantification of ligands secreted into the conditioned media of adipokine-incubated ovarian cancer cells

To determine if leptin or lipocalin-2 treatment of ovarian cancer cells resulted in an increase in potential pro-angiogenic molecules being secreted, ELISA was performed on the CM collected from the adipokine-incubated SKOV3 and A2780 cells (described in section 4.2.3).

Unexpectedly, neither ovarian cancer cell line (SKOV3 or A2780) secreted detectable levels of FGF-2 at either baseline or after incubation with lipocalin-2 or leptin (data not shown). In contrast, secretion of both VEGF and TGF-β1 from both ovarian cancer cell lines increased following lipocalin-2 or leptin incubation compared with the control (**Figure 53**).

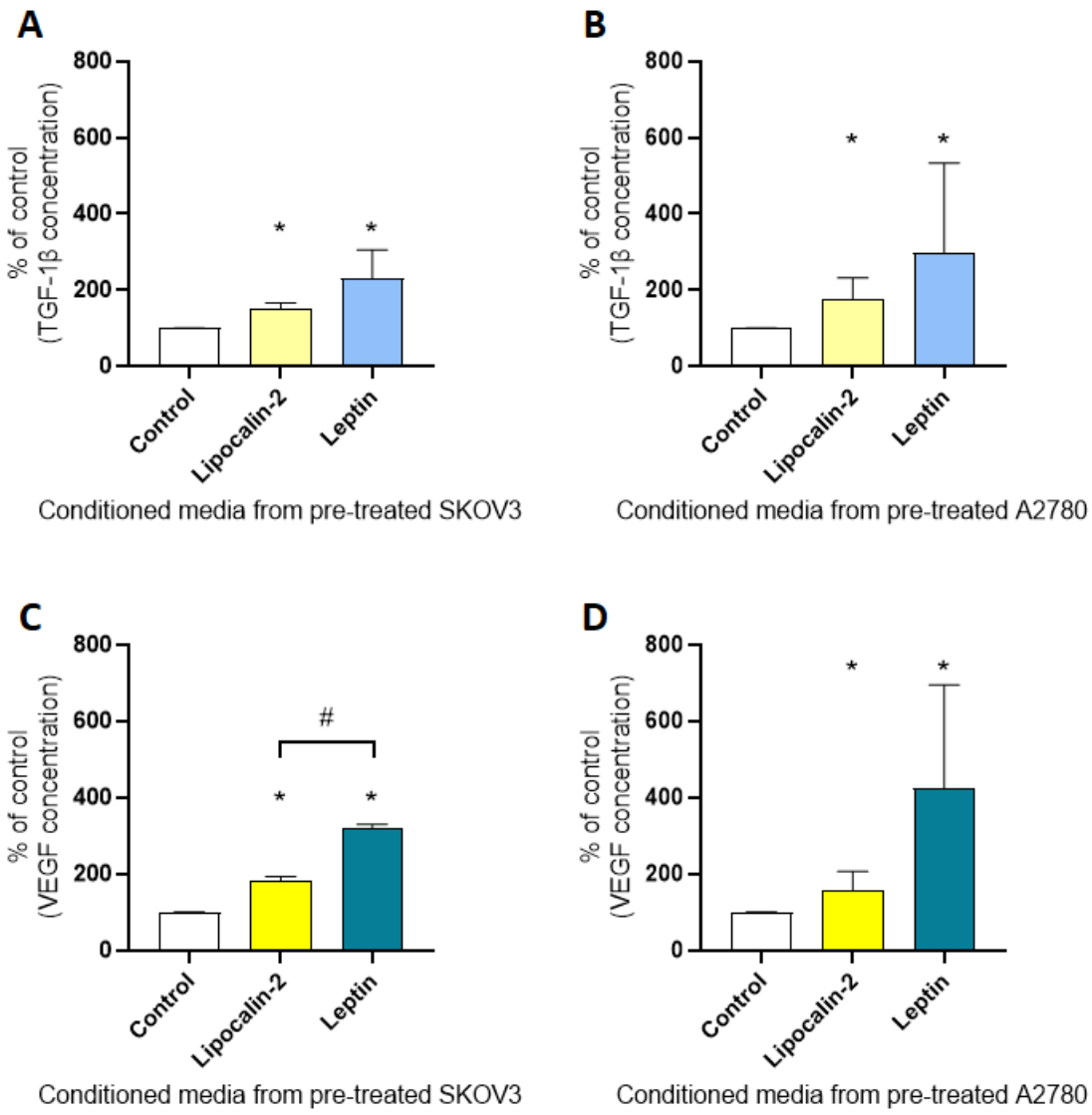

Figure 53. Incubation of SKOV3 and A2780 cells with lipocalin-2 or leptin increased TGF-β1 and VEGF secretion compared to the control. Ovarian cancer cells were incubated with leptin or lipocalin-2 for 24 hours and the CM was then collected for analysis by commercially available ELISA. For each ELISA kit, the supplied standards were diluted to the recommended range of concentrations. The standards and samples were assayed in triplicate and the absorbance was read at 450nm. The absorbance values, after subtracting the blank controls, were interpolated on the standard curve to determine the TGF-β1 (A, B) and VEGF (C, D) concentrations. Data are expressed as % of control and presented as mean ± SD. Data were analysed with Mann-Whitney U tests, n=3-4; *p<0.05 vs control; #p<0.05.

For instance, TGF-β1 levels were increased by 49% and 131% (vs control, 100%) in CM of SKOV3 cells incubated with lipocalin-2 and leptin, respectively, p<0.05 for both (**Figure 53A**). Similarly, in the A2780 CM, TGF-β1 secretion increased by 77% and 198% when the cells were incubated with lipocalin-2 and

leptin, respectively, p<0.05 for both (**Figure 53B**). VEGF secretion from SKOV3 cells was enhanced by 49% and 133% (vs control, 100%) following incubation with lipocalin-2 and leptin respectively, p<0.05 for both (**Figure 53C**). In A2780, lipocalin-2 incubation increased VEGF secretion by 55% and leptin incubation increased secretion by 324%, p<0.05 for both (**Figure 53D**). It can be seen that generally, the concentrations of both secreted VEGF and TGF-β1 were higher when the ovarian cancer cells were incubated with leptin than with lipocalin-2, although this difference was only statistically significant (p<0.05) for VEGF secretion from SKOV3 cells (**Figure 53C**).

4.3.3 Maximal non-toxic concentrations of receptor inhibitors

Alongside identifying and quantifying potential pro-angiogenic ligands in the ovarian cancer CM, the potential involvement of activated receptors in HOMEC proliferation was examined using specific inhibitors. Specifically, alectinib (CH5424802) is an ALK inhibitor, while AZD4547 is a FGFR inhibitor (for FGF-R1/2/3 inhibition). Semaxanib (SU5416) and SAR131675 are selective inhibitors of VEGFR2 and VEGFR3 respectively.

Prior to utilising these receptor inhibitors in conjunction with the ovarian cancer CM, their maximal non-toxic concentrations (in ranges determined from the literature) for use in HOMECs were first determined by WST8 assay (methods described in section 4.2.4). These toxicity experiments were performed for alectinib, SAR131675 and AZD4547 only, as the effective concentration of semaxanib (10μM) in HOMECs was previously determined in this laboratory. The results are shown in **Figure 54**. No statistical analysis was performed due to the low number of repeats (n=2) and that the experiments aimed to establish maximal inhibitor concentrations.

To select the maximal safe concentration for each inhibitor, the concentration with the greatest HOMEC viability (as a percentage of their respective controls) were chosen. Hence, in later experiments, alectinib was utilised at 10nM concentration (HOMEC numbers were 91% of control), AZD4547 at 100nM (82% of control) and SAR131675 at 1μM (117% of control).

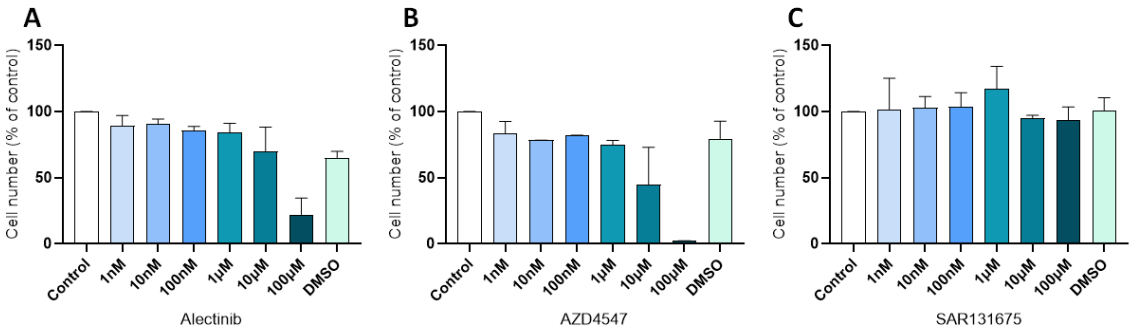

Figure 54. Low doses of alectinib, AZD4547 and SAR131675 were not highly toxic to HOMECs as assessed WST8 assay. HOMECs were seeded at 10,000 cells/well in 96-well plates and cultured for at least 24 hours before overnight treatment with the inhibitors alectinib (A), AZD4547 (B) and SAR131675 (C), diluted in starvation media. The cells were replenished with the same inhibitor treatment for a further 24 hours. Cell viability was determined by addition of WST8 reagent. Plates were read at 450nm after 2 hours. Results shown are mean ± SD and as a percentage of the control, n=2.

4.3.4 The effect of receptor inhibitors on HOMEC proliferation induced by conditioned media from adipokine-incubated ovarian cancer cells

HOMEC proliferation induced by CM collected from lipocalin-2- or leptin-incubated ovarian cancer cells was examined in the presence of the receptor inhibitors using BrdU and WST8 assays. DMSO was included as appropriate as the vehicle control. The methods were described in section 4.2.5. HOMEC proliferation was considered inhibited when treatment with the inhibitor reduced HOMEC proliferation significantly compared to both their respective control (CM without inhibitor) and DMSO control (CM with equivolume of DMSO as the inhibitor).

a) The effect of receptor inhibitors on HOMEC proliferation induced by conditioned media from adipokine-incubated SKOV3 cells

The VEGFR2 inhibitor, semaxanib, markedly decreased HOMEC proliferation induced by all SKOV3 CM as assessed BrdU assay (**Figure 55D**). Semaxanib reduced HOMEC proliferation induced by CM from lipocalin-2-incubated SKOV3 cells and leptin-incubated SKOV3 cells by 26% and 37% (vs control, 100%)

respectively, $p<0.05$ ($n=3$) for both. Similarly, when HOMECs were treated with control SKOV3 CM, semaxanib reduced proliferation by 34%. DMSO alone had no significant effect in any condition.

Treatment with the FGFR1/2/3 inhibitor, AZD4547, showed a similar trend to semaxanib (**Figure 55B**). AZD4547 reduced HOMEC proliferation observed with control SKOV3 CM and with CM from leptin-incubated SKOV3 cells, but these reductions were not statistically different compared to the DMSO control ($p>0.05$). Treatment with other inhibitors, alectinib (**Figure 55A**) and SAR131675 (**Figure 55C),** did not significantly affect HOMEC proliferation induced by SKOV3 CM; all $p>0.05$.

b) The effect of receptor inhibitors on HOMEC proliferation induced by conditioned media from adipokine-incubated A2780 cells

When HOMEC proliferation was measured using BrdU assay, in general none of the tested inhibitors reduced HOMEC proliferation compared to their respective control and DMSO control (**Figure 56**). The only exception was when HOMECs were treated with CM from leptin-incubated A2780 cells (**Figure 56D**); where proliferation was decreased by 17% in the presence of semaxanib when compared with control (100%) ($p<0.05$, $n=3$). Although not statistically significant, HOMEC proliferation was also decreased by 13% when co-treated with semaxanib and CM from lipocalin-2-incubated A2780 cells; and decreased by 19% when co-treated with semaxanib and basal A2780 CM.

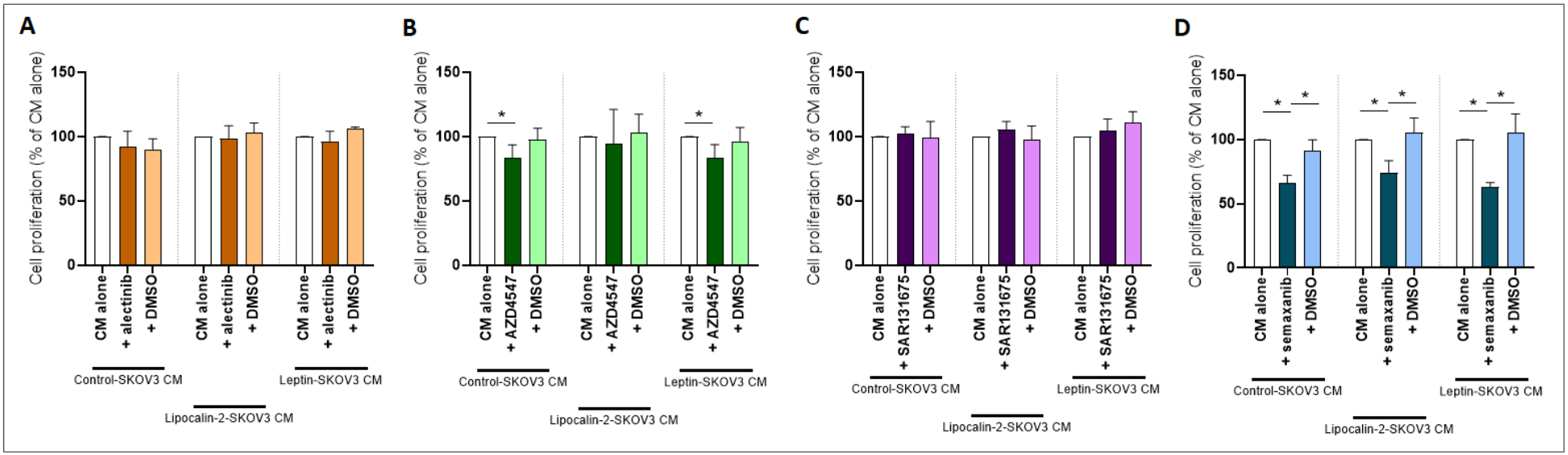

Figure 55. Semaxanib inhibited HOMEC proliferation induced by various conditioned media from SKOV3 cells as assessed by BrdU assay. HOMECs were seeded at 10,000 cells/well in 96-well plates and cultured for at least 24 hours before overnight treatment with alectinib (A), AZD4547 (B), SAR131675 (C) and semaxanib (D) diluted in starvation media. Cells were then treated with the same inhibitors diluted in CM from lipocalin-2- and leptin-incubated SKOV3 cells. The BrdU reagent was added after 24 hours of treatment incubation and cells fixed after a further 6 hours; plates were read at 450nm. Results shown are mean ± SD and as percentage of conditioned media alone; data were analysed with Mann-Whitney U tests; n=3; *p<0.05. CM: conditioned media.

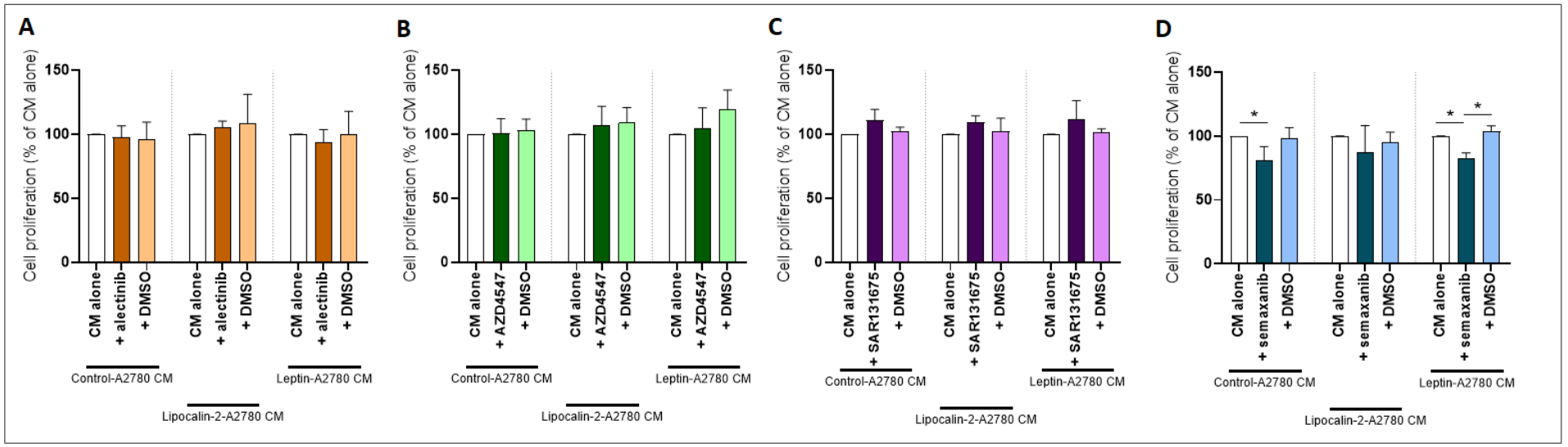

Figure 56. Semaxanib inhibited HOMEC proliferation induced by conditioned media from leptin-incubated A2780 cells as assessed by BrdU assay. HOMECs were seeded at 10,000 cells/well in 96-well plates and cultured for at least 24 hours before overnight treatment with alectinib (A), AZD4547 (B), SAR131675 (C) and semaxanib (D) diluted in starvation media. Cells were then treated with the same inhibitors diluted in CM from lipocalin-2- and leptin- incubated A2780 cells. The BrdU reagent was added after 24 hours of treatment incubation and cells fixed after a further 6 hours; plates were read at 450nm. Results shown are mean ± SD and as percentage of conditioned media alone; data were analysed with Mann-Whitney U tests; n=3; *p<0.05. CM: conditioned media.

4.3.5 The effect of adipokine-incubated ovarian cancer conditioned media on the activation of signalling kinases

After assessing the activated receptors and HOMEC proliferation in the presence of inhibitors of the receptors, it was determined that VEGFR2 activation may be responsible for the increased proliferation observed in cells treated with CM from adipokine-incubated cancer cells. HOMEC lysate collected after treatment with CM from lipocalin-2-incubated SKOV3 cells showed increased VEGFR2 activation by 19% compared with the control (**Table 10** in the appendix), which was slightly below the 20%-increment cut-off. This was also supported by the observation that increased levels of VEGF, the activating ligand for VEGFR2, were detected in these CM via ELISA (section 4.3.2).

This possibility was further investigated by examining which intracellular signalling molecules downstream of surface receptor activation are involved in HOMEC proliferation. Thus, lysates from CM-treated HOMECs were collected (section 4.2.1) and then screened with antibody arrays to detect phosphorylated (activated) protein kinases (section 4.2.2). These proteins are responsible for signal transduction, and their activation state regulates cellular processes such as cell proliferation.(368)

Prior to lysate collection, HOMECs were treated with CM from both SKOV3 and A2780 cells pre-incubated with adipokines. This allowed comparison of the protein kinases activated between the different CM types. Sample array images obtained from membranes incubated with HOMEC lysate generated from cells after treatment with SKOV3 CM and with A2780 CM are shown in **Figure 57** and **Figure 58** respectively. The intensities of the spots showing selected kinases are shown in **Figure 59** and limited to those with average pixel density increase of at least 10% above control to focus on the targets which showed the highest magnitude of activation.

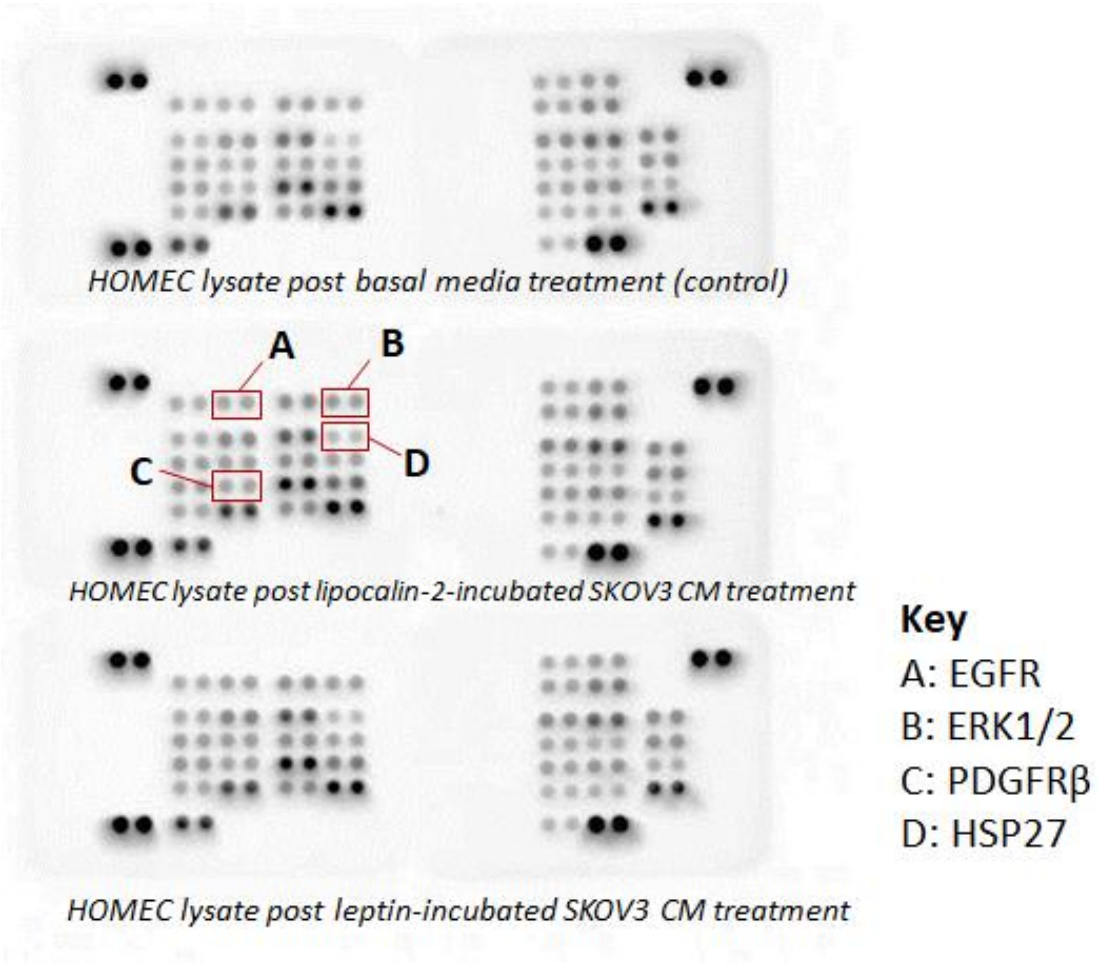

Figure 57. Adipokine-incubated SKOV3 conditioned media induced phosphorylation of multiple signalling kinases in HOMECs. HOMECs were treated with basal media, and CM from lipocalin-2-incubated SKOV3 cells and leptin-incubated SKOV3 cells for 5 minutes. HOMECs were then lysed, and lysate was incubated overnight with nitrocellulose membranes pre-spotted with capture antibodies for various phosphorylated kinases. Detection antibodies, streptavidin-HRP and chemiluminescent reagents were applied in between multiple washings, and the membranes imaged on the Azure 500 imager. Representative images are shown from n=2. Key activated kinases are labelled to show their position on the membrane. EGFR: epidermal growth factor receptor; ERK1/2: extracellular signal-regulated kinases1/2; PDGFRβ: platelet-derived growth factor receptor-beta; HSP27: heat shock protein 27; CM: conditioned media.

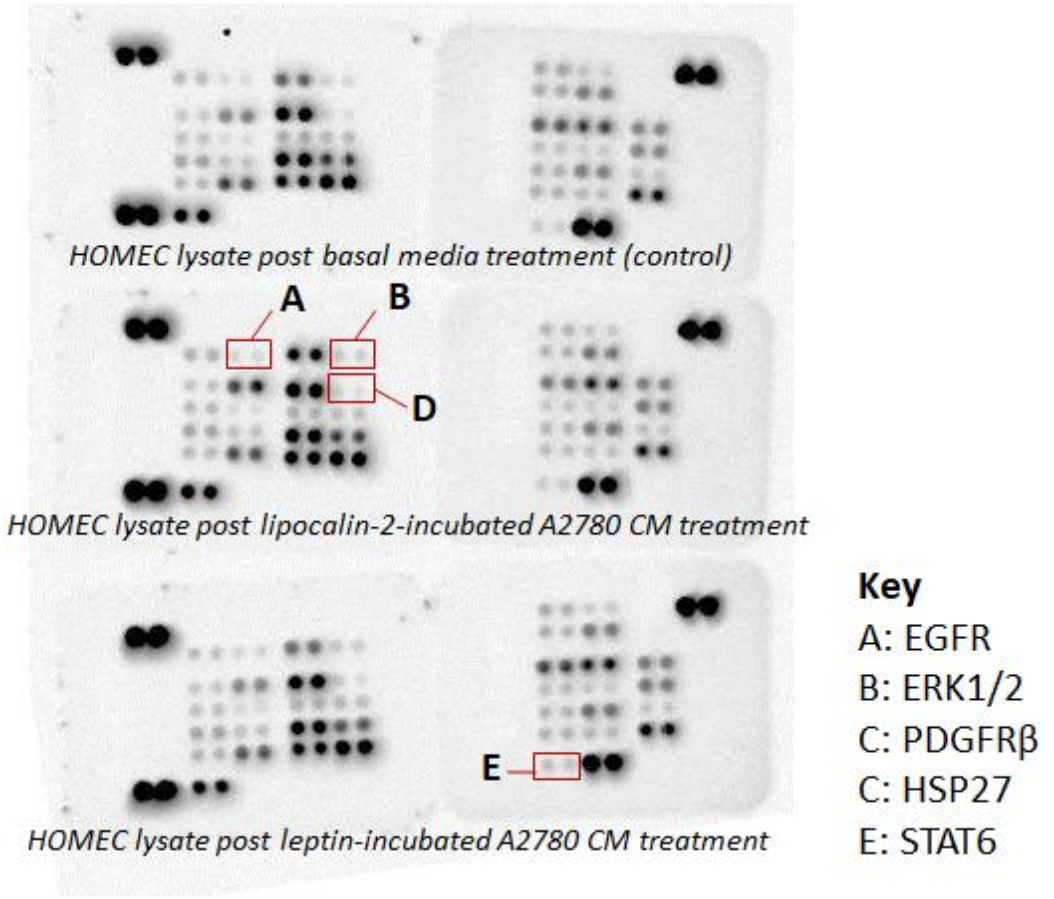

Figure 58. Adipokine-incubated A2780 conditioned media induced phosphorylation of multiple signalling kinases in HOMECs. HOMECs were treated with basal media, and CM from lipocalin-2-incubated A2780 cells and leptin-incubated A2780 cells for 5 minutes. HOMECs were then lysed, and lysate was incubated overnight with nitrocellulose membranes pre-spotted with capture antibodies for various phosphorylated kinases. Detection antibodies, streptavidin-HRP and chemiluminescent reagents were applied in between multiple washings, and the membranes imaged on the Azure 500 imager. Representative images are shown from n=2. Key activated kinases are labelled to show their position on the membrane. EGFR: epidermal growth factor receptor; ERK1/2: extracellular signal-regulated kinases1/2; HSP27: heat shock protein 27; STAT6: signal transducer and activator of transcription 6; CM: conditioned media.

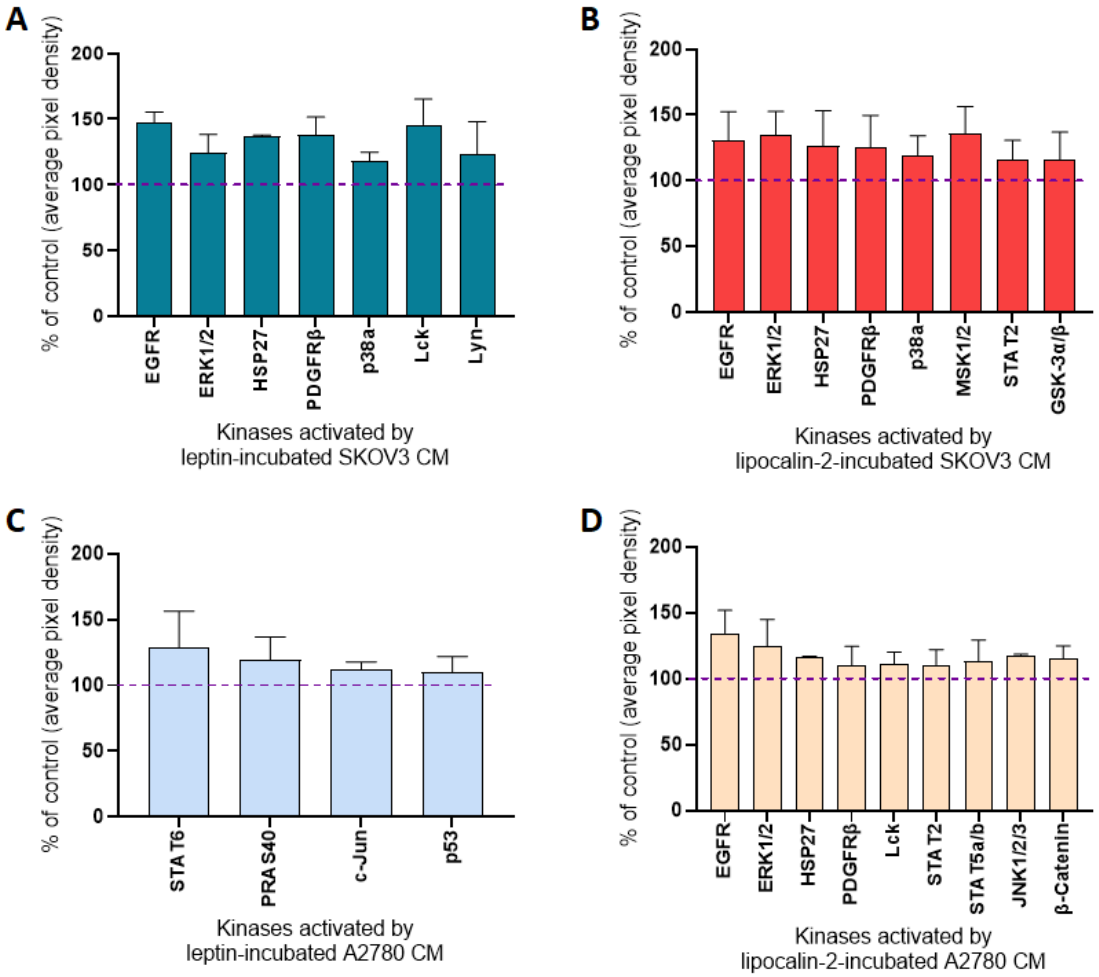

Figure 59. Multiple kinase targets were activated (phosphorylated) in HOMECs treated with conditioned media from adipokine-incubated ovarian cancer cells. HOMECs were treated for 5 minutes with CM from leptin-incubated SKOV3 cells (A), lipocalin-2-incubated SKOV3 cells (B), leptin-incubated A2780 cells (C) and lipocalin-2-incubated A2780 cells (D). HOMECs were then lysed, and lysate samples containing 200-400µg of total proteins were incubated overnight with nitrocellulose membranes pre-spotted with capture antibodies for various phosphorylated kinases. Following multiple washings, chemiluminescent reagents were applied prior to imaging the membranes. After subtracting negative control, the abundance of each target was calculated as a percentage of the corresponding control pixel density. Only targets with average increase in pixel density and activation ≥10% compared with control are shown. n=2 for each conditioned media type. CM: conditioned media.

Based on their cumulative pixel density as a percentage of the control, the epidermal growth factor receptor (EGFR) and extracellular signal-regulated kinases 1/2 (ERK1/2) appeared to be the most common targets within HOMECs. Compared with the control, an increase in EGFR activation was detected when HOMECs were treated with CM from lipocalin-2-incubated A2780 cells (35% increase), lipocalin-2-incubated SKOV3 cells (31% increase) and leptin-incubated SKOV3 cells (47% increase). ERK1/2 activation was detected in lysate from cells treated with CM from lipocalin-2-incubated A2780 cells (25% increase), lipocalin-2-incubated SKOV3 cells (34% increase) and leptin-incubated SKOV3 cells (25% increase).

In addition to EGFR and ERK1/2, other targets including HSP27, PDGFRβ and p38a showed increased activation when treated with CM from both leptin- and lipocalin-2-incubated SKOV3 cells (**Figure 59A** and **Figure 59B** respectively). Increased HSP27 and PDGFRβ activation was also observed with CM from lipocalin-2-incubated A2870 cells (**Figure 59D**).

The activated kinase targets were starkly different when HOMECs were treated with CM from leptin-incubated A2780 cells (**Figure 59C**). STAT6 (28% increase) showed the highest increase in activation compared to the control (100%).

4.3.6 Receptor tyrosine kinase activation with omental adipose tissue conditioned media

As described in chapter 3, HOMEC proliferation was induced by adipose tissue CM, although the secreted adipokine responsible for this response could not be identified. To examine whether proliferation induced by CM from both adipose tissue and adipokine-incubated cancer cells occurred via the same potential pathway(s), receptor activation in HOMECs treated with CM from adipose tissue was examined using the phospho-RTK array. Sample array images obtained from HOMEC lysate following treatment with adipose tissue CM are shown in **Figure 60**, and the phosphorylation changes in selected receptor tyrosine kinase are shown in **Figure 61**.

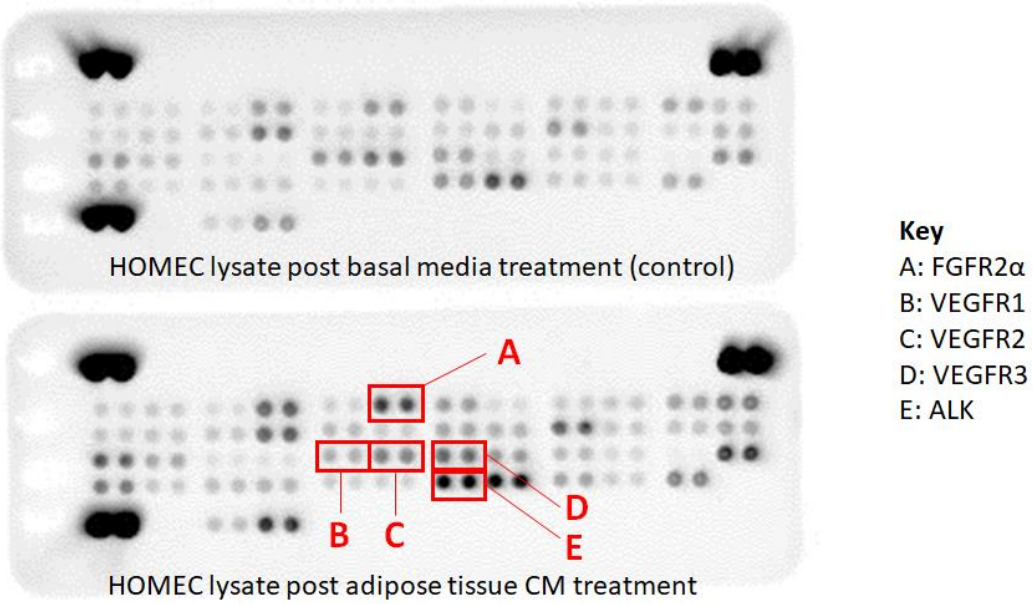

Figure 60. Adipose tissue conditioned media induced phosphorylation of multiple receptor tyrosine kinases in HOMECs. HOMECs were treated with basal media and adipose tissue CM for 5 minutes. HOMECs were then lysed, and lysate was incubated overnight with nitrocellulose membranes pre-spotted with capture antibodies for various phosphorylated receptor tyrosine kinase. Detection antibodies, streptavidin-HRP and chemiluminescent reagents were applied in between multiple washings, and the membranes imaged on the Azure 500 imager. Representative images are shown from n=2. Key activated receptor tyrosine kinases are labelled to show their position on the membrane. FGFR2α: fibroblast growth factor receptor-2-alpha; VEGFR3: vascular endothelial growth factor receptor-3; ALK: anaplastic lymphoma kinase; CM: conditioned media.

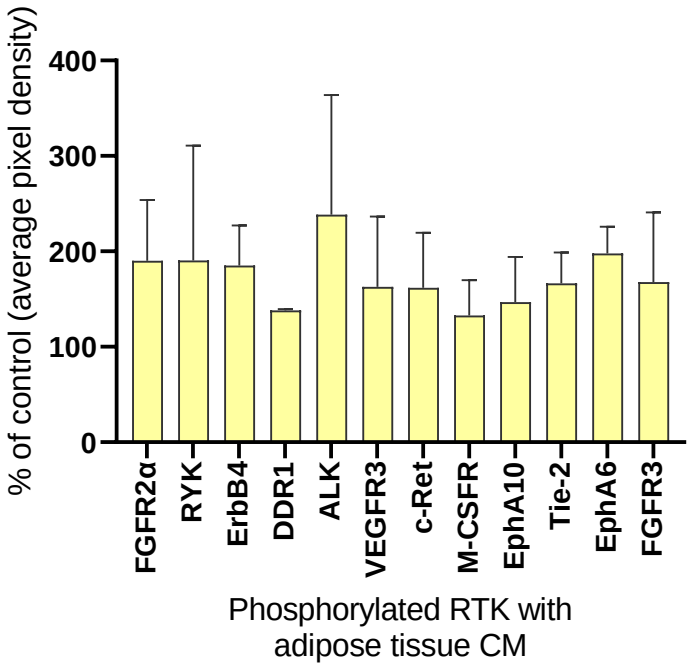

Figure 61. Multiple receptor tyrosine kinase targets were activated (phosphorylated) in HOMECs treated with adipose tissue conditioned media. HOMECs were treated for 5 minutes with adipose tissue CM, lysed and lysate samples containing 200-300µg of total proteins were incubated overnight with nitrocellulose membranes pre-spotted with capture antibodies for various phosphorylated receptor tyrosine kinases. Following multiple washings, chemiluminescent reagents were applied prior to imaging the membranes. After subtracting the negative control, the abundance of each target was calculated as a percentage of the pixel density on the corresponding control membrane. Only receptor targets with average increase in pixel density and activation ≥20% compared with control are shown, n=2. CM: conditioned media.

It is interesting to note that similar targets were activated in HOMECs when treated with adipose tissue CM to those treated with CM from adipokine-incubated ovarian cancer cells (section 4.3.1). Both FGFR2α and RYK showed increased activation (both showed 90% increase) compared with the control. Of all the tested receptor tyrosine kinases, ALK had the highest level of activation when HOMECs were treated with adipose tissue CM, with a 139% increase compared with the control. VEGFR3, but not VEGFR1 and VEGFR2, also showed increased activation (by 63%).

4.3.7 The effect of omental adipose tissue conditioned media on the activation of signalling kinases

Similarly, to compare signalling kinase activation when HOMECs were treated with different CM types, the phospho-kinase array was utilised to assess HOMEC lysates treated with adipose tissue CM. Sample array images obtained from array membranes incubated with HOMEC lysate collected after treatment with adipose tissue CM for 5 minutes are shown in **Figure 62**, and the relative intensities of selected kinases compared with control are shown in **Figure 63**.

The only kinase target which was clearly elevated upon treatment with adipose tissue CM was STAT3. Compared with control, STAT3 activation showed 161% increment, while the second highest activated target was Src (increase of 10%).

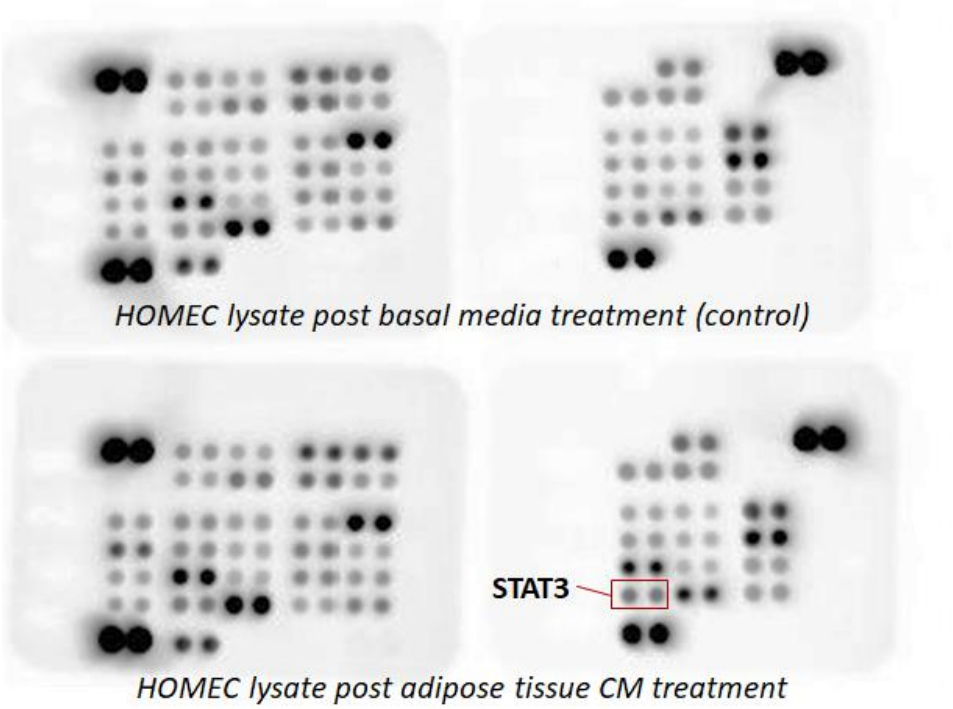

Figure 62. Adipose tissue conditioned media induced phosphorylation of STAT3 in HOMECs. HOMECs were treated with basal media and adipose tissue CM for 5 minutes and then lysed. The lysates were incubated overnight with nitrocellulose membranes pre-spotted with capture antibodies for various phosphorylated kinases. Detection antibodies, streptavidin-HRP and chemiluminescent reagents were applied in between multiple washings, and the membranes imaged on the Azure 500 imager. Representative images are shown from n=2. Signal transducer and activator of transcription 3 (STAT3), a key activated kinase is labelled to show its position on the membrane. CM: conditioned media.

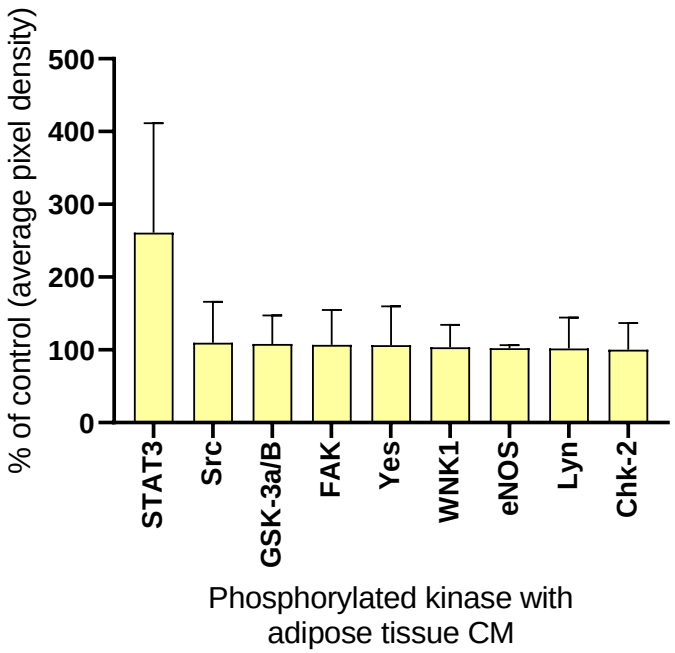

Figure 63. STAT3 activation was highest in HOMECs treated with adipose tissue conditioned media. HOMECs were treated for 5 minutes with adipose tissue CM, lysed and lysate samples containing 200-400µg of total proteins were incubated overnight on nitrocellulose membranes pre-spotted with capture antibodies for various phosphorylated kinases. Following multiple washings, chemiluminescent reagents were applied prior to imaging the membranes. After subtracting negative control, the abundance of each target was calculated as a percentage of the corresponding control membrane's pixel density. Only receptor targets which showed increased pixel density compared to the control (100%) are shown, n=2. CM: conditioned media.

4.3.8 Presence of VEGFR3 in HOMECs

It was interesting to note that increased activation of VEGFR3 was observed when HOMECs were treated with CM from adipose tissue (**Figure 61**) and adipokine-treated A2780 cells (**Figure 52C** and **Figure 52D**). This finding was unexpected as VEGFR3 has been reported to be present in lymphatic ECs, as opposed to vascular ECs such as HOMECs. Lymphatic ECs are mainly involved in lymphangiogenesis and immune response, with a lesser role in angiogenesis.(369) To confirm if HOMECs expressed this receptor which could then be available to interact with secreted VEGF, immunocytochemistry was performed as described in section 2.9.

Aside from VEGFR3, the HOMECs were also stained for CD31 and vWF simultaneously to verify their endothelial morphology. Furthermore, expression of CD31 and vWF is erratic and not well defined in human and mice lymphatic ECs,(370, 371) and thus these markers could help confirm the vascular origin of the HOMECs. Prior to immunocytochemistry, the HOMECs were not treated with CM; thus, the VEGFR3, CD31 and vWF detected in these cells reflect the proteins present in normal growth conditions.

The VEGFR3 antibody used binds to the extracellular domain of the receptor (372, 373) and thus, immunostaining was first performed without membrane permeabilisation in order to detect VEGFR3 on the HOMEC membrane surface. However, some studies have reported immunostaining of VEFGR3 in permeabilised human cells,(374, 375) hence immunocytochemistry was also performed on permeabilised HOMECs.

From the fluorescent microscope images, it was observed that HOMECs expressed VEGFR3 on the HOMEC surface and also dispersed within the cytoplasm (**Figure 64** and **Figure 65** respectively).

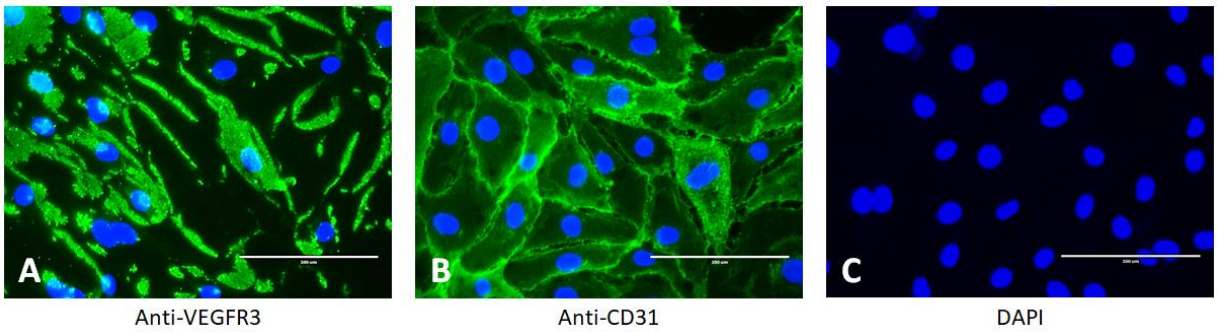

Figure 64. VEGFR3 detected extracellularly in HOMECs. HOMEC endothelial identity was confirmed by the expression of CD31. HOMECs were seeded at 10,000 cells/well in 8-well chamberslides and grown to confluence. Cells were fixed with 4% (v/v) paraformaldehyde at room temperature, and then incubated overnight with primary antibodies (anti-VEGFR3 (A), anti-CD31 (B) or PBS (C) for control); followed by incubation with fluorescent-conjugated secondary antibodies. Cell nuclei were stained blue with DAPI. After mounting with coverslips, slides were visualised at 10x magnification with EVOS Fluo. The negative control (C) shows background level of staining with no primary antibody. Similar results were obtained across two different HOMEC populations at different passage numbers. Scale bar 200µm.

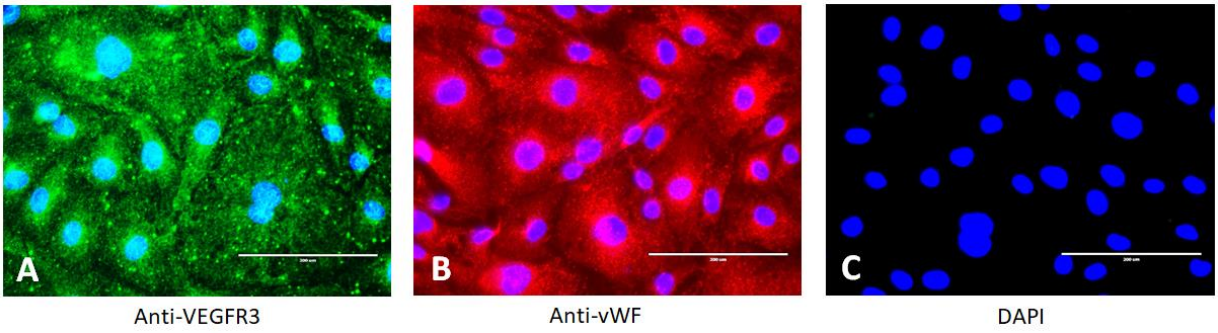

Figure 65. VEGFR3 detected intracellularly in HOMECs. HOMEC endothelial identity was confirmed by the expression of vWF. HOMECs were seeded at 10,000 cells/well in 8-well chamberslides and grown to confluence. Cells were fixed with 4% (v/v) paraformaldehyde at room temperature, and then permeabilised with methanol at -20°C. Cells were incubated overnight with primary antibodies (anti-VEGFR3 (A), anti-vWF (B) or PBS (C) for control); followed by incubation with fluorescent-conjugated secondary antibodies. Cell nuclei were stained blue with DAPI. After mounting with coverslips, slides were visualised at 10x magnification with EVOS Fluo. The negative control (C) shows background level of staining with no primary antibody. Similar results were obtained across two different HOMEC populations at different passage numbers. Scale bar 200µm.

4.4 Discussion

4.4.1 Identification of pro-proliferative pathways activated by factors secreted into conditioned media from adipokine-incubated ovarian cancer cells

From the results of the phospho-RTK array, it could be seen that many of the activated receptors in HOMECs were common to treatment with CM from adipokine-incubated SKOV3 and A2780 cells. Identification of these activated receptors highlighted two possible further approaches, a) identifying the possible candidates within the CM which activates these receptors to eventually enhance HOMEC proliferation, or b) inhibiting these receptors to observe if HOMEC proliferation was affected.

In the former approach, the possible candidates within the CM which induced HOMEC proliferation were narrowed down to VEGF, FGF-2 and TGF-β1. Co-incidentally, these three factors were also detected in omental adipocyte and

adipose tissue CM (**Figure 97** in the appendix). In the latter approach, focussing on receptor inhibition, VEGFR2, VEGFR3, ALK and FGFR2α were selected for further investigation based on their activation as assessed by the phospho-RTK array and their link to angiogenesis. The selected targets are discussed as follows.

a) VEGF and VEGFR2

From the phospho-RTK array, HOMEC treatment with leptin-treated ovarian cancer CM increased the activation of both VEGFR1 and VEGFR2, for which the common ligand for these receptors is VEGF. Both the VEGFR1 and VEGFR2 are commonly reported to be expressed in ECs; however, the latter is the predominant receptor for VEGF-mediated angiogenesis.(361) Additionally, leptin has been previously reported to increase VEGF secretion and VEGFR2 expression in cancer cells, such as breast and gallbladder cancers.(362) Thus, the VEGF-VEGFR2 axis was a potential candidate for further investigation.

b) VEGFR3

The activation of VEGFR3 was observed when the HOMECs were treated with CM from A2780 pre-incubated with leptin and lipocalin-2, but not CM from SKOV3. This was interesting as VEGFR3 signalling is conventionally associated with the lymphatic vasculature, and has been reported to be involved in lymphatic EC proliferation and migration (lymphangiogenesis).(376) However, later studies showed that VEGFR3 is upregulated in the tumour vasculature and is expressed in angiogenic sprouts in mouse models.(364) Genetic deletion of the receptor or using blocking antibodies resulted in decreased sprouting, vascular density and branching as well as EC proliferation; this implied that alongside VEGFR2, VEGFR3 also has a role in angiogenesis.(364)

The results presented suggest that there was a difference between factors released by A2780 and SKOV3 cells. For instance, A2780 cells appear to secrete factors which activate VEGFR3, with potential candidates being VEGF-C and VEGF-D. These were not tested in the present study, as the ELISA (section 4.3.2) only tested for VEGF, which is also known as VEGF-A. Immunohistochemical studies on ovarian cancer samples have shown increased VEGF-C and VEGF-D expression, especially when lymph node or

peritoneal metastases were present.(363, 377) Correspondingly, ECs adjacent to the tumour showed increased VEGFR3 expression.(363) This led to the hypothesis that lymphatic and peritoneal spread were regulated by the tumour's secretion of VEGF-C and VEGF-D which served to upregulate VEGFR3 in both lymphatic and vascular ECs.(363) In the present study, VEGFR3 was detected via immunocytochemistry in HOMECs which were not exposed to ovarian cancer CM prior (section 4.3.8). Since the HOMECs were only exposed to the CM for 5 minutes, it can be concluded that the A2780 CM contained a secreted factor that enhances VEGFR3 activation in HOMECs.

The apparent non-activation of VEGFR3 by leptin- or lipocalin-2-treated SKOV3 CM may be due to cancer phenotype (discussed in section 3.4.4b) Hence, future work could investigate whether SKOV3 or A2780 cells secrete VEGF-C and VEGF-D with or without adipokine pre-treatment.

c) FGF-2 and FGFR2α

FGFR2α is a docking protein downstream of receptor tyrosine kinases and it was activated by all cancer cell CM tested as assessed by the phospho-RTK arrays. An example of such receptors are the FGF receptors (FGFRs), where activation of the receptor leads to the phosphorylation of docking proteins.(366) Common subtypes of FGFRs are FGFR1, FGFR2, FGFR3 and FGFR4. FGFRs are also detected in ECs, with FGFR1 and FGFR2 being the most commonly reported (378) and their activation induces EC proliferation.(365) When HOMEC lysate was analysed using the phospho-RTK array, FGFR3 activation was also detected alongside FGFR1 and FGFR2 under various conditions (**Table 9** and **Table 10** in the appendix). Since FGFR1/2/3 showed increased activation in the array, they were further investigated using a pan-FGFR inhibitor which inhibits FGFR1/2/3.

Eponymously, the ligands for the FGFRs are the FGFs. The FGF/FGFR signalling pathway is involved in homeostasis, immune defence, as well as tumour angiogenesis.(379) Mutational changes in the FGFRs are associated with various cancers; for example in some ovarian cancer subtypes, aberrant FGFR1 or upregulated FGFR2 genes have been implicated in carcinogenesis.(378-380) Additionally, FGF-2 is a pro-angiogenic mediator often overexpressed in various cancers which acts directly on ECs or by

stimulating VEGF expression.(381) The crosstalk between FGF-2 and VEGF is recognised; in an in vitro study using bovine microvascular and aortic ECs, FGF-2-induced angiogenesis was inhibited when VEGFR inhibitors were utilised.(382) Conversely, FGF-2 treatment of bovine corpus luteal ECs induced FGFR, VEGFR1 and VEGFR2 mRNA upregulation.(383) Thus, with the increased activation of FGFR2α detected in the phospho-RTK array and the known angiogenic effects of FGF-2 which may be linked to VEGF, the FGF-2 ligand was a possible candidate involved in HOMEC proliferation and was investigated further.

Moreover, from the array results, FGFR2α has the highest cumulative activation amongst all other targets tested in the array. Considering that FGFR2α docks downstream to FGFR, ALK and possibly other receptors (e.g. neurotrophin and ret receptors),(366) treatment with the different CM types may have 'inflated' the level of FGFR2α activation. In other words, FGFR2α appeared to have the highest activation cumulatively, but the individual receptors upstream of this docking protein may have been activated to different levels by the different factors contained within the tested CM.

d) ALK

Similar to increased VEGFR3 activation, the leptin- and lipocalin-2-treated A2780 CM induced ALK activation. ALK belongs to the insulin receptor tyrosine kinase superfamily and activation of the ALK gene is associated with carcinogenesis.(384) This receptor tyrosine kinase is detected in ovarian cancer;(367) a study on ovarian cancer samples from patients showed that ALK phosphorylation was the highest amongst all other receptor tyrosine kinases.(367) Many past studies reported a link between ALK activation within the tumour cells and cancer progression, for example in anaplastic large cell lymphoma where it was first identified, breast cancer, colorectal cancer, and most notably, non-small cell lung cancer wherein most ALK inhibitor therapies have been developed.(384)

While activation of ALK leads to signalling pathways involved in cell proliferation, survival and differentiation, its activating ligand remains a mystery.(385) The growth factors midkine and pleiotrophin have been put forward as ligands for ALK.(386, 387) For instance, ALK mRNA upregulation

was associated with pleiotrophin-induced growth of HUVECs.(387) Also, midkine was shown to increase human cerebral microvascular EC (hCMEC) and HUVEC proliferation, which coincided with the activation (phosphorylation) of ALK; this finding was substantiated by the use of anti-midkine antibody which reduced levels of phosphorylated ALK.(386) Anti-pleiotrophin antibody, however, did not affect ALK phosphorylation.(386) Interestingly, other antibodies directed at the extracellular component of the ALK were able to activate signalling without the presence of ligands, thus questioning the actual identity of the receptor's ligand.(388)

A possible explanation for the increased ALK activation in HOMECs may be attributed to an activating ligand secreted from the adipokine-treated A2780. ALK activation was only detected when HOMECs were treated with A2780 CM, but not with SKOV3 CM. This observation again affirmed the difference between the two ovarian cancer subtypes.

Despite its unknown ligand, the ALK receptor was further examined due to its association with tumour angiogenesis and its increased activation as detected in the phospho-RTK array. Furthermore, the docking protein FGFR2α is associated downstream of the ALK receptor,(366) which also showed increased activation within the same array.

e) TGF-β1

The phospho-RTK array detects the receptor tyrosine kinases commonly activated (phosphorylated) in human cells during normal growth and development. However, the present study seeks to examine tumour angiogenesis. TGF-β signalling contributes to tumour angiogenesis alongside other tumorigenic effects discussed below. Even though this target was not incorporated in the phospho-RTK array, TGF-β1 was included for further investigation.

TGF-β1 is the most common isoform of the TGF-β family and is the predominant isoform in tumours.(389) The TGF-β signalling pathways are implicated in several types of cancer including ovarian cancer.(389, 390) Interestingly, TGF-β signalling is tumour-suppressive in normal cells and in early stages of cancer contributing to the maintenance of cell homeostasis and preventing uncontrollable growth, but this reverts to tumour-promoting in later

stages of cancer when the tumour has progressed.(391) For example, in normal ovarian epithelial cells TGF-β suppresses cell growth, but in 40% of ovarian cancers this inhibitory effect is lost and EMT is induced.(390)

As discussed in sections 1.3.5 and 1.6.5, TGF-β promotes cancer cell proliferation, metastatic colony establishment and chemoresistance. Additionally, aberrant TGF-β signalling is associated with cancer cell survival through apoptosis resistance, secretion of pro-inflammatory mediators which drives tumour invasion, as well as inhibition of immune surveillance which allows tumour progression.(391) Expectedly with its tumour promoting role, TGF-β is linked to tumour angiogenesis; in vitro experiments showed increased expression of pro-angiogenic mediators such as VEGF and FGF-2 after treatment with TGF-β.(392-394)

4.4.2 Identification and quantification of FGF-2, TGF-β1 and VEGF

a) Absence of FGF-2 in ovarian cancer cell CM

As assessed by ELISA, FGF-2 was undetectable in the CM from both the ovarian cancer cell types (SKOV3 and A2780) which were incubated with leptin or lipocalin-2. Notably, FGF-2 was also not detected by ELISA in the CM of ovarian cancer cells treated with basal media alone (control) indicating that these EOC did not secrete FGF-2 under resting or into CM from adipokine-activated cells. This was unexpected since treatment of HOMECs with these same CM did activate FGFR1, FGFR3 and FGFR2α as assessed by the phospho-RTK array.

These data were in contrast with findings from past studies, which reported the presence of FGF-2 and its mRNA in specimens of primary ovarian tumours,(259, 395, 396) and that endogenous FGF-2 and its mRNA were detected in SKOV3 cells in vitro and in vivo.(397)

A possible explanation might be that the FGF-2 originated from the HOMECs themselves, rather than being secreted by the ovarian cancer cells. The CM of leptin- and lipocalin-2-incubated ovarian cancer cells may have induced FGF-2 secretion from the HOMECs, which then activated the receptor associated with FGFR2α in an autocrine manner. This was supported by studies in HUVEC and

bovine aortic EC which showed that FGF-2 was endogenously present in ECs.(398, 399)

Another possible explanation for the apparent lack of FGF-2 in the cancer cell CM may be due to the detection limit of the ELISA itself. The lowest concentration of the FGF-2 standard was 15.6 pg/mL in the present study. In a previous study using two human prostate cancer cell lines, FGF-2 was detected by ELISA in the growth media from the prostate cancer cells treated with leptin, but at very low levels, in the range of 5-10pg/mL in one cell line and <1pg/mL in the other.(400) Thus, it is possible that FGF-2 was secreted by the adipokine-incubated ovarian cancer cell lines at levels below the detection limit of the ELISA.

b) Lipocalin-2 induced TGF-β1 and VEGF secretion from ovarian cancer cells

In contrast to FGF, the concentration of secreted VEGF and TGF-β1 was markedly increased compared to the control in the CM from both ovarian cancer cell types treated with lipocalin-2 (**Figure 53**). These data support a direct link between adipokines secreted from omental adipose tissue and the induction of secretion of pro-angiogenic factors from ovarian cancer cells for the first time.

Past studies found that it is the expression of lipocalin-2, rather than exposure to exogenously sourced lipocalin-2, in cancer cells which is associated with TGF-β1 secretion. Lipocalin-2 is expressed in many types of cancers (e.g. breast, gastric and liver cancers) (348) and in ovarian tissue, its expression is significantly higher in cancer than in normal tissue.(348, 349) Depending on cancer type, the increase or decrease in lipocalin-2 expression is correlated to TGF-β1 secretion, and TGF-β1 is one of the mediators which drives the cancer EMT process.(349, 401-405) However, no studies have yet shown that treating ovarian cancer cells with lipocalin-2 from a non-cancer source induces the secretion of TGF-β1, and the data presented support the hypothesis that the microenvironment of the omentum provides a rich “soil” for EOC metastasis.

Similarly, lipocalin-2 expression in cancer cells was associated with VEGF secretion. Immunohistochemical and serum studies in human colorectal cancer cases showed positive correlation between lipocalin-2 and VEGF expression.(345, 346) In breast cancer cell lines, lipocalin-2 upregulates VEGF

expression and its angiogenic effect was shown in the migration of HUVECs in vitro.(332) Within the female reproductive system, immunohistochemical studies showed positive correlation between lipocalin-2 and VEGF expression in endometrial cancer.(347) No previous studies showed that exposure of cancer cells to exogenous lipocalin-2 elicits VEGF secretion.

It is possible that the proliferative effect seen in HOMECs, following treatment with CM from cancer cells incubated with lipocalin-2, may be solely due to the increased VEGF secretion as detected via ELISA. The concomitant increase in TGF-β1 secretion may have other roles, e.g. EMT, not tested in the present study. However, a immunohistochemical study on colorectal cancer specimens found that TGF-β1 was associated with increased VEGF expression and increased microvascular density.(406) Thus, in the present study, the increased secretion of TGF-β1 may have also led to the observed increased VEGF secretion to induce angiogenesis, manifested as increased HOMEC proliferation.

c) Leptin induced TGF-β1 and VEGF secretion from ovarian cancer cells

Similar to lipocalin-2, treating SKOV3 and A2780 cells with leptin yielded CM with markedly increased VEGF and TGF-β1 concentrations compared to the control (**Figure 53**). This observation was similar to an in vitro study performed in human prostate cancer cell lines, DU145 and PC3, which showed that exogenous leptin treatment induced VEGF and TGF-β1 secretion.(400) The authors also showed that the level of VEGF and TGF-β1 secreted depended on the concentration of leptin used, which ranged from 4 to 80ng/mL;(400) these concentrations were higher than that utilised in the present study on ovarian cancer cells.

Leptin receptors were detected in breast, thyroid and pancreatic cancer cells and their activation was found to be responsible for tumour growth, reduction in apoptosis and induction of EMT.(407-409) Leptin receptors were also detected in primary ovarian tumour tissue, as well as in several ovarian cancer cell lines, including SKOV3 and A2780.(410) In this latter study, leptin treatment of SKOV3 cells resulted in increased migration and invasion; and induced the expression of genes related to EMT in another ovarian cancer cell line, HEY.(410) Furthermore, leptin treatment on lung and breast cancer cells

induces EMT concomitant with TGF-β upregulation.(409, 411) From these observations, the increased TGF-β1 levels detected via ELISA in the ovarian cancer CM post-leptin incubation may exert roles which are beyond the scope of this project. As mentioned in the previous subsection (section 4.4.2b) the enhanced proliferation detected in HOMECs treated with CM from leptin-incubated ovarian cancer cells may be a direct result of VEGF action instead of TGF-β1.

From past literature, treatment with leptin stimulates VEGF secretion from prostate cancer cells (400) and ECs (such as HUVECs and porcine aortic ECs).(412) Past studies mostly examined leptin expression within cancer cells, as opposed to exogenous leptin treatment of the cells, and its association with VEGF expression. Leptin expression is often higher in cancer tissues compared to normal tissues, and activation of its receptors on the cancer cells results in proliferation; which was observed in gastric and colorectal cancers.(413, 414) Additionally, immunohistochemical studies showed that increased leptin expression was associated with increased VEGF expression in samples of human gastric and colorectal cancers.(413-415) The present study, for the first time, showed that treating ovarian cancer cells with leptin induced significant levels of secreted VEGF.

4.4.3 The effect of specific receptor inhibitors on HOMEC proliferation induced by conditioned media from cancer cells incubated with adipokines

As shown in section 3.3.5c, HOMEC proliferation was induced by CM collected from both SKOV3 and A2780 cells pre-incubated with the adipokines leptin and lipocalin-2. It can be assumed that this enhanced proliferation is caused by factors secreted by the cancer cells and not by the residual adipokines within the CM, since the individual adipokines had no effect on HOMEC proliferation (section 3.3.5a).

Since the RTK arrays highlighted certain receptors as possible mediators of the proliferative effect of the cancer cell CM, their involvement in HOMEC proliferation was tested using specific inhibitors. The effects of inhibition of each

receptor target on HOMEC proliferation induced by cancer cell CM are discussed in the subsections that follow.

a) FGFR inhibition

FGFR inhibition was examined as these receptors are associated with FGFR2α and this docking protein was strongly activated, as assessed by the phospho-RTK array when HOMECs were treated with cancer cell CM (**Figure 52**). Even though FGF-2 was undetected via ELISA (section 4.3.2), it was possible that FGFR2α activation may be via a different FGF isoform or locally by HOMEC secreted FGF-2 at levels too low to be detected by ELISA as mentioned previously. Thus, AZD4547, which inhibits FGFR1/2/3, was utilised to examine the effect of this blockade.

Inhibition of the FGFRs with AZD4547 did not significantly affect HOMEC proliferation induced by ovarian cancer cell CM. Additionally, since the inhibitor is a pan-FGFR inhibitor, the data suggest that alternative FGF isoforms that activate these receptors are not secreted into the CM. This supported the absence of secreted FGF-2 in the ovarian cancer CM. These findings are in contrast to other types of solid tumours which have been shown to secrete various FGF isoforms capable of activating FGFR1/2/3; e.g. hepatocellular and lung cancers secrete FGF-3, pancreatic cancer secretes FGF-5, while prostate cancer secretes FGF-1, -6, -7, -8 and -9.(381)

It is also possible that FGFR activation, inferred from the increased FGFR2α activation, by factors within the tested CM was not associated with HOMEC proliferation. This was because the FGFR family of receptors regulates other cellular functions such as cell differentiation and survival,(381) which were not investigated in the present study.

In past studies FGFR activation was shown to induce not only proliferation, but migration and invasion in mouse brain microvascular EC in vitro.(416, 417) Treating HDMECs with vaccarin, an active ingredient of a medicinal herb, enhanced their proliferation, migration and tube formation via FGF-2/FGFR1 signalling.(418) In the present study, however, the combined data suggest that FGF-2 and FGFR signalling do not play a role in HOMEC proliferation in the in vitro model used here.

b) ALK inhibition

ALK showed increased activation when HOMECs were treated with CM from adipokine-incubated A2870 cells as assessed by the phospho-RTK array. Since the docking protein FGFR2α is also associated with ALK,(366) alectinib was utilised to inhibit this receptor.

Inhibition of ALK with alectinib did not also significantly affect HOMEC proliferation induced by ovarian cancer CM. It was initially expected that alectinib would reduce HOMEC proliferation induced by CM from leptin- and lipocalin-2-incubated A2780 CM since increased ALK activation was detected from the phospho-RTK array; but this was not the case. Thus, similar to the FGFRs, ALK activation by factors in the ovarian cancer CM was most likely not associated with HOMEC proliferation.

Only a few studies have focussed on the role of ALK within ECs especially in the context of cancer. Immunohistochemically, tumours induced in mice injected with human neuroblastoma cell lines showed decreased vascular density, with concomitant reductions in VEGF and VEGFR2 expression when the ALK gene was silenced.(419) ALK activation in HUVECs and primary human brain ECs induced proliferation as assessed by tetrazolium dye staining (similar to WST8 assay).(386) However, these findings from past studies may not be suitably extrapolated to the present observation due to heterogeneity in the ECs studied (macrovascular versus microvascular in HOMECs) and that they originate from a different tissue environment (non-ovarian or non-omental in origin).

c) VEGFR3 inhibition

VEGFR3 inhibition was examined since CM from adipokine-treated A2780 cells activated VEGFR3; notably, treatment with CM from leptin-treated A2780 cells activated the three VEGFR subtypes based on the results of the phospho-RTK array (**Figure 52**). Additionally, VEGFR3 may have roles in angiogenesis (discussed in section 4.4.1b). A VEGFR3 inhibitor, SAR131675, was utilised to examine HOMEC proliferation induced by cancer cell CM.

HOMEC proliferation was unaffected by SAR131675 compared with control and DMSO control. At face value, this was not aligned to past studies reporting the pro-angiogenic role of VEGFR3 signalling. VEGFR3 inhibition, via genetic deletion of the receptor or via blocking antibodies, resulted in decreased vessel

density, vessel branching and EC proliferation in mouse studies.(364) Furthermore, VEGFR3 activation promoted angiogenesis even with VEGFR2 inhibition in mice and in vitro human EC studies.(364, 420) However, in two other studies using mouse models, VEGFR3 inhibition suppressed the notch signalling in angiogenesis which resulted in the upregulation of VEGFR2.(376, 421) When ECs were depleted of VEGFR3, they more sensitive to VEGF due to increased amounts of VEGFR2; this was observed as increased vascular permeability due to enhanced VEGFR2 activation.(376) This compensatory mechanism explains the observed hypervascularity and hypersprouting in ECs following genetic deletion of VEGFR3.(421)

These data may also explain the observation here of increased HOMEC proliferation, although not statistically significant, induced by A2780 CM even with VEGFR3 inhibition. SAR131675 was applied overnight on the HOMECs which may have allowed the transcription and overexpression VEGFR2, and the enhanced VEGF levels in the CM (demonstrated by ELISA in section 4.3.2) interacted with the enhanced receptor levels to increase cell proliferation. As VEGFR3 is related to the sprouting process in angiogenesis, future work could utilise antibodies against CD34,(276) which are present in tip cells of angiogenic sprouts, to complement the proliferation assays.

d) VEGFR2 inhibition

A VEGFR2 inhibitor, semaxanib was tested because VEGFR2 is the main receptor for VEGF in terms of angiogenesis.(361) Both leptin- and lipocalin-2-incubated ovarian cancer CM showed increased VEGF secretion as assessed by ELISA (section 4.3.2). Given that the canonical VEGF-VEGFR2 interaction initiates angiogenic signalling in ECs, the inclusion of semaxanib was relevant in investigating HOMEC proliferation.

Treatment with semaxanib significantly reduced HOMEC proliferation induced by CM from adipokine-incubated SKOV3 cells when compared to their respective control and DMSO control (**Figure 55D**). The magnitude of HOMEC proliferation reduction with semaxanib treatment was similar between the control SKOV3 CM, leptin-incubated SKOV3 CM and lipocalin-2-incubated SKOV3 CM (reduction to 66%, 74%, 63% respectively, when compared to control 100%). This implied that even basal SKOV3 CM, i.e. without adipokine

pre-incubation, activates VEGFR2. Indeed, previous work in the lab demonstrated that SKOV3 cells secrete VEGF into their CM,(106) and the ELISA performed in section 4.3.2 showed that basal SKOV3 CM contained secreted VEGF.

Taking into account these data and the earlier observation where treating HOMECs with basal SKOV3 CM showed no increased proliferation (**Figure 29** and **Figure 30** in section 3.3.3b), it is possible that the basally-secreted VEGF in the CM maintains HOMEC proliferation but was insufficient to increase it to levels above the control. When the SKOV3 cells were incubated with leptin or lipocalin-2, higher levels of VEGF were secreted as assessed by ELISA (section 4.3.2). HOMEC proliferation induced by this CM was significantly inhibited by semaxanib. Thus, it appears that the enhanced proliferation in HOMECs treated with CM from adipokine-incubated SKOV3 can be attributed to the secretion of VEGF into the CM.

Similarly, when treated with CM from A2780 cells pre-incubated with adipokines, only treatment with semaxanib reduced HOMEC proliferation compared to control and DMSO control. Interestingly, only the CM from leptin-incubated A2780 cells showed statistically significant reduction in HOMEC proliferation in the presence of semaxanib; proliferation induced by CM from lipocalin-2-incubated A2780 cells was also reduced but was not statistically significant (**Figure 56D**). These data inferred that the factors secreted into the CM may be different depending on whether the A2780 cells were pre-incubated with leptin or lipocalin-2. A possible explanation may be that leptin induces a higher level of VEGF secretion in A2780 cells compared to lipocalin-2 (although this was not statistically different), thus VEGFR2 inhibition may be more prominent when HOMECs were co-treated with semaxanib and CM from leptin-incubated A2780 cells.

Indeed, the role of leptin in angiogenesis is well known. Depending on the cancer type, leptin functions as an angiogenic factor through multiple signalling pathways and by inducing expression of related molecules such as MMPs.(362) Collectively, leptin is associated with increased VEGF expression and VEGFR2 expression as well as VEGFR2 activation.(362) The close association between leptin and VEGF/VEGFR2 from past studies supports the observation that VEGFR2 inhibition with semaxanib decreased HOMEC proliferation to a greater

extent when treated with CM from leptin-, but not with CM from lipocalin-2-treated A2780 cells.

4.4.4 Intracellular pathways involved in HOMEC proliferation

The phospho-kinase array revealed the activation of different signalling targets by distinct types of CM (**Figure 59**). With a cut-off value of 10% increase in activation compared with the control, the common signalling kinase activated by both leptin- and lipocalin-2-treated SKOV3 CM were EGFR, ERK1/2, HSP27 and PDGFRβ. Similarly, HOMEC treatment with CM from lipocalin-2-treated A2780 cells induced activation of EGFR, ERK1/2 and HSP27. Interestingly, treatment with CM from leptin-treated A2780 cells increased activation of targets different to the other CM types, with STAT6 showing the greatest activation. This again highlights the heterogenous responses of the two cancer cell types.

The individual kinase targets are discussed and a possible signalling pathway leading to HOMEC proliferation is proposed, as follows.

a) STAT6

The increased activation of STAT6 in HOMECs treated with CM from A2780 cells incubated with leptin was unexpected. This was because in past studies STAT6 was often investigated in cancer cells or in macrophages;(422-424) although STAT6 has been reported to be present in ECs with roles other than proliferation.(425, 426) For example, in HUVECS STAT6 signalling was implicated in the upregulation of surface molecules involved in inflammatory responses.(425) In HMECs, the expression of STAT6 was associated with the expression of a transcription factor which transforms the vascular EC phenotype to the lymphatic phenotype.(425)

Angiogenesis-related roles of STAT6 were reported in studies on macrophages. The combination of the STAT3 and STAT6 signalling pathways in macrophages mediated tumour progression.(424) This was achieved via the secretion of cathepsins, proteases which degrade ECM and basement membranes to allow tumour invasion, and also angiogenic sprouting.(424) The polarisation of macrophages to the M2 phenotype, achieved via STAT6 signalling, is also

involved in stimulating angiogenesis in the context of atherosclerosis.(427) Thus, the robust activation of STAT6 observed is interesting, but the available evidence suggests that it may not be involved in HOMEC proliferation. Future studies could examine if indeed STAT6 in involved in HOMEC proliferation with the use of a STAT6 inhibitor.

b) EGFR and HSP27

EGFR and HSP27 activation were commonly induced by CM from lipocalin-2-incubated A2780 CM and both types of SKOV3 CM. The observed increased EGFR activation within the HOMEC lysate was not supported by past studies as most reported EGFR activation within cancer cells and its role in tumorigenesis, rather than in ECs.(428) One study reported that EGFRs were more commonly expressed in tumour-associated ECs as opposed to normal ECs.(429) However, the HOMECs in this thesis were only treated with the cancer cell CM for 5 minutes and induction of EGFR expression with this short duration of CM exposure is unlikely to convert normal EC to tumour-associated EC. Furthermore, the HOMECs were isolated from non-diseased omental tissue, with large vessels and fibrotic segments dissected away as a first step, thus decreasing the possibility of the isolated HOMECs being 'tumour-associated.'

The most possible explanation for activation of EGFR in HOMECs is EC heterogeneity. Representative EC types showed the absence of EGFR, for example in HMECs (which were derived from skin), HUVECs (derived from the macrovasculature), as well as, mice skin and adipose ECs.(429) EGFR may be present in HOMECs specifically but not in other EC types, thus future work may seek to confirm its presence in HOMECs e.g. via immunocytochemistry or ELISA.

The increased activation of HSP27 in HOMECs was also in contrast with past studies as HSP27 phosphorylation and activation were reported to be induced by angiogenic inhibitors.(430, 431) In a study using HUVECs and HDMECs, HSP27 phosphorylation was associated with an increase in actin cytoskeletal fibres which were theorised to inhibit cell motility.(430) Thus, angiogenesis inhibition was potentially achieved though HSP27 activation and subsequent decrease in cell migration.(430) In another study, treatment with the angiogenic inhibitor thiolutin inhibited HUVEC proliferation in vitro and at the same time

induced HSP27 phosphorylation.(431) Of note, the phosphorylated sites, S78 and S82,(431) match those detected in the phospho-RTK array utilised in the present study.

Interestingly, extracellular HSP27 has been detected in the tumour microenvironment, for instance in breast and hepatocellular cancers, where it is thought to be secreted from the tumour cells.(432) Experiments using exogenous recombinant human HSP27 induced the migration of HDMECs, which the authors attributed to increased VEGF and VEGFR2 expression.(432)

From data of these past studies, activation of intracellular HSP27 appeared to be anti-angiogenic, while activation of extracellular HSP27 was pro-angiogenic. In the present study, the increased HSP27 activation was detected from HOMEC lysates, and thus it can be assumed to be intracellular in origin. Due to heterogeneity in ECs based on location and vascular type, it was possible that HSP27 activation may be pro-angiogenic in the HOMEC population, or that its activation is unrelated to cell proliferation.

c) ERK1/2 and PDGFRβ

Similar to EGFR and HSP27, enhanced activation of ERK1/2 and PDGFRβ were commonly induced by CM from lipocalin-2-incubated A2780 CM and both types of SKOV3 CM. The enhanced ERK1/2 activation was in concordance with past studies showing the pro-angiogenic role of ERK. In HUVECs, for example, treatment with VEGF induced the phosphorylation of ERK1/2 and enhanced cell proliferation as assessed with BrdU assay.(359) Aortic and lung ECs extracted from mice with deleted ERK1/2 genes showed defective angiogenesis, characterised by decreased proliferation as assessed by BrdU incorporation and decreased migration as assessed by scratch wound assay.(433) In vitro, an ERK inhibitor decreased the proliferation, migration and tube formation of foetal human pulmonary artery ECs.(430) Thus, the ERK1/2 kinase is a potential candidate involved in HOMEC proliferation.

The PDGFR family consists of two main receptor types, PDGFRα and PDGFRβ, and many different isoforms of PDGF as activating ligands.(434) PDGFR activation upregulates VEGF which is largely responsible for the events in angiogenesis including angiogenic sprouting, as well as the recruitment of perivascular cells, e.g. pericytes, for vasculature formation and

stabilisation.(435, 436) Indeed, the phosphorylation of PDGFRβ has been postulated to activate downstream ERK1/2 signalling leading to increased VEGF expression.(435)

VEGF stimulates PDGF-B secretion from ECs, which has high affinity for PDGFRβ; the PDGF-B/PDGFRβ signalling is involved in perivascular cell recruitment.(437) In bovine aorta EC, PDGFRβ was exclusively detected in angiogenic sprouts and in EC tube formation; conversely, treatment with anti-PDGF-B antibodies reduced this tube formation.(438)

d) Possible signalling pathways for HOMEC proliferation induced by conditioned media from cancer cells

From the data, VEGF/VEGFR2 signalling appeared to be the driver for HOMEC proliferation when treated with CM from ovarian cancer cells pre-incubated with leptin or lipocalin-2. This is inferred from enhanced VEGF secretion in the cancer cell CM (confirmed via ELISA) which may have contributed to HOMEC proliferation in a paracrine manner; subsequently, reduced HOMEC proliferation was observed when co-treated with ovarian cancer cell CM and the VEGFR2 inhibitor, semaxanib. This VEGFR2 activation may have led to the increased ERK1/2 activation, seen in the phospho-kinase array, which ultimately induced cell proliferation.

Activation of the VEGF/VEGFR2 axis may have been enhanced by PDGFRβ signalling. A possible activating ligand for PDGFRβ, PDGF-B, may have originated from the cancer cells, or from the HOMECs themselves since VEGF have been shown to stimulate PDGF-B secretion from ECs.(437) As discussed earlier, PDGFRβ activation can lead to downstream ERK1/2 signalling (435) and induce HOMEC proliferation in synergy with the VEGF/VEGFR2 axis.

A schematic of the possible proliferative pathway within the HOMECs is depicted in **Figure 66**. Future work could investigate this potential synergy between VEGFR2 and PDGFRβ activation, by examining the effect of PDGFR blockade on HOMEC proliferation and elucidating the factors secreted in cancer cell CM which could activate PDGFRβ.

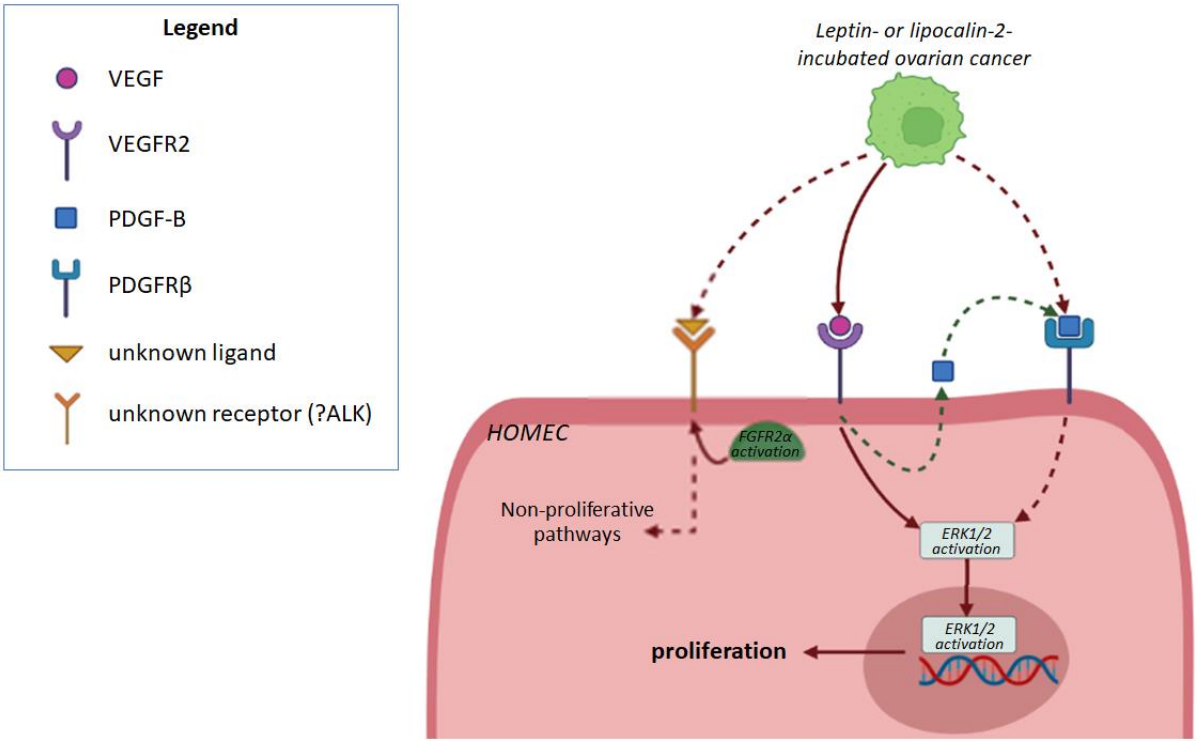

Figure 66. Schematic of the potential proliferative signalling pathway in HOMECs when treated with conditioned media from ovarian cancer cells. Leptin- or lipocalin-2-incubated cancer cells secrete VEGF which activates VEGFR2 (A) leading to downstream ERK1/2 activation and cell proliferation. PDGF-B may be secreted by cancer cells (B) or by ECs upon VEGFR2 activation (C), which activates PDGFRβ to induce cell proliferation. Activation of the docking protein, FGFR2α, is not involved in cell proliferation; FGFR2α activation may be a result of upstream receptor activation (possibly ALK receptor) by an, as yet, unidentified ligand secreted by cancer cells. Solid arrows indicate data from the present study; dashed arrows indicate data from past studies. Diagram created with BioRender.com.

4.4.5 The effect of omental adipose tissue conditioned media on the activation of receptor tyrosine kinases and signalling kinases

a) Activation of receptor tyrosine kinases

Similar to treatment with CM from adipokine-incubated cancer cells, treating HOMECs with adipose tissue CM induced the activation of multiple receptor tyrosine kinases as assessed by the phospho-RTK array; the highest activation being the ALK receptor. The ligand for this receptor is yet unknown (discussed in section 4.4.1d), and it may be possible that the receptor activation was

induced by an unknown factor secreted from omental adipocytes into the adipose tissue CM. Adipokines from adipose tissue could potentially contribute to tumour progression, as discussed in section 1.5. The various adipokines secreted by the omental adipose tissue are shown in **Figure 97** in the appendix, with the identification of these adipokines limited by what was pre-set on the array; but one or more of them may be responsible for this ALK activation in the HOMECs.

Treatment of HOMECs with adipose tissue CM also showed increased VEGFR3 activation in the phospho-RTK array. Similar to primary ovarian cancer cells, the omental adipocytes are in close proximity to the lymphatic network as peritoneal fluid drains through the lymphatic vessels of the omentum.(158) Thus, there is a possibility that adipocytes secrete factors which are involved in lymphatic maintenance. The adipokine array utilised (section 3.2.5) contained antibodies for the detection of VEGF (i.e. VEGF-A), but not for VEGF-C or VEGF-D, hence this is a potential investigation area for future studies. Indeed, one study showed upregulated VEGF-C and VEGF-D expression in adipocytes of mice subjected to a high fat diet,(439) which aligned with observations in obese individuals where serum VEGF-C was increased, and both VEGF-C and VEGF-D levels correlated with percentage of body fat.(440) Hence, a link between VEGFR3 activation and adipose tissue CM may be an activating ligand secreted from adipocytes, most possibly VEGF-C and/or VEGF-D.

Notably, no increased activation of VEGFR1 and VEGFR2 were detected when the HOMECs were treated with adipose tissue CM (**Table 11** in the appendix). This observation implied that HOMEC proliferation induced by factors secreted from adipose tissue may not VEGF-mediated; in contrast with the findings when HOMECs were treated with CM from adipokine-incubated cancer cells.

b) Activation of signalling kinases

From the results of the phospho-kinase array, when adipose tissue CM were applied onto HOMECs, STAT3 activation was increased drastically, at least twice the magnitude of the second highest activated kinase target. This contrasted with treatment with the cancer cell CM where high levels of STAT3 activation were not observed. This observation infers that different signalling pathways leading to HOMEC proliferation were induced by the different CM treatments. These data highlight the complexity of pro-angiogenic signalling in the omental tumour microenvironment.

STAT3 activation in HOMECs when treated with adipose tissue CM agreed with past studies in both macro- and microvascular ECs, where STAT3 signalling was associated with angiogenesis; specifically, in EC proliferation and migration.(441-443) STAT3 signalling is known to be downstream of the activation of FGFR and VEGFR by their pro-angiogenic ligands, FGF-2 and VEGF.(441-443) Both of these adipokines were detected in adipose tissue CM (**Figure 97** in the appendix) and could be responsible for the STAT3 activation observed.

However, the receptor for VEGF, VEGFR2, did not show increased activation in the phospho-RTK array when the HOMECs were treated with adipose tissue CM (**Table 11** in the appendix). This suggested that the observed STAT3 activation may not be linked to VEGF/VEGFR2 signalling.

c) Possible signalling pathways for HOMEC proliferation induced by adipose tissue conditioned media

Considering the results of both the phospho-RTK and phospho-kinase arrays, it is possible that the activation of receptors such as ALK or FGFRs may be responsible for HOMEC proliferation when treated with adipose tissue CM. The increased FGFR2α activation may be related to its docking to the FGFRs or to the ALK receptor, which in turn leads to STAT3 activation and subsequent cell proliferation. The various secreted adipokines in the omental adipose tissue may be responsible for the receptor activation. A schematic of this possible signalling pathway is depicted in **Figure 67**.

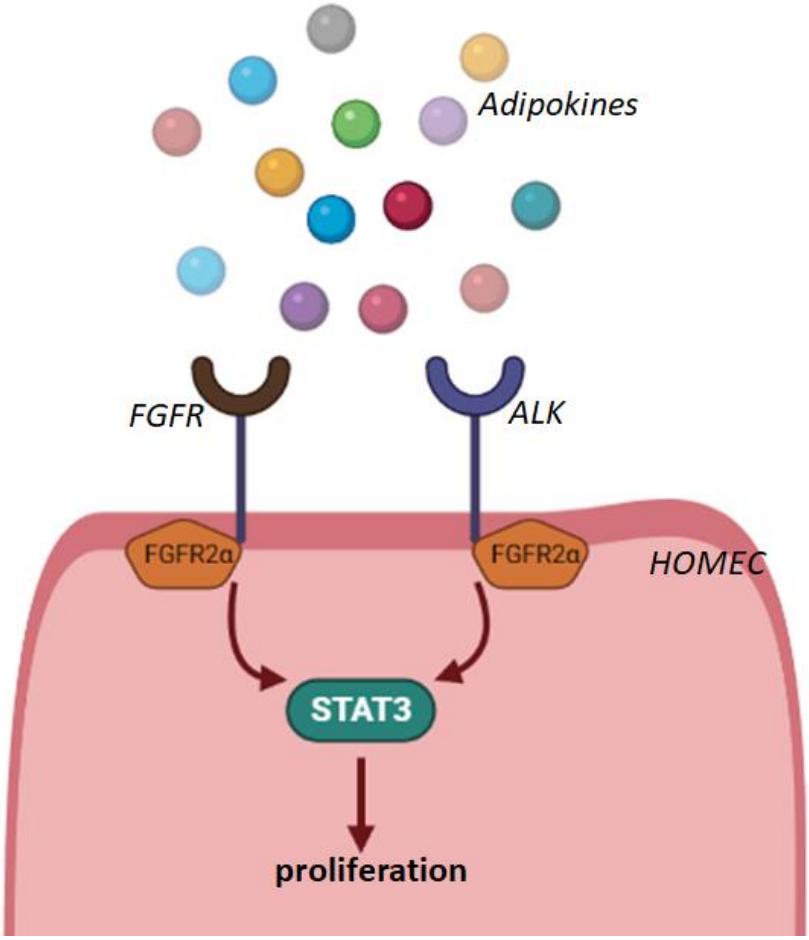

Figure 67. Schematic of the potential proliferative signalling pathway in HOMECs when treated with omental adipose tissue conditioned media. Adipokines secreted into the conditioned media may activate receptors such as FGFRs or ALK, leading to the docking and activation of FGFR2α. This in turn activates STAT3 signalling which leads to cell proliferation. Diagram created with BioRender.com.

Some studies reported an association between ERK1/2 and STAT3 activation in ECs. For example, in a mouse microvascular EC line, ERK1/2 and STAT3 signalling was found to be involved in EC migration as assessed by a scratch wound healing assay.(444) Another study in mouse brain EC reported that ERK1/2 activation subsequently led to STAT3 activation, and that this signalling pathway was involved in angiogenesis as assessed by a tube formation assay in vitro.(445) Thus, it is possible then that tumour angiogenesis in the omental environment may be a combined effect of both ERK1/2 activation (as a result of cancer-secreted factors) and STAT3 activation (due to the omental adipokines).

4.4.6 Limitations of the antibody arrays

The results of both the phospho-kinase and phospho-RTK arrays should be interpreted with caution. The kinase targets EGFR and PDGFRβ were featured on both arrays, but they appeared more prominent in the phospho-kinase array. This discrepancy may be due to the method of measurement. During the chemiluminescent image development of the array membranes, the length of exposure time was dependent on the strongest spots (larger magnitude of activation); the image was generated before the fainter spots could develop above the background (negative control) levels. Subsequently, when measuring pixel density of each spot, the density of the background and the fainter spots were not as contrasting as the stronger spots.

It was also not possible to combine the results of both the phospho-RTK and phospho-kinase arrays due to their different processing methods, i.e. difference in sample loading concentrations, antibody solutions provided within the commercial kit and image development processing times.

Thus, the arrays were considered as a screening tool to rapidly detect key activation targets. To quantify the difference in the degree of target phosphorylation or activation, more specific methods are required, e.g. ELISA for the specific targets.

4.4.7 VEGFR3 in HOMECs

Based on immunocytochemistry, VEGFR3 was detected on the surface of HOMECs and also within the cytoplasm. The reason for VEGFR3 detection in both extracellular and intracellular locations is unknown. Thus, future work may investigate the localisation of this receptor when treated with adipokine-incubated ovarian cancer CM.

Another distant possibility which cannot be excluded in the detection of VEGFR3 may be the identity of the isolated HOMECs. Considering that lymphatic vessels are also present near the omentum,(158) the VEGFR3 data raise the possibility that the ECs isolated were of lymphatic origin rather than

vascular. However, this possibility is unlikely since the isolated cells clearly express vWF, which is not expressed in lymphatic ECs.(371)

Future HOMEC isolation work may incorporate additional immunostaining markers. Examples include D2-40, podoplanin or integrin α1 to detect lymphatic ECs.(370, 426) If required, lymphatic ECs could be immunoselected, similar to HOMECs, using magnetic beads bound to antibodies against podoplanin.(426)

4.5 Chapter summary and conclusion

As previously discussed, EC proliferation is critical to angiogenesis and in tumour growth and metastasis. The “switching” of the host ECs from a proliferatively quiescent to an active state is considered a key step in new tumour blood vessel formation. It was shown in this chapter that during the metastasis of EOC, these pro-proliferative signals could be factors directly secreted from the omental adipose tissue or indirectly from the cancer cells in response to factors secreted from the adipose tissue, specifically leptin and lipocalin-2. There is currently limited understanding of the mechanisms underlying angiogenic activation of omental ECs during EOC metastasis and to investigate this further, this chapter describes a series of experiments designed to better understand which factors released from the cancer cells could be responsible for the observed enhanced proliferation.

Antibody arrays were utilised to examine which HOMEC receptors and intracellular kinase targets were activated (phosphorylated) by treatment with CM from adipokine-incubated A2780 and SKOV3 cells, as well as CM from adipose tissue. These data were interrogated to identify potential signalling mediators released from the EOC cells, and their role in inducing proliferation in HOMECs was investigated further by ELISA and receptor inhibitor studies.

VEGF and TGF-β1 were found to be secreted at high levels into all of the cancer cell CM i.e. from A2780 and SKOV3 cells incubated with leptin or lipocalin-2. However, only the VEGFR2 inhibitor significantly reduced proliferation induced by these CM, strongly suggesting a role for VEGF in the observed EC responses. This was particularly true for CM from SKOV3 cells,

again highlighting the difference between A2780 and SKOV3 cells in terms of their secretion of angiogenic factors.

VEGFR3, a receptor mostly expressed in the lymphatic vasculature, was shown to be expressed in HOMECs. Increased VEGFR3 activation in HOMECs were detected when the cells were treated with CM from A2780, but not with CM from SKOV3, further highlighting the difference between the cancer cell subtypes.

HOMEC proliferation induced by the cancer cell CM is most likely via ERK1/2 activation which is downstream of VEGF/VEGFR2 signalling and is possibly potentiated by PDGFRβ activation. A non-VEGF pathway involving the activation of STAT3 was put forward when HOMECs were treated with omental adipose tissue CM. These data highlight the complexity of the signals acting on host omental ECs during EOC metastasis.

Clearly, proangiogenic signals can derive from the adipocytes themselves and by their interaction with the invading tumour cells. It may be that the baseline secretome of the adipose tissue contributes to normal vascular homeostasis when ECs are in their normal quiescent state, but once they are “triggered” to become proliferative e.g. in in vitro cell culture, secreted factors instead induce proliferation. In the in vivo environment this “triggering” could be achieved by factors secreted from the tumour cells in response to adipokines released from the adipocytes. Thus, in the omental tumour microenvironment there are multiple pro-angiogenic inputs capable of initiating angiogenesis providing a receptive “soil” for new tumour growth.

In the management of EOC, new therapies are sorely needed as current treatments are inadequate or outdated (discussed in section 1.2.5). Therefore, understanding the interaction between the different players within the tumour microenvironment and their intracellular signalling processes serves to identify potential therapeutic targets.

Chapter 5. Human omental mesothelial cell isolation protocol development

5.1 Introduction

Mesothelial cells line the inner cavities of the human body (e.g. the pleural, pericardial and peritoneal cavities).(235) Within the peritoneal cavity, mesothelial cells also line the outer surface of the omentum and are the first point of contact for metastatic ovarian cancer cells, as discussed in section 1.6.5. In investigating the interaction between ovarian cancer cells and mesothelial cells, utilising tissue-specific mesothelial cells may better represent in vivo conditions; hence, a reliable protocol for isolating these cells is required.

However, there are drawbacks in utilising primary cells for experiments. One of which is their limited proliferative capacity. This concept is described as the Hayflick limit, in which the number of times the cells undergo division is pre-determined by intracellular mechanisms.(446, 447) When the cells have exhausted their dividing capabilities, the cell cycle then becomes irreversibly arrested and they enter into a senescent phase.(446) Hence, primary cells are viable for experiments mostly at early passages.

Another drawback related to primary cell culture is contamination with fibroblasts, which are cells involved in ECM generation and maintenance.(448) During primary cell isolation, fibroblasts may be inadvertently ‘harvested’ as they are present within the connective tissue. When present in cultures even at low levels, fibroblasts proliferate faster than isolated primary cells and have the tendency to outgrow them.(449, 450) Therefore, addressing fibroblast contamination may increase the probability of obtaining successful primary cell cultures.

When isolating HOMECs from the omental tissue samples (detailed in section 2.4), most of the digested tissue is discarded in the enzyme solution. This discarded solution contains a mixture of omental components, such as mesothelial cells, adipocytes, ECM and connective tissue. In investigating ovarian cancer metastasis, this enzyme solution presents a rich source of mesothelial cells which could be extracted for experimental use.

Thus, the aims of this chapter are to develop a reliable method to isolate mesothelial cells from the human omentum (section 5.3) and to optimise their growth in in vitro culture (section 5.4).

5.2 Methods

5.2.1 Mesothelial cell isolation protocol

Mesothelial cells were isolated from omental tissue according to the method described in section 2.5. The development of this method is detailed in section 5.3.

5.2.2 Immunocytochemistry

Mesothelial cells were seeded at 30,000 cells in a glass-bottomed culture dish and grown to confluence before immunocytochemistry was performed (described in section 2.9). The selection of suitable primary antibodies is detailed as follows.

Mesothelial cells contain cytoskeletal components such as cytokeratin-18 and vimentin.(451-453) Vimentin is generally accepted as a marker for fibroblasts,(454-456) a frequent contaminant in cell isolation procedures; and thus, could be used to differentiate between the two cell types.

It was also possible that the cell populations could be contaminated with ECs. Indeed the mesothelial cobblestone appearance is also characteristic of ECs.(451) Therefore, the cell populations were also examined for the endothelial markers CD31 and von Willebrand factor (vWF).(278) CD31 is ubiquitous in ECs but should not be observed in the isolated mesothelial cells or in fibroblasts.(457) vWF, an intracellular protein, is characteristic of ECs (278) and is absent in fibroblasts.(458) However, there is some disagreement whether vWF is present in mesothelial cells.(451, 453, 459) **Table 7** summarises the cellular markers which are present or absent in the three cell types – mesothelial cells, ECs and fibroblasts.

Table 7. Cellular markers present or absent in mesothelial cells, endothelial cells and fibroblasts. The four markers – cytokeratin-18, vimentin, CD31 and von Willebrand factor – were utilised in immunocytochemistry to differentiate between the cell phenotypes. Table partially adapted from Lachaud et al (2015).(282)

	Cellular markers			
	Cytokeratin-18	**Vimentin**	**CD31**	**von Willebrand factor**
Mesothelial cells (451-453, 459)	Present	Present	Absent	Present/ Absent
Endothelial cells (278, 451, 452)	Absent	Present	Present	Present
Fibroblasts (454-458)	Absent	Present	Absent	Absent

The purity of the isolated mesothelial cells was assessed based on co-staining with cytokeratin-18 and vimentin. The mesothelial cell majority appear red/yellow due to the presence of both cytokeratin-18 and vimentin, but areas of green-stained vimentin indicated contamination with fibroblasts. In order to assess the purity of the culture, ImageJ was used to interrogate the images taken at 10x magnification. Both the green-coloured regions and the total area encompassed by all cells were selected using the thresholding method on ImageJ (Image > Adjust > Color Threshold > Hue). The area of these selected regions was then measured and compared.

5.2.3 Fibroblast depletion using magnetic bead technology

The principle of this procedure is based on the premise that magnetic beads (MicroBeads® by Miltenyi Biotec), affixed to a fibroblast-specific antibody (unknown identity due to proprietary information), bind specifically to fibroblasts in a mixed cell suspension. When the bead/cell suspension is then flowed through a magnetised column (LS column), the beads with fibroblasts attached

are retained and the non-attached cells that flow through the column should then be depleted of fibroblasts.

For mesothelial purification a mixed cell population was collected after isolation or by trypsinisation as indicated, centrifuged at 200*g* for 5 minutes at room temperature and then depleted of fibroblasts using commercially supplied devices. The cell pellet was resuspended in 1mL of anti-fibroblast microbead buffer (composition as described in section 2.3.3), transferred to a 2mL tube, and microcentrifuged at 1300 rpm for 10 minutes. The buffer was aspirated and 80µLof fresh buffer was added, together with 20µL of the anti-fibroblast beads (20µL for up to 10 million cells, according to manufacturer's recommendation). The mixture was pipetted gently to ensure even mixing before being placed on a roller mixer at room temperature for 30 minutes.

As a washing step, 1mL of fresh anti-fibroblast microbead buffer was added and the tube microcentrifuged at 1300 rpm for 10 minutes. All buffer was aspirated and fresh 500µL buffer was added to resuspend the cell pellet. The LS column was pre-washed with this same buffer before use. The washed LS column was affixed to the MidiMACS™ Separator, which functions as the magnetic field source; and the MidiMACS™ Separator was affixed upright onto the MACS Multistand as shown in **Figure 68**.

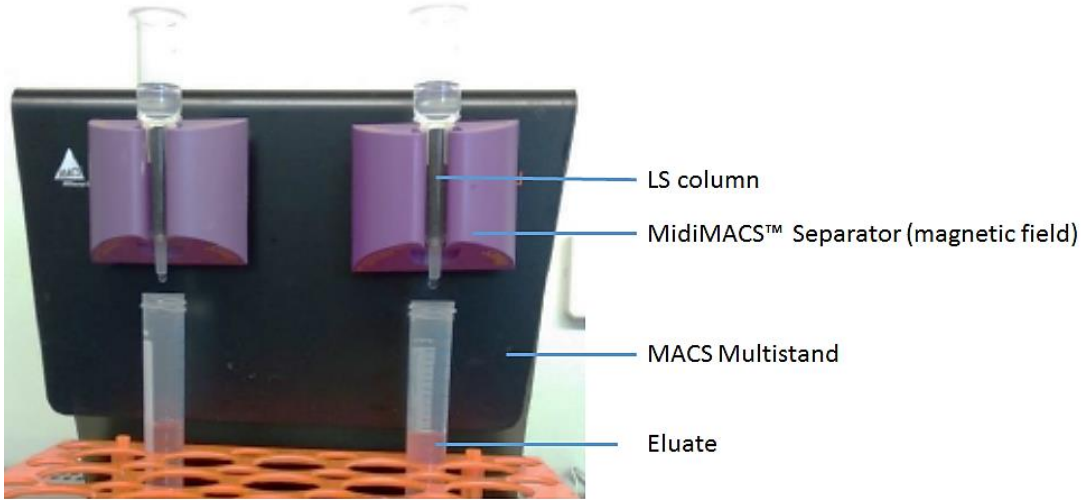

Figure 68. A photograph depicting the magnetic separation of fibroblasts using an LS column attached to a magnetic separator. The mixed cell population combined with magnetic anti-fibroblast beads was passed through the column under the influence of gravity. This was followed by three buffer washes, and all the eluate was collected. In this protocol, the cells attached to the beads (purportedly fibroblasts) remained in the column, while the non-attached cells were rinsed out as the eluate.

For the separation step, the suspension was pipetted into the LS column followed by three 3mL buffer washes, and all eluate collected. In principle, this eluate should only contain cells without magnetised beads attached, i.e. the mesothelial cells. The LS column was removed from the magnetic field and further rinsed with buffer. This eluate should only contain the beaded fibroblasts. The separate eluates were both centrifuged at 200*g* for 5 minutes at room temperature and both of the final cell pellets were cultured in lab cultureware coated with collagen IV and in mesothelial cell complete growth medium.

5.2.4 Assessment of mesothelial cell proliferation on different coating substrates

Mesothelial cells were seeded at 5,000 cells per well in 96-well plates in complete growth media. The plates were pre-coated with four different coating substrates – collagen I 3.33µg/mL, collagen IV 5µg/mL, gelatin 2% (v/v) and gelatin 0.2% (v/v); with at least 10 replicates per coating type. After 24 hours, the BrdU reagent was added to each well (20 µL per well), except wells which were designated as background wells. After 18 hours of incubation at 37°C/5% CO_2, the plates were fixed and subsequently processed as described in section 2.11.

5.2.5 Assessment of mesothelial cell doubling time

Mesothelial cells were seeded at 20,000 cells per well (equivalent to 10,000 cells/cm^2) in 500µL complete growth media, in collagen IV-coated 24-well plates. After 2 to 3 days in culture, cells were trypsinised (150µL/well), neutralised with 600µL/well growth media, and transferred to 1.5mL tubes for microcentrifugation at 1500 rpm for 5 minutes. The media was carefully removed from the pellet using a 10µL pipette tip affixed to the aspirator. Before counting with an automated haemocytometer, the cell pellet was resuspended in 100µL growth media and mixed thoroughly. These procedures were performed in quadruplicate, and at the same time daily to ensure 24-hour

interval between the recorded cell population numbers. The remaining cells in culture were changed with fresh growth media every 2 to 3 days.

With the calculated cell numbers recorded, the steepest growth indicates the log phase. The difference in cell numbers during this interval was used to calculate the population doubling time according to the formula derived from Greenwood et al (2002) (460):

$$\text{Population doubling time} = \frac{t \cdot \log_{10} 2}{(\log_{10} N_2 - \log_{10} N_1)}$$

where t = elapsed time in hours ($t_2 - t_1$) i.e. 24 hours

N = calculated cell number

5.2.6 Determination of the optimum FBS concentration required for omental mesothelial cell growth

Mesothelial cells were seeded at 10,000 cells per well in 96-well plates, initially in DMEM 10% (v/v) FBS. After 24 hours, all media were aspirated and replaced with DMEM with different FBS concentrations (5%, 10% and 20% (v/v)), with six replicates per condition. The plates were incubated at 37°C/5% CO_2 for another 24 hours. BrdU reagent were added to each well, except for designated background wells, and incubated for 20 hours. The plates were fixed and subsequently processed as described in section 2.11.

5.2.7 Determination of the optimum seeding density for omental mesothelial cell growth

Mesothelial cells were seeded in DMEM 10% (v/v) FBS, at various densities in 24-well plates, with three replicates per condition. Each collagen IV-coated well had a growth area of 2 cm^2; cells were counted with a haemocytometer and seeded at 5000 to 40,000 per well (2500 to 20,000 cells/cm^2). Wells were imaged with a phase contrast microscope at the same time daily to observe when they reached confluence. In a separate experiment, the same design was employed but with the growth media replaced with DMEM 20% (v/v) FBS.

5.3 Development of a protocol to isolate mesothelial cells

5.3.1 Non-enzymatic method of mesothelial cell isolation

Initially a non-enzymatic methodology was investigated; based on a protocol adapted from Hewett and Murray (1994).(461) This method was based on the premise that mesothelial cells form an external layer on the surface of the omentum, thus they would eventually dissociate from the surface of the omental tissue without any enzymatic digestion.

Method

Omental tissue, obtained as described in section 2.4, was minced into 1cm^3 pieces with a scalpel and washed once in cold PBS. The pieces were then placed into a 50mL centrifuge tube to a volume of 10mL. 20mL of fresh cold PBS containing gentamicin (50µg/mL) was added and the tube was placed on a roller mixer at 2-8°C for 4 hours or 9 hours.

The PBS was then removed from the tissue pieces, transferred into a fresh centrifuge tube, and centrifuged at 200*g* at 4°C for 10 minutes. The resultant cell pellet was plated into a 0.2% (w/v)-gelatin coated well of a 6-well plate and cultured in DMEM with 10% (v/v) FBS. This medium was originally chosen as it is considered a basic medium for general cell culture, such as those cited in past literature.(461-463)

Results

This non-enzymatic method of omental mesothelial cell isolation was performed twice. Incubation in cold PBS was initially performed for 4 hours, which yielded very few cells; hence in the second attempt, this incubation duration was increased to 9 hours to improve cell yield. With both the 4-hour and the 9-hour incubation, cell growth was sparse with not enough cells present to generate a confluent monolayer even after 11 or 20 days post isolation (**Figure 69**). Thus, a more efficient isolation method was investigated; specifically, a method based on enzymatic digestion.

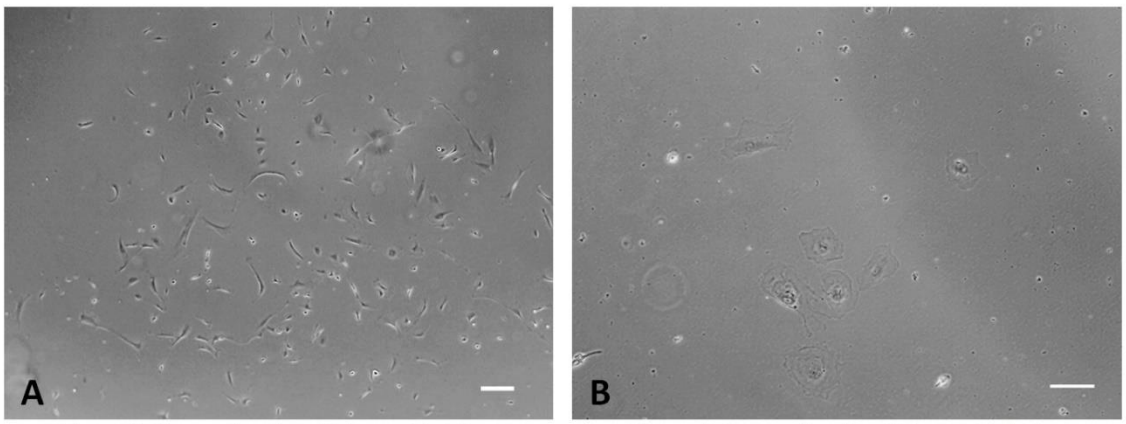

Figure 69. Mesothelial cell yield was low when a non-enzymatic isolation method was employed. Minced and washed omental tissue segments were placed in PBS on a roller mixer and the shed cells were collected, cultured and then imaged by phase contrast microscopy (EVOS XL Core) at 4x magnification. (A) four-hour agitation on a roller mixer and 11 days in culture, (B) nine-hour agitation on a roller mixer and 20 days in culture; scale bar 200µm.

5.3.2 Enzymatic method of mesothelial cell isolation

Due to the unsuccessful harvesting of mesothelial cells using the non-enzymatic method, an enzyme-based protocol for mesothelial cell isolation was adapted from Takahashi et al (1991).(279)

Method

The omental tissue sample was minced, using a scalpel, into 1cm^3 pieces and then mixed with pre-warmed enzyme solution containing collagenase type II (tissue : enzyme solution ratio of 1:1.5 v/v). The mixture was then placed on a rotary mixer at 37°C for 20 minutes. At the end of the digestion, the enzyme was neutralised by adding FBS (1:10 v/v) to the mixture.

Large undigested tissue pieces were manually removed using tweezers, and the mixture then passed through one layer of gauze swab with multiple cold PBS washings. The filtrate was then centrifuged at 300*g* at 4°C for 10 minutes. The resultant cell pellet, red in colour due to the presence of erythrocytes, was resuspended in 1mL of DMEM with 10% (v/v) FBS and then gently layered on top of 10mL cold modified PBS solution (composition as described in section

2.3.3). Over the course of 10-15 minutes, this top layer gradually seeped downwards (**Figure 70**).

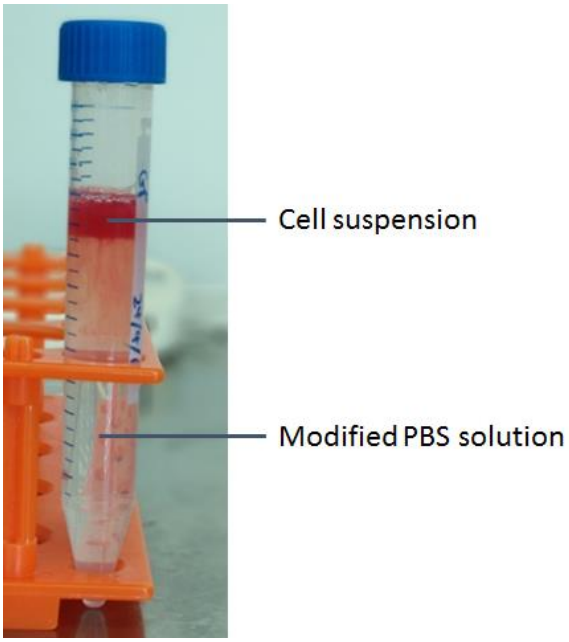

Figure 70. A photograph showing the layering of the isolated cell suspension mixture onto the modified PBS solution. A mixed cell population obtained from enzyme-digested omental tissue was layered onto the modified PBS solution and left to seep downwards under the influence of gravity; the red colour of the seepage is due to the presence of erythrocytes from the mixed cell suspension in the top layer.

This layering step, adapted from Takahashi et al (1991),(279) utilised gravity and the viscosity of the modified PBS solution to separate the mixed cell population. Although not mentioned in the original article, this method is a form of cell density separation; with the premise that the mesothelial cells became suspended within the modified PBS solution. Since the original top layer contained erythrocytes, their red colour provided an indication of the extent of the downward seepage into the modified PBS solution.

If the top layer was too dense or heavy, this slow seepage did not occur and instead the whole top layer fell straight into the modified PBS solution. In this case, there was no distinction between the top layer and the rest of the modified PBS solution, and the whole solution appeared totally red in colour due to the

presence of erythrocytes. If this occurred, the whole mixture was centrifuged at 300*g* at 4°C for 10 minutes and the cell pellet resuspended in a larger volume i.e. 2mL of DMEM with 10% (v/v) FBS. 1mL aliquots were then layered on top of two separate 10mL cold modified PBS cushions.

Alternatively, the modified PBS solution was gently rocked top-to-bottom to create a layer of foam bubbles (<1cm in height) at the upper surface. This layer of foam prevented the fall of the top layer and thus, allowed the gradual seepage into the modified PBS solution. This method was serendipitously discovered: the modified PBS solution aliquots were initially frozen, and to speed up thawing prior to use, the tubes were shaken by tilting them upside down several times.

Once the top layer had seeped into the modified PBS solution, the top and bottom 1mL 'layers' were discarded, and the middle 9mL portion was centrifuged at 300*g* at 4°C for 10 minutes. The resultant cell pellet mostly contained erythrocytes (red in colour) and mesothelial cells. Generally, 10-15 minutes of this layering step was sufficient, as assessed by the extent of the red coloured seepage into the modified PBS solution. The layering step was considered complete when the downward seepage had reached at least half the length of the tube.

After the first layering step, a second layering step was performed in the same manner to further purify the cell yield. The cell pellet was again suspended in 1mL of DMEM with 10% (v/v) FBS and layered onto fresh 10mL cold modified PBS solution. After 10 minutes, the middle 9mL portion was collected and centrifuged at 300*g* at 4°C for 10 minutes. This final cell pellet was resuspended in DMEM with 10% (v/v) FBS and cultured in a well of a 6-well plate coated with 0.2% (w/v) gelatin. Two to three days later, wells were washed twice with DMEM with 10% (v/v) FBS to remove erythrocytes and fresh media was added. The isolation procedure is summarised in **Figure 71**.

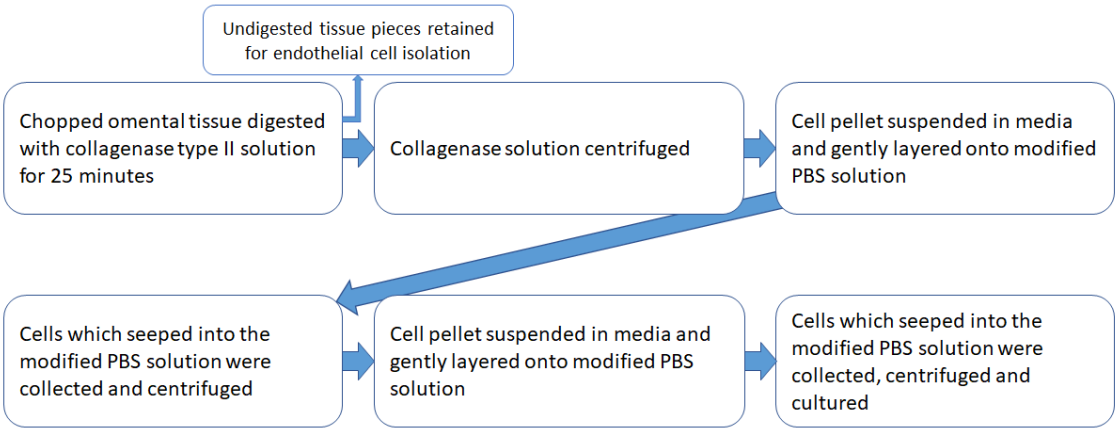

Figure 71. A schematic of the enzyme-based mesothelial cell isolation protocol. The protocol consists of an enzymatic digestion step to detach the mesothelial cells from the tissue, followed by two layering steps to further purify the cell yield. Endothelial cell (HOMEC) isolation is detailed in chapter 3.

Results

The enzymatic method of isolating omental mesothelial cells was performed on 47 tissue samples. Compared to the non-enzymatic method, this protocol yielded increased mesothelial cell numbers, which were able to form a confluent monolayer in 6-well plates nearly 45% of the time (21 of 47 samples). In the remaining samples, fibroblast contamination was noted, as determined by microscopy. Further method development was thus required to improve the purity of isolation; thus, a magnetic bead purification protocol was tested (refer to section 5.2.3).

Contamination of erythrocytes was also observed; this was indicated by the red colour of the cell pellet and subsequently, the colour of the downward seepage into the modified PBS solution. These were easily washed away after 2 to 3 days of culture once the isolated mesothelial cells adhered to the bottom of the well.

One key advantage of this enzymatic isolation technique was that the undigested tissue sample could subsequently be utilised for HOMEC isolation (described in section 2.4), thus ensuring that the donated human sample was used appropriately.

5.3.3 Depletion of fibroblasts from the isolated mesothelial cell population

It was noted, using phase contrast microscopy, that prior to reaching confluence, mesothelial cells were spindle-shaped i.e. similar to fibroblasts. Thus, fibroblast contamination was difficult to determine in sub-confluent primary cell populations. In contrast, a confluent mesothelial population displayed a cobblestone appearance, whereas fibroblasts retained their spindle-like phenotype (**Figure 72**). Therefore, the purity of a mesothelial culture was initially determined by microscopy of a confluent culture.

From the 47 tissue samples processed, 21 yielded confluent mesothelial cell populations which were later expanded, 26 samples resulted in cultures with more than 50% fibroblast coverage (cultures were then discarded), while the remaining 10 had <50% fibroblast coverage. Cultures with less than 50% fibroblast population were subjected to a fibroblast depletion procedure using anti-fibroblast magnetic beads as described in section 5.2.3.

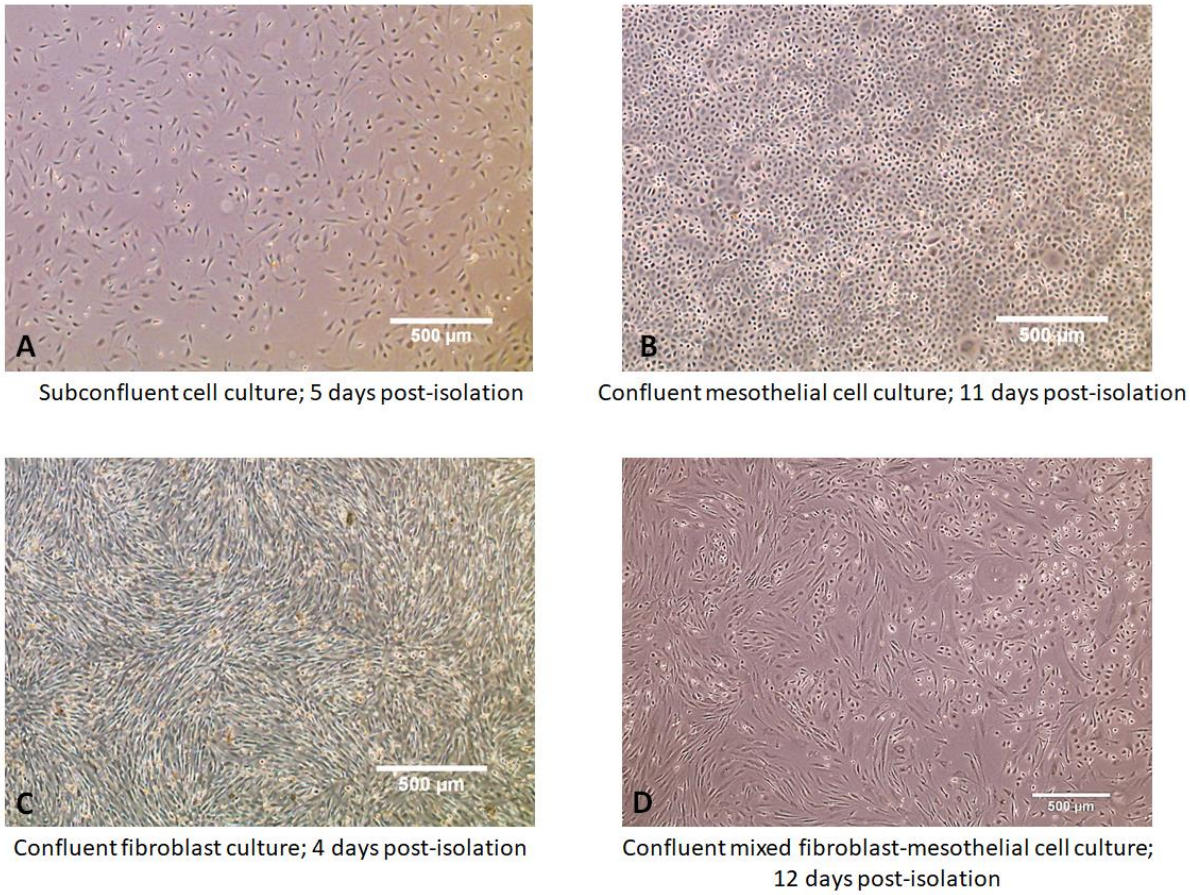

Figure 72. The purity of a mesothelial cell culture can be determined by microscopy of a confluent culture. Mesothelial cells were isolated from human omentum by collagenase type II digestion and density separation. Freshly isolated cells were cultured in DMEM with 10% (v/v) FBS and cell phenotype was examined by phase contrast microscopy. Representative images, captured at 4x magnification on EVOS XL Core, of cells at passage 0 are shown: sub-confluent cells after 5 days of culture post-isolation (A); confluent mesothelial cells after 11 days of culture post-isolation (B); confluent fibroblasts after 4 days of culture post-isolation (C) and confluent mixed fibroblasts and mesothelial cells after 12 days of culture post-isolation (D). Scale bar 500µm.

Results

This fibroblast depletion procedure was performed on 10 of the isolated samples, when it was determined visually that mesothelial cells were present and that the fibroblast contamination was less than 50%. This method was effective 60% of the time (6 of 10) i.e. the non-magnetised cells (cells that did not bind to the beads) appeared as a cobblestone-like monolayer after culturing them to confluence, which suggested a mesothelial phenotype. Their mesothelial cell identity was confirmed by immunocytochemistry (section 5.2.2).

However, upon culturing the magnetised portion, a mixed cell population of both cobblestone and fibroblastoid cells was observed by microscopy. Immunocytochemistry confirmed their identities as mesothelial cells and fibroblasts, respectively. Both the magnetised and non-magnetised portion are depicted in **Figure 73** and **Figure 74**.

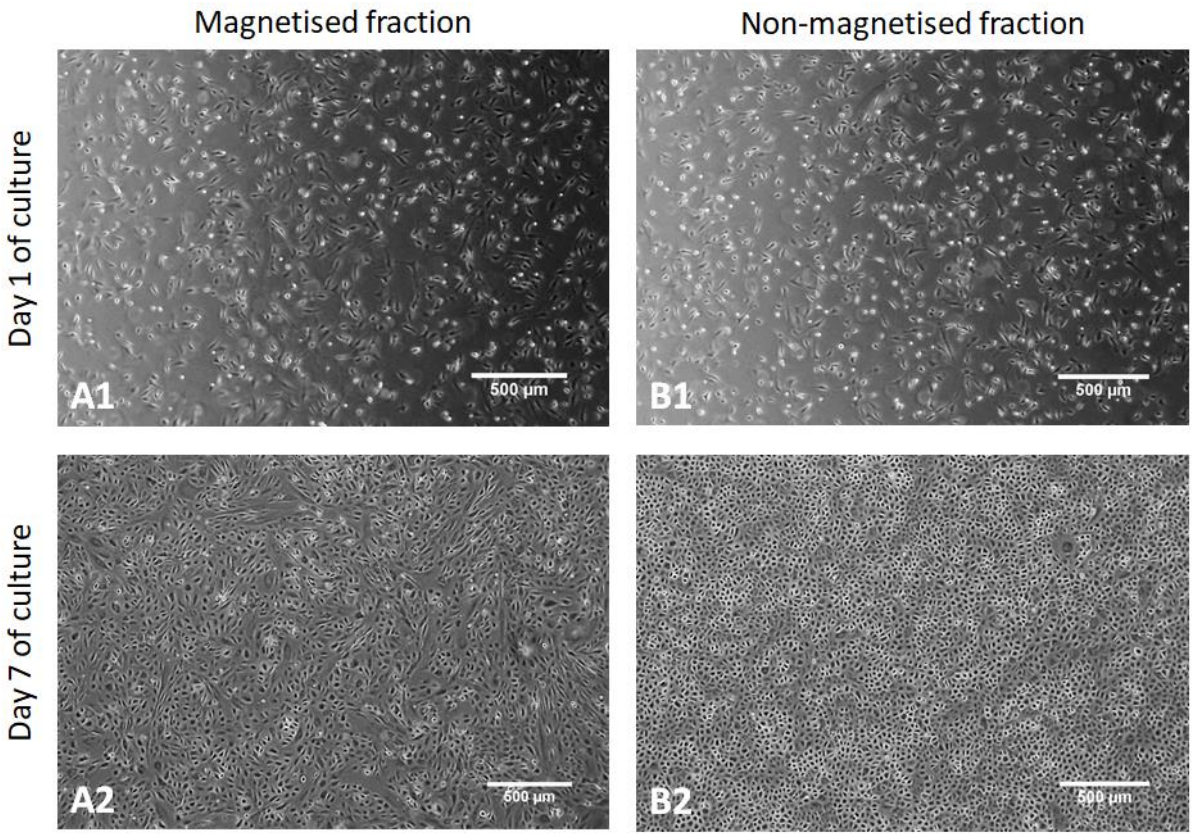

Figure 73. Anti-fibroblast magnetic beads depleted fibroblasts from a mixed cell population but bound to both fibroblasts and mesothelial cells. Mesothelial cells were isolated from omental tissue by collagenase II digestion and cultured to confluence prior to fibroblast depletion by magnetic bead technology. Both the eluate fraction (non-magnetic) and the cells retained on the beads (magnetic) were collected and cultured. Representative images of cells at passage 1, captured on EVOS XL Core at 4x magnification, show both the “fibroblast”/magnetic (A1, A2) and “mesothelial”/non-magnetic fractions (B1, B2) after culturing for 1 day (A1, B1) and 7 days (A2, B2). Scale bar 500µm.

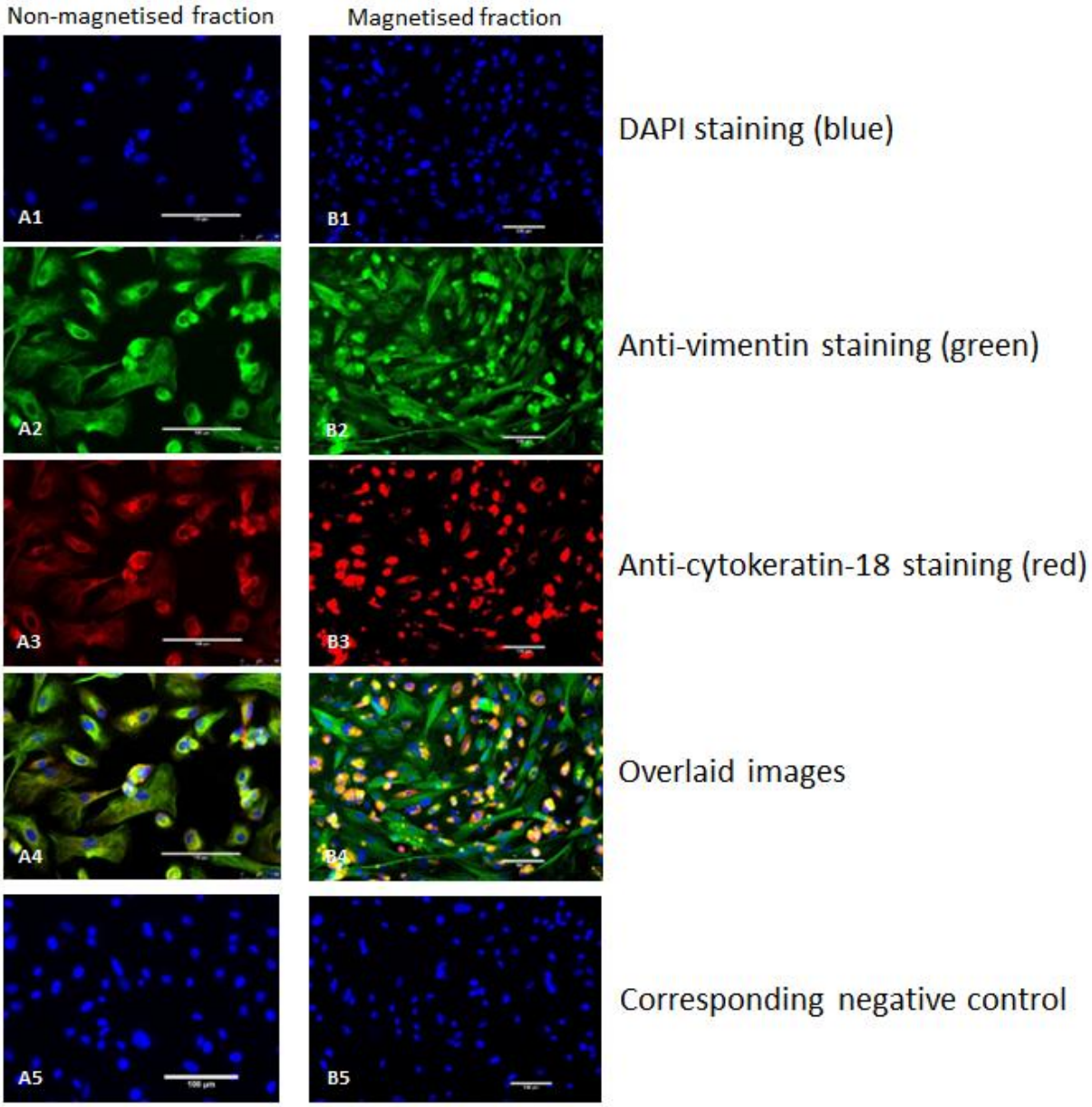

Figure 74. Magnetic anti-fibroblast beads bound to fibroblasts and mesothelial cells, generating a non-magnetised mesothelial cell fraction as assessed by staining for vimentin and cytokeratin-18. Mesothelial cells were isolated from omental tissue by collagenase II digestion and 5 days later treated to deplete fibroblasts by magnetic bead technology. Cells, at passage 1, obtained after the fibroblast depletion procedure were seeded at 30,000 cells in a glass-bottomed culture dish to confluence; cells were with 4% (v/v) paraformaldehyde at room temperature and then permeabilised with methanol at -20°C. Primary antibodies (anti-vimentin and anti-cytokeratin-18) were applied, followed by fluorescent-conjugated secondary antibodies; cell nuclei were stained blue with DAPI (A1, B1). Culture dishes were visualised at 10x magnification with Leica DM4000 B LED. Mesothelial cells appear yellow (A4, B4) as the green of the vimentin (A2, B2) and the red of cytokeratin-18 (A3, B3) were overlaid, while fibroblasts only stained for vimentin. The non-magnetised fraction (A4) showed a mesothelial cell majority while the magnetised fraction (B4) showed a mixed population of mesothelial cells and fibroblasts. The negative control (PBS only, in place of primary antibodies) (A5, B5) showed background level of staining. Scale bar 100µm.

These data suggested non-specificity of the anti-fibroblast beads. They appeared to bind to a surface marker common to both mesothelial cells and fibroblasts. While the beads were successful in depleting fibroblasts from the mixed population culture to produce a pure mesothelial cell culture, some mesothelial cells were lost in the process as they were discarded with the beads.

To reiterate, this fibroblast depletion procedure was performed on a mixed population of mesothelial cells and fibroblasts between passages 0 to 1, with a 60% success rate. The remaining 40% were deemed unsuccessful when the non-magnetised portion (mesothelial cells) appeared senescent-like when cultured post-fibroblast depletion.

The senescent-like cells were characterised by their flattened and enlarged morphology as determined by phase contrast microscopy. Visually, their features were similar to the senescent omental mesothelial cells from past studies.(464, 465) An example of a culture containing senescent-like mesothelial cells is later shown in **Figure 75**.

However, these senescent-like cells were not investigated further in this project. Cultures were discarded when these cells occupy ≥10% (visually determined) of the culture area. Furthermore, the regular supply of omental tissue samples together with the establishment of a reliable method of mesothelial cell isolation provided sufficient numbers of cells for experimental use.

5.3.4 A second depletion of fibroblasts on the magnetised portion consisting of mesothelial cells and fibroblasts

After the first round of magnetic fibroblast depletion, it was noted that the magnetised portion (at passage 1) contained both mesothelial cells and fibroblasts. In an attempt to salvage the mesothelial cells in this mixed population, the population were first expanded (1:5 split) to increase their cell numbers (passage 2) and then subjected to the same fibroblast depletion procedure a second time (as described in section 5.2.3).

Results

Only one mixed cell population was subjected to the fibroblast depletion procedure twice. No further repeats were performed due to the high rate of senescent-like cells as observed by microscopy after the second depletion procedure. These senescent-like mesothelial cells are characterised by a flattened and enlarged phenotype (465) and the morphological changes in the cell population can be clearly observed in **Figure 75**. It was possible that the multiple depletion procedures reduced cell numbers and thus, resulted in decreased seeding density, which may have contributed to the high rate of senescence. This is later discussed in section 5.5.2b.

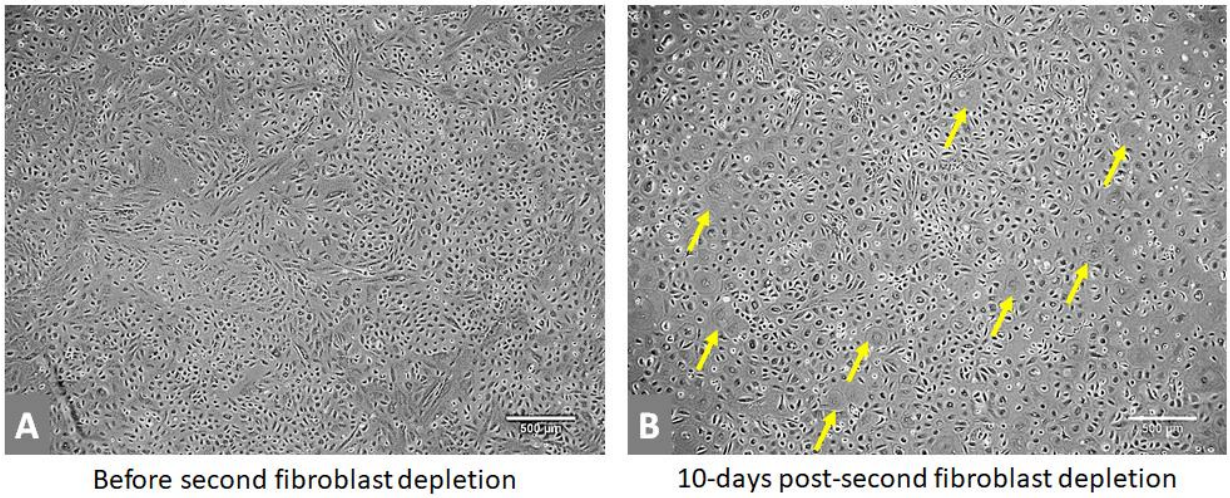

Figure 75. Repeated fibroblast depletion increases the number of senescent-like cells. Cells were subjected to fibroblast-depletion 6 days post-isolation from tissue. The mixed cell population that attached to the magnetic beads was expanded and then subjected to a second fibroblast depletion procedure 16 days later. Images were captured at 4x magnification with EVOS XL Core prior to the second fibroblast depletion procedure at passage 2 (A), and ten days later at passage 3 (B). Senescent-like cells, as assessed visually by microscopy are marked with arrows. Scale bar 500µm.

5.3.5 Depletion of fibroblasts during the enzymatic isolation of mesothelial cells

The previous described attempts to eliminate fibroblast contamination were performed on cultured isolates at passage 0 and 1. This approach had a success rate of 60%. Performing the fibroblast depletion a second time increased the number of senescent-like cells.

In an attempt to improve isolation efficiency, further experiments attempted to remove fibroblast contamination during the original isolation process to obtain a pure population of mesothelial cells at passage 0.

The mixed cell suspension generated prior to the density separation step (described in section 5.3.2) contains erythrocytes, as evidenced by the red colour. To reduce the number of cells in the suspension and thus maximise the binding of the anti-fibroblast beads, the erythrocytes were lysed by adding 900µL of autoclaved deionised distilled water. After 30 seconds, 100µL of 10x PBS was added to halt the lysis reaction. This mixture was centrifuged at 1300 rpm for 10 minutes, and the supernatant aspirated to remove the lysed erythrocytes. The mixed cell population was then subjected to a fibroblast depletion procedure as described in section 5.2.3 and the cells cultured in 6-well plates.

Results

In the earlier mesothelial cell isolation protocol, the cell pellet produced after collagenase type II digestion was subjected to a density separation using modified PBS solution. Incorporating the magnetic fibroblast depletion step at the point of isolation replaced this separation step, since the ultimate goal was to separate contaminant cells from the mesothelial cells.

When the population of cells that did not attach to the beads was cultured to confluence, the cells appeared cobblestone similar to that observed after previous fibroblast depletion attempts (**Figure 76A**) and subsequent immunocytochemistry analysis confirmed their mesothelial cell identity. Meanwhile, the population of cells that did attach to the beads appeared fibroblast-like (**Figure 76B**) by phase contrast microscopy, which initially suggested that the magnetic selection of fibroblasts at the point of isolation

offered improved efficacy compared to when it was performed after passage 0, i.e. fewer mesothelial cells were lost by attachment to the beads. However, immunocytochemistry analysis of the magnetically-selected cells showed both fibroblasts and mesothelial cells, similar to previous observations.

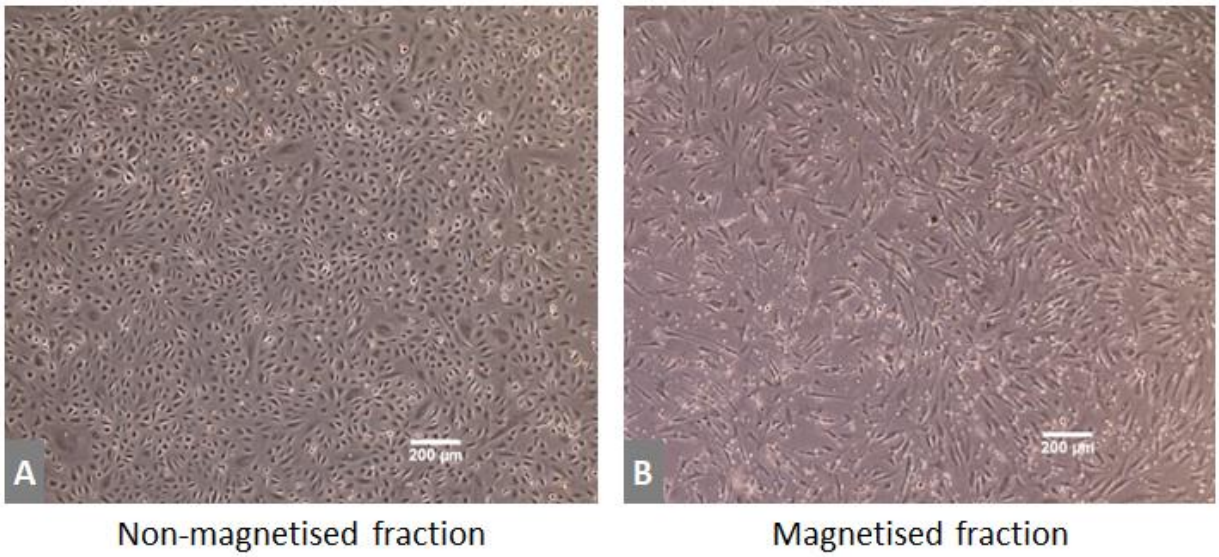

Figure 76. Cell phenotype in the magnetised (fibroblast-like) and non-magnetised (cobblestone-like) populations were distinctly different when observed under phase contrast microscopy. Cells were isolated from omental tissue by collagenase II digestion, subjected to erythrocyte lysis, and immediately followed by fibroblast separation using magnetic bead technology. Both magnetised (A, cells that attached to the beads, nominally fibroblasts) and non-magnetised (B, unattached cells e.g. mesothelial) fractions were cultured in separate wells of a 6-well plate. Images were captured at 4x magnification with EVOS XL Core after 5 days (A) and 9 days (B) of culture. Scale bar 200µm.

Based on all the experimental data collected, the final isolation protocol adopted was that described in section 5.3.2, and fibroblast depletion protocol was only utilised when the isolated cells at passage 0 displayed fibroblast contamination of <50% coverage. The reasons for this are discussed in section 5.5.2.

5.3.6 Characterisation of isolated mesothelial cells

The phenotype of the mesothelial cells (isolated using the final isolation protocol described in section 5.3.2) was confirmed by negative staining for CD31 (**Figure 77**), and positive staining for both vimentin and cytokeratin-18 (**Figure 78**). Depending on the omental specimen, some of the cells stained positive for vWF while some did not (**Figure 79**). Where vWF was observed, it was less abundant than observed in ECs (451) (previously depicted in **Figure 26** and **Figure 65**).

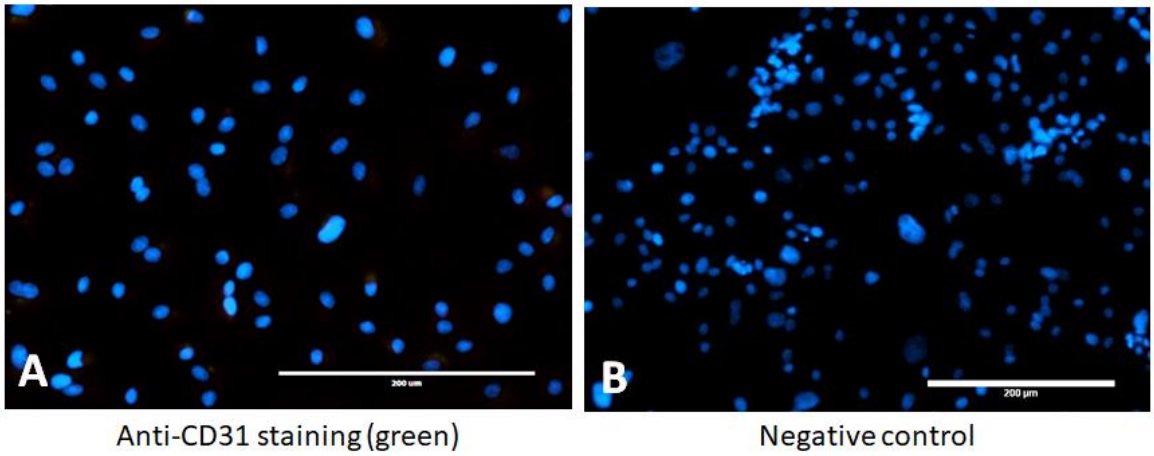

Figure 77. Isolated omental mesothelial cells do not express CD31. Cells were seeded at 30,000 cells in a glass-bottomed culture dish and cultured to confluence. Cells were fixed with 4% (v/v) paraformaldehyde at room temperature. Anti-CD31 primary antibodies were applied (A) but PBS replaced primary antibodies in negative control (B), followed by fluorescent-conjugated secondary antibodies. Cell nuclei were stained blue with DAPI. After mounting with coverslips, culture dishes were visualised at 10x magnification with EVOS Fluo. Scale bar 200µm.

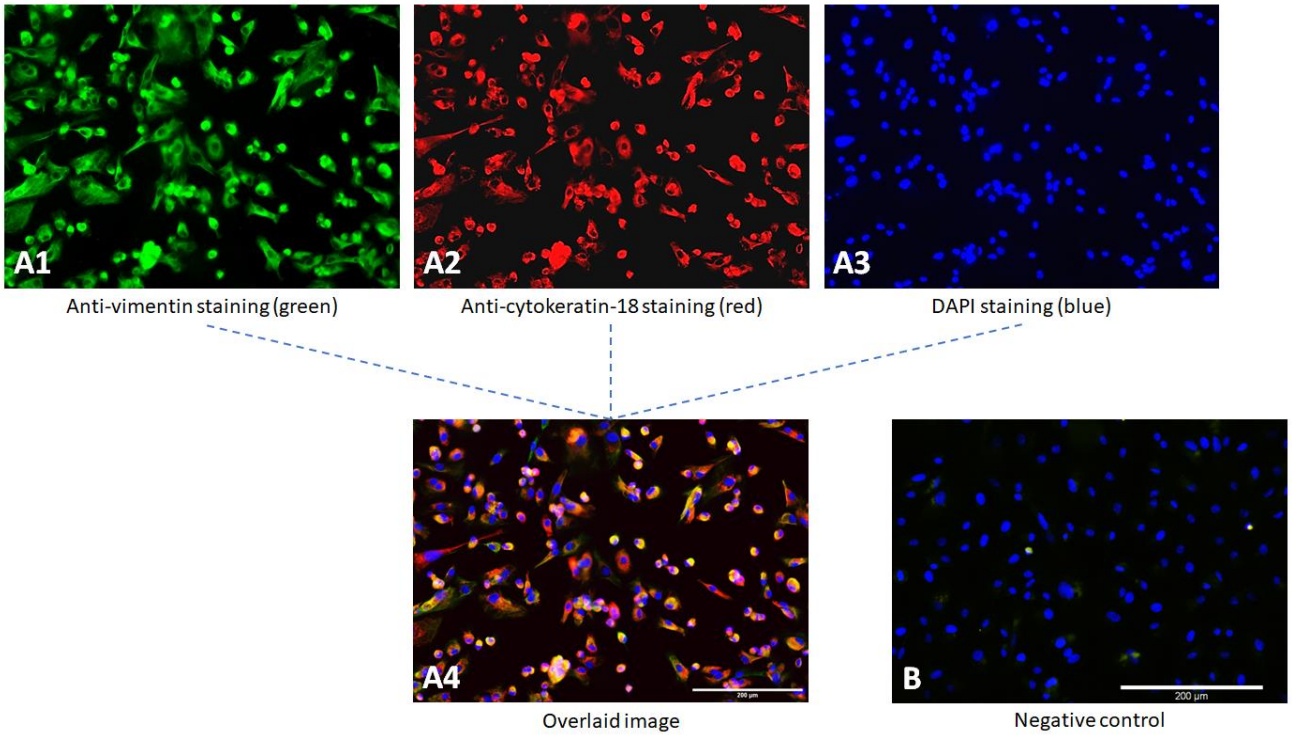

Figure 78. Isolated omental mesothelial cells express cytokeratin-18 and vimentin. Cells were seeded at 30,000 cells in a glass-bottomed culture dish and cultured to confluence. Cells were fixed with 4% (v/v) paraformaldehyde at room temperature, and then permeabilised with methanol at -20°C. Primary antibodies (anti-vimentin and anti-cytokeratin-18) were applied, followed by fluorescent-conjugated secondary antibodies; cell nuclei were stained blue with DAPI (A3, B). After mounting with coverslips, culture dishes were visualised at 10x magnification with Leica DM4000 B LED. Mesothelial cells appear yellow (A4) as the green of the vimentin (A1) and the red of cytokeratin-18 (A2) were overlaid. The negative control (PBS only, in place of primary antibodies) (B) showed background level of staining. Scale bar 200µm.

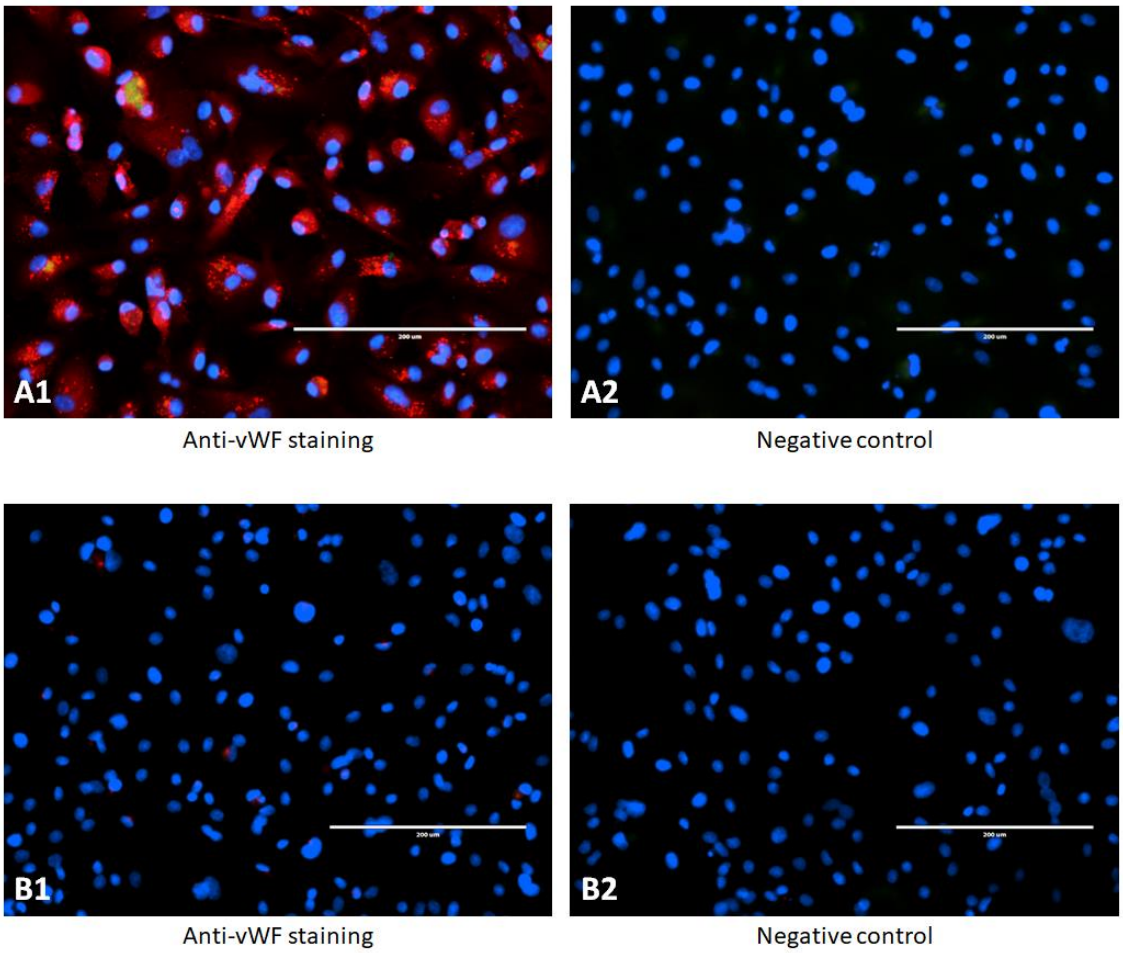

Figure 79. Some isolates of omental mesothelial cells stained positive for vWF (A1) and others negative for vWF (B1). The cells were of the same passage number (p2). Images A2 and B2 are the corresponding negative controls for A1 and B1 respectively. Cells were seeded at 30,000 cells in a glass-bottomed culture dish and cultured to confluence. Cells were fixed with 4% (v/v) paraformaldehyde at room temperature, and then permeabilised with methanol at -20°C. Anti-vWF antibody was applied, except in negative controls where PBS was applied, followed by fluorescent-conjugated secondary antibodies. Cell nuclei were stained blue with DAPI. After mounting with coverslips, culture dishes were visualised at 10x magnification with EVOS Fluo. Scale bar 200µm.

Purity of the isolated mesothelial cell population, as assessed by immunocytochemistry was performed on cells isolated via collagenase type II digestion without fibroblast depletion (n=2), and on cells which underwent fibroblast depletion (n=2). In both circumstances, there were less than 5% of contamination of other cell types, namely fibroblasts (representative image in **Figure 80**).

The mesothelial cells were only utilised in experiments up to passage 5 as there was a higher occurrence of senescent-like cells at later passage numbers; only cultures with less than 10% senescent-like cells (determined visually by phase contrast microscopy) were used. Cell senescence is discussed in section 5.5.4.

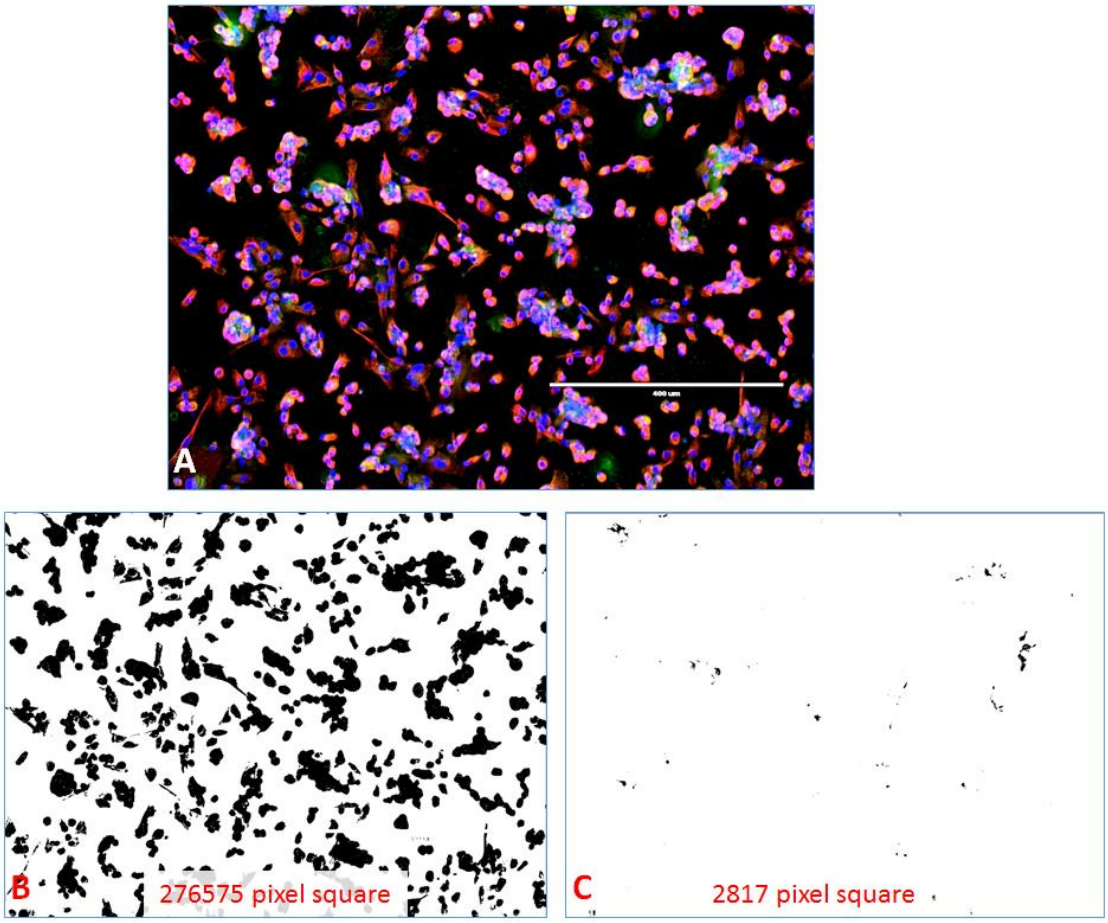

Figure 80. Isolated mesothelial cell culture with less than 5% contamination from other cell types. Cells were isolated from omental tissue by collagenase II digestion and treated to deplete fibroblasts by magnetic bead technology. Cells were seeded at 30,000 cells in a glass-bottomed culture dish and cultured to confluence; cells were fixed with 4% (v/v) paraformaldehyde at room temperature and then permeabilised with methanol at -20°C. Primary antibodies (anti-vimentin and anti-cytokeratin-18) were applied, followed by fluorescent-conjugated secondary antibodies (green for vimentin, red for cytokeratin-18); cell nuclei were stained blue with DAPI. The proportion of contaminating fibroblasts (stained green) was calculated by ImageJ. Representative image visualised at 20x magnification using EVOS Fluo (A); total cell area, marked black on ImageJ (B) and green-stained areas, marked black on ImageJ (C). Scale bar 400µm.

5.4 Optimisation of mesothelial cell growth conditions

Once the isolation method for human omental mesothelial cells was established and optimised, the optimum culture conditions were examined to maximise the viability of the cells for use in future experiments. The aspects investigated were: a) optimum coating substrate for tissue culture plasticware; b) population doubling time; c) optimum FBS concentration in the complete growth media; and d) optimum seeding density.

5.4.1 Coating surface type for tissue culture plasticware

Cultureware coating aids the adhesion and subsequent proliferation of cultured cells. Therefore, simulating basement membrane conditions could, in theory, improve cell viability. In the initial isolations, the mesothelial cells were cultured in wells coated with 0.2% (v/v) gelatin, according to the method by Takahashi et al (1991).(279) However, in vivo, the basement membrane of adipose tissue (where the isolated mesothelial cells originate) mostly consists of collagen IV,(466, 467) although some studies mention that collagen I is the most abundant.(468, 469) Therefore, experiments were carried out to identify the growth environment required for optimal mesothelial cell growth.

Initially, freshly isolated cells were seeded onto collagen IV or gelatin 0.2% (v/v). From visual observation, cells adhered to the gelatin coating faster than to the collagen IV, however, they proliferated faster on collagen IV than on gelatin (**Figure 81**). This was further investigated using a commercially available cell proliferation assay and with a wider range of coating materials, as described in section 5.2.4.

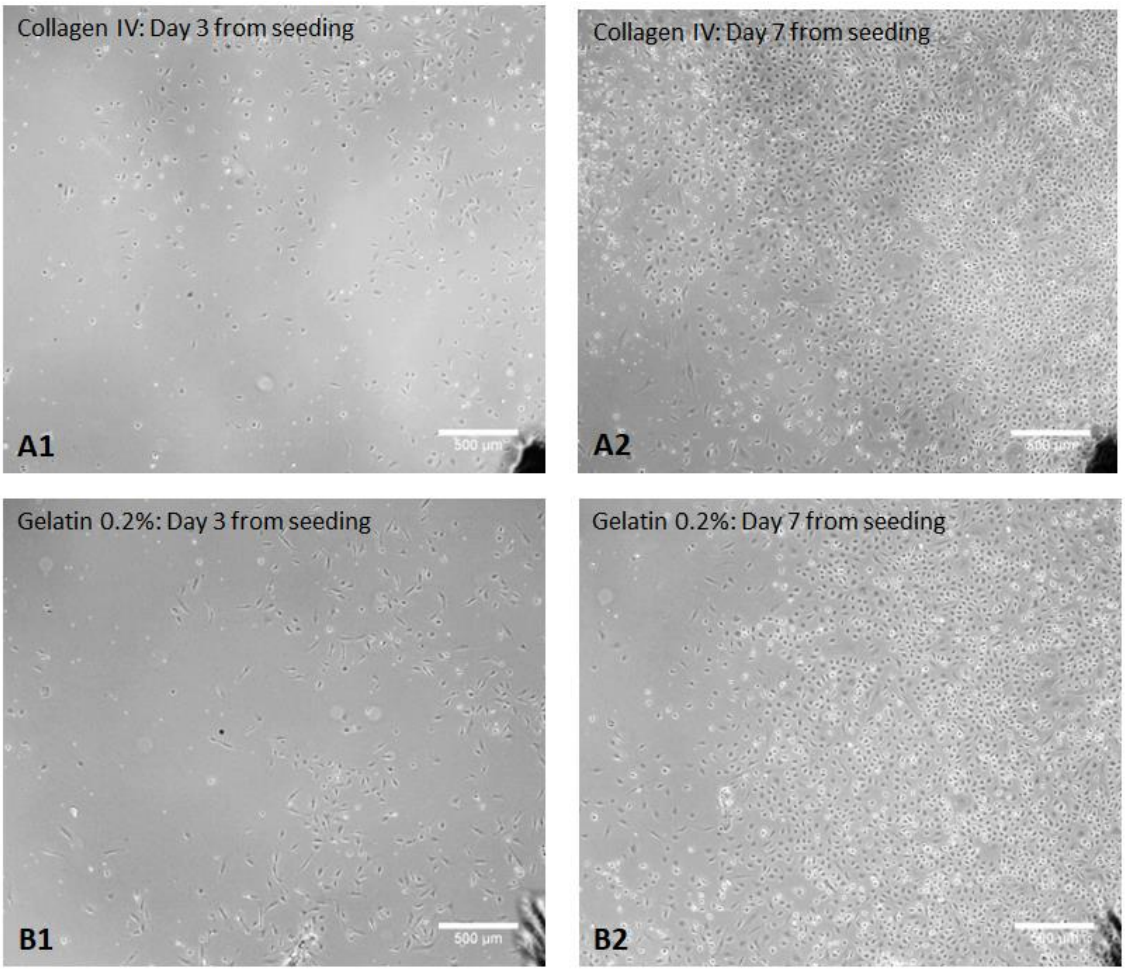

Figure 81. Collagen IV enhanced mesothelial cell growth. Freshly isolated mesothelial cells were seeded equally in each well of a 6-well plate with DMEM 10% (v/v) FBS media and growth was assessed visually. More mesothelial cells adhered onto gelatin 0.2% v/v (B1) than to collagen IV (A1) after three days of seeding (n=2); but those on collagen IV (A2) proliferated faster compared to those on gelatin 0.2% v/v (B2) four days later. Representative images from n=2 are shown. Cells were imaged at 4x magnification with EVOS XL Core in the same location; scale bar 500µm.

The collagen IV coated surface proved to be best for mesothelial cell proliferation (**Figure 82**). Cells on collagen I and collagen IV surfaces generally had higher proliferation rates i.e. the highest cell number based on absorbance values, compared with gelatin-coated surfaces. Based on these findings, all laboratory cultureware for mesothelial cell culture was subsequently coated with collagen IV in future experiments.

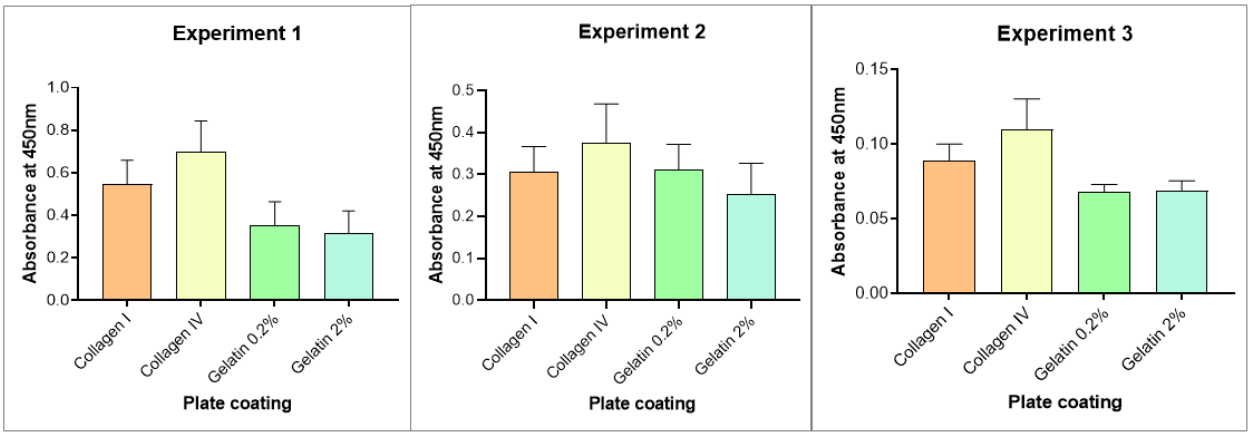

Figure 82. Mesothelial cell proliferation was greatest when cells were seeded on collagen IV. Mesothelial cells were seeded at 5,000 cells/well in 96-well plates. After 24 hours, BrdU was applied and the cells cultured for an additional 18 hours before cell fixation and analysis; plates were read at 450nm. Data are presented as mean ± SD of the absorbance values. Three different mesothelial cell populations were used, and at different passage numbers (experiment 1 at passage 3, experiment 2 at passage 2, experiment 3 at passage 4).

5.4.2 Population doubling time

To optimise the culture and experimental use of the isolated mesothelial cells, it is useful to determine their growth rate. This was achieved using a population doubling assay as described in section 5.2.5.

The experiment was performed on three separate occasions with three different mesothelial cell populations and at different passage numbers as indicated in **Figure 83**. In all three experiments, the log phase was identified between days 4 and 5, despite the varying passage numbers. The population doubling time was calculated from these cell number values. The average population doubling time of the mesothelial cells was estimated to be 25.9 hours, with a range from 17.6 to 32.8 hours.

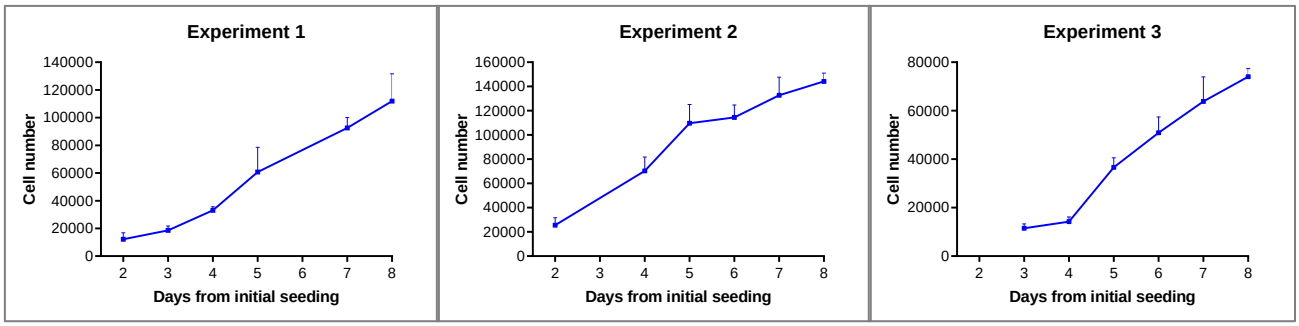

Figure 83. Mesothelial cell growth curves. Mesothelial cells were seeded at 20,000 cells/well in 24-well plates. Each day, between days 2 to 8, cells were trypsinised, pelleted, and resuspended for cell counting at the same time. Data are presented as mean ± SD. Three different mesothelial cell population were used, at different passage numbers (experiment 1 at passage 2, experiment 2 at passage 3, experiment 3 at passage 4).

5.4.3 FBS concentration in mesothelial cell complete growth media

When utilising a basic growth media such as DMEM, the concentration of FBS used is user-defined and is tailored to the cells in question. To investigate the optimum concentration of FBS for mesothelial cell culture, a cell proliferation assay was employed as described in section 5.2.6.

The experiment was performed twice on two separate populations of mesothelial cells. Compared to the proliferation in media containing 5% (v/v) FBS, there appeared to be greater mesothelial cell proliferation when cells were cultured in media containing 10% and 20% (v/v) FBS (**Figure 84**). However, there was no calculated statistical significance between them due to the low number of repeats (n=2). Based on these findings, DMEM with 20% (v/v) FBS was used for culture of isolated mesothelial cells in all experiments.

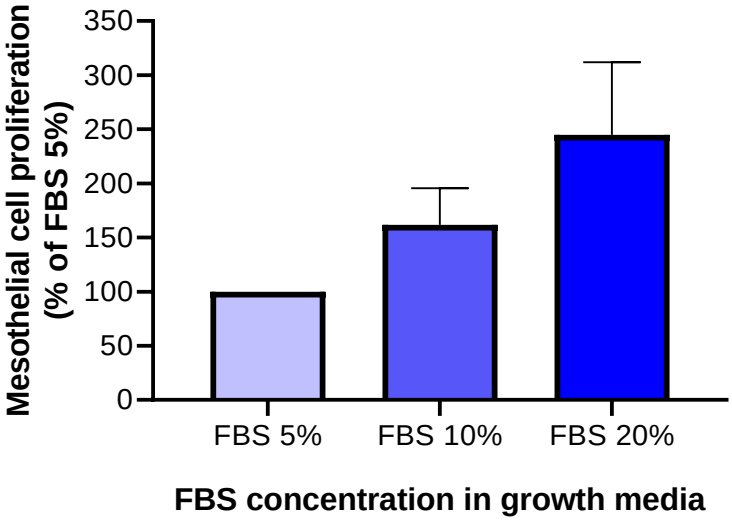

Figure 84. Enhanced mesothelial cell proliferation was observed with increased FBS concentration. Cells were seeded at 10,000 cells/well in 96-well plates and after 24 hours the culture media was replaced with media containing increasing FBS concentrations as indicated. After another 24 hours, BrdU was applied and incubated for 20 hours before cell fixation and analysis; plates were read at 450nm. Data are mean ± SD of the absorbance values (n=2).

5.4.4 Mesothelial cell seeding density

For mesothelial cells to form confluent cobblestone monolayers, they must first adhere to their growth surface, form filopodia and come into contact with neighbouring cells for active proliferation to occur.(462) Hence, at early stages, mesothelial cells appear fibroblast-like (refer to **Figure 72A**). Consequently, with low seeding density, the cell-to-cell contact is reduced and the confluent cobblestone layer does not form. It was possible that the initial isolation and culturing methods did not take seeding density into account, resulting in the occurrence of senescent-like cells or fibroblast contamination. Therefore, an experiment to determine the ideal seeding density was performed as described in section 5.2.7.

The experiment was performed at least three times with three different mesothelial populations. When mesothelial cells were grown in DMEM 10% (v/v) FBS media, they required an average of 6.5 days to achieve confluence when seeded at 2500 cells/cm^2, 4.3 days at 5000 cells/cm^2, 3.3 days at 10,000 cells/cm^2 and 2 days when seeded at 20,000 cells/cm^2 (**Figure 85A**).

At double the FBS concentration i.e. 20% (v/v), the mesothelial cells achieved confluence at least 11% quicker. A confluent monolayer was observed after 5.7 days when seeded at 2500 cells/cm^2, 3.6 days at 5000 cells/cm^2, 2.9 days at 10,000 cells/cm^2 and 1.7 days at 20,000 cells/cm^2 (**Figure 85B**).

Based on these data, mesothelial cells were seeded at least 10,000 cells/cm^2 for experiments or for population expansion, as an optimum monolayer could be achieved by day 3.

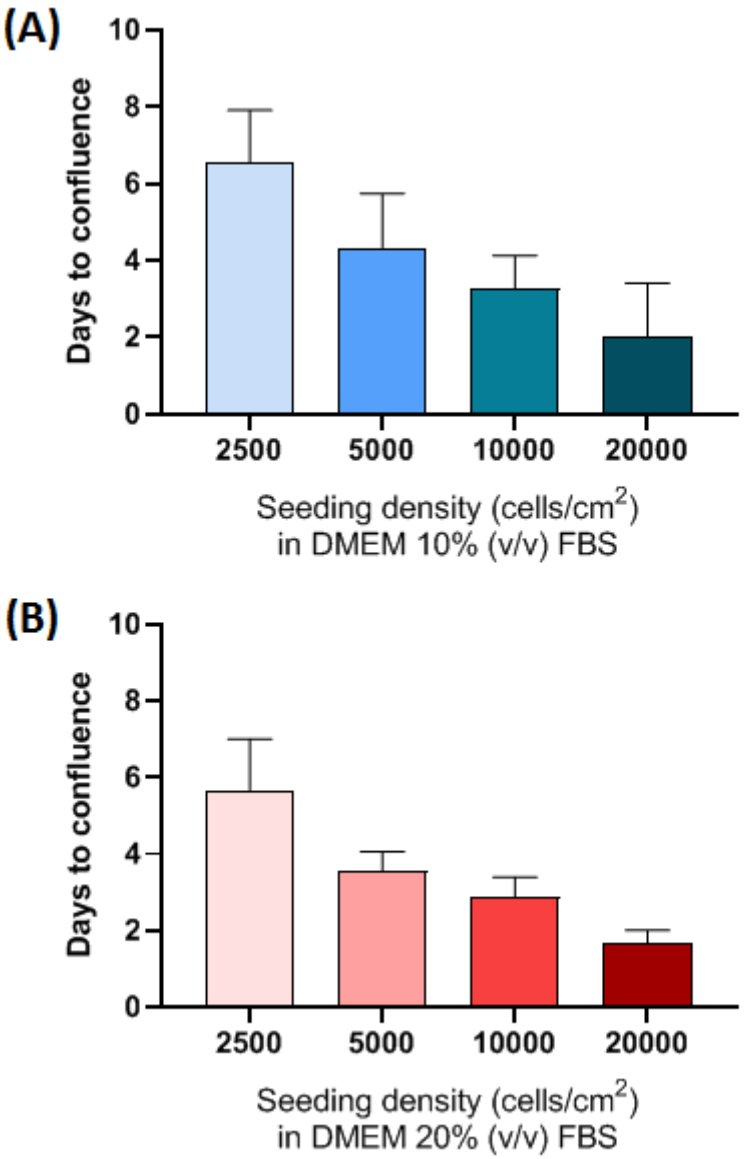

Figure 85. Determining the ideal seeding density of mesothelial cells by adjusting seeding density and FBS concentration. Cells were seeded at increasing densities, as indicated, in 24-well plates containing DMEM 10% (v/v) FBS (A) or DMEM 20% (v/v) FBS (B). Confluence was determined via phase contrast microscopy at the same time daily. Data presented as mean ± SD (n=3-4).

5.5 Discussion

5.5.1 Isolation of mesothelial cells using an enzymatic method

A method based on enzyme-digestion was successfully developed to isolate mesothelial cells from the human omentum, and was found to be more effective than the initial non-enzyme-based method. The latter relied on the shedding of the outer mesothelial cell layer through agitation but the yield was too poor for the cells to propagate.

During the enzymatic isolation procedure, the layering of the mixed cell suspension into the modified PBS solution was found to be crucial. With the foam layer at the top of the solution, introduced by agitation, the rate of the downward seepage of the mixed cell suspension was controlled; as opposed to the whole suspension falling straight through the solution when the foam layer was not present. This foam is a result of the proteinaceous BSA denaturing upon agitation to form a layer at the liquid-air interface.(470)

Freshly isolated cells were seeded into 6-well plates. From observation, if they did not form confluent cobblestone-like cultures by day 5, the plates could be safely discarded. This was because if the cell numbers were too few, cell-to-cell contact was reduced and cell growth was reduced. At the same time, the culture could be overrun by fibroblasts. In nearly half (45%) of the isolation attempts, a confluent cobblestone cell monolayer was successfully attained, which could be later passaged and expanded. If a mixed culture of both mesothelial cells and fibroblasts was obtained, the proportion of fibroblasts was assessed via phase contrast microscopy and cultures with <50% fibroblasts were processed using magnetic fibroblast depletion to obtain cultures containing pure mesothelial cells.

5.5.2 Fibroblast depletion using magnetic beads

a) Anti-fibroblast magnetic bead specificity

After fibroblast depletion using magnetic bead technology, the culture of the non-magnetised portion resulted in cobblestone monolayer suggestive of mesothelial cells, while the culture of the magnetised portion showed a mix of fibroblastoid and cobblestone appearance. This suggested that the anti-fibroblast beads have increased affinity for fibroblasts, but were not specific to fibroblasts alone since the mesothelial cells appeared to bind to the beads. From the product description, the magnetic anti-fibroblast beads were “based on a fibroblast-specific antigen.” An enquiry to the manufacturer did not reveal the specific marker recognised by the anti-fibroblast beads (proprietary information), but the product website pointed towards references for D7-Fib and CD271.(471) Both D7-Fib and CD271 were previously studied in fibroblasts of various origins, but not studied in mesothelial cells. It is possible that mesothelial cells may contain these markers; detection via immunocytochemistry or flow cytometry could have been performed to determine this. Additionally, CD271 is present in mesenchymal stromal cells, which are precursors of diverse differentiated tissues including adipose tissue,(472) and thus may be a mutual mesenchymal marker for both the omental fibroblasts and mesothelial cells.

b) Second fibroblast depletion procedure

Further purification of the mesothelial cells (in the mixed magnetised fraction of section 5.3.4) by a second magnetic fibroblast depletion procedure resulted in increased numbers of senescent-like cells. A possible explanation might be that at this point, the cells would have been subjected to multiple passaging – twice for fibroblast depletion and once for culture expansion. A recent critical review reported that at higher passage numbers, the cell cycle elongates and cell proliferation declines leading to cell senescence,(446) which may be the case in the present study. Hence, subjecting the isolated primary cells to multiple depletion procedures to purify cell yield was not suitable, as the cells would be of a higher passage number and no longer suitable for experiments.

Further discussion on cell senescence is elaborated in section 5.5.4.

c) Fibroblast depletion during mesothelial cell isolation

An alternative to performing the magnetic fibroblast depletion twice, was to perform the procedure at the point of cell isolation from the tissue. This would reduce unnecessary passaging and potentially yield a purer mesothelial cell population at passage 0 itself. The protocol also saved time as the twice-layering steps were omitted and the purity of the mesothelial cell yield was similar to when the procedure was performed at later passages post-tissue isolation.

In practical terms, however, incorporating the fibroblast depletion step into the isolation protocol was technically challenging. This was because both the mesothelial cell and HOMEC isolation protocols needed to be performed concurrently, since collagenase type II digestion step was a shared early processing step, and within 24 hours of tissue collection to retain cell viability. Presently, the enzymatic method of mesothelial cell isolation (described in section 5.3.2) has a success rate of 45%. Since fibroblast depletion at the point of isolation did not improve the overall success rate of achieving a pure mesothelial culture and it was impractical, it was not routinely adopted.

5.5.3 Mesothelial cell characterisation via immunocytochemistry

Confirmation of mesothelial cell identity was performed via immunocytochemistry. Since fibroblasts were a major contaminant and the mesothelial cell isolation procedure incorporated the initial step of HOMEC isolation, a combination of primary antibodies was utilised to differentiate between the three cell types, i.e. the anti-vimentin and anti-cytokeratin-18 (to distinguish between mesothelial cells and fibroblasts), and anti-CD31 and anti-vWF (to distinguish mesothelial cells and HOMECs).

The mesothelial cells from different omental samples variously stained positive or negative for vWF. However, even when present, vWF was observed to be less abundant than that found in HOMECs. Due to this observation, which has been previously reported,(451, 473) vWF is not a reliable marker to differentiate between mesothelial cells and ECs. Hence, as a minimum, the three antibodies – vimentin, cytokeratin-18 and CD31 – were used to differentiate mesothelial

cells from fibroblasts and ECs. Overall, the enzymatic isolation and the fibroblast depletion procedures were successful in yielding pure populations of mesothelial cells.

5.5.4 Optimal growth conditions for mesothelial cells

With the establishment of the mesothelial cell isolation protocol, confirmed by immunocytochemistry, the next step was to optimise the growth conditions of the cells. Coating of lab cultureware was performed to mimic the basement membrane in vivo. As assessed by BrdU assay, the collagen I and collagen IV coated surfaces showed greater cell proliferation compared with the gelatin 0.2% and 2% (v/v) surfaces. Collagen IV was shown to be the best coating for mesothelial cell proliferation. This is likely to be because the collagen family most closely resembles the in vivo basement membrane. Being of human origin, the isolated mesothelial cells may possess higher affinity for the collagen IV than collagen I, as the collagen IV was derived from human placenta, while the latter from rat's tail.

When comparing growth in media containing FBS 10% (v/v) and 20% (v/v), confluence was achieved slightly quicker at the higher FBS concentration. This was expected, as a higher concentration of serum contains a higher concentration of growth factors, which in turn supports cell growth.

When investigating the mesothelial cell seeding density, confluence within a well was achieved quicker with a higher seeding density. Doubling the seeding density reduced the time to achieve confluence by a day. At a higher density, cell-to-cell contact is greater which enhances proliferation via contact-mediated signalling.(462, 474) This can be seen from the projection of filopodia on the mesothelial cells which form contacts with neighbouring cells. Conversely, when mesothelial cells were seeded at a low density, cell-to-cell contact was minimal and the cells were less likely to form a confluent monolayer and eventually senesced or died. This suggests that mesothelial cell proliferation is dependent on the physical interaction between the cells i.e. juxtacrine signalling, rather than a secreted factor through paracrine signalling. Possible interactions between the cells may activate proliferative pathways including the

phosphatidylinositol 3-kinase pathway implicated in ECs,(474) or connexin gap junction proteins implicated in mesothelioma or osteosarcoma.(475, 476) Using receptor/pathway inhibitors, further experiments could be performed to investigate the mechanisms by which physical interactions between the mesothelial cells leads to their proliferation.

Another advantage of seeding the mesothelial cells at high density is to reduce the risk of senescence. With greater cell-to-cell contact, a phenomenon termed 'contact inhibition' occurs where the cells experience cell cycle arrest. It has been proposed that contact inhibition inhibits the mammalian target of rapamycin (mTOR) pathway within cells. Since mTOR activation is involved in converting the cell cycle arrest into the irreversible senescence state, mTOR inhibition might decrease senescence.(477) Additionally, the high density of cells is able to inhibit mTOR by exhausting essential growth factors within the medium.(478)

The results of the cell seeding density experiment may also explain the observation of senescent-like cells in cultures from post-fibroblast depletion (sections 5.3.3 and 5.3.4). Loss of cells during the procedure, because some mesothelial cells bind to the magnetic beads and were eliminated, may have resulted in low seeding densities post-procedure. To improve, a cell counting step could be incorporated post-fibroblast depletion to ensure that the cells were seeded at the prescribed minimum density of 10,000 cells/cm^2.

A common approach to cell senescence is the Hayflick limit, wherein cell division occurs for a finite number of times before entering the senescent phase.(447) This limit was related to the number of cell division and not the duration of time in culture, since previously frozen cells retained their 'memory' of the number of times they have divided previously.(447) For the omental mesothelial cells, the Hayflick limit is yet unknown and the mesothelial cells were utilised for experiments up to passage 5 only. Future work may determine what is the maximum number of cell doublings or passaging in these primary cells before senescent-like cells are detected. Additionally, markers to differentiate senescent from non-senescent cells, such as senescence-associated beta-galactosidase (SA-β-gal) and ribosomal protein S6 (RPS6),(478) may be utilised.

In the present study, the mesothelial cell population doubling time was found to be nearly 26 hours based on three different mesothelial cell populations. As a comparison, the doubling time of murine mesothelial cells ranged from 18 to 40 hours.(479-481) However, there were limited past studies informing the doubling time of human mesothelial cells. One study mentioned that their omental mesothelial cell doubling time ranged from 4 to 6 days when cultured in media also containing FBS 20% (v/v),(451) but the growth media (M199 media) was different than that used in the present experiment, which may explain the disparity in doubling time. Furthermore, the method of doubling time calculation may be different; it was possible that the previous study's calculation was not performed during the log phase of cell growth, but was based on a general cell count after a defined period of days. Using the present cell count data, the interval of days between the cell number on the final day of the experiment and its half value was approximately 3 to 4 days, closely resembling that obtained in the previous study.

5.6 Chapter conclusion

In conclusion, a protocol to obtain pure cultures of mesothelial cells from human omental tissue was successfully developed using an enzyme-based digestion protocol. This protocol did not routinely include fibroblast depletion, but this was utilised using magnetic bead technology when fibroblast contamination in the initial isolate was less than 50% coverage. Both approaches generated a pure population of mesothelial cells (<95%) with a low enough passage number for experimental use. In experiments, mesothelial cells were only utilised up to passage 5 due to the higher occurrence of senescent-like cells at higher passage numbers.

Additionally, these studies identified optimum growth conditions for the isolated mesothelial cells for subsequent routine culture. Specifically, (i) all cell cultureware was pre-coated with collagen IV, (ii) the seeding density was maintained at least 10,000 cells/cm^2 for routine passage or for experiments, to generate confluent monolayer in two to three days and reduce the risk of senescent-like cells, and (iii) cells were maintained with DMEM 20% FBS throughout the isolation procedure and during culture.

This cell isolation and culture protocol was then followed to carry out further experimental studies examining the role of omental mesothelial cells in metastasis of EOC cells to the omentum (chapter 6).

Chapter 6. An investigation into whether factors secreted from omental adipocytes, mesothelial cells or ovarian cancer cells impact adhesion of ovarian cancer cells onto the mesothelial cell monolayer

6.1 Introduction

During metastasis of ovarian cancer to the omentum, cancer cells dislodge from the primary tumour and are transported via the peritoneal fluid to reach the omentum. The mesothelial layer on the omental surface is the first point of contact for the invading cancer cells, and the adhesion of the cancer cells to the mesothelial layer is thought to mediated by factors secreted by various cells in the omental microenvironment. Expectedly, most studies have focused on the role of cancer cells and mesothelial cells.

Many studies examined cancer cells and their secreted factors which contribute to their metastatic potential within the abdomen (previously discussed in section 1.6.5). For example, ovarian and colorectal cancer cells secrete factors such as such as TGF-β and IL-1β to stimulate the transition of mesothelial cells to a phenotype more receptive towards cancer cell invasion.(254, 273, 482, 483) Additionally, TGF-β can stimulate mesothelial cells to secrete fibronectin, an ECM component, that the cancer cells can adhere to as part of the invasion process.(263) IL-1β was also discovered to upregulate adhesion molecules, e.g. ICAM-1 and VCAM-1, on rat mesothelial cells which aids the adhesion of metastatic colon cancer cells.(254)

As for the role of mesothelial cells in cancer invasion, mesothelial cells synthesise molecules such as CXCL12 and hyaluronan which can bind to their corresponding receptors, CXCR4 and CD44 respectively, on the ovarian cancer cells.(144, 264) These interactions were postulated to be the first step in cancer invasion. The fibronectin secreted by mesothelial cells also renders the mesothelial cell layer more susceptible to physical clearance by the invading ovarian cancer cells.(271)

However, the role of omental secreted adipokines in facilitating ovarian cancer cells adhesion to the outer mesothelial cell layer of the omentum has not been widely studied. Adipocytes, a major component of omental adipose tissue, have

been previously shown provide an energy source to the growing cancer in the form of fatty acids. They also secrete a wide range of factors which allow the cancer cells to thrive, e.g. by supporting the EMT process during cancer dissemination, by acting as a chemoattractant for the homing of cancer cells towards the omentum, or by inducing chemoresistant mechanisms within the cancer cells (these and more were discussed in section 1.5).

Since the omentum is a major secondary site for EOC it is possible that these secreted factors may play a role in the metastatic process. Therefore, this chapter will examine, using relevant human cell types, the effect of various CM (collected from ovarian cancer cells, omental adipose tissue and omental mesothelial cells themselves) on the adhesion of ovarian cancer cells onto the mesothelial cell monolayer. SKOV3 cells, an ovarian cancer cell line originally derived from ascites, were utilised in the following experiments. Due to their ascitic origin, SKOV3 cells represent metastatic cancer which has exfoliated from the primary tumour, and are thus suited for investigating cancer cell adhesion onto the omental mesothelial cells.

Thus, the specific aims of this chapter are to:

a) develop a reliable method to assess the adhesion of ovarian cancer cells onto the mesothelial cell layer which closely resembles in vivo conditions (sections 6.3.1 to 6.3.5);
b) investigate the effect of adipose tissue CM (plus ovarian cancer cell and mesothelial cell CM for comparison) on the adhesion of ovarian cancer cells to the mesothelium (section 6.3.6); and
c) visualise the ovarian cancer cell adhesion onto the mesothelial cell layer via immunocytochemistry (section 6.3.7).

6.2 General methods

6.2.1 Culture and seeding of omental mesothelial cells

Mesothelial cells were isolated from omental tissue samples, as described in section 2.5. For experiments, the mesothelial cells were seeded at 30,000 cells/well in 24-well plates coated with collagen IV. The cultures were maintained in DMEM 20% FBS (v/v) and fed every 2 to 3 days until they reached confluence, as determined by phase contrast microscopy.

6.2.2 Labelling SKOV3 cells with calcein-AM

SKOV3 cells were labelled with calcein-AM to allow assessment of their adherence to the mesothelial cells. The calcein-AM dye fluoresces green under fluorescent microscopy which allows both manual counting of the cells and fluorescence spectrophotometry.

Trypsinised SKOV3 cells were suspended in DMEM/F12 with 10% (v/v) FBS and calcein-AM added to a concentration of 1µM; equivalent to 1:2000 (v/v) dilution of stock, i.e. 1µL of 2mM calcein-AM in 2mL of media. The cell suspension was placed on a rotary mixer at 20 rpm for 20 minutes at 37°C to allow the calcein-AM dye to enter the SKOV3 cells. The cells were then centrifuged at 200*g* for 5 minutes, and supernatant aspirated to remove excess calcein-AM solution. The labelled SKOV3 cells were suspended in treatment media, as indicated in later sections, ready for use in experiments.

6.2.3 SKOV3 adhesion onto mesothelial cell layer (preliminary protocol)

Calcein-AM-labelled SKOV3 cells (section 6.2.2) were suspended in media (media type indicated in later sections), applied onto mesothelial cells (cell numbers indicated in later sections) and incubated at 37°C/5% CO_2. After the indicated duration of incubation, unadhered SKOV3 cells were removed by washing with warmed PBS or mesothelial cell growth media. Wells were filled with 500µL of PBS before being analysed by fluorescence spectrophotometry or fluorescence microscopy. Each experimental condition was conducted in

triplicate as a minimum (intra-experimental n ≥ 3), and experiments were conducted at least 3 times unless otherwise noted (n ≥ 3).

6.2.4 Fluorescence spectrophotometry

Prior to fluorescence reading, the wells were filled with PBS (section 6.2.3) since mesothelial cell growth media contains phenol red which may increase background fluorescence (484) and thus, affect subsequent fluorescence measurements.

On the fluorescence spectrophotometer, the excitation/emission wavelength was set to 495/515nm, as recommended by the manufacturer of calcein-AM. The readings were expressed as relative fluorescence units (RFU).

6.2.5 Quantification of labelled SKOV3 cells using images from fluorescence microscopy

After washing off the unadhered SKOV3 cells (in section 6.2.3), the plates were imaged on the green channel of a fluorescence microscope. **Figure 86** depicts the location of the imaged areas in each well. For standardisation during imaging, the regions of interest comprised of a straight line from centre to the edge of the well. The labelled SKOV3 cells appeared green in the images (**Figure 87**); cells were counted manually and averaged across all images from the same well.

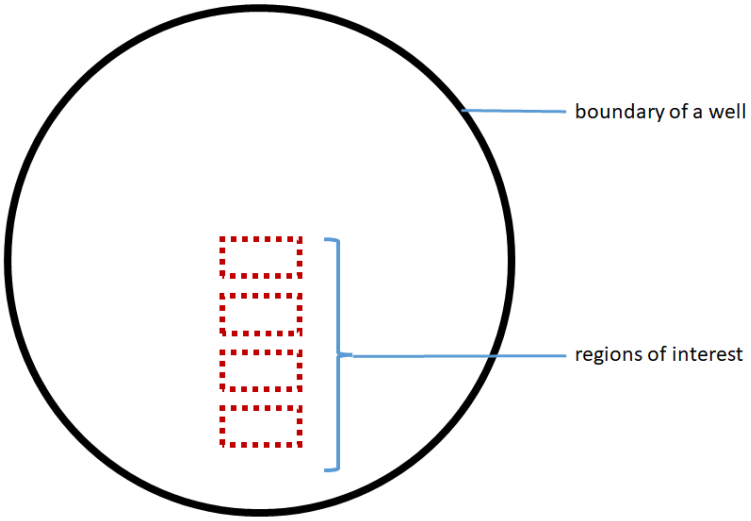

Figure 86. Location of the imaged areas (regions of interest) in each well of a 24-well plate. Each well was imaged using the green channel of the EVOS Fluo microscope at 10x magnification.

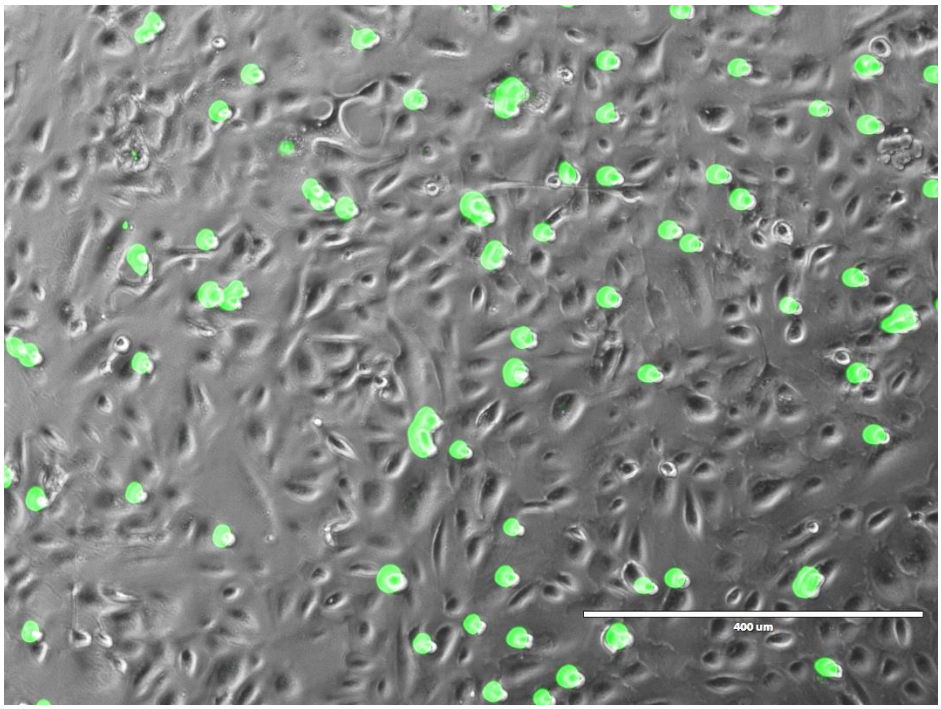

Figure 87. Calcein-AM-labelled SKOV3 cells adhere onto a layer of mesothelial cells. Representative image depicts SKOV3 cells adhered to mesothelial cells when treated with adipose tissue CM. Mesothelial cells were seeded at 30,000 cells/well on a 24-well plate and grown to confluence. Labelled SKOV3 cells suspended in treatment media were applied onto the mesothelial cells (20,000 cells/500µL/well) for 24 hours and the wells washed with mesothelial cell growth media to remove any unadhered SKOV3 before imaging with EVOS Fluo at 10x magnification. Scale bar 400µm.

6.2.6 Calculation of fluid shear stress

To simulate peritoneal fluid flow conditions, the 24-well plates containing mesothelial cells and labelled SKOV3 cells are placed on a see-saw rocker. The settings of the rocker were derived from a formula by Zhou et al (2010).(485) The formula calculates the fluid shear stress in the centre of a circular well and is given as follows.

$$\tau = \frac{\pi\mu\theta}{2\delta^2 T}$$

where τ is the shear stress (dyn/cm^2) in the centre of the well

μ is fluid viscosity (Pa.s)

θ is the angle of tilt (°)

δ is the ratio of media depth to the well diameter, i.e. height/diameter

T is the time (s) to complete one oscillation on the see-saw rocker

Fluid viscosity (μ) was set to 0.001 Pa.s, which is the viscosity of water since the treatment media is >90% water, and was also the value set in Zhou et al (2010).(485) The angle of tilt (θ) was given in the product specification of the Stuart see-saw rocker (model SSL4) as 7°.

The product specification of the Corning Costar® 24-well plate were considered in calculating the ratio of media depth to diameter (δ). The diameter of each well was given as 1.56cm, and the bottom surface area as 1.9cm^2. With a media volume of 500µL (or 0.5cm^3), the media height was calculated as 0.263cm (0.5 / 1.9). Hence, δ was fixed at 0.169 (0.263 / 1.56) with 500µL of media per well.

Experimentally, the only amendable parameter is the oscillation time (T), which is inversely proportional to the fluid shear stress (τ). This parameter was adjustable via the rocker's oscillations per minute (osc/min) setting, where osc/min = 60 / T.

There is variation in the physiological shear stress values within the peritoneum; proposed values ranged between <0.1 to 11 dyn/cm^2 ,(486-488) or even lower

at 0.002 to 0.02 dyn/cm^2.(140) In the present study, the target shear stress value was set at or near to 0.05 dyn/cm^2, which translates to a setting of 30 osc/min on the see-saw rocker. The chosen target shear stress value was also due to the technical limitation of the rocker. For example, to obtain 0.1 dyn/cm^2 in the present experimental set up, the rocker oscillation must be set to its maximum setting of 70 osc/min, which would cause the media within the wells to splash onto the lid of the plate. However, the experimental conditions used were able to recreate the very low shear stress values reported for the peritoneal fluid and so recreated the physiological conditions more effectively compared to other studies using a static system, e.g. previously reported by Kenny et al (2014),(263) Sandoval et al (2013),(273) and Kenny et al (2007).(468)

The shear stress values were extrapolated from the example given in Zhou et al (2010): 1500µL of media within a dish of 0.35cm diameter (media height 0.156cm, δ = 0.0446) rocked at a 5.1° angle at 1 oscillation per second is equivalent to 0.70 dyn/cm^2. Correspondingly with the current setup, 500µL of media in a 1.56cm diameter well (media height 0.263cm, δ = 0.169) rocked at 7° at 1 oscillation per 2 seconds (osc/min = 30) results in a fluid shear stress of 0.0426 dyn/cm^2.

6.2.7 Assessing SKOV3 adhesion onto a mesothelial cell layer by manual counting (final protocol)

Mesothelial cells were seeded in standard clear 24-well plates, as described in section 6.2.1. Labelled SKOV3 cells (section 6.2.2) were suspended in treatment media which consisted of various conditioned media (control CM, SKOV3 CM, mesothelial cell CM, or adipose tissue CM) diluted 1:1 (v/v) with basal media and supplemented with 10% (v/v) FBS.

Media from the mesothelial cells were aspirated and exchanged with the labelled SKOV3 suspended in the equivalent conditioned media as above; SKOV3 cells were seeded at 20,000 cells/ 500µL/ well. For wells designated as blanks, fresh mesothelial growth media (DMEM 20% (v/v) FBS) was replaced without the SKOV3 cells. Plates were incubated for 24 hours or 48 hours at

37°C/5% CO_2 on a see-saw rocker set to 30 osc/min. Each experimental condition was conducted in quadruplicate (intra-experimental n ≥ 4).

Plates were then removed from the rocker and the wells were rinsed with warmed DMEM 20% (v/v) FBS before cell fixation with 4% paraformaldehyde (w/v, 300µL/well) for 20 minutes at room temperature. The wells were rinsed 4 times with PBS, filled with 500µL/well PBS, and imaged at 4x magnification with the green channel of the EVOS Fluo microscope (described in section 6.2.5). The settings on the green channel of the microscope were standardised throughout the experiments for all images captured. During image capture, intensity was set to 90% with 250 millisecond exposure time; while during image adjustment, the brightness was set to 90% and the contrast at 95%.

SKOV3 adhesion onto the mesothelial cells, i.e. areas marked by the green colour of the calcein-AM, was measured on ImageJ and expressed as square pixels (Image > Adjust > Color Threshold > Hue: 0-255, Saturation: 0-255, Brightness 7-14). The values obtained from the background wells were averaged and subtracted from all the other wells, to give the net area of adhered SKOV3 cells.

6.2.8 Immunocytochemistry

Mesothelial cells and the adhered SKOV3 cells in 24-well plates were subjected to immunocytochemistry as described in section 2.9.

6.3 Results

An initial series of developmental studies were carried out to establish an experimental methodology that could accurately and reproducibly assess adhesion of ovarian cancer cells to a mesothelial monolayer. It was initially intended that adhered cancer cells would be quantified by fluorescence spectrophotometry and thus preliminary studies were carried out to validate this approach, specifically to determine (a) if fluorescence intensity correlated with number of fluorescently labelled cells measured, (b) optimum type of multiwell plate required to reduce any background fluorescence.

6.3.1 Determination of fluorescence with different seeding densities of labelled SKOV3 and different types of 24-well plates

To assess if fluorescence readings correlate with labelled SKOV3 cell numbers, mesothelial cells were first seeded in 24-well plates as described in section 6.2.1. Both clear- and black-coloured wall plates were utilised. SKOV3 cells were labelled with calcein-AM as described in section 6.2.2, then suspended in basal media containing FBS 10% (v/v) and added onto mesothelial cells at various seeding densities as indicated. The plates were analysed by fluorescence spectrophotometry, described in section 6.2.4.

The fluorescence readings are shown in **Figure 88**. Fluorescence readings in the clear- and black-walled plates were comparable. The fluorescence readings were proportional to the seeding density of the SKOV3 cells: specifically, the greater the seeding density, the greater the fluorescence reading. However, wells containing only mesothelial cells without the fluorescently labelled SKOV3 (i.e. background wells) also generated low fluorescence readings, which suggested that mesothelial cells autofluoresce at the spectrophotometer settings used (495/515nm).

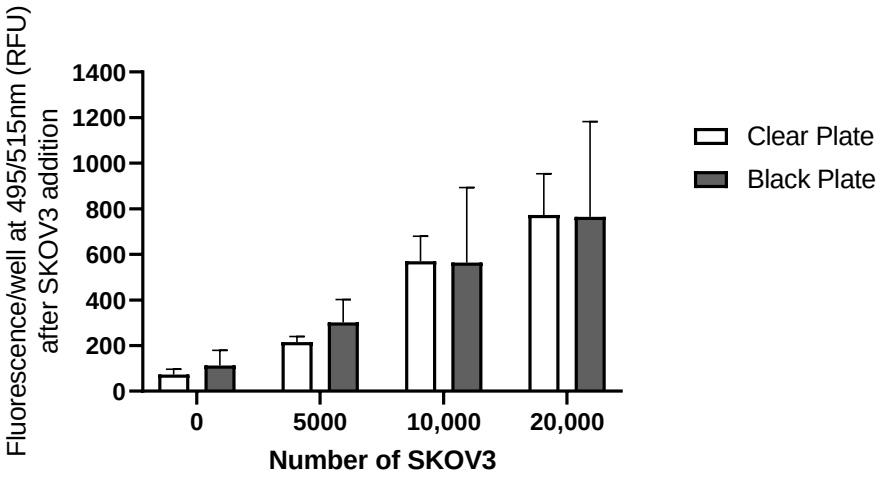

Figure 88. The fluorescence per well was similar in both clear and black plates when measured after SKOV3 addition. Mesothelial cells were seeded at 30,000 cells/well on clear and black 24-well plates and grown to confluence. Calcein-AM-labelled SKOV3 cells were suspended in basal media + 10% (v/v) FBS and applied to mesothelial cells at increasing densities (0 to 20,000 SKOV3/ 500µL/ well). Wells with zero SKOV3 cells contained mesothelial cells only. Plates were analysed by fluorescence spectrophotometry at 495/515nm before 24-hour incubation. Data presented as mean ± SD of replicates from one experiment.

6.3.2 Seeding density of SKOV3 and their adhesion to mesothelial cells as visualised by fluorescence microscopy

The data presented above indicate that the fluorescence readings generated reflected the number of SKOV3 cells seeded. Thus, a further validation study was performed to determine visually if SKOV3 adhesion onto the mesothelial cell monolayer was affected by the seeding density of SKOV3 and if cells remained attached after washing.

Mesothelial cells were seeded as described in section 6.2.1. Labelled SKOV3 cells (section 6.2.2) were suspended in basal media containing FBS 10% (v/v). As described in section 6.2.3, the suspension was added onto mesothelial cells at various seeding densities as indicated, incubated for 24 hours and the unadhered SKOV3 cells removed by rinsing with mesothelial cell growth media

to mimic experimental conditions. The wells were imaged using fluorescence microscopy and sample images are shown in **Figure 89**.

The number of SKOV3 cells adhering to the mesothelial cell layer increased with increasing number of applied cells. This indicated that cancer cells remain adhered to the mesothelial layer after washing, and this was reflected by increased fluorescence.

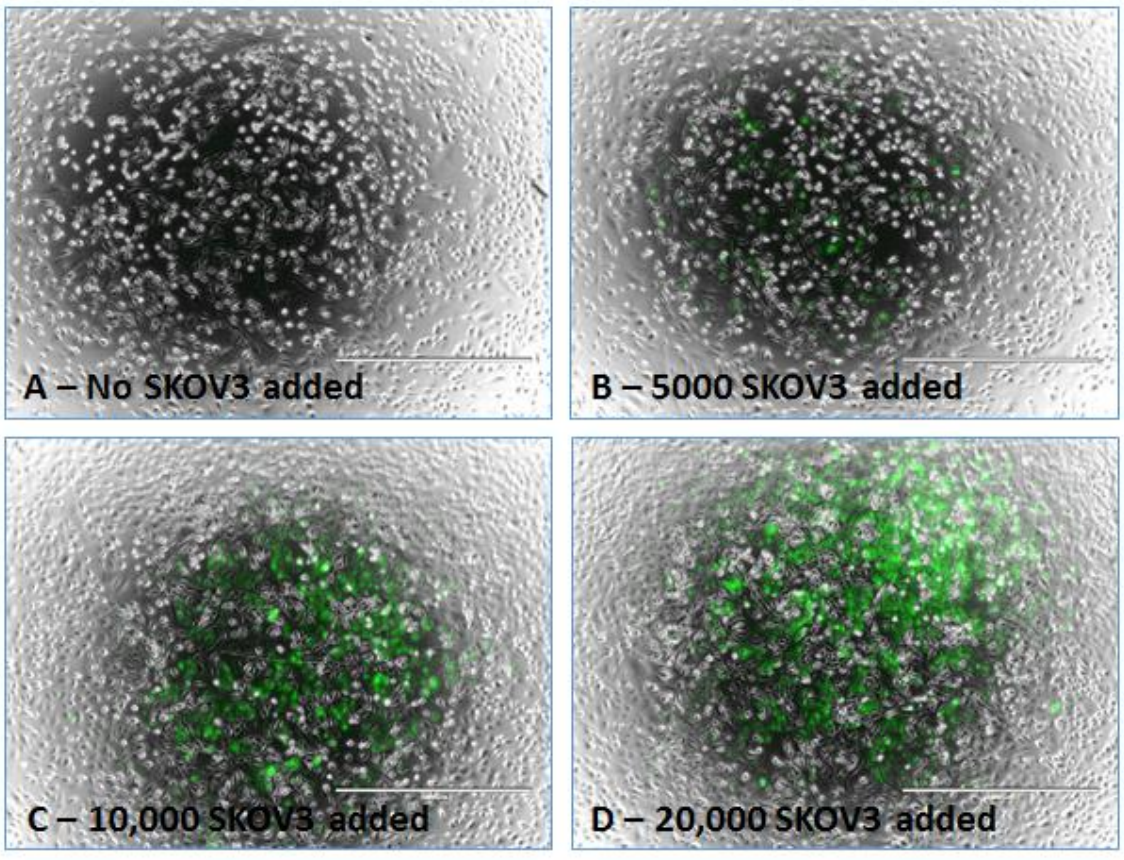

Figure 89. The greater the numbers of SKOV3 added, the greater the area of adhesion onto mesothelial cells. Mesothelial cells were seeded at 30,000 cells/well in 24-well plates and grown to confluence. Calcein-AM-labelled SKOV3 cells were suspended in basal media + 10% (v/v) FBS and applied to mesothelial cells at increasing densities (0-20,000 SKOV3/ 500µL/ well). Unadhered SKOV3 cells were removed by washing after 24 hours. Each well was then imaged by fluorescence microscopy using the green and transmitted light channels. Representative images, captured at 4x magnification using EVOS Fluo, depict SKOV3 adhesion (green colour) after washing post-24-hour incubation (A: background/ no SKOV3 added, B: 5000 SKOV3, C: 10,000 SKOV3, D: 20,000 SKOV3; n=1. Scale bar 1000µm.

6.3.3 Comparing fluorescence readings and manual counting of adhered SKOV3 cells

The results described in sections 6.3.1 and 6.3.2 suggest that fluorescence spectrophotometry can be used to reliably assess attachment of fluorescently labelled cancer cells. This approached was finally validated by comparing data obtained by measured fluorescence values with manual counting of the number of adhered SKOV3 cells.

Mesothelial cells were seeded as described in section 6.2.1. As pre-treatment of mesothelial cells, the media was exchanged with basal media (control) or adipose tissue CM (500µL/well) and incubated overnight. Labelled SKOV3 cells (section 6.2.2) were suspended in basal media or adipose tissue CM, added onto their respective pre-treated mesothelial cells at 10,000 cells/well and incubated for 6 hours; unadhered SKOV3 cells were removed by rinsing with PBS (described in section 6.2.3). The plates were subjected to fluorescence spectrophotometry (section 6.2.4), followed by fluorescence microscopy at 10x magnification with 7 images captured per well (section 6.2.5).

Overnight treatment with adipose tissue CM did not affect mesothelial cell phenotype, as examined by phase contrast microscopy (**Figure 90**) and also by immunocytochemistry (later described in section 6.3.7). However, there was a marked difference in the SKOV3 adhesion data obtained using the two assessment methods (**Figure 91**). The adipose tissue CM treatment induced a three-fold increase in SKOV3 adhesion compared with control based on fluorescence readings, but this increase was not reflected in the cell counting results.

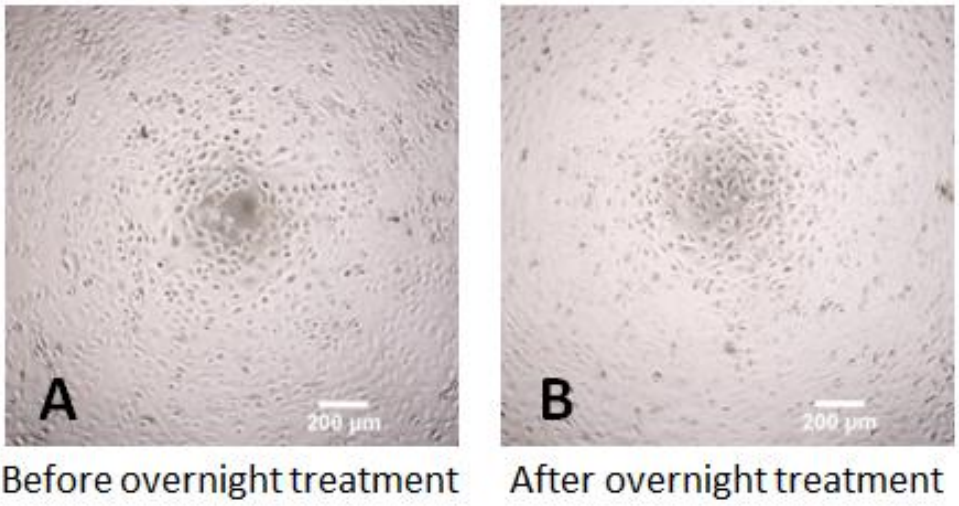

Figure 90. Overnight treatment with adipose tissue conditioned media did not alter mesothelial cell phenotype. Mesothelial cells were seeded at 30,000 cells/well on a 24-well plate and grown to confluence. Adipose tissue conditioned media were applied overnight. Representative images, captured at 4x magnification using EVOS XL Core, show cells prior to treatment (A) and after overnight treatment (B). Scale bar 200µm.

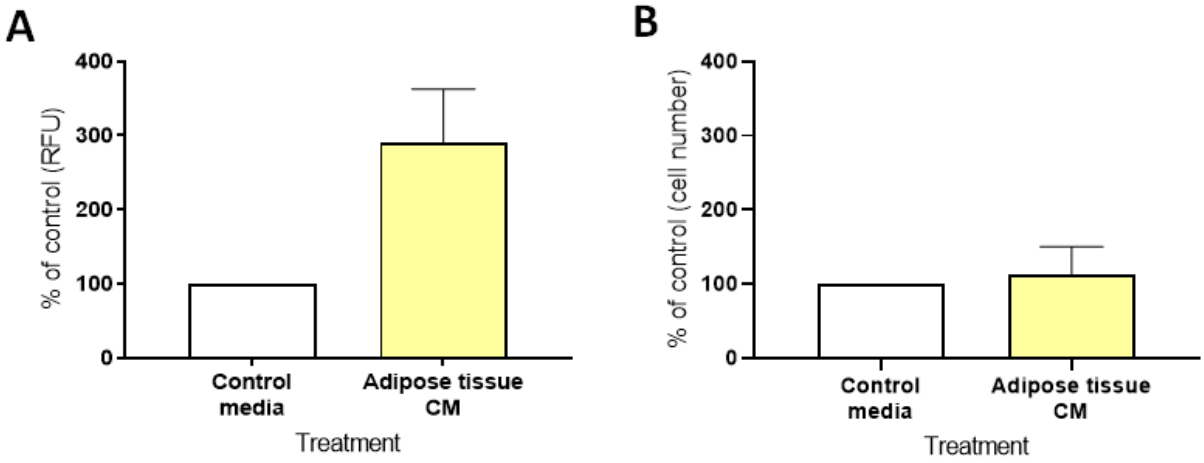

Figure 91. Adherence of SKOV3 onto mesothelial cells was dissimilar when determined by fluorescence emission (A) or manual cell count (B). Mesothelial cells were seeded at 30,000 cells/well on a 24-well plate, grown to confluence and treated with basal media (control) or adipose tissue CM overnight. Fluorescently-labelled SKOV3 cells were applied for 6 hours before washing off unattached cells with PBS. The plates were subjected to fluorescence spectrophotometry; then imaged using the green channel of a fluorescence microscope and the adhered SKOV3 calculated. Data are presented as mean ± SD of replicates from one experiment and expressed as a percentage of control media. CM: conditioned media.

6.3.4 Fluorescence spectrophotometry of blank 24-well plates

The inconsistency in the fluorescence readings and manual cell counts (section 6.3.3) suggested issues with fluorescence spectrophotometry. It has already been shown that the mesothelial cells autofluoresced in the absence of labelled SKOV3 cells (section 6.3.1), thus any background fluorescence generated by the liquid in the wells or by the plates themselves was investigated.

The 24-well plates were pre-coated with collagen IV, but not seeded with mesothelial cells (left blank). The wells were filled (500µL/well) with PBS, SKOV3 growth media, basal media with 10% (v/v) FBS or left dry (no media). The plates were then subjected to fluorescence spectrophotometry (described in section 6.2.4) prior to and after overnight incubation at 37°C/5% CO_2.

A wide range of background fluorescent values were obtained with the different conditions. The standard clear-walled plates showed higher variability between the individual wells, as depicted by their larger standard deviation values, compared with the black plates (**Figure 92**). Furthermore, the different media type used in each well resulted in different readings, even though the volume was consistent in all wells (500µL/well). The results suggested that the plates and media themselves contribute to variability in fluorescence readings.

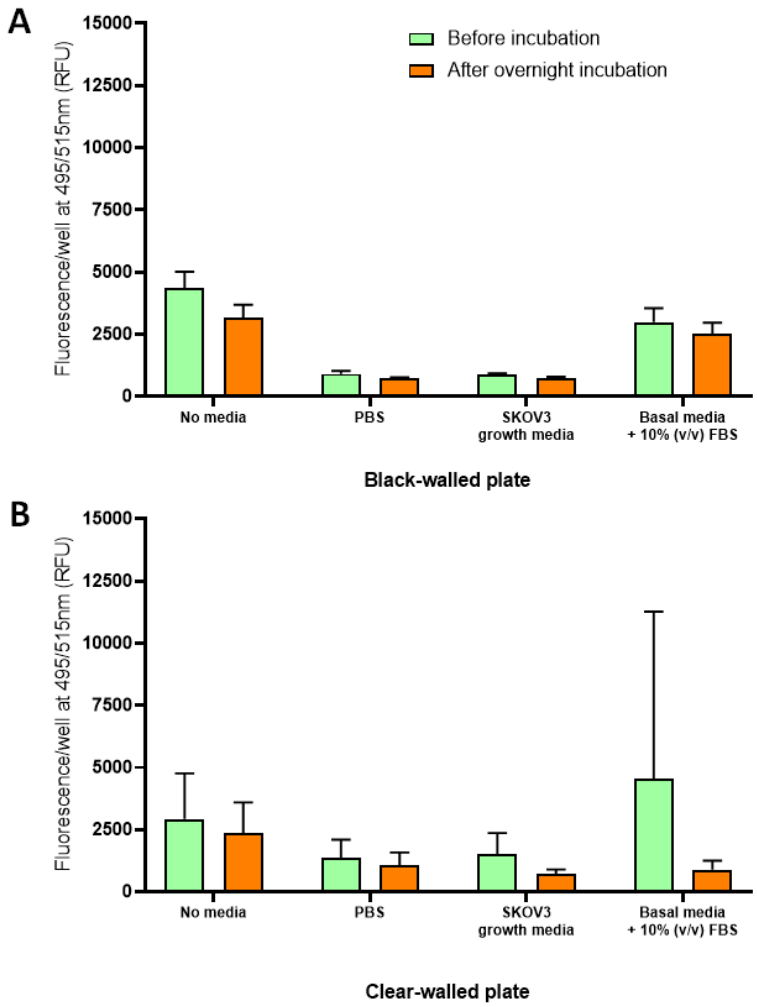

Figure 92. Fluorescence spectrophotometry of blank black-walled and clear-walled plates demonstrated erratic readings. Collagen IV-coated black (A) or clear (B) 24-well plates were filled with various media (500µL/well). The plates were subjected to fluorescence spectrophotometry at 495/515nm before and after overnight incubation. Data presented as mean ± SD of replicates from one experiment.

6.3.5 Seeding density of SKOV3 and their adhesion to mesothelial cells as assessed by fluorescence spectrophotometry

The previous data suggest that background fluorescence may generate unreliable data when using fluorescence spectrophotometry to assess SKOV3 cell adhesion. However, the results presented in section 6.3.1 did show that fluorescence readings were proportional to fluorescent cell number which suggests that this methodology is reliable. Therefore, one final validation study

was performed to assess the ability of fluorescence spectrophotometry to measure the increasing number of adhered fluorescently labelled cells remaining after washing, when cells were seeded at increasing densities (previously assessed visually, with no quantification, in section 6.3.2).

Mesothelial cells were seeded in clear- and black-coloured 24-well plates (described in section 6.2.1). SKOV3 cells were labelled with calcein-AM (section 6.2.2) and suspended in basal media containing FBS 10% (v/v) and added onto mesothelial cells at various seeding densities as indicated. After 24 hours of incubation, unadhered SKOV3 cells were removed (section 6.2.3) and the plates analysed by fluorescence spectrophotometry (section 6.2.4).

The results are shown in **Figure 93**. Fluorescence readings in the clear- and black-walled plates were comparable. Similar to **Figure 88**, the background wells (containing only mesothelial cells without the labelled SKOV3 cells) generated fluorescence readings which inferred the autofluorescence property of mesothelial cells.

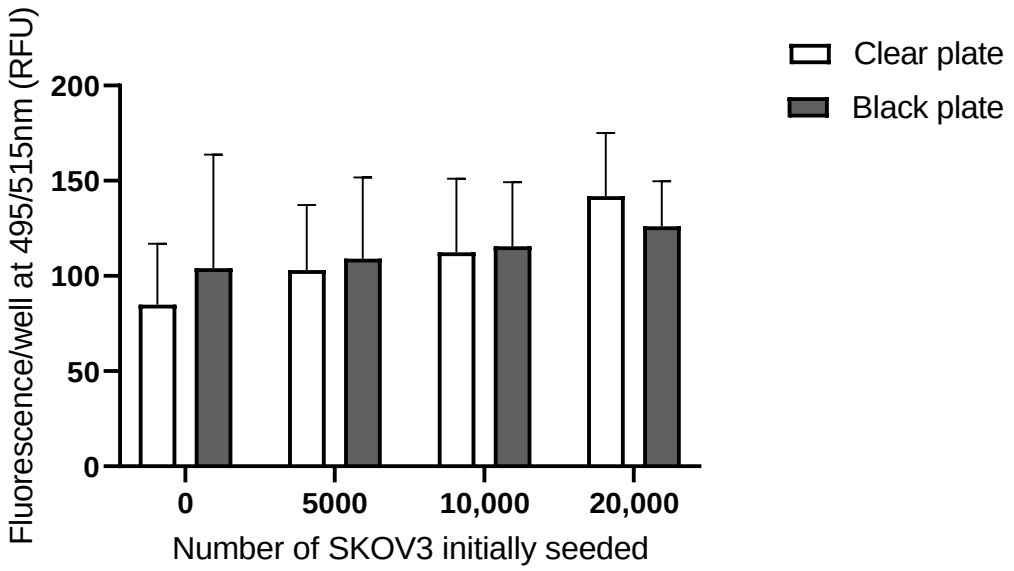

Figure 93. The fluorescence readings of the background wells were similar to the wells with adhered SKOV3. Mesothelial cells were seeded at 30,000 cells/well on clear and black 24-well plates and grown to confluence. Calcein-AM-labelled SKOV3 cells were suspended in basal media + 10% (v/v) FBS and applied onto mesothelial cells at increasing densities (0 to 20,000 SKOV3/ 500µL/ well). Wells with zero SKOV3 cells contained mesothelial cells only (background wells). Plates were incubated at 37°C/5% CO2 for 24 hours, washed and then analysed by fluorescence spectrophotometry at 495/515nm. Data are presented as mean ± SD of replicates from one experiment.

After the unadhered SKOV3 were removed by washing, the readings of the background wells were similar to the wells with the adhered SKOV3. These data therefore suggest that the fluorescence spectrophotometry method did not appear sensitive enough to distinguish the fluorescence of the adhered SKOV3 cells from the background fluorescence.

These data and the previous data suggested that utilising fluorescence spectrophotometry to determine the amount of SKOV3 adhesion onto mesothelial cells was unreliable. Therefore, an alternative method to quantify SKOV3 adhesion was required.

6.3.6 The effect of adipose, SKOV3 and mesothelial cell conditioned media on SKOV3 cell adhesion to a mesothelial monolayer under fluid flow conditions as assessed by manual cell counting

The previous data indicated that analysing adherence of SKOV3 by fluorescence spectrophotometry was not a reproducible and reliable methodology. Therefore, manual counting was used for all future experiments. With this method, the type of plate (clear or black) used becomes immaterial and thus, standard clear 24-well plates were utilised.

In the previous experiments, SKOV3 adhesion to mesothelial cells was examined under static conditions, i.e. the media with suspended SKOV3 cells was unmoving on top of the mesothelial cell surface. To better simulate the passive flow conditions of the peritoneal fluid on the omental surface, the fluid shear stress commonly encountered in the peritoneum were generated within the wells via mechanical rocking, i.e. by placing the plates on a see-saw rocker. The settings of the see-saw rocker to generate the required shear stress are detailed in section 6.2.6.

The experiment was conducted and analysed as described in section 6.2.7. Most of the observed SKOV3 adhesion occurred in the middle part of the well, where the SKOV3 cells were congregated in a parallel direction to the rocking motion (**Figure 94**), i.e. the ‘pivot’ of the see-saw.

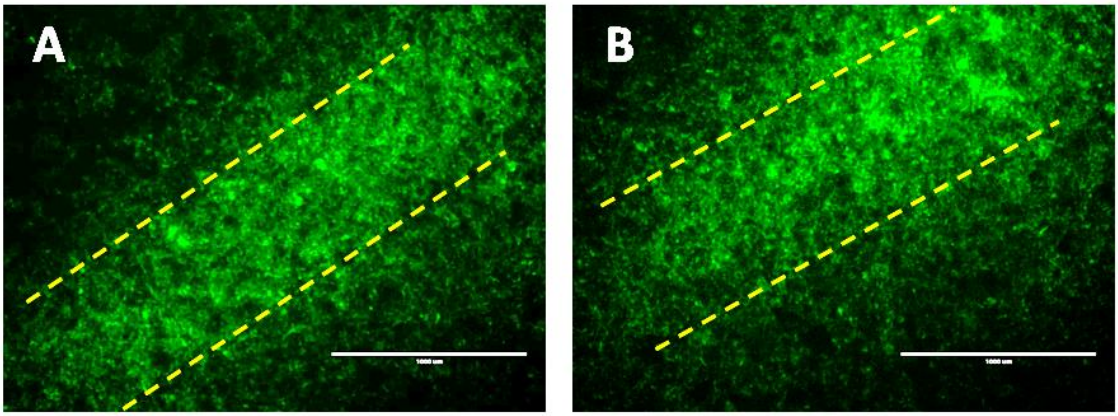

Figure 94. SKOV3 adhesion onto mesothelial cells was mostly observed in the central region of the well, parallel (marked with dotted lines) to the rocking direction. Mesothelial cells were seeded at 30,000 cells/well in 24-well plates and grown to confluence. Calcein-AM-labelled SKOV3 cells were suspended in various treatment media and applied onto mesothelial cells (20,000 SKOV3/ 500µL/ well) on a see-saw rocker for 24 or 48 hours. Unadhered SKOV3 cells were removed by washing and the wells imaged on a fluorescence microscope; labelled SKOV3 cells appear green when imaged on the green channel. Representative images, captured at 4x magnification with EVOS Fluo, depict SKOV3 adhesion after 48 hours when treated with mesothelial CM (A) and adipose tissue CM (B). Scale bar 1000µm.

Compared to the control CM after 24 hours, there was no significant difference in SKOV3 adhesion to mesothelial cells in the presence of SKOV3 CM or adipose tissue CM (**Figure 95**). Interestingly, less SKOV3 adhesion was observed when cells were incubated with mesothelial CM ($p<0.05$, compared to control CM). However, this reduced adhesion was not observed after 48 hours when SKOV3 adhesion in all treatment CM (mesothelial cell CM, SKOV3 CM, adipose tissue CM) were similar to control.

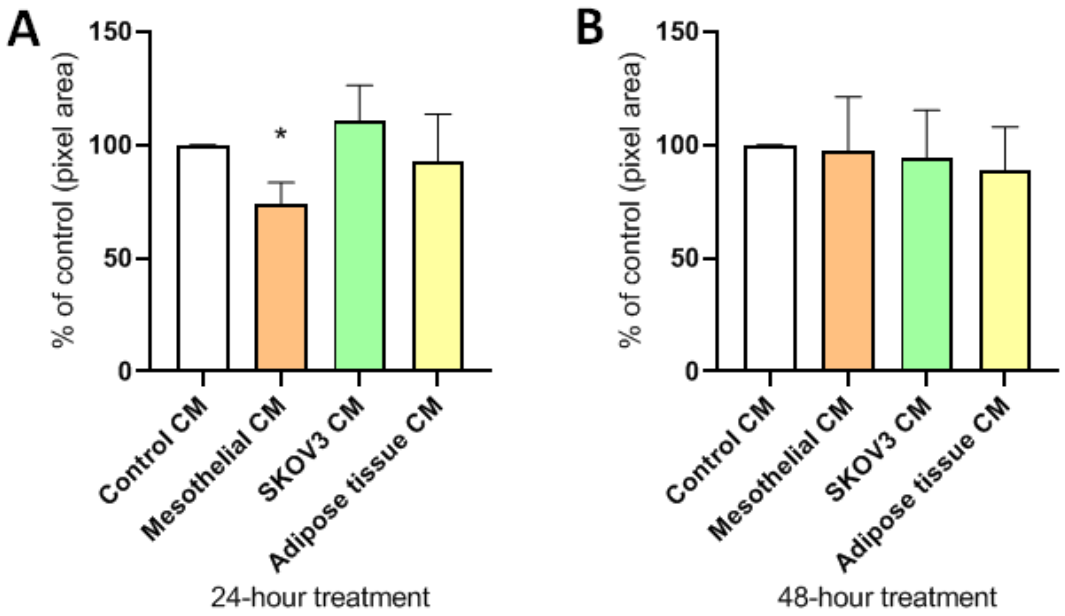

Figure 95. Mesothelial cell CM reduced SKOV3 adhesion after 24 hours, but not after 48 hours. Mesothelial cells were seeded at 30,000 cells/well in 24-well plates and grown to confluence. Calcein-AM-labelled SKOV3 cells were suspended in treatment media and applied onto mesothelial cells (20,000 SKOV3/ 500µL/ well) on a see-saw rocker for 24 (A) or 48 (B) hours. Unadhered SKOV3 cells were removed by washing and the wells imaged on a fluorescence microscope. The total area of adhered SKOV3 cells was calculated on ImageJ and compared between treatments. Data are presented as mean ± SD and expressed as a percentage of control media (n=4), *$p<0.05$, Mann-Whitney test. CM: conditioned media.

6.3.7 Visualisation of SKOV3 adhesion onto mesothelial cells via immunocytochemistry

After SKOV3 cells adhered to the mesothelial cell monolayer, immunocytochemistry was performed (described in section 6.2.8) to detect any changes in mesothelial cell morphology, either induced by the treatment media overnight incubation, or induced by the SKOV3 cells. In terms of the latter, previous studies reported that cancer cells were able to cause the migration or clearance of mesothelial cells and subsequently, the cancer cells adhered to the ECM in the exposed sub-mesothelial layer (discussed in section 1.6.5). Thus, immunocytochemistry investigated whether the SKOV3 cells adhered to the mesothelial cells themselves or to the collagen coating underneath the mesothelial cell layer.

Immunocytochemistry confirmed the identity of mesothelial cells by the presence of both cytokeratin-18 and vimentin, and their general morphology appeared unchanged after prolonged incubation (≥24 hours) with treatment media and SKOV3 cells (**Figure 96**). The green of the calcein-AM within the SKOV3 cytosol appeared diffuse, while the green of the vimentin within the mesothelial cells appeared fibrous; hence the two cell types could be distinguished. The nuclei of the SKOV3 cells appeared larger than that of mesothelial cells, identified from the blue dye of DAPI staining. Immunocytochemistry images showed that the SKOV3 cells adhered to the mesothelial cells rather than to the matrix in between them, based on cytokeratin-18 staining, which indicated the location of the adhered mesothelial cells.

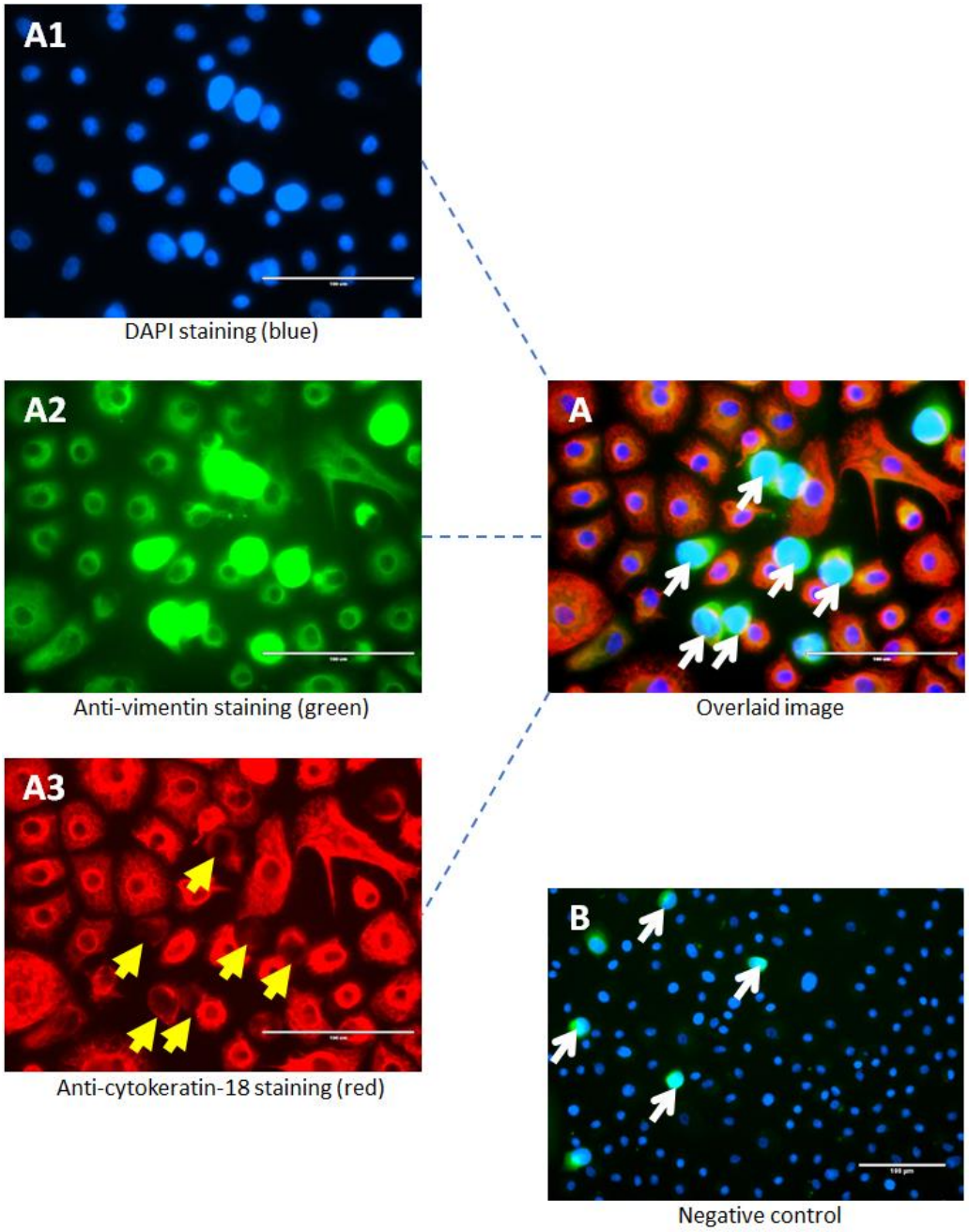

Figure 96. SKOV3 cell adhere to mesothelial cells. The presence of vimentin (green, A2) and cytokeratin-18 (red, A3) confirmed the identity of mesothelial cells and their location. White arrows mark the calcein-AM-labelled SKOV3 and yellow arrows mark SKOV3 cells adhered to the mesothelial cells. Mesothelial cells were seeded at 30,000 cells/well on a 24-well plate, grown to confluence and treated with SKOV3 CM overnight. Fluorescent-labelled SKOV3 cells were applied for 6 hours before removing unadhered cells with PBS. Cell fixation was performed with 4% (v/v) paraformaldehyde at room temperature and cells were then permeabilised with methanol at -20°C. Primary antibodies (anti-vimentin and anti-cytokeratin-18) were applied, followed by fluorescent-conjugated secondary antibodies; cell nuclei were stained blue with DAPI (A1), and the plate was visualised via fluorescence microscopy. Representative images, captured at 40x magnification using EVOS Fluo, show SKOV3 adhesion on mesothelial cells stained for vimentin and cytokeratin-18 (A) with the individual channels (A1, A2, A3) shown separately. The negative control (PBS in place of primary antibodies) showed background level of staining (B). Scale bar 100µm.

6.4 Discussion

Since the interaction between ovarian cancer cells and the omental mesothelial cells is crucial in cancer metastasis to the omentum, a method to analyse the initial adhesion of ovarian cancer cells to the mesothelial surface layer was developed. SKOV3 cells were selected to represent metastatic ovarian cancer, as they were derived from the ascitic fluid of EOC,(284) and thus would come into contact with the omental surface. The SKOV3 cells were fluorescently labelled to ease their detection via fluorescence spectrophotometry or fluorescence microscopy. However, the former method proved to be unreliable and thus manual cell counting was eventually performed using images captured via fluorescence microscopy. Furthermore, to closely resemble in vivo fluid shear stress conditions encountered in the peritoneal cavity at the omental surface, cells in the culture plates was subjected to mechanical rocking during treatment.

When comparing SKOV3 adhesion under different treatment conditions, treatment with mesothelial cell CM resulted in reduced SKOV3 adhesion compared with control, adipose tissue CM and SKOV3 CM after 24 hours. However, after 48 hours, SKOV3 adhesion was of similar levels in all CM types.

6.4.1 Fluorescence spectrophotometry readings were unreproducible and unreliable

In studying the adhesion of the ovarian cancer cells onto mesothelial cells, labelling the SKOV3 cells with calcein-AM, a fluorescent dye, and leaving the mesothelial cells unlabelled, was a simple approach to differentiate between the two different cell types.

Fluorescence spectrophotometry was initially thought to be the most objective measurement of fluorescence, and also allowed for higher throughput, but proved unreliable in these experiments. Examination of fluorescence per well immediately after seeding with different numbers of labelled SKOV3 confirmed that the level of fluorescence was proportional to cell numbers added. However, after 24 hours incubation and washing off the unadhered SKOV3 cells, the

fluorescence readings were greatly reduced and were similar to the background wells (mesothelial cells without the labelled SKOV3).

Images of the wells showed greater numbers of adhered SKOV3 when they were seeded at a higher density, but this observation was only measured as marginal in the fluorescence readings. Importantly, the background wells themselves emitted fluorescence in the absence of SKOV3, suggesting that the mesothelial cells autofluoresce. This is supported by literature showing that cellular components were found to naturally autofluoresce.(489) These data suggest that the utility of fluorescence spectrophotometry was limited since it could not discern between the fluorescence of the adhered SKOV3 cells and the background readings.

Discrepancies also arose in the fluorescence readings generated and the manual cell count numbers. It was proposed initially that the discrepancy could be explained by the multiwell plates used in the experiments. Black plates are often marketed as suitable for fluorescence-based experiments, since the black-coloured walls absorb light and thus, reduce intra-well light reflection. In the experiment using blank (no cells, media only) clear and black 24-well plates, the difference between the readings obtained from the clear and black plates were obvious; the standard clear-walled plates showed higher variability (larger standard deviation values) between the individual wells, possibly due to the light reflection within the walls resulting in high background fluorescence. Additionally, a 24-well plate is considered as a low-density plate (as opposed to the higher density 384-well plates where the walls of each well are closer together) with a wide bottom surface Thus, the clear-bottomed surfaces of both the standard and black plates may also cause light reflection and in turn, contribute to the background fluorescence.

Another contributory factor to background fluorescence is the autofluorescence of compounds within the media itself.(490, 491) This was shown earlier when the different types of media within the blank wells generated different fluorescence values. From the data shown it was concluded that fluorescence spectrophotometry was not suitable method to measure calcein-AM-labelled SKOV3 adhesion onto mesothelial cells. Therefore, a visual-based method was used instead i.e. by analysing microscope images of fluorescent SKOV3 cells.

6.4.2 Fluid shear stress generation in culture wells

To date, this is the first time the adhesion of ovarian cancer cells onto omental mesothelial cell layer was investigated under physiological shear stress conditions. Previous studies adopted a static system,(273, 468) while another study generated fluid shear stress using a gyro-rocker instead of a see-saw rocker in order to examine the changes induced in ovarian cancer cells.(492) The gyro-rocker method was not utilised as the calculation of shear stress did not appear reliable, since it was based on the equation for a see-saw rocker as stated in the Zhou et al (2010) study.

The method of using a see-saw rocker to generate fluid shear stress was chosen due to the ease of set up and operation. Cells were cultured as usual in 24-well plates, and placed on the rocker within the incubator itself; with no need for extra tubing, additional temperature control or other specialist equipment. Furthermore, the authors of the article that the fluid shear stress equation was adapted from, proposed that their method and equation is applicable for rocking systems with a low magnitude, i.e. ≤1 dyn/cm^2;(485) which is appropriate to simulate peritoneal fluid shear stress in the current experiment.

In terms of the fluid shear stress experienced by the mesothelial cell layer, the calculated shear stress, 0.0426 dyn/cm^2, applies to the centre of the well as stated in the original article.(485) The authors of the article also stated that the shear stress values do not differ greatly (<17% difference) within the central 50% of the well, as long as the bottom of the well is fully covered by media during rocking. Such a situation is applicable in these experiments as the volume of media was sufficient and the angle of tilt small enough to prevent the mesothelial cells at the bottom being exposed to air at any point. By extrapolation, the maximal shear stress within the central 50% of the well is 0.0498 dyn/cm^2, which is within the physiological peritoneal shear stress value of <0.1 dyn/cm^2.(140) Hence, to analyse SKOV3 adhesion, microscope images were positioned in the centre of the well to encompass the central 50% region.

It was observed that the pattern of SKOV3 adhesion was concentrated in the middle of the well and formed a parallel band in the same direction as the rocking see-saw motion. This suggests that higher shear stress enhanced SKOV3 adhesion. This is supported by the literature indicating that the

application of fluid shear stress increases the invasiveness of many types of cancers. For example, in ovarian cancer cells shear stress induced cytoskeletal changes (486) and increased secretion of IL-8, both of which are linked to enhanced tumour adhesion.(487) In chondrosarcoma, shear stress increased MMP-12 expression and subsequent ECM degradation.(493) In hepatocellular carcinoma shear stress led to upregulation of autophagy and conservation of resources during tumour invasion.(494)

6.4.3 The effect of treatment with conditioned media on SKOV3 adhesion onto mesothelial cells

Interestingly, none of the CM tested i.e. adipose tissue, mesothelial cell or SKOV3 CM, increased SKOV3 adhesion to the mesothelium above control levels. This was unexpected since the CM were sourced from cells reported to be capable of secreting factors which contribute to cancer metastasis. For example, adipocytes, a major component of adipose tissue, are linked to cancer metastasis through the secretion of adipokines for tumour invasion and angiogenesis (section 1.5). Mesothelial cells are also recognised as active participants in tumour metastasis through the upregulation of adhesion factors and receptors in ovarian cancer cells (discussed in section 1.6.5).(464, 468, 495) Factors secreted from SKOV3 cells have been reported to induce MMT, making mesothelial cells more conducive towards cancer invasion.(273)

Interestingly, incubating SKOV3 and mesothelial cells in mesothelial cell CM reduced adhesion of the cancer cells to the mesothelium after 24 hours, although no difference from control was seen after 48 hours. These data suggest that mesothelial cells secrete factors that protect against cancer cell adhesion, at least in the short term (≤24 hours). At the 24-hour timepoint, the findings were similar to a previous study by Kenny et al (2007) who compared SKOV3 adhesion to human omental mesothelial cells or fibroblasts.(468) They showed that SKOV3 adhesion to mesothelial cells was considerably lower than adhesion to fibroblasts, and inferred that the mesothelial cells inhibited cancer cell adhesion while fibroblasts induced it. Adhesion to fibroblasts was lower when the SKOV3 cells were pre-treated with mesothelial cell CM, but the pre-treatment of the SKOV3 cells did not further reduce adhesion to mesothelial

cells.(468) The authors postulated that SKOV3 adhesion to mesothelial cells was mediated by direct cell-contact since mesothelial cell CM had no effect.(468)

In the experimental setup described in Kenny et al (2007), the pre-treatment of SKOV3 with mesothelial cell CM was for 18 hours, and then the SKOV3 cells suspended in mesothelial cell CM was added to the mesothelial cell layer for a further 4 hours to allow SKOV3 adhesion.(468) This is equivalent to a 22-hour exposure time of the SKOV3 to the mesothelial cell CM. This was similar to the present experiment where the SKOV3 cells, suspended in the treatment CM, were incubated with the mesothelial cells for 24-hours. The difference in the present setup was that the SKOV3 cells were not pre-treated with treatment CM prior to addition to the mesothelial cell layer.

The decreased SKOV3 adhesion observed in cells incubated with mesothelial cell CM for 24 hours may be due to the presence of factors in the CM which protects against cancer cell adhesion. A possible candidate may be free-floating hyaluronan which had previously detached from the mesothelial cells during CM collection.(268) This exogenous hyaluronan may have served as a decoy for the SKOV3 cells to bind to. However, at the 48-hour timepoint, SKOV3 adhesion in all treatment CM types was similar to control CM. It was possible that the free-floating hyaluronan had been depleted or ‘mopped up’ by the SKOV3 cells by 48 hours, thus the SKOV3 cells could then go on to bind to the mesothelial cell layer.

In a previous study, omental mesothelial cells which had converted to the mesenchymal phenotype showed greater SKOV3 adhesion compared to the epithelial-like mesothelial cells.(273) This same study showed that MMT in the omental mesothelial cells could be induced by incubating them with either SKOV3 CM or a treatment containing both TGF-β1 and IL-1β for 6 days; the spindle-shaped morphology of mesenchymal-like mesothelial cells was observed by day 3.(273) Interestingly, both TGF-β1 and IL-1β were detected in the omental adipose tissue CM of the present study (**Figure 97** in the appendix), and these factors have been implicated in the MMT process from other studies.(496, 497) Altered morphology in mesothelial cells was not observed in the present study, possibly due to the shorter incubation time (≤48 hours) with CM from SKOV3 or adipose tissue. By extrapolation, it is possible

that extending the incubation duration to at least 72 hours may have resulted in increased SKOV3 adhesion to the mesothelial cell layer compared with the control when incubated in CM from SKOV3 or adipose tissue.

It is also possible that the method by which the media in the wells were removed, i.e. by pipette aspiration, may have contributed to the lack of difference observed in SKOV3 adhesion when treated with the different CM types, especially at the 48-hour timepoint. Media aspiration was performed in the wells containing mesothelial cells prior to SKOV3 seeding. It was possible that media aspiration via pipette may have mechanically destroyed the surface structure of mesothelial cells, possibly the hyaluronan coating (discussed in section 1.6.5), which then allowed SKOV3 adhesion regardless of the type of CM treatment present including the control. A study by Jones et al (1995),(268) showed that the mesothelial cell pericellular coat, consisting of hyaluronan, conferred protection against ovarian cancer cell adhesion. They reported that media aspiration resulted in a greater loss of this coat compared to when the media was poured out, and that cancer cell adhesion was greater when the former method was employed.

The mechanism of SKOV3 adhesion was not explored in this project. Possible mechanisms from past studies, as discussed in subsections 1.6.5b and 1.6.5c, proposed the role of integrins (bind to the fibronectin secreted by mesothelial cells), the CD44 receptor (binds to surface hyaluronan on mesothelial cells), or the CXCR4 receptor (binds to CXCL12 secreted by mesothelial cells). Thus, future work could include investigating the roles of these molecules.

6.4.4 SKOV3 adhere to mesothelial cells and not the extracellular matrix

From immunocytochemistry, it could be seen that SKOV3 cells adhered to the mesothelial cells themselves rather than the extracellular matrix in between them. Images from fluorescence microscopy showed that the structure of the cytokeratin-18 and vimentin within the mesothelial cells were not altered when SKOV3 were adhered. While vimentin was also present in SKOV3,(498) this was not apparent in the images as the diffused appearance of the green calcein-AM masked the fibres of the also green vimentin.

It is interesting to note that this finding was not aligned to previous studies which suggested that cancer cell adhesion is enhanced by the 'clearing away' of mesothelial cells to expose the underlying matrix, where the initial adhesion then occurs.(271, 272) Specifically, it has been suggested that the ovarian cancer cells in contact with the mesothelial cell layer use traction force to disassemble mesothelial cells from their underlying matrix.(271) It is possible that these differential results are due to the different coating substrates used or different cancer cells. For instance, Davidowitz et al (2014) used fibronectin to coat their cultureware,(272) whereas the present experiment used collagen IV. Additionally, these authors did not test SKOV3 cells in their study. Metastatic ovarian cancer cells may preferentially bind to fibronectin, with previous studies reporting interactions between cancer cell integrins and fibronectin.(141, 142, 263) In the present study, collagen IV coating was utilised when culturing mesothelial cells as it was tested to be the most suitable (demonstrated in section 5.4.1), and also because collagen most closely resembles the basement membrane of adipose tissue in vivo.(466, 467)

It is possible that the mechanism of ovarian cancer invasion (mesothelial clearance or adhesion) may be dependent on the coating substrate utilised. Thus, for future experiments, it would be interesting to compare the effect of fibronectin or collagen coating on SKOV3 adhesion to mesothelial cells, and subsequently identify the cancer cell integrins involved.

Davidowitz et al (2014) also reported that ovarian cancer cells (derived from primary cancer or cancer cell lines) with greater gene expression of mesenchymal markers showed better mesothelial cell clearance ability; while those with greater expression of epithelial markers showed poor clearance ability.(272) This was confirmed by the increased expression of vimentin (a mesenchymal marker) or the decreased expression of E-cadherin (an epithelial marker) in the clearance-competent cancer cell types.(272) The role of EMT was also implicated in the binding of cancer cells to fibronectin, observed as increased binding when E-cadherin expression was inhibited.(141)

These findings implied that the extent of EMT in the cancer cells correlates with their ability to clear the mesothelial cell layer and thus, facilitate cancer invasion. Indeed, the significance of the EMT process in ovarian cancer dissemination was discussed in section 1.3.5. Additionally, increased E-cadherin mRNA

expression in ovarian cancer cells in peritoneal and pleural fluid correlated with better patient survival.(499) Therefore, future work could examine the role of EMT and whether the adhered SKOV3 cells showed changes in levels of mesenchymal and epithelial markers. Although vimentin expression was detected via immunocytochemistry, this was not quantified in the present study.

Since the mesothelial cell layer appeared intact in the present study, adhesion molecules on the mesothelial cells such as ICAM-1 or VCAM-1 may be implicated in their interaction with the SKOV3 cells, based on a study investigating colon cancer cell adhesion to rat mesothelial cells.(254) This study attributed the increased expression of adhesion molecules to the action of IL-1β,(254) which is also one of the mediators secreted by omental adipose tissue. A more recent study reported that SKOV3 cells migrate across the mesothelial cell layer (human mesothelial cell line cultured in pore filter chambers) through the interaction between VCAM-1 expressed on the mesothelial cells and the α4β1 integrin on the cancer cells.(500) Additionally, mesothelial VCAM-1 expression was negatively correlated to patient survival in EOC.(501) Future work could focus on identifying the molecules involved in ovarian cancer adhesion and invasion, and the mediators which regulate their expression.

The immunocytochemistry images also showed that the adhered SKOV3 retained their circular morphology. This was also noted by Sandoval et al (2013) (273) in mesothelial cells which retained their cobblestone or epithelial-like characteristics as per normal physiology (as observed here). However, these authors noted that when the mesothelial cells transdifferentiated to a mesenchymal phenotype (via MMT), the adhered SKOV3 cells produced pseudopodial projections on the mesothelial cell surface.(273) This phenomenon was not observed in the current experiment, possibly because the experiment was carried out for 24 hours, whereas that of Sandoval et al was for 72 hours.(273) Indeed, such pseudopodial projections on the adhered SKOV3 were observed after 48 hours, based on fluorescent microscopy images from early experiments (**Figure 99** in the appendix).

6.5 Chapter summary

The omental mesothelial cells are the first point of contact for ovarian cancer cells metastasising via the peritoneal fluid. Since the omentum is a favoured site of metastasis it was hypothesised that the release of soluble adipokines by this adipose tissue organ may contribute to the rich “soil” that encourages cancer cells to “seed” onto this organ. Thus, the effect of adipose tissue CM on cancer cell adhesion onto the outer mesothelial layer of the omentum was examined. Since both the cancer cells and mesothelial cells can also potentially secrete pro-adhesive factors in the tumour cell microenvironment the effect of CM collected from these two cell types on cancer cell/mesothelial cell adhesion were also examined for comparison.

To facilitate these studies an in vitro experimental system was successfully established. This identified that quantification of the adhesion of SKOV3, as a model for metastatic ovarian cancer, onto mesothelial cells by manual cell count was optimum rather than the use of fluorescence spectrophotometry. To simulate peritoneal fluid flow conditions, experienced in the microenvironment of the omental mesothelial cells, fluid shear stress was generated by mechanical rocking of the culture plates.

Interestingly, after 24 hours incubation the adipose CM had no effect on SKOV3 adhesion onto mesothelial cells and similarly no changes in adhesion were induced by cancer cell CM. However, the mesothelial cell CM significantly reduced mesothelial cell adhesion compared with the control. After 48 hours, SKOV3 adhesion was similar in all treatments which suggests that secreted factors in the CM did not enhance SKOV3 adhesion. These data suggest that none of the CM in isolation contain factors that enhance cancer cell adhesion, at least in the experimental system studied. It is possible that a combination of CM may have different effects, and this could be studied in the future

In contrast, these data support the conclusion that factors secreted from mesothelial cells actively contribute to maintaining a relatively low adhesive surface for migrating cancer cells and that removal of these factors may disrupt this homeostatic process. Thus, it would be interesting to examine whether a mixture of CM would suppress this effect, i.e. would mixing SKOV3 CM with mesothelial cell CM override the protective effects of the mesothelial cell CM.

This serves as a potential direction for future studies in elucidating the mechanism of SKOV3 adhesion onto the omental mesothelial cells.

Chapter 7. General discussion and future work

Of all the gynaecological cancers, EOC is the most lethal. In the UK, survival rate after 10 years is only 35%.(57) Most patients are diagnosed at stage III and IV, and 10-year survival at stage IV is a paltry 13%.(58) Some of the reasons for this advanced stage at diagnosis are non-specific symptoms during the early stages of the cancer, lack of awareness, lack of effective screening methods and relatively ineffective long term treatment. Chemotherapy post-surgery is the mainstay treatment, however, advancement in this aspect has been slow. The current platinum-taxane combination chemotherapy was first established in 1996, and still remains mostly unchanged, except for slight regimen changes in dosage and administration duration.(95-97)

Anti-angiogenic treatments were heralded as a new era in anti-cancer therapies. The premise for their development was the discovery of VEGF. Solid tumours, including ovarian cancers, secrete this pro-angiogenic factor which is reported to stimulate tumour angiogenesis to supply the growing primary and metastatic tumours with nutrients and oxygen.(44, 45) Anti-angiogenic therapies targeting VEGF are designed to prevent VEGF signalling in host ECs, which in turn should inhibit new vessel growth and regression of newly formed vasculature, ultimately leading to tumour death.(502)

The anti-angiogenic therapy bevacizumab (anti-VEGF antibody) was approved for use in ovarian cancer and appeared promising in the short term, with quality of life scores comparable to standard chemotherapy.(102, 103) However, improvements were not sustained in the long term, as evidenced by the lack of clinical benefit. Unfortunately, clinical endpoints such as overall survival and progression-free survival showed modest or no improvement with the addition of bevacizumab to standard treatment.(101-103) This lack of impact could be the result of compensatory pro-angiogenic pathways in tumours, inappropriateness of administration route of the therapies, or drug resistance. In fact, resistance to bevacizumab is increasingly recognised, whereby treatment induces resistance genes in cancer cells, leading to adaptive mechanisms to circumvent bevacizumab’s action,(104, 105) again suggesting compensation by alternative pro-angiogenic pathways to the VEGF-VEGFR axis. Thus, tumour angiogenesis is a complex process, and more research is required to

understand the mechanisms involved and translate findings into clinically useful therapy.

In ovarian cancer metastasis, the transcoelomic dissemination route is the most common, whereby the tumour cells break away from the primary tumour and are transported by peritoneal fluid into the peritoneal cavity. The metastatic cells then preferentially attach to peritoneal surfaces which are composed of mesothelial cells. One such location is the surface of the omentum, a large abdominal organ composed of adipose tissue. The preference, or tropism, of the tumour cells for the omentum is not coincidental. It is partly due to the structure of the omentum itself, especially the ‘milky spot’ areas where peritoneal fluid containing the tumour cells enters through fenestrations and the action of macrophages and mesothelial cells aid tumour colonisation.

Adipocytes are the main component cells of adipose tissue and previous studies showed that they may also play a role in tumour metastasis and progression. Not only can the adipocytes provide fatty acids as an energy source for the metastatic tumour cells, but other elements of the secretome, including adipokines, can promote cancer EMT (supporting the survival of exfoliated tumour cells), function as an attractant for metastatic cells and aid their adhesion, promote chemoresistance in tumour cells and promote tumour angiogenesis.(159, 186) It is also possible that EOC metastasis to the omentum is so successful because the secreted adipokines also contribute to the process of angiogenesis initiated by the growing tumour to support delivery of nutrients and oxygen. However, the specific mechanisms by which the latter may occur have not been fully investigated.

Clearly, a greater understanding of the influence of adipokines on the metastatic process may reveal potential pathways for future therapeutic targets, and given the relatively poor advances in this area over the past 30 years, new therapeutic options for sufferers of ovarian cancer are urgently needed. Thus, the aim of this thesis was to examine, using disease relevant human cell types, whether secreted omental adipokines support EOC metastasis to the omentum by (a) influencing initial ovarian cancer cell adhesion to the surface of the omentum (mesothelial cell layer), and (b) by inducing pro-angiogenic changes in the microvascular ECs within the omentum (i.e. the HOMECs).

To investigate this, the existing protocol to isolate HOMECs was improved to reliably increase their yield. Key changes included extending the duration of enzymatic digestion of the omental tissue (a greater proportion of the tissue sample is digested away to release a higher number of the intended cells) and extending the incubation duration of the immunoselection step (allowing more time for the antibody to bind to the HOMEC surface marker, CD31). The identity of the isolated cells was confirmed via immunocytochemistry for known endothelial cell markers including CD31 and vWF.(278, 281)

EC activation is critical for angiogenesis, and this activation was measured by EC proliferation (assessed by WST8 and BrdU assays) and migration (assessed by scratch assay). Initial studies examined the ability of factors secreted from omental adipose to induce HOMEC proliferation. Importantly, the complete secretome of the adipose tissue, in the form of CM, significantly enhanced HOMEC proliferation, suggesting that the adipose tissue alone is a rich “soil” for metastatic EOCs. However, although analysis of the CM identified key secreted adipokines with potential angiogenic effects (adiponectin, cathepsin L, leptin, lipocalin-2 and MIF), none of these proteins alone or in combination, enhanced HOMEC proliferation suggesting that the secreted pro-proliferative factor(s) is still to be identified. However, antibody array analysis of the HOMEC receptors and intracellular signalling pathways activated by adipose tissue CM suggested activation of a pro-proliferative pathway involving STAT3 signalling. Based on the existing literature, STAT3 is possibly activated upstream by receptors such as ALK, FGFR, or another as yet unidentified receptor (**Figure 67**).(385, 503, 504)

The range of adipokines secreted by adipose tissue (**Figure 97** in the appendix) may act as ligands for these receptors. A possible candidate is HGF, which was shown to induce HUVEC and human aortic EC proliferation as assessed by a [^{3}H]Thymidine assay (similar to BrdU assay).(505, 506) Moreover, treatment with HGF was associated with increased STAT3 activation in ECs.(506)[refH6b] Other potential pro-angiogenic factors derived from the adipocyte secretome are CCL5 and IGFBP-3, which were shown to induce tube formation in HUVECs in vitro and in murine models in vivo.(507, 508)

It was interesting to note that neither the adipose tissue CM nor the selected individual adipokines enhanced cell migration, raising the possibility that adipokines play a larger role in HOMEC proliferation than migration.

Since it is generally accepted that the cancer cells themselves contribute to their own metastasis, the effect of basal cancer CM on HOMEC proliferation was also examined. Interestingly, while CM from A2780 cells, (ovarian cancer cells derived from the primary tumour) did enhance EC proliferation, CM from SKOV3 cells (an ovarian cancer cell line originating from a metastatic tumour), did not. This contrasting observation showcased the different angiogenic and thus, invasive capabilities of the cancer cells. It was also unexpected, since most solid tumours, including EOC, have been shown to secrete VEGF, a prominent pro-angiogenic growth factor.(509, 510)

Since both cell types i.e. adipocytes and EOC cells, are present in the complex omental microenvironment of the invaded omentum during metastasis, it was hypothesised that the interaction between secreted adipokines and the cancer cells may be further driving angiogenesis. Thus, the ovarian cancer cells were exposed to the individual identified adipokines prior to collection of their CM which was then applied onto the HOMECs. Excitingly, it was shown for the first time that CM from both SKOV3 and A2780 cells, pre-incubated with leptin or lipocalin-2, significantly enhanced HOMEC proliferation compared with cancer cell CM alone. These data strongly suggested that these two adipokines induced the release of proangiogenic factors from the cancer cells, highlighting the complexity of the cellular crosstalk occurring in the omentum during EOC metastasis.

A series of experiments were then carried out to try to identify the pro-angiogenic factors secreted from the cancer cells in response to leptin and lipocalin-2 and the signalling pathways activated in the HOMECs. It was found that VEGF and TGF-β1 secretion was induced by both adipokines in both SKOV3 and A2780 cells. However, inhibitor studies confirmed that only VEGFR2 inhibition significantly reduced the proliferative effects of the CM from adipokine treated cancer cells. The CM activated a range of common intracellular signalling kinase targets in the HOMECs including ERK1/2, HSP27 and PDGFRβ. These combined data strongly suggested that activation of the VEGF-VEGFR2/ERK1/2 axis was responsible for the observed HOMEC

proliferation and that additionally the VEGF/VEGFR2 activation may have been potentiated by PDGFRβ signalling (**Figure 66**).

Separately, increased VEGFR3 activation was detected in the HOMECs which prompted additional immunocytochemistry of HOMECs with an anti-VEGFR3 antibody. Indeed, VEGFR3 was detected in two separate populations of the isolated HOMECs. This was interesting since this VEGF receptor type has been reported to be mostly expressed in lymphatic ECs in previous studies, highlighting the heterogeneity of ECs and the importance of using relevant ECs when studying a specific disease (in this case HOMECs).

In summary, the data presented here indicate that the secretome of omental adipocytes not only contains (as yet unidentified) factors that alone or in combination are able to activate a pro-angiogenic i.e. pro-proliferative, phenotype in HOMECs, but also leptin and lipocalin-2 which interact with EOCs to induce secretion of VEGF. Thus, the resident microvasculature in the omentum is exposed to two sources of pro-angiogenic signals originating from the adipocytes, one direct and one indirect via the cancer cells and this double trigger may be enough to initiate the angiogenic switch and induce new vessel growth. Thus, the highly complex interactions between adipocytes, cancer cell and ECs in the omentum during EOC metastasis may promote metastasis growth and partly explain the high rate of successful secondary spread to this tissue i.e. it provides a fertile “soil” for the “seeded” cancer cells.

Aside from targeting angiogenesis, methods to overcome the establishment of metastasis in the first place would be beneficial in treating EOC. Mesothelial cells form the outer layer of the omentum and are the first point of contact for the invading cancer cells. It was thus hypothesised that factors secreted from the omental adipocytes may also contribute to this stage of EOC metastasis.

To investigate the adhesion of the ovarian cancer cells onto the mesothelial layer, a reliable protocol to isolate the omental mesothelial cells was first developed. The identity of the isolated cells was confirmed via immunocytochemistry. Next, a series of studies to optimise in vitro omental mesothelial cell growth conditions established that cultured cells should be grown in vessels or plates coated with collagen IV, maintained in DMEM with

20% FBS and seeded at a density of at least 10,000 cells/cm^2 to reduce the risk of senescent-like cells.

Once this was established, the cells were used to develop an assay to examine cancer cell adhesion to the mesothelium under flow conditions similar to those found in vivo, where peritoneal fluid movement along the omental surface generates fluid shear stress. Interestingly neither the CM from SKOV3 cells or adipose tissue had any effect on adhesion of SKOV3 cells to the mesothelial layer. However, CM from the mesothelial cells themselves reduced SKOV3 adhesion to the mesothelium at 24 hours, suggesting that mesothelial cells secrete protective factors against cancer cell adhesion in the short term (<24 hours). However, by 48 hours, SKOV3 adhesion was similar across all CM types. Free-floating hyaluronan was proposed as a possible protective factor secreted by the mesothelial cells and is a possible candidate for future work. Thus, the factors secreted from mesothelial cells could be further investigated in the future, to determine if they could be exploited for therapeutic use.

Additionally, it was observed from the microscopy images that the SKOV3 cells adhered to the mesothelial cells rather than the ECM in between them, as suggested by previous studies.(271, 272) Future work could explore the mechanism of this adhesion, possibly by examining the surface molecules of both the mesothelial and SKOV3 cells, and how these are affected by shear stress.

To summarise, the data presented in thesis suggest that activation of HOMECs by ovarian cancer cells during metastasis to the omentum is significantly enhanced by adipokines (particularly leptin or lipocalin-2) secreted from the resident adipocytes. These adipokines enhance secretion of VEGF from the cancer cells which in turn activates the VEGFR2 on the HOMECs, triggering downstream ERK1/2 phosphorylation and initiating cell proliferation. This added to the direct pro-proliferative effects of the adipocytes, triggers angiogenesis.

Clearly, these data provide additional evidence for the involvement of VEGF in metastasis of EOC to the omentum. However, as mentioned many anti-angiogenic therapies have targeted the VEGF pathway, including bevacizumab which has been trialled with disappointing results in advanced, i.e. metastasised, EOC. The data obtained provide insights into the

pathophysiology of the metastatic cancer itself and possible reasons behind this lack of clinical success. Firstly, bevacizumab is intravenously administered into the blood circulation system and relies on leaky tumour vessels for the drug to be delivered to the tumour mass or to the peritoneal ascites (since the therapy is an antibody, incapable of passing through the intact vessel wall). However, during the transcoelomic metastasis of ovarian cancer, metastatic tumour cells colonise non-diseased omental tissue where the vasculature is intact. Then, as shown here, they initially interact with the omental adipocytes to create an environment which stimulates angiogenesis in the growing tumour. Thus, perhaps the therapy is simply not able to initially access the areas where is it most required and the metastases are too established for the bevacizumab to induce clinically relevant effects. Secondly, perhaps the anti-VEGF therapies are administered too late in the cancer pathogenesis to bring about their full impact i.e. they are usually administered once metastasis has occurred.

The greater insight into the mechanisms involved in angiogenesis in omental metastases, shown here, suggest that anti-VEGF therapies that can be delivered at less advanced stages and through the intact microvasculature might be more effective than bevacizumab. However, this situation can only be addressed with earlier diagnosis, and as mentioned previously this is challenging for several reasons. It appears that the most likely way forward for improving the outcome of patients with EOC is an effective screening programme; proverbially, ‘prevention is better than cure.’

Several screening strategies were previously put forward, but no particular method has stood out due to the challenges they presented. For example, pelvic examination failed for a number of reasons: it was not sensitive enough to detect early tumours in asymptomatic patients;(511) the cancer could have metastasised elsewhere before growing large enough to be detected via ultrasound;(512) inter-observer variation in visualising and interpreting ultrasonography images of ovaries especially those in post-menopausal women.(513-515) Additionally, the blood biomarker CA125, commonly associated with ovarian cancer, is not sensitive or reliable as the cut-off threshold levels vary between different cancer subtypes.(64, 512)

Thus, ovarian cancer screening is not currently a viable option, and targeting angiogenesis in omental metastases may be the next best thing. A possible

strategy is to develop anti-angiogenic therapies which can be delivered much more efficiently to the adipose tissue of the omentum (for patients with omental metastases). This thesis highlights additional possible targets for therapeutic intervention. For instance, perhaps targeting leptin or lipocalin-2 or their signalling pathways in the EOC cells to reduce the overall VEGF burden could be considered. The pathways activated by these two adipokines resulting in enhanced VEGF production by the cancer cells were not investigated, and thus could be an important area for future work. A simple way to examine this is to collect the cancer cell lysate upon treatment with the adipokines and subject it to antibody arrays to detect the phosphorylation of relevant receptors and other signalling targets, similar to the procedures used to interrogate the lysate from CM-treated HOMECs.

Additionally, identifying the pro-angiogenic factor(s) secreted from the omental adipocytes could provide further targets for intervention. Inhibitor studies, like those performed in HOMECs when treated with cancer cell CM, could be replicated when HOMECs are treated with adipose tissue CM. As discussed earlier (section 4.4.5c), potential targets for inhibition include FGFRs and ALK to inform which receptor(s) upstream of STAT3 is/are implicated in HOMEC proliferation induced by the adipocyte secretome. Identifying the relevant receptor, and subsequently its activating ligand presents another target for anti-angiogenic therapy development.

Aside from targeting angiogenesis, therapies which aim to inhibit the initial tumour adhesion and colonisation in the target organ (omentum) may be beneficial. The data suggests that factors originating from mesothelial cells may inhibit the adhesion of ovarian cancer cells onto the outer mesothelial cell layer of the omentum, thus amplifying these protective factors presents a possible treatment strategy. Future work may involve electron microscopy to visualise the outer surface of the mesothelial cells, possibly visualising the theorised protective hyaluronan or the other components of the mesothelial glycocalyx, to better understand the physical communication between the adhering cancer cells and the mesothelial cell surface. This may provide insight into designing therapies which target the relevant adhesion molecules present on the metastatic cancer cells and on the mesothelial cells in order to curb the initial tumour colonisation.

While the use of antibody arrays in detecting the secretome of adipocytes in this thesis was convenient, the range of targets were limited by what was pre-set in the array, which are common or known targets from existing literature. Mass spectrometry is a possible alternative method especially in detecting the components in the secretome collected and utilised in this study, i.e. CM from adipose tissue, adipokine-incubated cancer cells, as well as mesothelial cells. For example, HOMECs treated with adipose tissue CM showed increased ALK activation but to date, its corresponding ligand is still unknown. Activating ligands such as midkine, which has cancer-promoting roles including angiogenesis,(516) were put forward in past studies (section 4.4.1d), however midkine is not included in the commercial antibody arrays. In such cases, mass spectrometry may be beneficial in revealing lesser-known ligands. Similarly, this method may be utilised to reveal the components of CM obtained from cancer cells incubated with leptin or lipocalin-2 (which may have induced HOMEC proliferation alongside VEGFR2 activation), or of mesothelial cell CM (which conferred protection against cancer cell adhesion onto the mesothelium).

As mentioned previously, the use of disease relevant human cells is pertinent to mimic in vivo conditions as much as possible. In the present study, the ECs for angiogenesis studies and the mesothelial cells for cancer adhesion studies were isolated from the omental tissue itself (primary cells). Furthermore, the omental tissue is non-diseased, i.e. normal omental tissue, to better represent the process of metastasis when cancer cells colonise healthy tissue. However, the ovarian cancer cells utilised in the present study, SKOV3 and A2780, are cell lines. Compared to primary cells, cell lines contain genetic alterations which may have changed their structure and function,(517) however in the case of SKOV3 and A2780, a mice study showed that injecting these cells resulted in tumour formation implying that their tumorigenicity appeared unaffected.(305) One study sought to profile several ovarian cancer cell lines, including SKOV3 and A2780, in terms of their clinical origin, morphology and genetic makeup; and the authors concluded that their extensive usage in in vitro studies are justified.(304) Contrastingly, another genetic profiling study on ovarian cancer cell lines reported that SKOV3 and A2780 cells have little genetic resemblance to HGSC.(518) Thus, it would be interesting to utilise primary ovarian cancer cells alongside these cell lines as a comparison, for example in terms of their

ability to induce HOMEC proliferation and in terms of adhesion to the mesothelium, as they may potentially reveal new targets for therapy development.

Building on the in vitro (2D) experiments conducted in the present study, 3D modelling studies is a viable option for future work. Examples include scaffold-based gels (e.g. Matrigel, alginate) or bioreactors (e.g. rotatable culture flasks), both of which consist of a mixture of cell types resembling the studied tissue, to better recreate the tumour microenvironment.(519) Presently, the investigation into the adhesion of cancer cells onto the mesothelial cell layer which utilises collagen IV as a suitable ECM for mesothelial cells, together with mechanical rocking to simulate peritoneal fluid movement, may potentially be classified as a 3D model. To improve the power of this model, other components or cell types may be included and structured within a scaffold-based gel, or bio-printed into a microfluidic chip device; e.g. inclusion of fibronectin and laminins with the collagen IV to better resemble the ECM, together with HOMECs, adipocytes and macrophages to better resemble native omental tissue.

In vivo animal studies are also avenues for future work and serve to verify the results of in vitro studies. For example, the present study postulated that leptin from omental adipocytes triggered the nearby metastatic cancer cells to secrete a pro-angiogenic factor to induce EC activation; thus inhibiting the action of leptin is a potential therapeutic target. In vivo studies may be useful to evaluate the efficacy of a leptin inhibitor in terms of inhibiting angiogenesis. Since leptin also has other roles in the body, e.g. appetite regulation and lipogenesis,(520, 521) the route of administration of a leptin inhibitor is also of significance as the therapeutic target ought to be leptin secreted by the omental adipocytes. Similarly, targeting adhesion molecules on the mesothelial cell surface requires precision in the route of therapy administration since mesothelial cells are present in other body cavities, such as the pleural (lung) cavity. Thus, animal studies are a suitable next step further work, and bridge the gap between in vitro studies and subsequent clinical studies in humans.

In summary, the data presented in this thesis highlight the complexity of the interaction between omental adipocytes, EOC cells and the host ECs during metastasis of ovarian cancer to the omentum. Additionally, it provides a possible rationale behind the disappointing results of the existing anti-VEGF

therapies and may be a useful starting point for development of future therapies that would ideally target multiple aspects of metastasis development.

Appendix

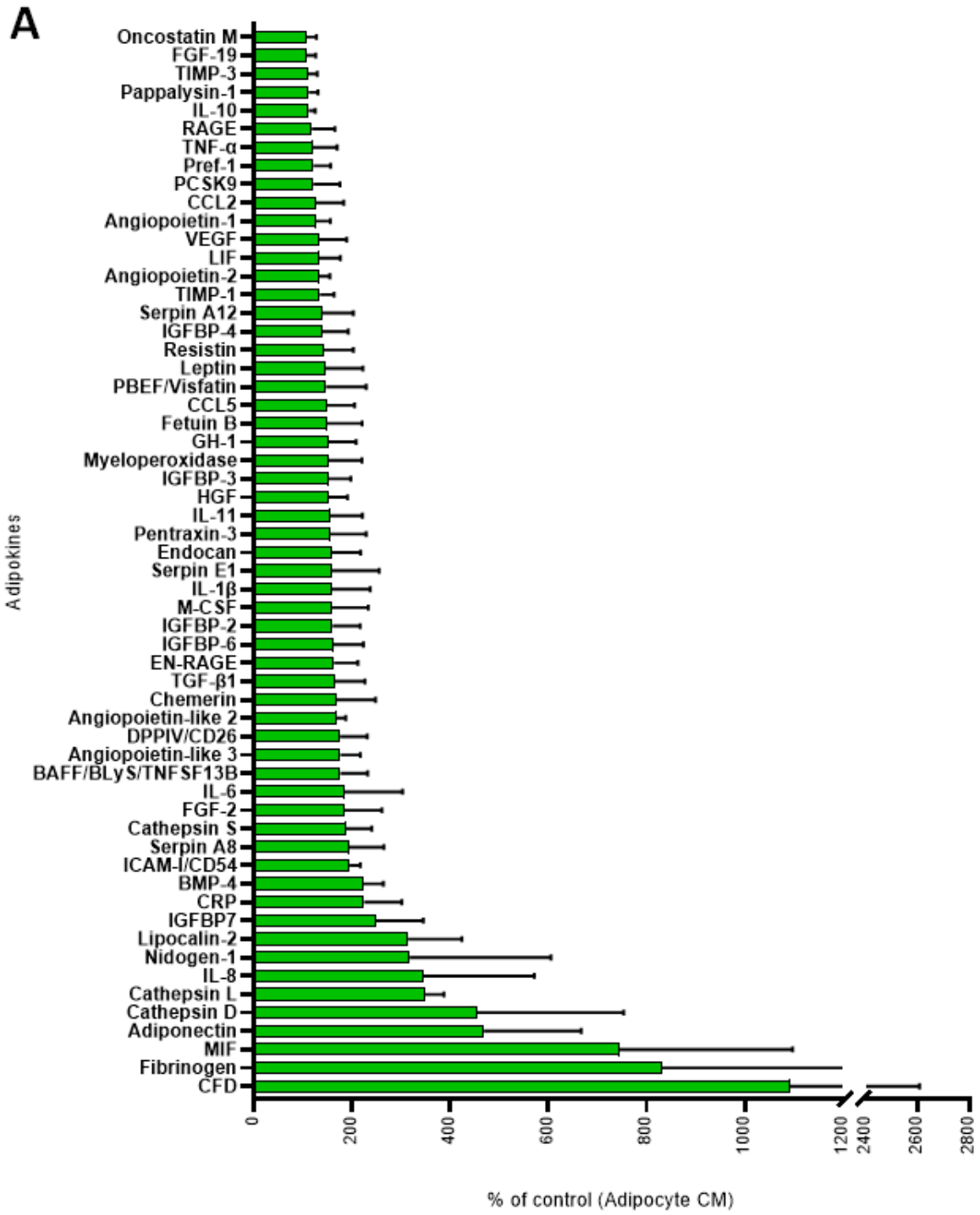
A
Oncostatin M
FGF-19
TIMP-3
Pappalysin-1
IL-10
RAGE
TNF-α
Pref-1
PCSK9
CCL2
Angiopoietin-1
VEGF
LIF
Angiopoietin-2
TIMP-1
Serpin A12
IGFBP-4
Resistin
Leptin
PBEF/Visfatin
CCL5
Fetuin B
GH-1
Myeloperoxidase
IGFBP-3
HGF
IL-11
Pentraxin-3
Endocan
Serpin E1
IL-1β
M-CSF
IGFBP-2
IGFBP-6
EN-RAGE
TGF-β1
Chemerin
Angiopoietin-like 2
DPPIV/CD26
Angiopoietin-like 3
BAFF/BLyS/TNFSF13B
IL-6
FGF-2
Cathepsin S
Serpin A8
ICAM-1/CD54
BMP-4
CRP
IGFBP7
Lipocalin-2
Nidogen-1
IL-8
Cathepsin L
Cathepsin D
Adiponectin
MIF
Fibrinogen
CFD
Adipokines
0
200
400
600
800
1000
1200
2400
2600
2800
% of control (Adipocyte CM)

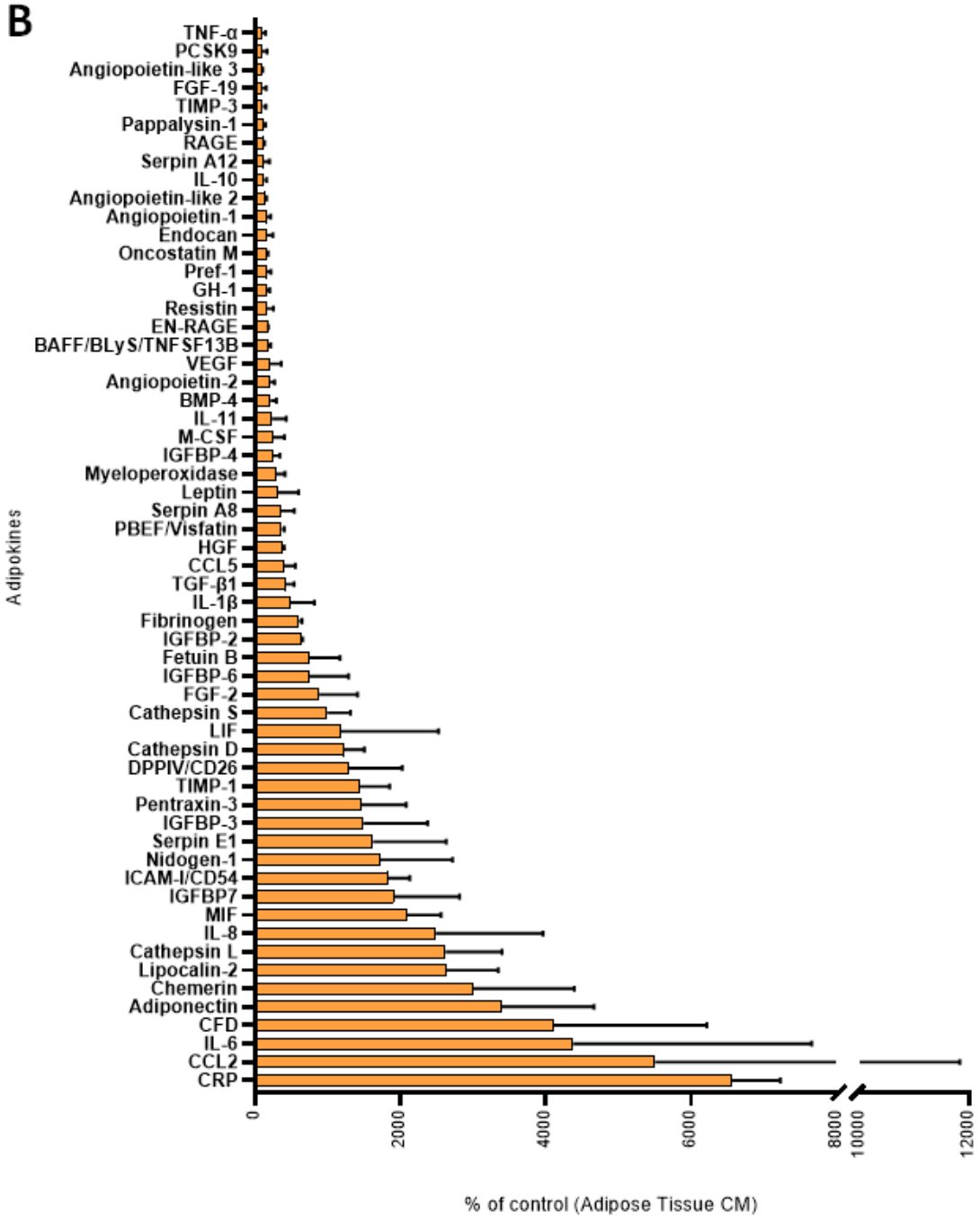

Figure 97. Range of adipokines secreted by omental adipocytes and adipose tissue. The average relative abundance, compared to control, of the 58 adipokines tested in adipocyte CM (n=3) (A) and adipose tissue CM (n=2) (B). CM containing 200µg of total protein, and equivalent volume of basal media as matched control, were incubated overnight on nitrocellulose membranes pre-spotted with capture antibodies for various adipokines. Following multiple washings, chemiluminescent reagents were applied prior to imaging the membranes. After subtracting the negative control, the abundance of each adipokine was calculated as a percentage of the basal media's (control) pixel density and averaged across replicates. CM: conditioned media.

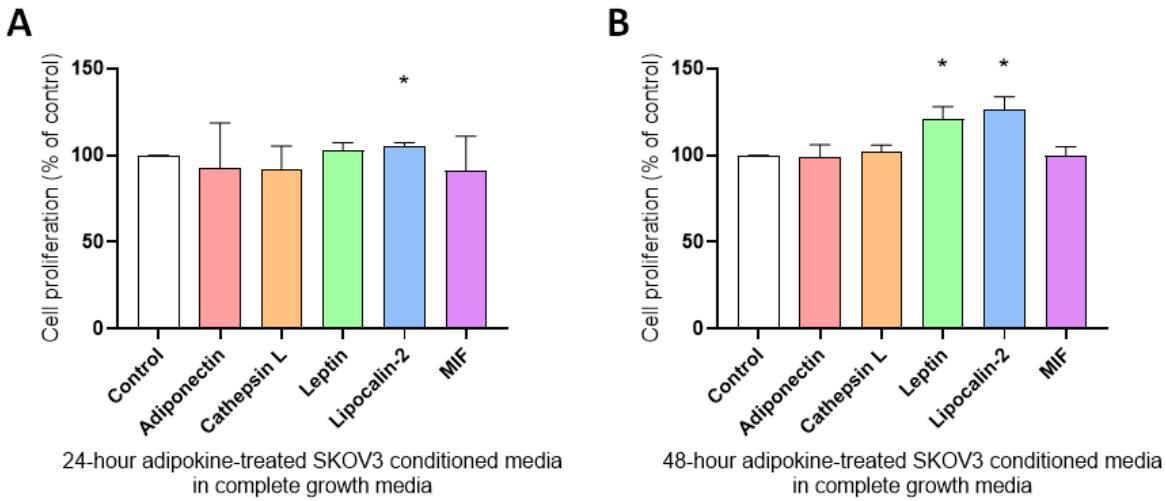

Figure 98. Conditioned media from SKOV3 pre-incubated with leptin or lipocalin-2 for 48 hours enhanced HOMEC proliferation as assessed by WST8 assay. HOMECs were seeded at 10,000 cells/well in 96-well plates and cultured for at least 24 hours before overnight serum starvation. SKOV3 conditioned media, composed of complete growth media, after incubation with individual adipokines for 24 (A) or 48 (B) hours, were applied onto cells. WST8 reagent was added after 24-hour treatment incubation and plates were read at 450nm after 2 hours. Results shown are mean ± SD and as a percentage of the control; data were analysed with Mann-Whitney U tests, n=3-4, *p<0.05 vs control.

Table 8. VEGF concentration in freshly derived CM is different from previously frozen CM from A2780 cells. A2780 cells were incubated with basal media (control) or leptin for 24 hours and the CM was then collected. Half of the CM was analysed by ELISA immediately, while the other half was frozen at -80°C for 10 days. The frozen CM was then thawed and analysed by ELISA. The supplied VEGF standards were diluted to the recommended range of concentrations, assayed in triplicate by ELISA and the absorbance read at 450nm. The absorbance values, after subtracting the blank controls, were interpolated on the standard curve to determine the VEGF concentrations.

	VEGF concentration intrapolated from standard curve (pg/mL)	
	Freshly derived CM	***CM thawed after frozen at -80°C for 10 days***
CM from control A2780	651	1197
CM from leptin-treated A2780	957	1876

Table 9. Activation (phosphorylation) of receptor tyrosine kinase targets in HOMECs treated with conditioned media from adipokine-incubated A2780 cells. HOMECs were treated with basal media, and CM from lipocalin-2-incubated A2780 cells and leptin-incubated A2780 cells for 5 minutes. HOMECs were then lysed, and lysate was incubated overnight with nitrocellulose membranes pre-spotted with capture antibodies for various phosphorylated receptor tyrosine kinases. Detection antibodies, streptavidin-HRP and chemiluminescent reagents were applied in between multiple washings, and the membranes imaged on the Azure 500 imager. Each target receptor was quantified by pixel density analysis; after subtracting background values, the abundance of each target was calculated as a percentage of the control. Only targets with values above the background levels are shown. CM: conditioned media.

	HOMEC treatment (average pixel density as a % of control CM)			
Target	**CM from lipocalin-2-incubated A2780 (A)**	**CM from lipocalin-2-incubated A2780 (B)**	**CM from leptin-incubated A2780 (A)**	**CM from leptin-incubated A2780 (B)**
ALK	138.9	143.2	175.3	145.0
Axl	88.6	155.5	137.9	142.1
c-Ret	106.5	128.8	126.0	99.0
DDR1	127.4	145.9	128.4	133.5
DDR2	93.3	106.9	113.4	81.6
Dtk	-	131.4	-	177.9
EGFR	-	63.9	-	65.4
EphA1	93.4	83.8	110.3	113.0
EphA10	79.8	138.7	123.5	115.2
EphA2	-	77.3	-	94.1
EphA4	93.5	156.9	140.6	163.3
EphA5	-	96.2	-	140.1
EphA6	100.1	-	92.8	-
EphB2	-	109.2	-	95.1
ErbB4	119.4	149.8	128.8	53.9
FGFR2α	127.0	152.5	156.0	101.5
FGFR3	-	186.2	-	222.7
HGFR	84.4	101.7	99.5	104.1
IGF-I R	-	73.3	-	37.5
M-CSFR	120.9	106.0	150.0	148.6
MSPR	103.0	-	125.9	-
PDGFRβ	92.3	-	111.6	-
ROR1	-	93.5	-	91.0
ROR2	-	153.4	-	177.0
RYK	115.3	139.5	139.1	118.6
Tie-1	76.0	131.3	131.0	137.4
Tie-2	98.3	97.7	109.8	88.3
VEGFR1	67.0	117.8	113.5	228.2
VEGFR2	66.3	109.8	130.4	115.8
VEGFR3	118.5	120.0	172.4	150.3

Table 10. Activation (phosphorylation) of receptor tyrosine kinase targets in HOMECs treated with conditioned media from adipokine-incubated SKOV3 cells. HOMECs were treated with basal media, and CM from lipocalin-2-incubated SKOV3 cells and leptin-incubated SKOV3 cells for 5 minutes. HOMECs were then lysed, and lysate was incubated overnight with nitrocellulose membranes pre-spotted with capture antibodies for various phosphorylated receptor tyrosine kinases. Detection antibodies, streptavidin-HRP and chemiluminescent reagents were applied in between multiple washings, and the membranes imaged on the Azure 500 imager. Each target receptor was quantified by pixel density analysis; after subtracting background values, the abundance of each target was calculated as a percentage of the control. Only targets with values above the background levels are shown. CM: conditioned media.

	HOMEC treatment (average pixel density as a % of control CM)			
Target	**CM from lipocalin-2-incubated SKOV3 (A)**	**CM from lipocalin-2-incubated SKOV3 (B)**	**CM from leptin-incubated SKOV3 (A)**	**CM from leptin-incubated SKOV3 (B)**
ALK	87.4	119.7	124.7	66.4
Axl	-	65.4	-	78.4
c-Ret	122.4	127.7	187.4	87.9
DDR1	107.8	219.2	121.0	105.8
DDR2	95.9	109.6	144.5	93.7
Dtk	-	83.2	-	95.1
EGFR	-	151.9	-	104.3
EphA1	-	75.6	-	92.7
EphA10	124.2	115.0	147.0	90.7
EphA2	-	49.9	-	109.9
EphA4	88.9	91.7	117.9	96.0
EphA5	-	78.9	-	100.5
EphB2	-	123.4	-	118.1
EphB3	-	101.2	-	70.7
ErbB4	155.0	214.0	245.6	115.4
FGFR1	-	106.8	-	118.3
FGFR2α	130.0	136.4	258.2	171.4
FGFR3	-	79.4	-	72.5
Flt-3	97.9	105.6	216.8	88.4
IGF-I R	-	61.4	-	94.2
M-CSFR	-	86.7	-	98.8
MSPR	-	140.7	-	121.5
PDGFRβ	-	105.4	-	120.0
ROR1	-	88.5	-	88.5
ROR2	-	80.9	-	83.6
RYK	159.0	143.4	238.9	123.3
Tie-1	106.5	89.8	127.4	85.6
Tie-2	102.9	120.6	153.0	100.5
VEGFR1	113.5	80.1	139.9	102.8
VEGFR2	90.2	148.3	201.0	119.8
VEGFR3	87.3	108.8	128.0	85.0

Table 11. Activation (phosphorylation) of receptor tyrosine kinase targets in HOMECs treated with conditioned media from omental adipose tissue. HOMECs were treated with basal media and adipose tissue CM for 5 minutes. HOMECs were then lysed, and lysate was incubated overnight with nitrocellulose membranes pre-spotted with capture antibodies for various phosphorylated receptor tyrosine kinases. Detection antibodies, streptavidin-HRP and chemiluminescent reagents were applied in between multiple washings, and the membranes imaged on the Azure 500 imager. Each target receptor was quantified by pixel density analysis; after subtracting background values, the abundance of each target was calculated as a percentage of the control. Only targets with values above the background levels are shown. CM: conditioned media.

	HOMEC treatment (average pixel density as a % of control CM)	
Target	**Adipose tissue CM (A)**	**Adipose tissue CM (B)**
ALK	327.2	149.9
Axl	112.5	95.7
c-Ret	202.7	120.8
DDR1	139.1	137.3
Dtk	318.7	-
EGFR	-	77.3
EphA10	180.4	113.5
EphA4	202.1	98.0
EphA6	217.7	178.3
ErbB4	214.7	155.3
FGFR2α	235.3	144.9
FGFR3	219.4	116.4
HGFR	-	78.2
M-CSFR	158.9	107.0
PDGFRα	120.5	-
RYK	275.5	105.3
Tie-1	127.9	97.3
Tie-2	189.3	143.8
TrkA	173.4	-
VEGFR1	64.6	58.3
VEGFR2	85.2	89.0
VEGFR3	214.9	111.0

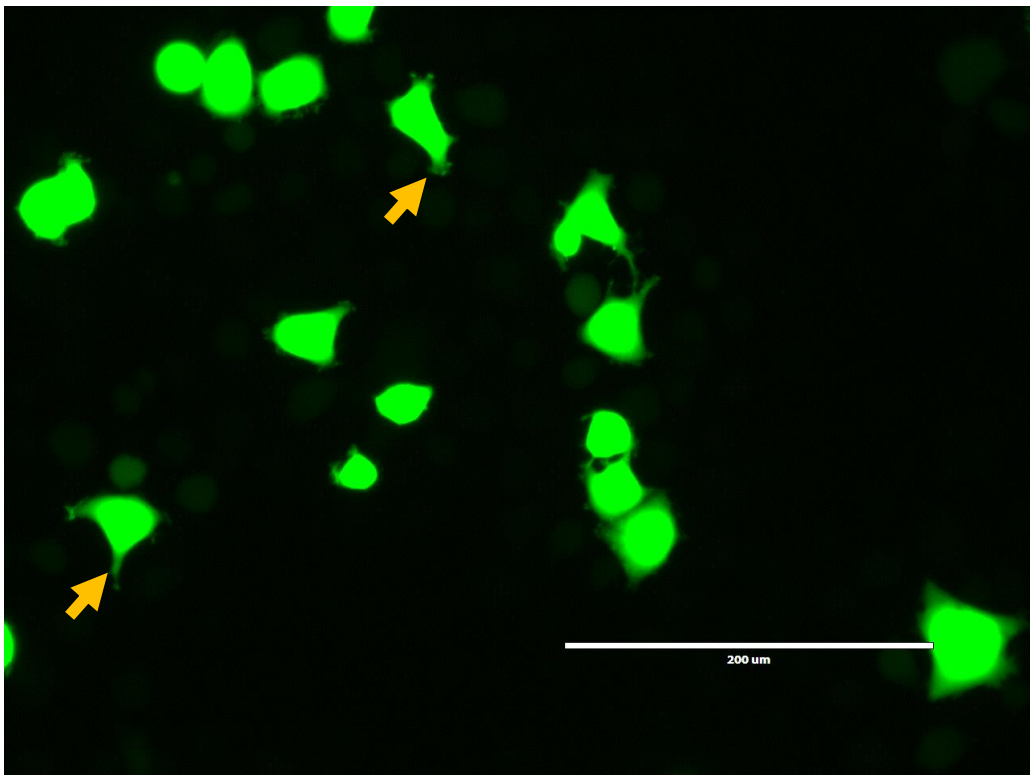

Figure 99. Pseudopodial projections of SKOV3 cells, marked with arrows. Calcein AM-labelled SKOV3 cells suspended in SKOV3 CM (10,000 cells/500µL) were applied onto confluent mesothelial cells in 24-well plates. After 48 hours the wells were washed with complete growth media. Cells were fixed with 4% (v/v) paraformaldehyde at room temperature and visualised using EVOS Fluo at 20x magnification. Scale bar 200µm.

References

1. Sung H, Ferlay J, Siegel RL, Laversanne M, Soerjomataram I, Jemal A, et al. Global Cancer Statistics 2020: GLOBOCAN Estimates of Incidence and Mortality Worldwide for 36 Cancers in 185 Countries. CA Cancer J Clin. 2021;71(3):209-49.
2. Matz M, Coleman MP, Carreira H, Salmeron D, Chirlaque MD, Allemani C, et al. Worldwide comparison of ovarian cancer survival: Histological group and stage at diagnosis (CONCORD-2). Gynecol Oncol. 2017;144(2):396-404.
3. Cancer Research UK. Ovarian cancer survival by stage at diagnosis [updated November 2019. Available from: https://www.cancerresearchuk.org/health-professional/cancer-statistics/statistics-by-cancer-type/ovarian-cancer/survival#heading-Three.
4. Pugsley MK, Tabrizchi R. The vascular system. An overview of structure and function. J Pharmacol Toxicol Methods. 2000;44(2):333-40.
5. Yuan SY, Rigor RR. Chapter 2, Structure and Function of Exchange Microvessels. Regulation of Endothelial Barrier Function. San Rafael (CA): Morgan & Claypool Life Sciences; 2010.
6. Kruger-Genge A, Blocki A, Franke RP, Jung F. Vascular Endothelial Cell Biology: An Update. Int J Mol Sci. 2019;20(18).
7. Eelen G, de Zeeuw P, Treps L, Harjes U, Wong BW, Carmeliet P. Endothelial Cell Metabolism. Physiol Rev. 2018;98(1):3-58.
8. Chi JT, Chang HY, Haraldsen G, Jahnsen FL, Troyanskaya OG, Chang DS, et al. Endothelial cell diversity revealed by global expression profiling. Proc Natl Acad Sci U S A. 2003;100(19):10623-8.
9. Aird WC. Phenotypic heterogeneity of the endothelium: I. Structure, function, and mechanisms. Circ Res. 2007;100(2):158-73.
10. Curry FE, Adamson RH. Endothelial glycocalyx: permeability barrier and mechanosensor. Ann Biomed Eng. 2012;40(4):828-39.
11. Tarbell JM, Pahakis MY. Mechanotransduction and the glycocalyx. J Intern Med. 2006;259(4):339-50.
12. Dejana E. Endothelial cell-cell junctions: happy together. Nat Rev Mol Cell Biol. 2004;5(4):261-70.
13. Gao C, Sun W, Christofidou-Solomidou M, Sawada M, Newman DK, Bergom C, et al. PECAM-1 functions as a specific and potent inhibitor of mitochondrial-dependent apoptosis. Blood. 2003;102(1):169-79.
14. DeLeve LD, Maretti-Mira AC. Liver Sinusoidal Endothelial Cell: An Update. Semin Liver Dis. 2017;37(4):377-87.
15. Frank PG, Pavlides S, Lisanti MP. Caveolae and transcytosis in endothelial cells: role in atherosclerosis. Cell Tissue Res. 2009;335(1):41-7.
16. Dvorak HF. Reconciling VEGF With VPF: The Importance of Increased Vascular Permeability for Stroma Formation in Tumors, Healing Wounds, and Chronic Inflammation. Front Cell Dev Biol. 2021;9:660609.
17. Dvorak AM, Feng D. The vesiculo-vacuolar organelle (VVO). A new endothelial cell permeability organelle. J Histochem Cytochem. 2001;49(4):419-32.
18. Sandoo A, van Zanten JJ, Metsios GS, Carroll D, Kitas GD. The endothelium and its role in regulating vascular tone. Open Cardiovasc Med J. 2010;4:302-12.
19. Edwards G, Feletou M, Weston AH. Endothelium-derived hyperpolarising factors and associated pathways: a synopsis. Pflugers Arch. 2010;459(6):863-79.

20. Alonso D, Radomski MW. The nitric oxide-endothelin-1 connection. Heart Fail Rev. 2003;8(1):107-15.
21. Yau JW, Teoh H, Verma S. Endothelial cell control of thrombosis. BMC Cardiovasc Disord. 2015;15:130.
22. Feletou M. The Endothelium: Part 1: Multiple Functions of the Endothelial Cells-Focus on Endothelium-Derived Vasoactive Mediators. Integrated Systems Physiology: from Molecule to Function to Disease. San Rafael (CA)2011.
23. Reitsma S, Slaaf DW, Vink H, van Zandvoort MA, oude Egbrink MG. The endothelial glycocalyx: composition, functions, and visualization. Pflugers Arch. 2007;454(3):345-59.
24. Jackson CJ, Nguyen M. Human microvascular endothelial cells differ from macrovascular endothelial cells in their expression of matrix metalloproteinases. Int J Biochem Cell Biol. 1997;29(10):1167-77.
25. Grafe M, Auch-Schwelk W, Hertel H, Terbeek D, Steinheider G, Loebe M, et al. Human cardiac microvascular and macrovascular endothelial cells respond differently to oxidatively modified LDL. Atherosclerosis. 1998;137(1):87-95.
26. Snopko R, Guffy T, Rafelson M, Hall E. Serum stimulation of prostacyclin synthesis in aortically, venously and microvascularly derived endothelial cells. Clin Physiol Biochem. 1987;5(2):70-6.
27. Pepper MS, Montesano R, el Aoumari A, Gros D, Orci L, Meda P. Coupling and connexin 43 expression in microvascular and large vessel endothelial cells. Am J Physiol. 1992;262(5 Pt 1):C1246-57.
28. Cavallaro U, Castelli V, Del Monte U, Soria MR. Phenotypic alterations in senescent large-vessel and microvascular endothelial cells. Mol Cell Biol Res Commun. 2000;4(2):117-21.
29. Adair TH, Montani JP. Angiogenesis. Integrated Systems Physiology: from Molecule to Function to Disease. San Rafael (CA)2010.
30. Alberts B, Johnson A, Lewis J, Raff M, Roberts K, Walter P. Blood Vessels and Endothelial Cells. Molecular Biology of the Cell. 4th ed. New York: Garland Science; 2002.
31. Carmeliet P, Jain RK. Molecular mechanisms and clinical applications of angiogenesis. Nature. 2011;473(7347):298-307.
32. van Hinsbergh VW, Koolwijk P. Endothelial sprouting and angiogenesis: matrix metalloproteinases in the lead. Cardiovasc Res. 2008;78(2):203-12.
33. Lugano R, Ramachandran M, Dimberg A. Tumor angiogenesis: causes, consequences, challenges and opportunities. Cell Mol Life Sci. 2020;77(9):1745-70.
34. Peach CJ, Mignone VW, Arruda MA, Alcobia DC, Hill SJ, Kilpatrick LE, et al. Molecular Pharmacology of VEGF-A Isoforms: Binding and Signalling at VEGFR2. Int J Mol Sci. 2018;19(4).
35. Bates DO, Cui TG, Doughty JM, Winkler M, Sugiono M, Shields JD, et al. VEGF165b, an inhibitory splice variant of vascular endothelial growth factor, is down-regulated in renal cell carcinoma. Cancer Res. 2002;62(14):4123-31.
36. Hellstrom M, Phng LK, Hofmann JJ, Wallgard E, Coultas L, Lindblom P, et al. Dll4 signalling through Notch1 regulates formation of tip cells during angiogenesis. Nature. 2007;445(7129):776-80.
37. Gelfand MV, Hong S, Gu C. Guidance from above: common cues direct distinct signaling outcomes in vascular and neural patterning. Trends Cell Biol. 2009;19(3):99-110.

38. Iragavarapu-Charyulu V, Wojcikiewicz E, Urdaneta A. Semaphorins in Angiogenesis and Autoimmune Diseases: Therapeutic Targets? Front Immunol. 2020;11:346.
39. Wang Y, Nakayama M, Pitulescu ME, Schmidt TS, Bochenek ML, Sakakibara A, et al. Ephrin-B2 controls VEGF-induced angiogenesis and lymphangiogenesis. Nature. 2010;465(7297):483-6.
40. Lawler PR, Lawler J. Molecular basis for the regulation of angiogenesis by thrombospondin-1 and -2. Cold Spring Harb Perspect Med. 2012;2(5):a006627.
41. Walia A, Yang JF, Huang YH, Rosenblatt MI, Chang JH, Azar DT. Endostatin's emerging roles in angiogenesis, lymphangiogenesis, disease, and clinical applications. Biochim Biophys Acta. 2015;1850(12):2422-38.
42. Li T, Kang G, Wang T, Huang H. Tumor angiogenesis and anti-angiogenic gene therapy for cancer. Oncol Lett. 2018;16(1):687-702.
43. Huang X, Jia L, Qian Z, Jia Y, Chen X, Xu X, et al. Diversity in human placental microvascular endothelial cells and macrovascular endothelial cells. Cytokine. 2018;111:287-94.
44. Hanahan D, Weinberg RA. Hallmarks of cancer: the next generation. Cell. 2011;144(5):646-74.
45. Bielenberg DR, Zetter BR. The Contribution of Angiogenesis to the Process of Metastasis. Cancer J. 2015;21(4):267-73.
46. Liao D, Johnson RS. Hypoxia: a key regulator of angiogenesis in cancer. Cancer Metastasis Rev. 2007;26(2):281-90.
47. Mandriota SJ, Pepper MS. Vascular endothelial growth factor-induced in vitro angiogenesis and plasminogen activator expression are dependent on endogenous basic fibroblast growth factor. J Cell Sci. 1997;110 (Pt 18):2293-302.
48. Li T, Jiang S. Effect of bFGF on invasion of ovarian cancer cells through the regulation of Ets-1 and urokinase-type plasminogen activator. Pharm Biol. 2010;48(2):161-5.
49. Kumar V, Patel S, Tcyganov E, Gabrilovich DI. The Nature of Myeloid-Derived Suppressor Cells in the Tumor Microenvironment. Trends Immunol. 2016;37(3):208-20.
50. Kujawski M, Kortylewski M, Lee H, Herrmann A, Kay H, Yu H. Stat3 mediates myeloid cell-dependent tumor angiogenesis in mice. J Clin Invest. 2008;118(10):3367-77.
51. Ardi VC, Kupriyanova TA, Deryugina EI, Quigley JP. Human neutrophils uniquely release TIMP-free MMP-9 to provide a potent catalytic stimulator of angiogenesis. Proc Natl Acad Sci U S A. 2007;104(51):20262-7.
52. Chung AS, Lee J, Ferrara N. Targeting the tumour vasculature: insights from physiological angiogenesis. Nat Rev Cancer. 2010;10(7):505-14.
53. Majidpoor J, Mortezaee K. Angiogenesis as a hallmark of solid tumors - clinical perspectives. Cell Oncol (Dordr). 2021;44(4):715-37.
54. Egeblad M, Nakasone ES, Werb Z. Tumors as organs: complex tissues that interface with the entire organism. Dev Cell. 2010;18(6):884-901.
55. Hosaka K, Yang Y, Seki T, Fischer C, Dubey O, Fredlund E, et al. Pericyte-fibroblast transition promotes tumor growth and metastasis. Proc Natl Acad Sci U S A. 2016;113(38):E5618-27.
56. Monk BJ, Minion LE, Coleman RL. Anti-angiogenic agents in ovarian cancer: past, present, and future. Ann Oncol. 2016;27 Suppl 1:i33-i9.
57. Cancer Research UK. One-, five- and ten-year survival for ovarian cancer [updated April 2020. Available from:

https://www.cancerresearchuk.org/health-professional/cancer-statistics/statistics-by-cancer-type/ovarian-cancer/survival#heading-Zero.
58. Office for National Statistics. Cancer Survival in England: adults diagnosed between 2013 and 2017 and followed up to 2018 2019 [updated November 2019. Available from: https://www.ons.gov.uk/peoplepopulationandcommunity/healthandsocialcare/conditionsanddiseases/datasets/cancersurvivalratescancersurvivalinenglandadultsdiagnosed.
59. Prat J, Figo Committee on Gynecologic Oncology. Staging classification for cancer of the ovary, fallopian tube, and peritoneum. Int J Gynaecol Obstet. 2014;124(1):1-5.
60. Kim J, Park EY, Kim O, Schilder JM, Coffey DM, Cho CH, et al. Cell Origins of High-Grade Serous Ovarian Cancer. Cancers (Basel). 2018;10(11).
61. Sundar S, Neal RD, Kehoe S. Diagnosis of ovarian cancer. BMJ. 2015;351:h4443.
62. Vargas AN. Natural history of ovarian cancer. Ecancermedicalscience. 2014;8:465.
63. Low EL, Waller J, Menon U, Jones A, Reid F, Simon AE. Ovarian cancer symptom awareness and anticipated time to help-seeking for symptoms among UK women. J Fam Plann Reprod Health Care. 2013;39(3):163-71.
64. Stewart C, Ralyea C, Lockwood S. Ovarian Cancer: An Integrated Review. Semin Oncol Nurs. 2019;35(2):151-6.
65. Shaaban AM, Rezvani M, Elsayes KM, Baskin H, Jr., Mourad A, Foster BR, et al. Ovarian malignant germ cell tumors: cellular classification and clinical and imaging features. Radiographics. 2014;34(3):777-801.
66. Simone CG, Markham MJ, Dizon DS. Chemotherapy in ovarian germ cell tumors: A systematic review. Gynecol Oncol. 2016;141(3):602-7.
67. Veneris JT, Mahajan P, Frazier AL. Contemporary management of ovarian germ cell tumors and remaining controversies. Gynecol Oncol. 2020;158(2):467-75.
68. Al Harbi R, McNeish IA, El-Bahrawy M. Ovarian sex cord-stromal tumors: an update on clinical features, molecular changes, and management. Int J Gynecol Cancer. 2021;31(2):161-8.
69. Schultz KA, Harris AK, Schneider DT, Young RH, Brown J, Gershenson DM, et al. Ovarian Sex Cord-Stromal Tumors. J Oncol Pract. 2016;12(10):940-6.
70. Zafrakas M, Grimbizis G, Timologou A, Tarlatzis BC. Endometriosis and ovarian cancer risk: a systematic review of epidemiological studies. Front Surg. 2014;1:14.
71. Bouchard-Fortier G, Panzarella T, Rosen B, Chapman W, Gien LT. Endometrioid Carcinoma of the Ovary: Outcomes Compared to Serous Carcinoma After 10 Years of Follow-Up. J Obstet Gynaecol Can. 2017;39(1):34-41.
72. Iida Y, Okamoto A, Hollis RL, Gourley C, Herrington CS. Clear cell carcinoma of the ovary: a clinical and molecular perspective. Int J Gynecol Cancer. 2021;31(4):605-16.
73. Babaier A, Ghatage P. Mucinous Cancer of the Ovary: Overview and Current Status. Diagnostics (Basel). 2020;10(1).
74. Maringe C, Walters S, Butler J, Coleman MP, Hacker N, Hanna L, et al. Stage at diagnosis and ovarian cancer survival: evidence from the International Cancer Benchmarking Partnership. Gynecol Oncol. 2012;127(1):75-82.

75. Kurman RJ, Shih Ie M. The origin and pathogenesis of epithelial ovarian cancer: a proposed unifying theory. Am J Surg Pathol. 2010;34(3):433-43.
76. Rosenblatt KA, Thomas DB. Reduced risk of ovarian cancer in women with a tubal ligation or hysterectomy. The World Health Organization Collaborative Study of Neoplasia and Steroid Contraceptives. Cancer Epidemiol Biomarkers Prev. 1996;5(11):933-5.
77. Kvaskoff M, Mahamat-Saleh Y, Farland LV, Shigesi N, Terry KL, Harris HR, et al. Endometriosis and cancer: a systematic review and meta-analysis. Hum Reprod Update. 2021;27(2):393-420.
78. Marquez RT, Baggerly KA, Patterson AP, Liu J, Broaddus R, Frumovitz M, et al. Patterns of gene expression in different histotypes of epithelial ovarian cancer correlate with those in normal fallopian tube, endometrium, and colon. Clin Cancer Res. 2005;11(17):6116-26.
79. Medeiros F, Muto MG, Lee Y, Elvin JA, Callahan MJ, Feltmate C, et al. The tubal fimbria is a preferred site for early adenocarcinoma in women with familial ovarian cancer syndrome. Am J Surg Pathol. 2006;30(2):230-6.
80. Antoniou A, Pharoah PD, Narod S, Risch HA, Eyfjord JE, Hopper JL, et al. Average risks of breast and ovarian cancer associated with BRCA1 or BRCA2 mutations detected in case Series unselected for family history: a combined analysis of 22 studies. Am J Hum Genet. 2003;72(5):1117-30.
81. Carcangiu ML, Radice P, Manoukian S, Spatti G, Gobbo M, Pensotti V, et al. Atypical epithelial proliferation in fallopian tubes in prophylactic salpingo-oophorectomy specimens from BRCA1 and BRCA2 germline mutation carriers. Int J Gynecol Pathol. 2004;23(1):35-40.
82. Berek JS, Kehoe ST, Kumar L, Friedlander M. Cancer of the ovary, fallopian tube, and peritoneum. Int J Gynaecol Obstet. 2018;143 Suppl 2:59-78.
83. Chui MH, Shih IM. Oncogenic BRAF and KRAS mutations in endosalpingiosis. J Pathol. 2020;250(2):148-58.
84. Dubeau L. The cell of origin of ovarian epithelial tumours. Lancet Oncol. 2008;9(12):1191-7.
85. Fathalla MF. Incessant ovulation--a factor in ovarian neoplasia? Lancet. 1971;2(7716):163.
86. Fleming JS, Beaugie CR, Haviv I, Chenevix-Trench G, Tan OL. Incessant ovulation, inflammation and epithelial ovarian carcinogenesis: revisiting old hypotheses. Mol Cell Endocrinol. 2006;247(1-2):4-21.
87. Momenimovahed Z, Tiznobaik A, Taheri S, Salehiniya H. Ovarian cancer in the world: epidemiology and risk factors. Int J Womens Health. 2019;11:287-99.
88. Ness RB, Grisso JA, Cottreau C, Klapper J, Vergona R, Wheeler JE, et al. Factors related to inflammation of the ovarian epithelium and risk of ovarian cancer. Epidemiology. 2000;11(2):111-7.
89. Yue W, Yager JD, Wang JP, Jupe ER, Santen RJ. Estrogen receptor-dependent and independent mechanisms of breast cancer carcinogenesis. Steroids. 2013;78(2):161-70.
90. Mizushima T, Miyamoto H. The Role of Androgen Receptor Signaling in Ovarian Cancer. Cells. 2019;8(2).
91. Ford CE, Werner B, Hacker NF, Warton K. The untapped potential of ascites in ovarian cancer research and treatment. Br J Cancer. 2020;123(1):9-16.
92. Szender JB, Emmons T, Belliotti S, Dickson D, Khan A, Morrell K, et al. Impact of ascites volume on clinical outcomes in ovarian cancer: A cohort study. Gynecol Oncol. 2017;146(3):491-7.

93. Cavazzoni E, Bugiantella W, Graziosi L, Franceschini MS, Donini A. Malignant ascites: pathophysiology and treatment. Int J Clin Oncol. 2013;18(1):1-9.
94. Vergote I, Trope CG, Amant F, Kristensen GB, Ehlen T, Johnson N, et al. Neoadjuvant chemotherapy or primary surgery in stage IIIC or IV ovarian cancer. N Engl J Med. 2010;363(10):943-53.
95. Cortez AJ, Tudrej P, Kujawa KA, Lisowska KM. Advances in ovarian cancer therapy. Cancer Chemother Pharmacol. 2018;81(1):17-38.
96. McGuire WP, Hoskins WJ, Brady MF, Kucera PR, Partridge EE, Look KY, et al. Cyclophosphamide and cisplatin compared with paclitaxel and cisplatin in patients with stage III and stage IV ovarian cancer. N Engl J Med. 1996;334(1):1-6.
97. Kumar S, Mahdi H, Bryant C, Shah JP, Garg G, Munkarah A. Clinical trials and progress with paclitaxel in ovarian cancer. Int J Womens Health. 2010;2:411-27.
98. Garcia J, Hurwitz HI, Sandler AB, Miles D, Coleman RL, Deurloo R, et al. Bevacizumab (Avastin(R)) in cancer treatment: A review of 15 years of clinical experience and future outlook. Cancer Treat Rev. 2020;86:102017.
99. Liu S, Kasherman L, Fazelzad R, Wang L, Bouchard-Fortier G, Lheureux S, et al. The use of bevacizumab in the modern era of targeted therapy for ovarian cancer: A systematic review and meta-analysis. Gynecol Oncol. 2021;161(2):601-12.
100. Shimizu Y, Kajiyama H, Yoshida K, Tamauchi S, Nakanishi T, Kikkawa F. The usefulness of bevacizumab for relief from symptomatic malignant ascites in patients with heavily treated recurrent ovarian cancer. J Obstet Gynaecol Res. 2019;45(12):2435-9.
101. Tewari KS, Burger RA, Enserro D, Norquist BM, Swisher EM, Brady MF, et al. Final Overall Survival of a Randomized Trial of Bevacizumab for Primary Treatment of Ovarian Cancer. J Clin Oncol. 2019;37(26):2317-28.
102. Perren TJ, Swart AM, Pfisterer J, Ledermann JA, Pujade-Lauraine E, Kristensen G, et al. A phase 3 trial of bevacizumab in ovarian cancer. N Engl J Med. 2011;365(26):2484-96.
103. Burger RA, Brady MF, Bookman MA, Fleming GF, Monk BJ, Huang H, et al. Incorporation of bevacizumab in the primary treatment of ovarian cancer. N Engl J Med. 2011;365(26):2473-83.
104. Deng Z, Zhou J, Han X, Li X. TCEB2 confers resistance to VEGF-targeted therapy in ovarian cancer. Oncol Rep. 2016;35(1):359-65.
105. Mesange P, Poindessous V, Sabbah M, Escargueil AE, de Gramont A, Larsen AK. Intrinsic bevacizumab resistance is associated with prolonged activation of autocrine VEGF signaling and hypoxia tolerance in colorectal cancer cells and can be overcome by nintedanib, a small molecule angiokinase inhibitor. Oncotarget. 2014;5(13):4709-21.
106. Winiarski BK, Wolanska KI, Rai S, Ahmed T, Acheson N, Gutowski NJ, et al. Epithelial ovarian cancer-induced angiogenic phenotype of human omental microvascular endothelial cells may occur independently of VEGF signaling. Transl Oncol. 2013;6(6):703-14.
107. Li L, Nan F, Guo Q, Guan D, Zhou C. Resistance to bevacizumab in ovarian cancer SKOV3 xenograft due to EphB4 overexpression. J Cancer Res Ther. 2019;15(6):1282-7.
108. Basu P, Mukhopadhyay A, Konishi I. Targeted therapy for gynecologic cancers: Toward the era of precision medicine. Int J Gynaecol Obstet. 2018;143 Suppl 2:131-6.

109. Shao F, Liu J, Duan Y, Li L, Liu L, Zhang C, et al. Efficacy and safety of PARP inhibitors as the maintenance therapy in ovarian cancer: a meta-analysis of nine randomized controlled trials. Biosci Rep. 2020;40(3).
110. Huang XZ, Jia H, Xiao Q, Li RZ, Wang XS, Yin HY, et al. Efficacy and Prognostic Factors for PARP Inhibitors in Patients With Ovarian Cancer. Front Oncol. 2020;10:958.
111. Delgado A, Guddati AK. Clinical endpoints in oncology - a primer. Am J Cancer Res. 2021;11(4):1121-31.
112. van Zijl F, Krupitza G, Mikulits W. Initial steps of metastasis: cell invasion and endothelial transmigration. Mutat Res. 2011;728(1-2):23-34.
113. Mack GS, Marshall A. Lost in migration. Nat Biotechnol. 2010;28(3):214-29.
114. Hapach LA, Mosier JA, Wang W, Reinhart-King CA. Engineered models to parse apart the metastatic cascade. NPJ Precis Oncol. 2019;3:20.
115. Jiang WG, Sanders AJ, Katoh M, Ungefroren H, Gieseler F, Prince M, et al. Tissue invasion and metastasis: Molecular, biological and clinical perspectives. Semin Cancer Biol. 2015;35 Suppl:S244-S75.
116. Naora H, Montell DJ. Ovarian cancer metastasis: integrating insights from disparate model organisms. Nat Rev Cancer. 2005;5(5):355-66.
117. Lengyel E. Ovarian cancer development and metastasis. Am J Pathol. 2010;177(3):1053-64.
118. Tan DS, Agarwal R, Kaye SB. Mechanisms of transcoelomic metastasis in ovarian cancer. Lancet Oncol. 2006;7(11):925-34.
119. Yousefi M, Dehghani S, Nosrati R, Ghanei M, Salmaninejad A, Rajaie S, et al. Current insights into the metastasis of epithelial ovarian cancer - hopes and hurdles. Cell Oncol (Dordr). 2020;43(4):515-38.
120. Heitz F, Harter P, Ataseven B, Heikaus S, Schneider S, Prader S, et al. Stage- and Histologic Subtype-Dependent Frequency of Lymph Node Metastases in Patients with Epithelial Ovarian Cancer Undergoing Systematic Pelvic and Paraaortic Lymphadenectomy. Ann Surg Oncol. 2018;25(7):2053-9.
121. Pano B, Sebastia C, Ripoll E, Paredes P, Salvador R, Bunesch L, et al. Pathways of lymphatic spread in gynecologic malignancies. Radiographics. 2015;35(3):916-45.
122. Griffin N, Burke C, Grant LA. Common primary tumours of the abdomen and pelvis and their patterns of tumour spread as seen on multi-detector computed tomography. Insights Imaging. 2011;2(3):205-14.
123. Wong SY, Hynes RO. Lymphatic or hematogenous dissemination: how does a metastatic tumor cell decide? Cell Cycle. 2006;5(8):812-7.
124. Tarin D, Price JE, Kettlewell MG, Souter RG, Vass AC, Crossley B. Mechanisms of human tumor metastasis studied in patients with peritoneovenous shunts. Cancer Res. 1984;44(8):3584-92.
125. Romero-Laorden N, Olmos D, Fehm T, Garcia-Donas J, Diaz-Padilla I. Circulating and disseminated tumor cells in ovarian cancer: a systematic review. Gynecol Oncol. 2014;133(3):632-9.
126. Cui L, Kwong J, Wang CC. Prognostic value of circulating tumor cells and disseminated tumor cells in patients with ovarian cancer: a systematic review and meta-analysis. J Ovarian Res. 2015;8:38.
127. Zhang X, Li H, Yu X, Li S, Lei Z, Li C, et al. Analysis of Circulating Tumor Cells in Ovarian Cancer and Their Clinical Value as a Biomarker. Cell Physiol Biochem. 2018;48(5):1983-94.

128. Pradeep S, Kim SW, Wu SY, Nishimura M, Chaluvally-Raghavan P, Miyake T, et al. Hematogenous metastasis of ovarian cancer: rethinking mode of spread. Cancer Cell. 2014;26(1):77-91.
129. Yoo E, Kim JH, Kim MJ, Yu JS, Chung JJ, Yoo HS, et al. Greater and lesser omenta: normal anatomy and pathologic processes. Radiographics. 2007;27(3):707-20.
130. Weidle UH, Birzele F, Kollmorgen G, Rueger R. Mechanisms and Targets Involved in Dissemination of Ovarian Cancer. Cancer Genomics Proteomics. 2016;13(6):407-23.
131. Bandyopadhyay A, Raghavan S. Defining the role of integrin alphavbeta6 in cancer. Curr Drug Targets. 2009;10(7):645-52.
132. Saldanha RG, Molloy MP, Bdeir K, Cines DB, Song X, Uitto PM, et al. Proteomic identification of lynchpin urokinase plasminogen activator receptor protein interactions associated with epithelial cancer malignancy. J Proteome Res. 2007;6(3):1016-28.
133. Liew PL, Hsu CS, Liu WM, Lee YC, Lee YC, Chen CL. Prognostic and predictive values of Nrf2, Keap1, p16 and E-cadherin expression in ovarian epithelial carcinoma. Int J Clin Exp Pathol. 2015;8(5):5642-9.
134. Bacic B, Haller H, Mrklic I, Kosta V, Caric A, Tomic S. Prognostic role of E-cadherin in patients with advanced serous ovarian cancer. Arch Gynecol Obstet. 2013;287(6):1219-24.
135. Zhang S, Balch C, Chan MW, Lai HC, Matei D, Schilder JM, et al. Identification and characterization of ovarian cancer-initiating cells from primary human tumors. Cancer Res. 2008;68(11):4311-20.
136. Cheng KW, Lahad JP, Kuo WL, Lapuk A, Yamada K, Auersperg N, et al. The RAB25 small GTPase determines aggressiveness of ovarian and breast cancers. Nat Med. 2004;10(11):1251-6.
137. Salceda S, Tang T, Kmet M, Munteanu A, Ghosh M, Macina R, et al. The immunomodulatory protein B7-H4 is overexpressed in breast and ovarian cancers and promotes epithelial cell transformation. Exp Cell Res. 2005;306(1):128-41.
138. Qian Y, Shen L, Cheng L, Wu Z, Yao H. B7-H4 expression in various tumors determined using a novel developed monoclonal antibody. Clin Exp Med. 2011;11(3):163-70.
139. Cheng L, Jiang J, Gao R, Wei S, Nan F, Li S, et al. B7-H4 expression promotes tumorigenesis in ovarian cancer. Int J Gynecol Cancer. 2009;19(9):1481-6.
140. Ip CK, Li SS, Tang MY, Sy SK, Ren Y, Shum HC, et al. Stemness and chemoresistance in epithelial ovarian carcinoma cells under shear stress. Sci Rep. 2016;6:26788.
141. Sawada K, Mitra AK, Radjabi AR, Bhaskar V, Kistner EO, Tretiakova M, et al. Loss of E-cadherin promotes ovarian cancer metastasis via alpha 5-integrin, which is a therapeutic target. Cancer Res. 2008;68(7):2329-39.
142. Shield K, Riley C, Quinn MA, Rice GE, Ackland ML, Ahmed N. Alpha2beta1 integrin affects metastatic potential of ovarian carcinoma spheroids by supporting disaggregation and proteolysis. J Carcinog. 2007;6:11.
143. Casey RC, Skubitz AP. CD44 and beta1 integrins mediate ovarian carcinoma cell migration toward extracellular matrix proteins. Clin Exp Metastasis. 2000;18(1):67-75.
144. Cannistra SA, Kansas GS, Niloff J, DeFranzo B, Kim Y, Ottensmeier C. Binding of ovarian cancer cells to peritoneal mesothelium in vitro is partly mediated by CD44H. Cancer Res. 1993;53(16):3830-8.

145. Nakamura K, Sawada K, Kinose Y, Yoshimura A, Toda A, Nakatsuka E, et al. Exosomes Promote Ovarian Cancer Cell Invasion through Transfer of CD44 to Peritoneal Mesothelial Cells. Mol Cancer Res. 2017;15(1):78-92.
146. Heath RM, Jayne DG, O'Leary R, Morrison EE, Guillou PJ. Tumour-induced apoptosis in human mesothelial cells: a mechanism of peritoneal invasion by Fas Ligand/Fas interaction. Br J Cancer. 2004;90(7):1437-42.
147. Chen L, Park SM, Tumanov AV, Hau A, Sawada K, Feig C, et al. CD95 promotes tumour growth. Nature. 2010;465(7297):492-6.
148. Ren J, Xiao YJ, Singh LS, Zhao X, Zhao Z, Feng L, et al. Lysophosphatidic acid is constitutively produced by human peritoneal mesothelial cells and enhances adhesion, migration, and invasion of ovarian cancer cells. Cancer Res. 2006;66(6):3006-14.
149. Klymenko Y, Bos B, Campbell L, Loughran E, Liu Y, Yang J, et al. Lysophosphatidic acid modulates ovarian cancer multicellular aggregate assembly and metastatic dissemination. Sci Rep. 2020;10(1):10877.
150. Jesionowska A, Cecerska-Heryc E, Matoszka N, Dolegowska B. Lysophosphatidic acid signaling in ovarian cancer. J Recept Signal Transduct Res. 2015;35(6):578-84.
151. Mitra AK, Chiang CY, Tiwari P, Tomar S, Watters KM, Peter ME, et al. Microenvironment-induced downregulation of miR-193b drives ovarian cancer metastasis. Oncogene. 2015;34(48):5923-32.
152. Sehouli J, Senyuva F, Fotopoulou C, Neumann U, Denkert C, Werner L, et al. Intra-abdominal tumor dissemination pattern and surgical outcome in 214 patients with primary ovarian cancer. J Surg Oncol. 2009;99(7):424-7.
153. Arie AB, McNally L, Kapp DS, Teng NN. The omentum and omentectomy in epithelial ovarian cancer: a reappraisal: part II--The role of omentectomy in the staging and treatment of apparent early stage epithelial ovarian cancer. Gynecol Oncol. 2013;131(3):784-90.
154. Isaza-Restrepo A, Martin-Saavedra JS, Velez-Leal JL, Vargas-Barato F, Riveros-Duenas R. The Peritoneum: Beyond the Tissue - A Review. Front Physiol. 2018;9:738.
155. Langley RR, Fidler IJ. The seed and soil hypothesis revisited--the role of tumor-stroma interactions in metastasis to different organs. Int J Cancer. 2011;128(11):2527-35.
156. Di Nicola V. Omentum a powerful biological source in regenerative surgery. Regen Ther. 2019;11:182-91.
157. Platell C, Cooper D, Papadimitriou JM, Hall JC. The omentum. World J Gastroenterol. 2000;6(2):169-76.
158. Meza-Perez S, Randall TD. Immunological Functions of the Omentum. Trends Immunol. 2017;38(7):526-36.
159. Dai L, Song K, Di W. Adipocytes: active facilitators in epithelial ovarian cancer progression? J Ovarian Res. 2020;13(1):115.
160. Ben Arie A, McNally L, Kapp DS, Teng NN. The omentum and omentectomy in epithelial ovarian cancer: a reappraisal. Part I--Omental function and history of omentectomy. Gynecol Oncol. 2013;131(3):780-3.
161. Singh AK, Patel J, Litbarg NO, Gudehithlu KP, Sethupathi P, Arruda JA, et al. Stromal cells cultured from omentum express pluripotent markers, produce high amounts of VEGF, and engraft to injured sites. Cell Tissue Res. 2008;332(1):81-8.
162. Litbarg NO, Gudehithlu KP, Sethupathi P, Arruda JA, Dunea G, Singh AK. Activated omentum becomes rich in factors that promote healing and tissue regeneration. Cell Tissue Res. 2007;328(3):487-97.

163. Konturek SJ, Brzozowski T, Majka I, Pawlik W, Stachura J. Omentum and basic fibroblast growth factor in healing of chronic gastric ulcerations in rats. Dig Dis Sci. 1994;39(5):1064-71.
164. Benezech C, Luu NT, Walker JA, Kruglov AA, Loo Y, Nakamura K, et al. Inflammation-induced formation of fat-associated lymphoid clusters. Nat Immunol. 2015;16(8):819-28.
165. Rangel-Moreno J, Moyron-Quiroz JE, Carragher DM, Kusser K, Hartson L, Moquin A, et al. Omental milky spots develop in the absence of lymphoid tissue-inducer cells and support B and T cell responses to peritoneal antigens. Immunity. 2009;30(5):731-43.
166. Ansel KM, Harris RB, Cyster JG. CXCL13 is required for B1 cell homing, natural antibody production, and body cavity immunity. Immunity. 2002;16(1):67-76.
167. Mills CD, Ley K. M1 and M2 macrophages: the chicken and the egg of immunity. J Innate Immun. 2014;6(6):716-26.
168. Zhu H, Naito M, Umezu H, Moriyama H, Takatsuka H, Takahashi K, et al. Macrophage differentiation and expression of macrophage colony-stimulating factor in murine milky spots and omentum after macrophage elimination. J Leukoc Biol. 1997;61(4):436-44.
169. Lopes Cardozo AM, Gupta A, Koppe MJ, Meijer S, van Leeuwen PA, Beelen RJ, et al. Metastatic pattern of CC531 colon carcinoma cells in the abdominal cavity: an experimental model of peritoneal carcinomatosis in rats. Eur J Surg Oncol. 2001;27(4):359-63.
170. Krist LF, Kerremans M, Broekhuis-Fluitsma DM, Eestermans IL, Meyer S, Beelen RH. Milky spots in the greater omentum are predominant sites of local tumour cell proliferation and accumulation in the peritoneal cavity. Cancer Immunol Immunother. 1998;47(4):205-12.
171. Buscher K, Wang H, Zhang X, Striewski P, Wirth B, Saggu G, et al. Protection from septic peritonitis by rapid neutrophil recruitment through omental high endothelial venules. Nat Commun. 2016;7:10828.
172. Krishnan V, Tallapragada S, Schaar B, Kamat K, Chanana AM, Zhang Y, et al. Omental macrophages secrete chemokine ligands that promote ovarian cancer colonization of the omentum via CCR1. Commun Biol. 2020;3(1):524.
173. Oosterling SJ, van der Bij GJ, Bogels M, van der Sijp JR, Beelen RH, Meijer S, et al. Insufficient ability of omental milky spots to prevent peritoneal tumor outgrowth supports omentectomy in minimal residual disease. Cancer Immunol Immunother. 2006;55(9):1043-51.
174. Sangisetty SL, Miner TJ. Malignant ascites: A review of prognostic factors, pathophysiology and therapeutic measures. World J Gastrointest Surg. 2012;4(4):87-95.
175. Clark R, Krishnan V, Schoof M, Rodriguez I, Theriault B, Chekmareva M, et al. Milky spots promote ovarian cancer metastatic colonization of peritoneal adipose in experimental models. Am J Pathol. 2013;183(2):576-91.
176. Son KN, Hwang J, Kwon BS, Kim J. Human CC chemokine CCL23 enhances expression of matrix metalloproteinase-2 and invasion of vascular endothelial cells. Biochem Biophys Res Commun. 2006;340(2):498-504.
177. Mantovani A, Sozzani S, Locati M, Allavena P, Sica A. Macrophage polarization: tumor-associated macrophages as a paradigm for polarized M2 mononuclear phagocytes. Trends Immunol. 2002;23(11):549-55.
178. Liu J, Geng X, Hou J, Wu G. New insights into M1/M2 macrophages: key modulators in cancer progression. Cancer Cell Int. 2021;21(1):389.

179. Cui L, Johkura K, Liang Y, Teng R, Ogiwara N, Okouchi Y, et al. Biodefense function of omental milky spots through cell adhesion molecules and leukocyte proliferation. Cell Tissue Res. 2002;310(3):321-30.
180. Maruo Y, Gochi A, Kaihara A, Shimamura H, Yamada T, Tanaka N, et al. ICAM-1 expression and the soluble ICAM-1 level for evaluating the metastatic potential of gastric cancer. Int J Cancer. 2002;100(4):486-90.
181. Schroder C, Witzel I, Muller V, Krenkel S, Wirtz RM, Janicke F, et al. Prognostic value of intercellular adhesion molecule (ICAM)-1 expression in breast cancer. J Cancer Res Clin Oncol. 2011;137(8):1193-201.
182. Reina M, Espel E. Role of LFA-1 and ICAM-1 in Cancer. Cancers (Basel). 2017;9(11).
183. Wang S, Yin C, Zhang Y, Zhang L, Tao L, Liang W, et al. Overexpression of ICAM-1 Predicts Poor Survival in High-Grade Serous Ovarian Carcinoma: A Study Based on TCGA and GEO Databases and Tissue Microarray. Biomed Res Int. 2019;2019:2867372.
184. Vucenik I, Stains JP. Obesity and cancer risk: evidence, mechanisms, and recommendations. Ann N Y Acad Sci. 2012;1271:37-43.
185. Fasshauer M, Bluher M. Adipokines in health and disease. Trends Pharmacol Sci. 2015;36(7):461-70.
186. Cao Y. Adipocyte and lipid metabolism in cancer drug resistance. J Clin Invest. 2019;129(8):3006-17.
187. Nieman KM, Romero IL, Van Houten B, Lengyel E. Adipose tissue and adipocytes support tumorigenesis and metastasis. Biochim Biophys Acta. 2013;1831(10):1533-41.
188. Foong KW, Bolton H. Obesity and ovarian cancer risk: A systematic review. Post Reprod Health. 2017;23(4):183-98.
189. Bae HS, Kim HJ, Hong JH, Lee JK, Lee NW, Song JY. Obesity and epithelial ovarian cancer survival: a systematic review and meta-analysis. J Ovarian Res. 2014;7:41.
190. Lv H, Wu S. Influence of obesity on surgical complications of patients with ovarian tumors. Oncol Lett. 2019;17(5):4590-4.
191. Vergara D, Merlot B, Lucot JP, Collinet P, Vinatier D, Fournier I, et al. Epithelial-mesenchymal transition in ovarian cancer. Cancer Lett. 2010;291(1):59-66.
192. Bruun JM, Pedersen SB, Richelsen B. Regulation of interleukin 8 production and gene expression in human adipose tissue in vitro. J Clin Endocrinol Metab. 2001;86(3):1267-73.
193. Nieman KM, Kenny HA, Penicka CV, Ladanyi A, Buell-Gutbrod R, Zillhardt MR, et al. Adipocytes promote ovarian cancer metastasis and provide energy for rapid tumor growth. Nat Med. 2011;17(11):1498-503.
194. Yin J, Zeng F, Wu N, Kang K, Yang Z, Yang H. Interleukin-8 promotes human ovarian cancer cell migration by epithelial-mesenchymal transition induction in vitro. Clin Transl Oncol. 2015;17(5):365-70.
195. Nowak M, Glowacka E, Szpakowski M, Szyllo K, Malinowski A, Kulig A, et al. Proinflammatory and immunosuppressive serum, ascites and cyst fluid cytokines in patients with early and advanced ovarian cancer and benign ovarian tumors. Neuro Endocrinol Lett. 2010;31(3):375-83.
196. Lokshin AE, Winans M, Landsittel D, Marrangoni AM, Velikokhatnaya L, Modugno F, et al. Circulating IL-8 and anti-IL-8 autoantibody in patients with ovarian cancer. Gynecol Oncol. 2006;102(2):244-51.
197. Colomiere M, Ward AC, Riley C, Trenerry MK, Cameron-Smith D, Findlay J, et al. Cross talk of signals between EGFR and IL-6R through

JAK2/STAT3 mediate epithelial-mesenchymal transition in ovarian carcinomas. Br J Cancer. 2009;100(1):134-44.
198. Celis JE, Moreira JM, Cabezon T, Gromov P, Friis E, Rank F, et al. Identification of extracellular and intracellular signaling components of the mammary adipose tissue and its interstitial fluid in high risk breast cancer patients: toward dissecting the molecular circuitry of epithelial-adipocyte stromal cell interactions. Mol Cell Proteomics. 2005;4(4):492-522.
199. Arora N, Ahmed N, Luwor RB. The Potential Role of Interleukin-11 in Epithelial Ovarian Cancer. Journal of Cancer Science and Clinical Therapeutics. 2019;3:28-47.
200. Wood IS, Wang B, Trayhurn P. IL-33, a recently identified interleukin-1 gene family member, is expressed in human adipocytes. Biochem Biophys Res Commun. 2009;384(1):105-9.
201. Tong X, Barbour M, Hou K, Gao C, Cao S, Zheng J, et al. Interleukin-33 predicts poor prognosis and promotes ovarian cancer cell growth and metastasis through regulating ERK and JNK signaling pathways. Mol Oncol. 2016;10(1):113-25.
202. D'Esposito V, Passaretti F, Hammarstedt A, Liguoro D, Terracciano D, Molea G, et al. Adipocyte-released insulin-like growth factor-1 is regulated by glucose and fatty acids and controls breast cancer cell growth in vitro. Diabetologia. 2012;55(10):2811-22.
203. Cai Q, Yan L, Xu Y. Anoikis resistance is a critical feature of highly aggressive ovarian cancer cells. Oncogene. 2015;34(25):3315-24.
204. Sun X-M, Dong W-G, Gao L-C, Jiang X. Detection of VEGF levels in ascites and peritoneal fluid. Chin J Cancer Res. 2003;15.
205. Mick GJ, Wang X, McCormick K. White adipocyte vascular endothelial growth factor: regulation by insulin. Endocrinology. 2002;143(3):948-53.
206. Zhang QX, Magovern CJ, Mack CA, Budenbender KT, Ko W, Rosengart TK. Vascular endothelial growth factor is the major angiogenic factor in omentum: mechanism of the omentum-mediated angiogenesis. J Surg Res. 1997;67(2):147-54.
207. Wei LH, Kuo ML, Chen CA, Chou CH, Lai KB, Lee CN, et al. Interleukin-6 promotes cervical tumor growth by VEGF-dependent angiogenesis via a STAT3 pathway. Oncogene. 2003;22(10):1517-27.
208. Popko K, Gorska E, Stelmaszczyk-Emmel A, Plywaczewski R, Stoklosa A, Gorecka D, et al. Proinflammatory cytokines Il-6 and TNF-alpha and the development of inflammation in obese subjects. Eur J Med Res. 2010;15 Suppl 2:120-2.
209. Muthukumaran N, Miletti-Gonzalez KE, Ravindranath AK, Rodriguez-Rodriguez L. Tumor necrosis factor-alpha differentially modulates CD44 expression in ovarian cancer cells. Mol Cancer Res. 2006;4(8):511-20.
210. Gao Y, Foster R, Yang X, Feng Y, Shen JK, Mankin HJ, et al. Up-regulation of CD44 in the development of metastasis, recurrence and drug resistance of ovarian cancer. Oncotarget. 2015;6(11):9313-26.
211. Martincuks A, Li PC, Zhao Q, Zhang C, Li YJ, Yu H, et al. CD44 in Ovarian Cancer Progression and Therapy Resistance-A Critical Role for STAT3. Front Oncol. 2020;10:589601.
212. Lin J, Ding D. The prognostic role of the cancer stem cell marker CD44 in ovarian cancer: a meta-analysis. Cancer Cell Int. 2017;17:8.
213. Bell LN, Ward JL, Degawa-Yamauchi M, Bovenkerk JE, Jones R, Cacucci BM, et al. Adipose tissue production of hepatocyte growth factor

contributes to elevated serum HGF in obesity. Am J Physiol Endocrinol Metab. 2006;291(4):E843-8.
214. Chen C, Zhao S, Karnad A, Freeman JW. The biology and role of CD44 in cancer progression: therapeutic implications. J Hematol Oncol. 2018;11(1):64.
215. Dirat B, Bochet L, Dabek M, Daviaud D, Dauvillier S, Majed B, et al. Cancer-associated adipocytes exhibit an activated phenotype and contribute to breast cancer invasion. Cancer Res. 2011;71(7):2455-65.
216. Guaita-Esteruelas S, Bosquet A, Saavedra P, Guma J, Girona J, Lam EW, et al. Exogenous FABP4 increases breast cancer cell proliferation and activates the expression of fatty acid transport proteins. Mol Carcinog. 2017;56(1):208-17.
217. Yue S, Li J, Lee SY, Lee HJ, Shao T, Song B, et al. Cholesteryl ester accumulation induced by PTEN loss and PI3K/AKT activation underlies human prostate cancer aggressiveness. Cell Metab. 2014;19(3):393-406.
218. Wang W, Guan KL. AMP-activated protein kinase and cancer. Acta Physiol (Oxf). 2009;196(1):55-63.
219. Bochet L, Lehuede C, Dauvillier S, Wang YY, Dirat B, Laurent V, et al. Adipocyte-derived fibroblasts promote tumor progression and contribute to the desmoplastic reaction in breast cancer. Cancer Res. 2013;73(18):5657-68.
220. Cirri P, Chiarugi P. Cancer-associated-fibroblasts and tumour cells: a diabolic liaison driving cancer progression. Cancer Metastasis Rev. 2012;31(1-2):195-208.
221. Maia A, Wiemann S. Cancer-Associated Fibroblasts: Implications for Cancer Therapy. Cancers (Basel). 2021;13(14).
222. Iyoshi S, Yoshihara M, Nakamura K, Sugiyama M, Koya Y, Kitami K, et al. Pro-tumoral behavior of omental adipocyte-derived fibroblasts in tumor microenvironment at the metastatic site of ovarian cancer. Int J Cancer. 2021;149(11):1961-72.
223. Iyengar NM, Gucalp A, Dannenberg AJ, Hudis CA. Obesity and Cancer Mechanisms: Tumor Microenvironment and Inflammation. J Clin Oncol. 2016;34(35):4270-6.
224. Robinson-Smith TM, Isaacsohn I, Mercer CA, Zhou M, Van Rooijen N, Husseinzadeh N, et al. Macrophages mediate inflammation-enhanced metastasis of ovarian tumors in mice. Cancer Res. 2007;67(12):5708-16.
225. Cardenas C, Montagna MK, Pitruzzello M, Lima E, Mor G, Alvero AB. Adipocyte microenvironment promotes Bclxl expression and confers chemoresistance in ovarian cancer cells. Apoptosis. 2017;22(4):558-69.
226. Wang Y, Qu Y, Niu XL, Sun WJ, Zhang XL, Li LZ. Autocrine production of interleukin-8 confers cisplatin and paclitaxel resistance in ovarian cancer cells. Cytokine. 2011;56(2):365-75.
227. Wang Y, Niu XL, Qu Y, Wu J, Zhu YQ, Sun WJ, et al. Autocrine production of interleukin-6 confers cisplatin and paclitaxel resistance in ovarian cancer cells. Cancer Lett. 2010;295(1):110-23.
228. Sheng X, Parmentier JH, Tucci J, Pei H, Cortez-Toledo O, Dieli-Conwright CM, et al. Adipocytes Sequester and Metabolize the Chemotherapeutic Daunorubicin. Mol Cancer Res. 2017;15(12):1704-13.
229. Nilsson MB, Langley RR, Fidler IJ. Interleukin-6, secreted by human ovarian carcinoma cells, is a potent proangiogenic cytokine. Cancer Res. 2005;65(23):10794-800.

230. Gopinathan G, Milagre C, Pearce OM, Reynolds LE, Hodivala-Dilke K, Leinster DA, et al. Interleukin-6 Stimulates Defective Angiogenesis. Cancer Res. 2015;75(15):3098-107.
231. Incio J, Ligibel JA, McManus DT, Suboj P, Jung K, Kawaguchi K, et al. Obesity promotes resistance to anti-VEGF therapy in breast cancer by up-regulating IL-6 and potentially FGF-2. Sci Transl Med. 2018;10(432).
232. Herold J, Kalucka J. Angiogenesis in Adipose Tissue: The Interplay Between Adipose and Endothelial Cells. Front Physiol. 2020;11:624903.
233. Sato N, Beitz JG, Kato J, Yamamoto M, Clark JW, Calabresi P, et al. Platelet-derived growth factor indirectly stimulates angiogenesis in vitro. Am J Pathol. 1993;142(4):1119-30.
234. Beitz JG, Kim IS, Calabresi P, Frackelton AR, Jr. Human microvascular endothelial cells express receptors for platelet-derived growth factor. Proc Natl Acad Sci U S A. 1991;88(5):2021-5.
235. Mutsaers SE. Mesothelial cells: their structure, function and role in serosal repair. Respirology. 2002;7(3):171-91.
236. Mutsaers SE. The mesothelial cell. Int J Biochem Cell Biol. 2004;36(1):9-16.
237. Nagai H, Chew SH, Okazaki Y, Funahashi S, Namba T, Kato T, et al. Metamorphosis of mesothelial cells with active horizontal motility in tissue culture. Sci Rep. 2013;3:1144.
238. Wagner WL, Zheng Y, Pierce A, Ackermann M, Horstmann H, Kuner T, et al. Mesopolysaccharides: The extracellular surface layer of visceral organs. PLoS One. 2020;15(9):e0238798.
239. Yung S, Chan TM. Pathophysiology of the peritoneal membrane during peritoneal dialysis: the role of hyaluronan. J Biomed Biotechnol. 2011;2011:180594.
240. Yung S, Chan TM. Hyaluronan--regulator and initiator of peritoneal inflammation and remodeling. Int J Artif Organs. 2007;30(6):477-83.
241. Evanko SP, Angello JC, Wight TN. Formation of hyaluronan- and versican-rich pericellular matrix is required for proliferation and migration of vascular smooth muscle cells. Arterioscler Thromb Vasc Biol. 1999;19(4):1004-13.
242. Ricciardelli C, Russell DL, Ween MP, Mayne K, Suwiwat S, Byers S, et al. Formation of hyaluronan- and versican-rich pericellular matrix by prostate cancer cells promotes cell motility. J Biol Chem. 2007;282(14):10814-25.
243. Tavianatou AG, Caon I, Franchi M, Piperigkou Z, Galesso D, Karamanos NK. Hyaluronan: molecular size-dependent signaling and biological functions in inflammation and cancer. FEBS J. 2019;286(15):2883-908.
244. Visser CE, Brouwer-Steenbergen JJ, Schadee-Eestermans IL, Meijer S, Krediet RT, Beelen RH. Ingestion of Staphylococcus aureus, Staphylococcus epidermidis, and Escherichia coli by human peritoneal mesothelial cells. Infect Immun. 1996;64(8):3425-8.
245. Tanaka S, Choe N, Iwagaki A, Hemenway DR, Kagan E. Asbestos exposure induces MCP-1 secretion by pleural mesothelial cells. Exp Lung Res. 2000;26(4):241-55.
246. Mierzejewski M, Paplinska-Goryca M, Korczynski P, Krenke R. Primary human mesothelial cell culture in the evaluation of the inflammatory response to different sclerosing agents used for pleurodesis. Physiol Rep. 2021;9(8):e14846.
247. Foussat A, Balabanian K, Amara A, Bouchet-Delbos L, Durand-Gasselin I, Baleux F, et al. Production of stromal cell-derived factor 1 by mesothelial cells

and effects of this chemokine on peritoneal B lymphocytes. Eur J Immunol. 2001;31(2):350-9.
248. Katayama H, Yokoyama A, Kohno N, Sakai K, Hiwada K, Yamada H, et al. Production of eosinophilic chemokines by normal pleural mesothelial cells. Am J Respir Cell Mol Biol. 2002;26(4):398-403.
249. Lanfrancone L, Boraschi D, Ghiara P, Falini B, Grignani F, Peri G, et al. Human peritoneal mesothelial cells produce many cytokines (granulocyte colony-stimulating factor [CSF], granulocyte-monocyte-CSF, macrophage-CSF, interleukin-1 [IL-1], and IL-6) and are activated and stimulated to grow by IL-1. Blood. 1992;80(11):2835-42.
250. Mutsaers SE, Birnie K, Lansley S, Herrick SE, Lim CB, Prele CM. Mesothelial cells in tissue repair and fibrosis. Front Pharmacol. 2015;6:113.
251. Day AJ, de la Motte CA. Hyaluronan cross-linking: a protective mechanism in inflammation? Trends Immunol. 2005;26(12):637-43.
252. Yung S, Chan TM. Pathophysiological changes to the peritoneal membrane during PD-related peritonitis: the role of mesothelial cells. Mediators Inflamm. 2012;2012:484167.
253. van der Wal BC, Hofland LJ, Marquet RL, van Koetsveld PM, van Rossen ME, van Eijck CH. Paracrine interactions between mesothelial and colon-carcinoma cells in a rat model. Int J Cancer. 1997;73(6):885-90.
254. van Rossen ME, Hofland LJ, van den Tol MP, van Koetsveld PM, Jeekel J, Marquet RL, et al. Effect of inflammatory cytokines and growth factors on tumour cell adhesion to the peritoneum. J Pathol. 2001;193(4):530-7.
255. Hofer SO, Shrayer D, Reichner JS, Hoekstra HJ, Wanebo HJ. Wound-induced tumor progression: a probable role in recurrence after tumor resection. Arch Surg. 1998;133(4):383-9.
256. Kuroki L, Guntupalli SR. Treatment of epithelial ovarian cancer. BMJ. 2020;371:m3773.
257. Rahimi N, Tremblay E, McAdam L, Roberts A, Elliott B. Autocrine secretion of TGF-beta 1 and TGF-beta 2 by pre-adipocytes and adipocytes: a potent negative regulator of adipocyte differentiation and proliferation of mammary carcinoma cells. In Vitro Cell Dev Biol Anim. 1998;34(5):412-20.
258. Abendstein B, Stadlmann S, Knabbe C, Buck M, Muller-Holzner E, Zeimet AG, et al. Regulation of transforming growth factor-beta secretion by human peritoneal mesothelial and ovarian carcinoma cells. Cytokine. 2000;12(7):1115-9.
259. Di Blasio AM, Carniti C, Vigano P, Vignali M. Basic fibroblast growth factor and ovarian cancer. J Steroid Biochem Mol Biol. 1995;53(1-6):375-9.
260. Cronauer MV, Stadlmann S, Klocker H, Abendstein B, Eder IE, Rogatsch H, et al. Basic fibroblast growth factor synthesis by human peritoneal mesothelial cells: induction by interleukin-1. Am J Pathol. 1999;155(6):1977-84.
261. Kuhn MC, Willenberg HS, Schott M, Papewalis C, Stumpf U, Flohe S, et al. Adipocyte-secreted factors increase osteoblast proliferation and the OPG/RANKL ratio to influence osteoclast formation. Mol Cell Endocrinol. 2012;349(2):180-8.
262. Qian J, LeSavage BL, Hubka KM, Ma C, Natarajan S, Eggold JT, et al. Cancer-associated mesothelial cells promote ovarian cancer chemoresistance through paracrine osteopontin signaling. J Clin Invest. 2021;131(16).
263. Kenny HA, Chiang CY, White EA, Schryver EM, Habis M, Romero IL, et al. Mesothelial cells promote early ovarian cancer metastasis through fibronectin secretion. J Clin Invest. 2014;124(10):4614-28.

264. Guo Q, Gao BL, Zhang XJ, Liu GC, Xu F, Fan QY, et al. CXCL12-CXCR4 Axis Promotes Proliferation, Migration, Invasion, and Metastasis of Ovarian Cancer. Oncol Res. 2014;22(5-6):247-58.
265. Jiang YP, Wu XH, Shi B, Wu WX, Yin GR. Expression of chemokine CXCL12 and its receptor CXCR4 in human epithelial ovarian cancer: an independent prognostic factor for tumor progression. Gynecol Oncol. 2006;103(1):226-33.
266. Natarajan S, Foreman KM, Soriano MI, Rossen NS, Shehade H, Fregoso DR, et al. Collagen Remodeling in the Hypoxic Tumor-Mesothelial Niche Promotes Ovarian Cancer Metastasis. Cancer Res. 2019;79(9):2271-84.
267. Pickup MW, Mouw JK, Weaver VM. The extracellular matrix modulates the hallmarks of cancer. EMBO Rep. 2014;15(12):1243-53.
268. Jones LM, Gardner MJ, Catterall JB, Turner GA. Hyaluronic acid secreted by mesothelial cells: a natural barrier to ovarian cancer cell adhesion. Clin Exp Metastasis. 1995;13(5):373-80.
269. Cannistra SA, DeFranzo B, Niloff J, Ottensmeir C. Functional heterogeneity of CD44 molecules in ovarian cancer cell lines. Clin Cancer Res. 1995;1(3):333-42.
270. Rump A, Morikawa Y, Tanaka M, Minami S, Umesaki N, Takeuchi M, et al. Binding of ovarian cancer antigen CA125/MUC16 to mesothelin mediates cell adhesion. J Biol Chem. 2004;279(10):9190-8.
271. Iwanicki MP, Davidowitz RA, Ng MR, Besser A, Muranen T, Merritt M, et al. Ovarian cancer spheroids use myosin-generated force to clear the mesothelium. Cancer Discov. 2011;1(2):144-57.
272. Davidowitz RA, Selfors LM, Iwanicki MP, Elias KM, Karst A, Piao H, et al. Mesenchymal gene program-expressing ovarian cancer spheroids exhibit enhanced mesothelial clearance. J Clin Invest. 2014;124(6):2611-25.
273. Sandoval P, Jimenez-Heffernan JA, Rynne-Vidal A, Perez-Lozano ML, Gilsanz A, Ruiz-Carpio V, et al. Carcinoma-associated fibroblasts derive from mesothelial cells via mesothelial-to-mesenchymal transition in peritoneal metastasis. J Pathol. 2013;231(4):517-31.
274. Pakula M, Uruski P, Niklas A, Wozniak A, Szpurek D, Tykarski A, et al. A Unique Pattern of Mesothelial-Mesenchymal Transition Induced in the Normal Peritoneal Mesothelium by High-Grade Serous Ovarian Cancer. Cancers (Basel). 2019;11(5).
275. Aroeira LS, Aguilera A, Selgas R, Ramirez-Huesca M, Perez-Lozano ML, Cirugeda A, et al. Mesenchymal conversion of mesothelial cells as a mechanism responsible for high solute transport rate in peritoneal dialysis: role of vascular endothelial growth factor. Am J Kidney Dis. 2005;46(5):938-48.
276. Siemerink MJ, Klaassen I, Vogels IM, Griffioen AW, Van Noorden CJ, Schlingemann RO. CD34 marks angiogenic tip cells in human vascular endothelial cell cultures. Angiogenesis. 2012;15(1):151-63.
277. Allemani C, Weir HK, Carreira H, Harewood R, Spika D, Wang XS, et al. Global surveillance of cancer survival 1995-2009: analysis of individual data for 25,676,887 patients from 279 population-based registries in 67 countries (CONCORD-2). Lancet. 2015;385(9972):977-1010.
278. Winiarski BK, Acheson N, Gutowski NJ, McHarg S, Whatmore JL. An improved and reliable method for isolation of microvascular endothelial cells from human omentum. Microcirculation. 2011;18(8):635-45.
279. Takahashi K, Hata J, Mukai K, Sawasaki Y. Close similarity between cultured human omental mesothelial cells and endothelial cells in cytochemical

markers and plasminogen activator production. In Vitro Cell Dev Biol. 1991;27A(7):542-8.
280. Chamchoy K, Pakotiprapha D, Pumirat P, Leartsakulpanich U, Boonyuen U. Application of WST-8 based colorimetric NAD(P)H detection for quantitative dehydrogenase assays. BMC Biochem. 2019;20(1):4.
281. Kanayasu-Toyoda T, Ishii-Watabe A, Kikuchi Y, Kitagawa H, Suzuki H, Tamura H, et al. Occludin as a functional marker of vascular endothelial cells on tube-forming activity. J Cell Physiol. 2018;233(2):1700-11.
282. Lachaud CC, Rodriguez-Campins B, Hmadcha A, Soria B. Use of Mesothelial Cells and Biological Matrices for Tissue Engineering of Simple Epithelium Surrogates. Front Bioeng Biotechnol. 2015;3:117.
283. Winiarski BK. Cross talk between ovarian cancer cells and microvascular omental endothelial cells: potential role in metastasis of ovarian cancer to the omentum [Doctoral thesis]: Exeter and Plymouth Peninsula Medical School; 2011.
284. Memorial Sloan Kettering Cancer Center. SK-OV-3: Human Ovarian Cancer Cell Line (ATCC HTB-79) [updated 2022. Available from: https://www.mskcc.org/research-advantage/support/technology/tangible-material/human-ovarian-cell-line-sk-ov-3.
285. UK Health Security Agency. Ovarian Cancer cell line A2780 (ECACC catalogue no. 93112519): Culture Collections; [updated 2021. Available from: https://www.culturecollections.org.uk/media/113526/a2780-cell-line-profile.pdf.
286. Adya R, Tan BK, Randeva HS. Differential effects of leptin and adiponectin in endothelial angiogenesis. J Diabetes Res. 2015;2015:648239.
287. Lopez-Jaramillo P, Gomez-Arbelaez D, Lopez-Lopez J, Lopez-Lopez C, Martinez-Ortega J, Gomez-Rodriguez A, et al. The role of leptin/adiponectin ratio in metabolic syndrome and diabetes. Horm Mol Biol Clin Investig. 2014;18(1):37-45.
288. Maskell ART. Pro-angiogenic and metastatic properties of galectin-1 during epithelial ovarian cancer metastasis to the omentum [Doctoral thesis]: University of Exeter; 2022.
289. Aghababazadeh M, Kerachian M. Cell Fasting: Cellular Response and Application of Serum Starvation. Journal of Nutrition, Fasting and Health. 2014;2(4):147-50.
290. Khammanit R, Chantakru S, Kitiyanant Y, Saikhun J. Effect of serum starvation and chemical inhibitors on cell cycle synchronization of canine dermal fibroblasts. Theriogenology. 2008;70(1):27-34.
291. Pranjol MZI, Zinovkin DA, Maskell ART, Stephens LJ, Achinovich SL, Los DM, et al. Cathepsin L-induced galectin-1 may act as a proangiogenic factor in the metastasis of high-grade serous carcinoma. J Transl Med. 2019;17(1):216.
292. Staton CA, Reed MW, Brown NJ. A critical analysis of current in vitro and in vivo angiogenesis assays. Int J Exp Pathol. 2009;90(3):195-221.
293. Bauman E, Granja PL, Barrias CC. Fetal bovine serum-free culture of endothelial progenitor cells-progress and challenges. J Tissue Eng Regen Med. 2018;12(7):1567-78.
294. Riss TL, Moravec RA, Niles AL, Duellman S, Benink HA, Worzella TJ, et al. Cell Viability Assays. In: Markossian S, Grossman A, Brimacombe K, Arkin M, Auld D, Austin CP, et al., editors. Assay Guidance Manual. Bethesda (MD)2004.

295. Xie N, Zhang L, Gao W, Huang C, Huber PE, Zhou X, et al. NAD(+) metabolism: pathophysiologic mechanisms and therapeutic potential. Signal Transduct Target Ther. 2020;5(1):227.
296. Geno Technology Inc. NAD+/NADH Assay [Colorimetric]: Geno Technology Inc; 2021 [updated 2021. Available from: https://www.gbiosciences.com/NAD-NADH_Assay_Colorimetric.
297. Greenshields AL, Shepherd TG, Hoskin DW. Contribution of reactive oxygen species to ovarian cancer cell growth arrest and killing by the anti-malarial drug artesunate. Mol Carcinog. 2017;56(1):75-93.
298. Zhang R, Chen J, Mao L, Guo Y, Hao Y, Deng Y, et al. Nobiletin Triggers Reactive Oxygen Species-Mediated Pyroptosis through Regulating Autophagy in Ovarian Cancer Cells. J Agric Food Chem. 2020;68(5):1326-36.
299. Kim B, Jung JW, Jung J, Han Y, Suh DH, Kim HS, et al. PGC1alpha induced by reactive oxygen species contributes to chemoresistance of ovarian cancer cells. Oncotarget. 2017;8(36):60299-311.
300. Zhang Y, Dai M, Yuan Z. Methods for the detection of reactive oxygen species. Anal Methods. 2018;10:4625-38.
301. Wu D, Yotnda P. Production and detection of reactive oxygen species (ROS) in cancers. J Vis Exp. 2011(57).
302. Lai F, Shen Z, Wen H, Chen J, Zhang X, Lin P, et al. A Morphological identification cell cytotoxicity assay using cytoplasm-localized fluorescent probe (CLFP) to distinguish living and dead cells. Biochem Biophys Res Commun. 2017;482(2):257-63.
303. Yang Y, Lu Y, Wu QY, Hu HY, Chen YH, Liu WL. Evidence of ATP assay as an appropriate alternative of MTT assay for cytotoxicity of secondary effluents from WWTPs. Ecotoxicol Environ Saf. 2015;122:490-6.
304. Beaufort CM, Helmijr JC, Piskorz AM, Hoogstraat M, Ruigrok-Ritstier K, Besselink N, et al. Ovarian cancer cell line panel (OCCP): clinical importance of in vitro morphological subtypes. PLoS One. 2014;9(9):e103988.
305. Hernandez L, Kim MK, Lyle LT, Bunch KP, House CD, Ning F, et al. Characterization of ovarian cancer cell lines as in vivo models for preclinical studies. Gynecol Oncol. 2016;142(2):332-40.
306. Sanders AJ, Ye L, Li J, Mason MD, Jiang WG. Tumour angiogenesis and repulsive guidance molecule b: a role in HGF- and BMP-7-mediated angiogenesis. Int J Oncol. 2014;45(3):1304-12.
307. Isozaki T, Arbab AS, Haas CS, Amin MA, Arendt MD, Koch AE, et al. Evidence that CXCL16 is a potent mediator of angiogenesis and is involved in endothelial progenitor cell chemotaxis : studies in mice with K/BxN serum-induced arthritis. Arthritis Rheum. 2013;65(7):1736-46.
308. Hallas-Potts A, Dawson JC, Herrington CS. Ovarian cancer cell lines derived from non-serous carcinomas migrate and invade more aggressively than those derived from high-grade serous carcinomas. Sci Rep. 2019;9(1):5515.
309. Hu X, Li D, Zhang W, Zhou J, Tang B, Li L. Matrix metalloproteinase-9 expression correlates with prognosis and involved in ovarian cancer cell invasion. Arch Gynecol Obstet. 2012;286(6):1537-43.
310. Devy L, Blacher S, Grignet-Debrus C, Bajou K, Masson V, Gerard RD, et al. The pro- or antiangiogenic effect of plasminogen activator inhibitor 1 is dose dependent. FASEB J. 2002;16(2):147-54.
311. Stefansson S, Petitclerc E, Wong MK, McMahon GA, Brooks PC, Lawrence DA. Inhibition of angiogenesis in vivo by plasminogen activator inhibitor-1. J Biol Chem. 2001;276(11):8135-41.

312. Michaelis UR. Mechanisms of endothelial cell migration. Cell Mol Life Sci. 2014;71(21):4131-48.
313. Yoshida A, Anand-Apte B, Zetter BR. Differential endothelial migration and proliferation to basic fibroblast growth factor and vascular endothelial growth factor. Growth Factors. 1996;13(1-2):57-64.
314. Lamalice L, Le Boeuf F, Huot J. Endothelial cell migration during angiogenesis. Circ Res. 2007;100(6):782-94.
315. Maeda N, Funahashi T, Matsuzawa Y, Shimomura I. Adiponectin, a unique adipocyte-derived factor beyond hormones. Atherosclerosis. 2020;292:1-9.
316. Shibata R, Ouchi N, Kihara S, Sato K, Funahashi T, Walsh K. Adiponectin stimulates angiogenesis in response to tissue ischemia through stimulation of amp-activated protein kinase signaling. J Biol Chem. 2004;279(27):28670-4.
317. Ouchi N, Kobayashi H, Kihara S, Kumada M, Sato K, Inoue T, et al. Adiponectin stimulates angiogenesis by promoting cross-talk between AMP-activated protein kinase and Akt signaling in endothelial cells. J Biol Chem. 2004;279(2):1304-9.
318. Lee HP, Lin CY, Shih JS, Fong YC, Wang SW, Li TM, et al. Adiponectin promotes VEGF-A-dependent angiogenesis in human chondrosarcoma through PI3K, Akt, mTOR, and HIF-alpha pathway. Oncotarget. 2015;6(34):36746-61.
319. Fruhbeck G, Catalan V, Rodriguez A, Gomez-Ambrosi J. Adiponectin-leptin ratio: A promising index to estimate adipose tissue dysfunction. Relation with obesity-associated cardiometabolic risk. Adipocyte. 2018;7(1):57-62.
320. Guadagni F, Roselli M, Martini F, Spila A, Riondino S, D'Alessandro R, et al. Prognostic significance of serum adipokine levels in colorectal cancer patients. Anticancer Res. 2009;29(8):3321-7.
321. Chen DC, Chung YF, Yeh YT, Chaung HC, Kuo FC, Fu OY, et al. Serum adiponectin and leptin levels in Taiwanese breast cancer patients. Cancer Lett. 2006;237(1):109-14.
322. Ashizawa N, Yahata T, Quan J, Adachi S, Yoshihara K, Tanaka K. Serum leptin-adiponectin ratio and endometrial cancer risk in postmenopausal female subjects. Gynecol Oncol. 2010;119(1):65-9.
323. Slomian GJ, Nowak D, Buczkowska M, Glogowska-Gruszka A, Slomian SP, Roczniak W, et al. The role of adiponectin and leptin in the treatment of ovarian cancer patients. Endokrynol Pol. 2019;70(1):57-63.
324. Ray A, Fornsaglio J, Dogan S, Hedau S, Naik D, De A. Gynaecological cancers and leptin: A focus on the endometrium and ovary. Facts Views Vis Obgyn. 2018;10(1):5-18.
325. Bouloumie A, Drexler HC, Lafontan M, Busse R. Leptin, the product of Ob gene, promotes angiogenesis. Circ Res. 1998;83(10):1059-66.
326. Sierra-Honigmann MR, Nath AK, Murakami C, Garcia-Cardena G, Papapetropoulos A, Sessa WC, et al. Biological action of leptin as an angiogenic factor. Science. 1998;281(5383):1683-6.
327. Pan T, Jin Z, Yu Z, Wu X, Chang X, Fan Z, et al. Cathepsin L promotes angiogenesis by regulating the CDP/Cux/VEGF-D pathway in human gastric cancer. Gastric Cancer. 2020;23(6):974-87.
328. Sudhan DR, Rabaglino MB, Wood CE, Siemann DW. Cathepsin L in tumor angiogenesis and its therapeutic intervention by the small molecule inhibitor KGP94. Clin Exp Metastasis. 2016;33(5):461-73.

329. Leung L, Radulovich N, Zhu CQ, Organ S, Bandarchi B, Pintilie M, et al. Lipocalin2 promotes invasion, tumorigenicity and gemcitabine resistance in pancreatic ductal adenocarcinoma. PLoS One. 2012;7(10):e46677.
330. Iannetti A, Pacifico F, Acquaviva R, Lavorgna A, Crescenzi E, Vascotto C, et al. The neutrophil gelatinase-associated lipocalin (NGAL), a NF-kappaB-regulated gene, is a survival factor for thyroid neoplastic cells. Proc Natl Acad Sci U S A. 2008;105(37):14058-63.
331. Cho H, Kim JH. Lipocalin2 expressions correlate significantly with tumor differentiation in epithelial ovarian cancer. J Histochem Cytochem. 2009;57(5):513-21.
332. Yang J, McNeish B, Butterfield C, Moses MA. Lipocalin 2 is a novel regulator of angiogenesis in human breast cancer. FASEB J. 2013;27(1):45-50.
333. Wu L, Du Y, Lok J, Lo EH, Xing C. Lipocalin-2 enhances angiogenesis in rat brain endothelial cells via reactive oxygen species and iron-dependent mechanisms. J Neurochem. 2015;132(6):622-8.
334. Choudhary S, Hegde P, Pruitt JR, Sielecki TM, Choudhary D, Scarpato K, et al. Macrophage migratory inhibitory factor promotes bladder cancer progression via increasing proliferation and angiogenesis. Carcinogenesis. 2013;34(12):2891-9.
335. Hira E, Ono T, Dhar DK, El-Assal ON, Hishikawa Y, Yamanoi A, et al. Overexpression of macrophage migration inhibitory factor induces angiogenesis and deteriorates prognosis after radical resection for hepatocellular carcinoma. Cancer. 2005;103(3):588-98.
336. Hussain F, Freissmuth M, Volkel D, Thiele M, Douillard P, Antoine G, et al. Human anti-macrophage migration inhibitory factor antibodies inhibit growth of human prostate cancer cells in vitro and in vivo. Mol Cancer Ther. 2013;12(7):1223-34.
337. Xu X, Wang B, Ye C, Yao C, Lin Y, Huang X, et al. Overexpression of macrophage migration inhibitory factor induces angiogenesis in human breast cancer. Cancer Lett. 2008;261(2):147-57.
338. Amin MA, Volpert OV, Woods JM, Kumar P, Harlow LA, Koch AE. Migration inhibitory factor mediates angiogenesis via mitogen-activated protein kinase and phosphatidylinositol kinase. Circ Res. 2003;93(4):321-9.
339. Achari AE, Jain SK. Adiponectin, a Therapeutic Target for Obesity, Diabetes, and Endothelial Dysfunction. Int J Mol Sci. 2017;18(6).
340. Brakenhielm E, Veitonmaki N, Cao R, Kihara S, Matsuzawa Y, Zhivotovsky B, et al. Adiponectin-induced antiangiogenesis and antitumor activity involve caspase-mediated endothelial cell apoptosis. Proc Natl Acad Sci U S A. 2004;101(8):2476-81.
341. Yi W, OuYang Q. Adiponectin improves diabetic nephropathy by inhibiting necrotic apoptosis. Arch Med Sci. 2019;15(5):1321-8.
342. Lu Y, Gao X, Wang R, Sun J, Guo B, Wei R, et al. Adiponectin inhibits proliferation of vascular endothelial cells induced by Ox-LDL by promoting dephosphorylation of Caveolin-1 and depolymerization of eNOS and up-regulating release of NO. Int Immunopharmacol. 2019;73:424-34.
343. Ricard N, Bailly S, Guignabert C, Simons M. The quiescent endothelium: signalling pathways regulating organ-specific endothelial normalcy. Nat Rev Cardiol. 2021;18(8):565-80.
344. Segeritz CP, Vallier L. Cell Culture: Growing Cells as Model Systems In Vitro. Basic Science Methods for Clinical Researchers. 2017:151-72.
345. Barresi V, Reggiani-Bonetti L, Di Gregorio C, Vitarelli E, Ponz De Leon M, Barresi G. Neutrophil gelatinase-associated lipocalin (NGAL) and matrix

metalloproteinase-9 (MMP-9) prognostic value in stage I colorectal carcinoma. Pathol Res Pract. 2011;207(8):479-86.
346. Swellam M, Abdelmaksoud MDE, Hassan AK. Clinical Significance of NGAL, MMP-9, and VEGF in Colorectal Cancer Patients. International Journal of Pharmaceutical and Clinical Research. 2016;8(1):117-22.
347. Xu H, Sun X, Sun WJ. Expression and clinical correlation of NGAL and VEGF in endometrial carcinoma. Eur Rev Med Pharmacol Sci. 2018;22(3):632-6.
348. Candido S, Maestro R, Polesel J, Catania A, Maira F, Signorelli SS, et al. Roles of neutrophil gelatinase-associated lipocalin (NGAL) in human cancer. Oncotarget. 2014;5(6):1576-94.
349. Lim R, Ahmed N, Borregaard N, Riley C, Wafai R, Thompson EW, et al. Neutrophil gelatinase-associated lipocalin (NGAL) an early-screening biomarker for ovarian cancer: NGAL is associated with epidermal growth factor-induced epithelio-mesenchymal transition. Int J Cancer. 2007;120(11):2426-34.
350. Gonzalez RR, Cherfils S, Escobar M, Yoo JH, Carino C, Styer AK, et al. Leptin signaling promotes the growth of mammary tumors and increases the expression of vascular endothelial growth factor (VEGF) and its receptor type two (VEGF-R2). J Biol Chem. 2006;281(36):26320-8.
351. Zhou W, Guo S, Gonzalez-Perez RR. Leptin pro-angiogenic signature in breast cancer is linked to IL-1 signalling. Br J Cancer. 2011;104(1):128-37.
352. Birmingham JM, Busik JV, Hansen-Smith FM, Fenton JI. Novel mechanism for obesity-induced colon cancer progression. Carcinogenesis. 2009;30(4):690-7.
353. Ghasemi A, Hashemy SI, Aghaei M, Panjehpour M. Leptin induces matrix metalloproteinase 7 expression to promote ovarian cancer cell invasion by activating ERK and JNK pathways. J Cell Biochem. 2018;119(2):2333-44.
354. Ito TK, Ishii G, Saito S, Yano K, Hoshino A, Suzuki T, et al. Degradation of soluble VEGF receptor-1 by MMP-7 allows VEGF access to endothelial cells. Blood. 2009;113(10):2363-9.
355. Ouh YT, Cho HW, Lee JK, Choi SH, Choi HJ, Hong JH. CXC chemokine ligand 1 mediates adiponectin-induced angiogenesis in ovarian cancer. Tumour Biol. 2019;42(4):1010428319842699.
356. Duncan JS, Turowec JP, Vilk G, Li SS, Gloor GB, Litchfield DW. Regulation of cell proliferation and survival: convergence of protein kinases and caspases. Biochim Biophys Acta. 2010;1804(3):505-10.
357. Paul MK, Mukhopadhyay AK. Tyrosine kinase - Role and significance in Cancer. Int J Med Sci. 2004;1(2):101-15.
358. Konopatskaya O, Shore AC, Tooke JE, Whatmore JL. A role for heterotrimeric GTP-binding proteins and ERK1/2 in insulin-mediated, nitric-oxide-dependent, cyclic GMP production in human umbilical vein endothelial cells. Diabetologia. 2005;48(3):595-604.
359. Bellou S, Hink MA, Bagli E, Panopoulou E, Bastiaens PI, Murphy C, et al. VEGF autoregulates its proliferative and migratory ERK1/2 and p38 cascades by enhancing the expression of DUSP1 and DUSP5 phosphatases in endothelial cells. Am J Physiol Cell Physiol. 2009;297(6):C1477-89.
360. Pranjol MZI, Gutowski NJ, Hannemann M, Whatmore JL. Cathepsin D non-proteolytically induces proliferation and migration in human omental microvascular endothelial cells via activation of the ERK1/2 and PI3K/AKT pathways. Biochim Biophys Acta Mol Cell Res. 2018;1865(1):25-33.
361. Apte RS, Chen DS, Ferrara N. VEGF in Signaling and Disease: Beyond Discovery and Development. Cell. 2019;176(6):1248-64.

362. Herrera-Vargas AK, Garcia-Rodriguez E, Olea-Flores M, Mendoza-Catalan MA, Flores-Alfaro E, Navarro-Tito N. Pro-angiogenic activity and vasculogenic mimicry in the tumor microenvironment by leptin in cancer. Cytokine Growth Factor Rev. 2021;62:23-41.
363. Yokoyama Y, Charnock-Jones DS, Licence D, Yanaihara A, Hastings JM, Holland CM, et al. Vascular endothelial growth factor-D is an independent prognostic factor in epithelial ovarian carcinoma. Br J Cancer. 2003;88(2):237-44.
364. Tammela T, Zarkada G, Wallgard E, Murtomaki A, Suchting S, Wirzenius M, et al. Blocking VEGFR-3 suppresses angiogenic sprouting and vascular network formation. Nature. 2008;454(7204):656-60.
365. Presta M, Dell'Era P, Mitola S, Moroni E, Ronca R, Rusnati M. Fibroblast growth factor/fibroblast growth factor receptor system in angiogenesis. Cytokine Growth Factor Rev. 2005;16(2):159-78.
366. Gotoh N. Regulation of growth factor signaling by FRS2 family docking/scaffold adaptor proteins. Cancer Sci. 2008;99(7):1319-25.
367. Ren H, Tan ZP, Zhu X, Crosby K, Haack H, Ren JM, et al. Identification of anaplastic lymphoma kinase as a potential therapeutic target in ovarian cancer. Cancer Res. 2012;72(13):3312-23.
368. Ardito F, Giuliani M, Perrone D, Troiano G, Lo Muzio L. The crucial role of protein phosphorylation in cell signaling and its use as targeted therapy (Review). Int J Mol Med. 2017;40(2):271-80.
369. Monaghan RM, Page DJ, Ostergaard P, Keavney BD. The physiological and pathological functions of VEGFR3 in cardiac and lymphatic development and related diseases. Cardiovasc Res. 2021;117(8):1877-90.
370. Pusztaszeri MP, Seelentag W, Bosman FT. Immunohistochemical expression of endothelial markers CD31, CD34, von Willebrand factor, and Fli-1 in normal human tissues. J Histochem Cytochem. 2006;54(4):385-95.
371. Pan J, Dinh TT, Rajaraman A, Lee M, Scholz A, Czupalla CJ, et al. Patterns of expression of factor VIII and von Willebrand factor by endothelial cell subsets in vivo. Blood. 2016;128(1):104-9.
372. Bio-Techne. Human VEGFR3/Flt-4 Antibody (Product datasheet) [updated 2019. Available from: https://www.bio-techne.com/p/antibodies/human-vegfr3-flt-4-antibody-54703_mab3491.
373. UniProt Consortium. Vascular endothelial growth factor receptor 3 [UniProtKB - P35916 (VGFR3_HUMAN)] [updated 2022. Available from: https://www.uniprot.org/uniprot/P35916.
374. Goertz L, Schneider SW, Desch A, Mayer FT, Koett J, Nowak K, et al. Heparins that block VEGF-A-mediated von Willebrand factor fiber generation are potent inhibitors of hematogenous but not lymphatic metastasis. Oncotarget. 2016;7(42):68527-45.
375. Deng Y, Zhang X, Simons M. Molecular controls of lymphatic VEGFR3 signaling. Arterioscler Thromb Vasc Biol. 2015;35(2):421-9.
376. Heinolainen K, Karaman S, D'Amico G, Tammela T, Sormunen R, Eklund L, et al. VEGFR3 Modulates Vascular Permeability by Controlling VEGF/VEGFR2 Signaling. Circ Res. 2017;120(9):1414-25.
377. Peng F, Zhong Y, Liu Y, Zhang Y, Xie Y, Lu Y, et al. SPARC suppresses lymph node metastasis by regulating the expression of VEGFs in ovarian carcinoma. Int J Oncol. 2017;51(6):1920-8.
378. Touat M, Ileana E, Postel-Vinay S, Andre F, Soria JC. Targeting FGFR Signaling in Cancer. Clin Cancer Res. 2015;21(12):2684-94.

379. Katoh M. Therapeutics Targeting FGF Signaling Network in Human Diseases. Trends Pharmacol Sci. 2016;37(12):1081-96.
380. Taniguchi F, Itamochi H, Harada T, Terakawa N. Fibroblast growth factor receptor 2 expression may be involved in transformation of ovarian endometrioma to clear cell carcinoma of the ovary. Int J Gynecol Cancer. 2013;23(5):791-6.
381. Korc M, Friesel RE. The role of fibroblast growth factors in tumor growth. Curr Cancer Drug Targets. 2009;9(5):639-51.
382. Tille JC, Wood J, Mandriota SJ, Schnell C, Ferrari S, Mestan J, et al. Vascular endothelial growth factor (VEGF) receptor-2 antagonists inhibit VEGF- and basic fibroblast growth factor-induced angiogenesis in vivo and in vitro. J Pharmacol Exp Ther. 2001;299(3):1073-85.
383. Gabler C, Plath-Gabler A, Killian GJ, Berisha B, Schams D. Expression pattern of fibroblast growth factor (FGF) and vascular endothelial growth factor (VEGF) system members in bovine corpus luteum endothelial cells during treatment with FGF-2, VEGF or oestradiol. Reprod Domest Anim. 2004;39(5):321-7.
384. Della Corte CM, Viscardi G, Di Liello R, Fasano M, Martinelli E, Troiani T, et al. Role and targeting of anaplastic lymphoma kinase in cancer. Mol Cancer. 2018;17(1):30.
385. Zhao Z, Verma V, Zhang M. Anaplastic lymphoma kinase: Role in cancer and therapy perspective. Cancer Biol Ther. 2015;16(12):1691-701.
386. Stoica GE, Kuo A, Powers C, Bowden ET, Sale EB, Riegel AT, et al. Midkine binds to anaplastic lymphoma kinase (ALK) and acts as a growth factor for different cell types. J Biol Chem. 2002;277(39):35990-8.
387. Stoica GE, Kuo A, Aigner A, Sunitha I, Souttou B, Malerczyk C, et al. Identification of anaplastic lymphoma kinase as a receptor for the growth factor pleiotrophin. J Biol Chem. 2001;276(20):16772-9.
388. Moog-Lutz C, Degoutin J, Gouzi JY, Frobert Y, Brunet-de Carvalho N, Bureau J, et al. Activation and inhibition of anaplastic lymphoma kinase receptor tyrosine kinase by monoclonal antibodies and absence of agonist activity of pleiotrophin. J Biol Chem. 2005;280(28):26039-48.
389. de Streel G, Lucas S. Targeting immunosuppression by TGF-beta1 for cancer immunotherapy. Biochem Pharmacol. 2021;192:114697.
390. Alsina-Sanchis E, Figueras A, Lahiguera A, Gil-Martin M, Pardo B, Piulats JM, et al. TGFbeta Controls Ovarian Cancer Cell Proliferation. Int J Mol Sci. 2017;18(8).
391. Tian M, Neil JR, Schiemann WP. Transforming growth factor-beta and the hallmarks of cancer. Cell Signal. 2011;23(6):951-62.
392. Sanchez-Elsner T, Botella LM, Velasco B, Corbi A, Attisano L, Bernabeu C. Synergistic cooperation between hypoxia and transforming growth factor-beta pathways on human vascular endothelial growth factor gene expression. J Biol Chem. 2001;276(42):38527-35.
393. Chen W, He S, Xiang D. Hypoxia-induced retinal pigment epithelium cell-derived bFGF promotes the migration and angiogenesis of HUVECs through regulating TGF-beta1/smad2/3 pathway. Gene. 2021;790:145695.
394. Moore-Smith LD, Isayeva T, Lee JH, Frost A, Ponnazhagan S. Silencing of TGF-beta1 in tumor cells impacts MMP-9 in tumor microenvironment. Sci Rep. 2017;7(1):8678.
395. Gan Y, Wientjes MG, Au JL. Expression of basic fibroblast growth factor correlates with resistance to paclitaxel in human patient tumors. Pharm Res. 2006;23(6):1324-31.

396. Davidson B, Goldberg I, Gotlieb WH, Kopolovic J, Ben-Baruch G, Nesland JM, et al. The prognostic value of metalloproteinases and angiogenic factors in ovarian carcinoma. Mol Cell Endocrinol. 2002;187(1-2):39-45.
397. Yoneda J, Kuniyasu H, Crispens MA, Price JE, Bucana CD, Fidler IJ. Expression of angiogenesis-related genes and progression of human ovarian carcinomas in nude mice. J Natl Cancer Inst. 1998;90(6):447-54.
398. Muthukrishnan L, Warder E, McNeil PL. Basic fibroblast growth factor is efficiently released from a cytolsolic storage site through plasma membrane disruptions of endothelial cells. J Cell Physiol. 1991;148(1):1-16.
399. Esser JS, Rahner S, Deckler M, Bode C, Patterson C, Moser M. Fibroblast growth factor signaling pathway in endothelial cells is activated by BMPER to promote angiogenesis. Arterioscler Thromb Vasc Biol. 2015;35(2):358-67.
400. Frankenberry KA, Somasundar P, McFadden DW, Vona-Davis LC. Leptin induces cell migration and the expression of growth factors in human prostate cancer cells. Am J Surg. 2004;188(5):560-5.
401. Cao L, Shao M, Schilder J, Guise T, Mohammad KS, Matei D. Tissue transglutaminase links TGF-beta, epithelial to mesenchymal transition and a stem cell phenotype in ovarian cancer. Oncogene. 2012;31(20):2521-34.
402. Wang YP, Yu GR, Lee MJ, Lee SY, Chu IS, Leem SH, et al. Lipocalin-2 negatively modulates the epithelial-to-mesenchymal transition in hepatocellular carcinoma through the epidermal growth factor (TGF-beta1)/Lcn2/Twist1 pathway. Hepatology. 2013;58(4):1349-61.
403. Yang J, Bielenberg DR, Rodig SJ, Doiron R, Clifton MC, Kung AL, et al. Lipocalin 2 promotes breast cancer progression. Proc Natl Acad Sci U S A. 2009;106(10):3913-8.
404. Hu L, Hittelman W, Lu T, Ji P, Arlinghaus R, Shmulevich I, et al. NGAL decreases E-cadherin-mediated cell-cell adhesion and increases cell motility and invasion through Rac1 in colon carcinoma cells. Lab Invest. 2009;89(5):531-48.
405. Ding G, Fang J, Tong S, Qu L, Jiang H, Ding Q, et al. Over-expression of lipocalin 2 promotes cell migration and invasion through activating ERK signaling to increase SLUG expression in prostate cancer. Prostate. 2015;75(9):957-68.
406. Xiong B, Gong LL, Zhang F, Hu MB, Yuan HY. TGF beta1 expression and angiogenesis in colorectal cancer tissue. World J Gastroenterol. 2002;8(3):496-8.
407. Xu Y, Tan M, Tian X, Zhang J, Zhang J, Chen J, et al. Leptin receptor mediates the proliferation and glucose metabolism of pancreatic cancer cells via AKT pathway activation. Mol Med Rep. 2020;21(2):945-52.
408. Uddin S, Hussain AR, Siraj AK, Khan OS, Bavi PP, Al-Kuraya KS. Role of leptin and its receptors in the pathogenesis of thyroid cancer. Int J Clin Exp Pathol. 2011;4(7):637-43.
409. Mishra AK, Parish CR, Wong ML, Licinio J, Blackburn AC. Leptin signals via TGFB1 to promote metastatic potential and stemness in breast cancer. PLoS One. 2017;12(5):e0178454.
410. Kato S, Abarzua-Catalan L, Trigo C, Delpiano A, Sanhueza C, Garcia K, et al. Leptin stimulates migration and invasion and maintains cancer stem-like properties in ovarian cancer cells: an explanation for poor outcomes in obese women. Oncotarget. 2015;6(25):21100-19.

411. Feng H, Liu Q, Zhang N, Zheng L, Sang M, Feng J, et al. Leptin promotes metastasis by inducing an epithelial-mesenchymal transition in A549 lung cancer cells. Oncol Res. 2013;21(3):165-71.
412. Lanier V, Gillespie C, Leffers M, Daley-Brown D, Milner J, Lipsey C, et al. Leptin-induced transphosphorylation of vascular endothelial growth factor receptor increases Notch and stimulates endothelial cell angiogenic transformation. Int J Biochem Cell Biol. 2016;79:139-50.
413. Geng Y, Wang J, Wang R, Wang K, Xu Y, Song G, et al. Leptin and HER-2 are associated with gastric cancer progression and prognosis of patients. Biomed Pharmacother. 2012;66(6):419-24.
414. Liu H, Wan D, Pan Z, Cao L, Wu X, Lu Z, et al. Expression and biological significance of leptin, leptin receptor, VEGF, and CD34 in colorectal carcinoma. Cell Biochem Biophys. 2011;60(3):241-4.
415. Zhao X, Huang K, Zhu Z, Chen S, Hu R. Correlation between expression of leptin and clinicopathological features and prognosis in patients with gastric cancer. J Gastroenterol Hepatol. 2007;22(8):1317-21.
416. Yang X, Qiao D, Meyer K, Friedl A. Signal transducers and activators of transcription mediate fibroblast growth factor-induced vascular endothelial morphogenesis. Cancer Res. 2009;69(4):1668-77.
417. Nakamura T, Mochizuki Y, Kanetake H, Kanda S. Signals via FGF receptor 2 regulate migration of endothelial cells. Biochem Biophys Res Commun. 2001;289(4):801-6.
418. Sun HJ, Cai WW, Gong LL, Wang X, Zhu XX, Wan MY, et al. FGF-2-mediated FGFR1 signaling in human microvascular endothelial cells is activated by vaccarin to promote angiogenesis. Biomed Pharmacother. 2017;95:144-52.
419. Di Paolo D, Ambrogio C, Pastorino F, Brignole C, Martinengo C, Carosio R, et al. Selective therapeutic targeting of the anaplastic lymphoma kinase with liposomal siRNA induces apoptosis and inhibits angiogenesis in neuroblastoma. Mol Ther. 2011;19(12):2201-12.
420. Tammela T, Zarkada G, Nurmi H, Jakobsson L, Heinolainen K, Tvorogov D, et al. VEGFR-3 controls tip to stalk conversion at vessel fusion sites by reinforcing Notch signalling. Nat Cell Biol. 2011;13(10):1202-13.
421. Zarkada G, Heinolainen K, Makinen T, Kubota Y, Alitalo K. VEGFR3 does not sustain retinal angiogenesis without VEGFR2. Proc Natl Acad Sci U S A. 2015;112(3):761-6.
422. Salguero-Aranda C, Sancho-Mensat D, Canals-Lorente B, Sultan S, Reginald A, Chapman L. STAT6 knockdown using multiple siRNA sequences inhibits proliferation and induces apoptosis of human colorectal and breast cancer cell lines. PLoS One. 2019;14(5):e0207558.
423. Cao H, Zhang J, Liu H, Wan L, Zhang H, Huang Q, et al. IL-13/STAT6 signaling plays a critical role in the epithelial-mesenchymal transition of colorectal cancer cells. Oncotarget. 2016;7(38):61183-98.
424. Yan D, Wang HW, Bowman RL, Joyce JA. STAT3 and STAT6 Signaling Pathways Synergize to Promote Cathepsin Secretion from Macrophages via IRE1alpha Activation. Cell Rep. 2016;16(11):2914-27.
425. Khew-Goodall Y, Wadham C, Stein BN, Gamble JR, Vadas MA. Stat6 activation is essential for interleukin-4 induction of P-selectin transcription in human umbilical vein endothelial cells. Arterioscler Thromb Vasc Biol. 1999;19(6):1421-9.
426. Petrova TV, Makinen T, Makela TP, Saarela J, Virtanen I, Ferrell RE, et al. Lymphatic endothelial reprogramming of vascular endothelial cells by the Prox-1 homeobox transcription factor. EMBO J. 2002;21(17):4593-9.

427. Gong M, Zhuo X, Ma A. STAT6 Upregulation Promotes M2 Macrophage Polarization to Suppress Atherosclerosis. Med Sci Monit Basic Res. 2017;23:240-9.
428. Sigismund S, Avanzato D, Lanzetti L. Emerging functions of the EGFR in cancer. Mol Oncol. 2018;12(1):3-20.
429. Amin DN, Hida K, Bielenberg DR, Klagsbrun M. Tumor endothelial cells express epidermal growth factor receptor (EGFR) but not ErbB3 and are responsive to EGF and to EGFR kinase inhibitors. Cancer Res. 2006;66(4):2173-80.
430. Keezer SM, Ivie SE, Krutzsch HC, Tandle A, Libutti SK, Roberts DD. Angiogenesis inhibitors target the endothelial cell cytoskeleton through altered regulation of heat shock protein 27 and cofilin. Cancer Res. 2003;63(19):6405-12.
431. Dai S, Jia Y, Wu SL, Isenberg JS, Ridnour LA, Bandle RW, et al. Comprehensive characterization of heat shock protein 27 phosphorylation in human endothelial cells stimulated by the microbial dithiole thiolutin. J Proteome Res. 2008;7(10):4384-95.
432. Thuringer D, Jego G, Wettstein G, Terrier O, Cronier L, Yousfi N, et al. Extracellular HSP27 mediates angiogenesis through Toll-like receptor 3. FASEB J. 2013;27(10):4169-83.
433. Srinivasan R, Zabuawala T, Huang H, Zhang J, Gulati P, Fernandez S, et al. Erk1 and Erk2 regulate endothelial cell proliferation and migration during mouse embryonic angiogenesis. PLoS One. 2009;4(12):e8283.
434. Raica M, Cimpean AM. Platelet-Derived Growth Factor (PDGF)/PDGF Receptors (PDGFR) Axis as Target for Antitumor and Antiangiogenic Therapy. Pharmaceuticals (Basel). 2010;3(3):572-99.
435. Magnusson PU, Looman C, Ahgren A, Wu Y, Claesson-Welsh L, Heuchel RL. Platelet-derived growth factor receptor-beta constitutive activity promotes angiogenesis in vivo and in vitro. Arterioscler Thromb Vasc Biol. 2007;27(10):2142-9.
436. Laschke MW, Elitzsch A, Vollmar B, Vajkoczy P, Menger MD. Combined inhibition of vascular endothelial growth factor (VEGF), fibroblast growth factor and platelet-derived growth factor, but not inhibition of VEGF alone, effectively suppresses angiogenesis and vessel maturation in endometriotic lesions. Hum Reprod. 2006;21(1):262-8.
437. Kano MR, Morishita Y, Iwata C, Iwasaka S, Watabe T, Ouchi Y, et al. VEGF-A and FGF-2 synergistically promote neoangiogenesis through enhancement of endogenous PDGF-B-PDGFRbeta signaling. J Cell Sci. 2005;118(Pt 16):3759-68.
438. Battegay EJ, Rupp J, Iruela-Arispe L, Sage EH, Pech M. PDGF-BB modulates endothelial proliferation and angiogenesis in vitro via PDGF beta-receptors. J Cell Biol. 1994;125(4):917-28.
439. Karaman S, Hollmen M, Robciuc MR, Alitalo A, Nurmi H, Morf B, et al. Blockade of VEGF-C and VEGF-D modulates adipose tissue inflammation and improves metabolic parameters under high-fat diet. Mol Metab. 2015;4(2):93-105.
440. Gomez-Ambrosi J, Catalan V, Rodriguez A, Ramirez B, Silva C, Gil MJ, et al. Involvement of serum vascular endothelial growth factor family members in the development of obesity in mice and humans. J Nutr Biochem. 2010;21(8):774-80.
441. Deo DD, Axelrad TW, Robert EG, Marcheselli V, Bazan NG, Hunt JD. Phosphorylation of STAT-3 in response to basic fibroblast growth factor occurs

through a mechanism involving platelet-activating factor, JAK-2, and Src in human umbilical vein endothelial cells. Evidence for a dual kinase mechanism. J Biol Chem. 2002;277(24):21237-45.
442. Yahata Y, Shirakata Y, Tokumaru S, Yamasaki K, Sayama K, Hanakawa Y, et al. Nuclear translocation of phosphorylated STAT3 is essential for vascular endothelial growth factor-induced human dermal microvascular endothelial cell migration and tube formation. J Biol Chem. 2003;278(41):40026-31.
443. Bartoli M, Platt D, Lemtalsi T, Gu X, Brooks SE, Marrero MB, et al. VEGF differentially activates STAT3 in microvascular endothelial cells. FASEB J. 2003;17(11):1562-4.
444. Chim SM, Kuek V, Chow ST, Lim BS, Tickner J, Zhao J, et al. EGFL7 is expressed in bone microenvironment and promotes angiogenesis via ERK, STAT3, and integrin signaling cascades. J Cell Physiol. 2015;230(1):82-94.
445. Santra M, Santra S, Zhang J, Chopp M. Ectopic decorin expression up-regulates VEGF expression in mouse cerebral endothelial cells via activation of the transcription factors Sp1, HIF1alpha, and Stat3. J Neurochem. 2008;105(2):324-37.
446. Ogrodnik M. Cellular aging beyond cellular senescence: Markers of senescence prior to cell cycle arrest in vitro and in vivo. Aging Cell. 2021;20(4):e13338.
447. Shay JW, Wright WE. Hayflick, his limit, and cellular ageing. Nat Rev Mol Cell Biol. 2000;1(1):72-6.
448. Plikus MV, Wang X, Sinha S, Forte E, Thompson SM, Herzog EL, et al. Fibroblasts: Origins, definitions, and functions in health and disease. Cell. 2021;184(15):3852-72.
449. Kisselbach L, Merges M, Bossie A, Boyd A. CD90 Expression on human primary cells and elimination of contaminating fibroblasts from cell cultures. Cytotechnology. 2009;59(1):31-44.
450. Linge C, Green MR, Brooks RF. A method for removal of fibroblasts from human tissue culture systems. Exp Cell Res. 1989;185(2):519-28.
451. Chung-Welch N, Patton WF, Shepro D, Cambria RP. Two-stage isolation procedure for obtaining homogenous populations of microvascular endothelial and mesothelial cells from human omentum. Microvasc Res. 1997;54(2):121-34.
452. Chung-Welch N, Patton WF, Yen-Patton GP, Hechtman HB, Shepro D. Phenotypic comparison between mesothelial and microvascular endothelial cell lineages using conventional endothelial cell markers, cytoskeletal protein markers and in vitro assays of angiogenic potential. Differentiation. 1989;42(1):44-53.
453. Fischereder M, Luckow B, Sitter T, Schroppel B, Banas B, Schlondorff D. Immortalization and characterization of human peritoneal mesothelial cells. Kidney Int. 1997;51(6):2006-12.
454. Tarbit E, Singh I, Peart JN, Rose'Meyer RB. Biomarkers for the identification of cardiac fibroblast and myofibroblast cells. Heart Fail Rev. 2019;24(1):1-15.
455. von Koskull H, Virtanen I. Induction of cytokeratin expression in human mesenchymal cells. J Cell Physiol. 1987;133(2):321-9.
456. Linxweiler J, Hajili T, Korbel C, Berchem C, Zeuschner P, Muller A, et al. Cancer-associated fibroblasts stimulate primary tumor growth and metastatic spread in an orthotopic prostate cancer xenograft model. Sci Rep. 2020;10(1):12575.

457. Li J, Huang NF, Zou J, Laurent TJ, Lee JC, Okogbaa J, et al. Conversion of human fibroblasts to functional endothelial cells by defined factors. Arterioscler Thromb Vasc Biol. 2013;33(6):1366-75.
458. Weber SC, Gratopp A, Akanbi S, Rheinlaender C, Sallmon H, Barikbin P, et al. Isolation and culture of fibroblasts, vascular smooth muscle, and endothelial cells from the fetal rat ductus arteriosus. Pediatr Res. 2011;70(3):236-41.
459. Morganti M, Budianto D, Takiy BA, Henze U, Mittermayer C, Sagripanti A, et al. Detection of minimal but significant amount of von Willebrand factor in human omentum mesothelial cell cultures. Biomed Pharmacother. 1996;50(8):369-72.
460. Greenwood SK, Hill RB, Sun JT, Armstrong MJ, Johnson TE, Gara JP, et al. Population doubling: a simple and more accurate estimation of cell growth suppression in the in vitro assay for chromosomal aberrations that reduces irrelevant positive results. Environ Mol Mutagen. 2004;43(1):36-44.
461. Hewett PW, Murray JC. Human omental mesothelial cells: a simple method for isolation and discrimination from endothelial cells. In Vitro Cell Dev Biol Anim. 1994;30A(3):145-7.
462. Chen KS, Chen WS. Experience in primary culture of human peritoneal mesothelial cell. Chin J Physiol. 2012;55(4):274-83.
463. Stylianou E, Jenner LA, Davies M, Coles GA, Williams JD. Isolation, culture and characterization of human peritoneal mesothelial cells. Kidney Int. 1990;37(6):1563-70.
464. Ksiazek K, Mikula-Pietrasik J, Korybalska K, Dworacki G, Jorres A, Witowski J. Senescent peritoneal mesothelial cells promote ovarian cancer cell adhesion: the role of oxidative stress-induced fibronectin. Am J Pathol. 2009;174(4):1230-40.
465. Herzog R, Tarantino S, Rudolf A, Aufricht C, Kratochwill K, Witowski J. Senescence-Associated Changes in Proteome and O-GlcNAcylation Pattern in Human Peritoneal Mesothelial Cells. Biomed Res Int. 2015;2015:382652.
466. Reggio S, Rouault C, Poitou C, Bichet JC, Prifti E, Bouillot JL, et al. Increased Basement Membrane Components in Adipose Tissue During Obesity: Links With TGFbeta and Metabolic Phenotypes. J Clin Endocrinol Metab. 2016;101(6):2578-87.
467. Zhou J, Ding M, Zhao Z, Reeders ST. Complete primary structure of the sixth chain of human basement membrane collagen, alpha 6(IV). Isolation of the cDNAs for alpha 6(IV) and comparison with five other type IV collagen chains. J Biol Chem. 1994;269(18):13193-9.
468. Kenny HA, Krausz T, Yamada SD, Lengyel E. Use of a novel 3D culture model to elucidate the role of mesothelial cells, fibroblasts and extra-cellular matrices on adhesion and invasion of ovarian cancer cells to the omentum. Int J Cancer. 2007;121(7):1463-72.
469. Moser TL, Pizzo SV, Bafetti LM, Fishman DA, Stack MS. Evidence for preferential adhesion of ovarian epithelial carcinoma cells to type I collagen mediated by the alpha2beta1 integrin. Int J Cancer. 1996;67(5):695-701.
470. Clarkson JR, Cui ZF, Darton RC. Protein Denaturation in Foam. J Colloid Interface Sci. 1999;215(2):323-32.
471. Miltenyi Biotec. Anti-Fibroblast MicroBeads, human 2022 [Available from: https://www.miltenyibiotec.com/GB-en/products/anti-fibroblast-microbeads-human.html.

472. Barilani M, Banfi F, Sironi S, Ragni E, Guillaumin S, Polveraccio F, et al. Low-affinity Nerve Growth Factor Receptor (CD271) Heterogeneous Expression in Adult and Fetal Mesenchymal Stromal Cells. Sci Rep. 2018;8(1):9321.
473. Potzsch B, Grulich-Henn J, Rossing R, Wille D, Muller-Berghaus G. Identification of endothelial and mesothelial cells in human omental tissue and in omentum-derived cultured cells by specific cell markers. Lab Invest. 1990;63(6):841-52.
474. Nelson CM, Chen CS. Cell-cell signaling by direct contact increases cell proliferation via a PI3K-dependent signal. FEBS Lett. 2002;514(2-3):238-42.
475. Gramsch B, Gabriel HD, Wiemann M, Grummer R, Winterhager E, Bingmann D, et al. Enhancement of connexin 43 expression increases proliferation and differentiation of an osteoblast-like cell line. Exp Cell Res. 2001;264(2):397-407.
476. Pelin K, Hirvonen A, Linnainmaa K. Expression of cell adhesion molecules and connexins in gap junctional intercellular communication deficient human mesothelioma tumour cell lines and communication competent primary mesothelial cells. Carcinogenesis. 1994;15(11):2673-5.
477. Leontieva OV, Demidenko ZN, Blagosklonny MV. Contact inhibition and high cell density deactivate the mammalian target of rapamycin pathway, thus suppressing the senescence program. Proc Natl Acad Sci U S A. 2014;111(24):8832-7.
478. Alessio N, Aprile D, Cappabianca S, Peluso G, Di Bernardo G, Galderisi U. Different Stages of Quiescence, Senescence, and Cell Stress Identified by Molecular Algorithm Based on the Expression of Ki67, RPS6, and Beta-Galactosidase Activity. Int J Mol Sci. 2021;22(6).
479. Hjelle JT, Golinska BT, Waters DC, Steidley KR, McCarroll DR, Dobbie JW. Isolation and propagation in vitro of peritoneal mesothelial cells. Perit Dial Int. 1989;9(4):341-7.
480. Jaurand MC, Bernaudin JF, Renier A, Kaplan H, Bignon J. Rat pleural mesothelial cells in culture. In Vitro. 1981;17(2):98-106.
481. Dauleh S, Santeramo I, Fielding C, Ward K, Herrmann A, Murray P, et al. Characterisation of Cultured Mesothelial Cells Derived from the Murine Adult Omentum. PLoS One. 2016;11(7):e0158997.
482. Rynne-Vidal A, Au-Yeung CL, Jimenez-Heffernan JA, Perez-Lozano ML, Cremades-Jimeno L, Barcena C, et al. Mesothelial-to-mesenchymal transition as a possible therapeutic target in peritoneal metastasis of ovarian cancer. J Pathol. 2017;242(2):140-51.
483. Strippoli R, Benedicto I, Perez Lozano ML, Cerezo A, Lopez-Cabrera M, del Pozo MA. Epithelial-to-mesenchymal transition of peritoneal mesothelial cells is regulated by an ERK/NF-kappaB/Snail1 pathway. Dis Model Mech. 2008;1(4-5):264-74.
484. Stadtfeld M, Varas F, Graf T. Fluorescent protein-cell labeling and its application in time-lapse analysis of hematopoietic differentiation. Methods Mol Med. 2005;105:395-412.
485. Zhou X, Liu D, You L, Wang L. Quantifying fluid shear stress in a rocking culture dish. J Biomech. 2010;43(8):1598-602.
486. Avraham-Chakim L, Elad D, Zaretsky U, Kloog Y, Jaffa A, Grisaru D. Fluid-flow induced wall shear stress and epithelial ovarian cancer peritoneal spreading. PLoS One. 2013;8(4):e60965.
487. Sun L, Wen J, Wang L, Wen Q, Wu J, Bie M. Fluid shear stress-induced IL-8/CXCR signaling in human ovarian cancer cells. Transl Cancer Res. 2019;8(4):1591-601.

488. Mitchell MJ, King MR. Computational and experimental models of cancer cell response to fluid shear stress. Front Oncol. 2013;3:44.
489. Surre J, Saint-Ruf C, Collin V, Orenga S, Ramjeet M, Matic I. Strong increase in the autofluorescence of cells signals struggle for survival. Sci Rep. 2018;8(1):12088.
490. Ryan PW, Li B, Shanahan M, Leister KJ, Ryder AG. Prediction of cell culture media performance using fluorescence spectroscopy. Anal Chem. 2010;82(4):1311-7.
491. Ettinger A, Wittmann T. Fluorescence live cell imaging. Methods Cell Biol. 2014;123:77-94.
492. Hyler AR, Baudoin NC, Brown MS, Stremler MA, Cimini D, Davalos RV, et al. Fluid shear stress impacts ovarian cancer cell viability, subcellular organization, and promotes genomic instability. PLoS One. 2018;13(3):e0194170.
493. Wang P, Chen SH, Hung WC, Paul C, Zhu F, Guan PP, et al. Fluid shear promotes chondrosarcoma cell invasion by activating matrix metalloproteinase 12 via IGF-2 and VEGF signaling pathways. Oncogene. 2015;34(35):4558-69.
494. Wang X, Zhang Y, Feng T, Su G, He J, Gao W, et al. Fluid Shear Stress Promotes Autophagy in Hepatocellular Carcinoma Cells. Int J Biol Sci. 2018;14(10):1277-90.
495. Rieppi M, Vergani V, Gatto C, Zanetta G, Allavena P, Taraboletti G, et al. Mesothelial cells induce the motility of human ovarian carcinoma cells. Int J Cancer. 1999;80(2):303-7.
496. Strippoli R, Benedicto I, Perez Lozano ML, Pellinen T, Sandoval P, Lopez-Cabrera M, et al. Inhibition of transforming growth factor-activated kinase 1 (TAK1) blocks and reverses epithelial to mesenchymal transition of mesothelial cells. PLoS One. 2012;7(2):e31492.
497. Loureiro J, Aguilera A, Selgas R, Sandoval P, Albar-Vizcaino P, Perez-Lozano ML, et al. Blocking TGF-beta1 protects the peritoneal membrane from dialysate-induced damage. J Am Soc Nephrol. 2011;22(9):1682-95.
498. Rosso M, Majem B, Devis L, Lapyckyj L, Besso MJ, Llaurado M, et al. E-cadherin: A determinant molecule associated with ovarian cancer progression, dissemination and aggressiveness. PLoS One. 2017;12(9):e0184439.
499. Elloul S, Elstrand MB, Nesland JM, Trope CG, Kvalheim G, Goldberg I, et al. Snail, Slug, and Smad-interacting protein 1 as novel parameters of disease aggressiveness in metastatic ovarian and breast carcinoma. Cancer. 2005;103(8):1631-43.
500. Slack-Davis JK, Atkins KA, Harrer C, Hershey ED, Conaway M. Vascular cell adhesion molecule-1 is a regulator of ovarian cancer peritoneal metastasis. Cancer Res. 2009;69(4):1469-76.
501. Scalici JM, Arapovic S, Saks EJ, Atkins KA, Petroni G, Duska LR, et al. Mesothelium expression of vascular cell adhesion molecule-1 (VCAM-1) is associated with an unfavorable prognosis in epithelial ovarian cancer (EOC). Cancer. 2017;123(6):977-84.
502. Rossi L, Verrico M, Zaccarelli E, Papa A, Colonna M, Strudel M, et al. Bevacizumab in ovarian cancer: A critical review of phase III studies. Oncotarget. 2017;8(7):12389-405.
503. Dong Z, Santeford A, Ban N, Lee TJ, Smith C, Ornitz DM, et al. FGF2-induced STAT3 activation regulates pathologic neovascularization. Exp Eye Res. 2019;187:107775.

504. Chiba R, Akiya M, Hashimura M, Oguri Y, Inukai M, Hara A, et al. ALK signaling cascade confers multiple advantages to glioblastoma cells through neovascularization and cell proliferation. PLoS One. 2017;12(8):e0183516.
505. Ding S, Merkulova-Rainon T, Han ZC, Tobelem G. HGF receptor up-regulation contributes to the angiogenic phenotype of human endothelial cells and promotes angiogenesis in vitro. Blood. 2003;101(12):4816-22.
506. Nakagami H, Morishita R, Yamamoto K, Taniyama Y, Aoki M, Matsumoto K, et al. Mitogenic and antiapoptotic actions of hepatocyte growth factor through ERK, STAT3, and AKT in endothelial cells. Hypertension. 2001;37(2 Pt 2):581-6.
507. Granata R, Trovato L, Lupia E, Sala G, Settanni F, Camussi G, et al. Insulin-like growth factor binding protein-3 induces angiogenesis through IGF-I- and SphK1-dependent mechanisms. J Thromb Haemost. 2007;5(4):835-45.
508. Suffee N, Hlawaty H, Meddahi-Pelle A, Maillard L, Louedec L, Haddad O, et al. RANTES/CCL5-induced pro-angiogenic effects depend on CCR1, CCR5 and glycosaminoglycans. Angiogenesis. 2012;15(4):727-44.
509. Li YL, Zhao H, Ren XB. Relationship of VEGF/VEGFR with immune and cancer cells: staggering or forward? Cancer Biol Med. 2016;13(2):206-14.
510. Masoumi Moghaddam S, Amini A, Morris DL, Pourgholami MH. Significance of vascular endothelial growth factor in growth and peritoneal dissemination of ovarian cancer. Cancer Metastasis Rev. 2012;31(1-2):143-62.
511. Doroudi M, Kramer BS, Pinsky PF. The bimanual ovarian palpation examination in the Prostate, Lung, Colorectal and Ovarian cancer screening trial: Performance and complications. J Med Screen. 2017;24(4):220-2.
512. Menon U, Ryan A, Kalsi J, Gentry-Maharaj A, Dawnay A, Habib M, et al. Risk Algorithm Using Serial Biomarker Measurements Doubles the Number of Screen-Detected Cancers Compared With a Single-Threshold Rule in the United Kingdom Collaborative Trial of Ovarian Cancer Screening. J Clin Oncol. 2015;33(18):2062-71.
513. Javadi S, Ganeshan DM, Qayyum A, Iyer RB, Bhosale P. Ovarian Cancer, the Revised FIGO Staging System, and the Role of Imaging. AJR Am J Roentgenol. 2016;206(6):1351-60.
514. Sharma A, Burnell M, Gentry-Maharaj A, Campbell S, Amso NN, Seif MW, et al. Factors affecting visualization of postmenopausal ovaries: descriptive study from the multicenter United Kingdom Collaborative Trial of Ovarian Cancer Screening (UKCTOCS). Ultrasound Obstet Gynecol. 2013;42(4):472-7.
515. Stott W, Campbell S, Franchini A, Blyuss O, Zaikin A, Ryan A, et al. Sonographers' self-reported visualization of normal postmenopausal ovaries on transvaginal ultrasound is not reliable: results of expert review of archived images from UKCTOCS. Ultrasound Obstet Gynecol. 2018;51(3):401-8.
516. Filippou PS, Karagiannis GS, Constantinidou A. Midkine (MDK) growth factor: a key player in cancer progression and a promising therapeutic target. Oncogene. 2020;39(10):2040-54.
517. Kaur G, Dufour JM. Cell lines: Valuable tools or useless artifacts. Spermatogenesis. 2012;2(1):1-5.
518. Domcke S, Sinha R, Levine DA, Sander C, Schultz N. Evaluating cell lines as tumour models by comparison of genomic profiles. Nat Commun. 2013;4:2126.
519. Yee C, Dickson KA, Muntasir MN, Ma Y, Marsh DJ. Three-Dimensional Modelling of Ovarian Cancer: From Cell Lines to Organoids for Discovery and Personalized Medicine. Front Bioeng Biotechnol. 2022;10:836984.

520. Amitani M, Asakawa A, Amitani H, Inui A. The role of leptin in the control of insulin-glucose axis. Front Neurosci. 2013;7:51.
521. Singh P, Peterson TE, Sert-Kuniyoshi FH, Glenn JA, Davison DE, Romero-Corral A, et al. Leptin signaling in adipose tissue: role in lipid accumulation and weight gain. Circ Res. 2012;111(5):599-603.